Lappeenrannan teknillinen korkeakoulu
Lappeenranta University of Technology

Pekka Savolainen

MODELING OF NON-ISOTHERMAL VAPOR MEMBRANE SEPARATION WITH THERMODYNAMIC MODELS AND GENERALIZED MASS TRANSFER EQUATIONS

Acta Universitatis
Lappeenrantaensis
125

Lappeenrannan teknillinen korkeakoulu
Lappeenranta University of Technology

Pekka Savolainen

MODELING OF NON-ISOTHERMAL VAPOR MEMBRANE SEPARATION WITH THERMODYNAMIC MODELS AND GENERALIZED MASS TRANSFER EQUATIONS

Dissertation for the degree of Doctor of Science (Technology) to be presented with due permission for public examination and criticism in the Auditorium 1383 at Lappeenranta University of Technology, Lappeenranta, Finland on the 30th of May in 2002, at noon.

Acta Universitatis
Lappeenrantaensis
125

ISBN 951-764-647-X
ISSN 1456-4491

Lappeenrannan teknillinen korkeakoulu
Digipaino 2002

ABSTRACT

Savolainen Pekka
Modeling of non-isothermal vapor membrane separation with thermodynamic models and generalized mass transfer equations
Lappeenranta 2002
179 p.
Acta Universitatis Lappeenrantaensis 125
Diss. Lappeenranta University of Technology
ISBN 951-764-647-X
ISSN 1456-4491

A rigorous unit operation model is developed for vapor membrane separation. The new model is able to describe temperature, pressure, and concentration dependent permeation as well real fluid effects in vapor and gas separation with hydrocarbon selective rubbery polymeric membranes.

The permeation through the membrane is described by a separate treatment of sorption and diffusion within the membrane. The chemical engineering thermodynamics is used to describe the equilibrium sorption of vapors and gases in rubbery membranes with equation of state models for polymeric systems. Also a new modification of the UNIFAC model is proposed for this purpose. Various thermodynamic models are extensively compared in order to verify the models' ability to predict and correlate experimental vapor-liquid equilibrium data. The penetrant transport through the selective layer of the membrane is described with the generalized Maxwell–Stefan equations, which are able to account for the bulk flux contribution as well as the diffusive coupling effect. A method is described to compute and correlate binary penetrant–membrane diffusion coefficients from the experimental permeability coefficients at different temperatures and pressures. A fluid flow model for spiral-wound modules is derived from the conservation equation of mass, momentum, and energy. The conservation equations are presented in a discretized form by using the control volume approach. A combination of the permeation model and the fluid flow model yields the desired rigorous model for vapor membrane separation. The model is implemented into an in-house process simulator and so vapor membrane separation may be evaluated as an integral part of a process flowsheet.

Keywords: modeling, vapor separation, membrane, permeation, sorption, diffusion, polymer, equation of state, UNIFAC, Maxwell–Stefan equations, control volume method, spiral-wound module

UDC 66.071.6.001.57 : 66.081 : 533.15

FOREWORD

This dissertation was carried out during the years 1997-2002 at Neste Engineering Oy, Process Engineering department in close co-operation with Lappeenranta University of Technology.

Many individuals have given their support and guidance along the way. Firstly, I would like to express my appreciation to Professor (emeritus) Seppo Palosaari and Professor Juha Kallas, my former and current supervisor, for leading me through the dissertation. Professor Juhani Aittamaa and Dr. Harri Järvelin are thanked for offering me this challenging research topic. The former was my industrial instructor before receiving the professorship at Helsinki University of Technology. I am indebted to my current industrial instructor, Dr. Kari I. Keskinen, for valuable discussions and, especially, for carefully reading and commenting on various manuscript versions. The official previewers, Professor (emeritus) Jorma Sohlo and Professor Henrik Saxén from Åbo Akademi University, are thanked for suggesting valuable corrections and pointing out the ambiguous sections in the manuscript of this dissertation. Finally, I would like to thank the staff at Process Engineering department for creating an enthusiastic and pleasant working atmosphere.

The financial support of Neste Research Foundation is gratefully acknowledged in the form of travel grant and research grants for the years 1997-2000. The support of the Graduate School in Chemical Engineering (GSCE) is also gratefully acknowledged in the form of defraying the expenses of participation to the GSCE courses and seminars. Neste Engineering Oy is gratefully acknowledged for providing computing and other working facilities during this work.

Porvoo, April 2002

Pekka Savolainen

TABLE OF CONTENTS

1 INTRODUCTION

The Loeb and Sourirajan (1963) invention of the phase-inverted reverse osmosis membranes was a breakthrough for the development of feasible membrane separation processes. These asymmetric membranes, which consisted of a thin dense skin and a porous support layer, provided reasonable fluxes for many membrane separation applications. Since then the development in membranes and membrane processes has been vigorous so that the current list of commercial membrane processes is long, including reverse osmosis, nanofiltration, ultrafiltration, microfiltration, electrodialysis, pervaporation, and gas separation.

Gas separation uses dense polymeric, porous ceramic, or porous carbon membranes. Polymeric membranes are either glassy or rubbery membranes. However, most modern applications make use of dense glassy polymeric membranes such as PRISM® polysulfone membranes that were launched by Monsanto Co. in 1980 (MacLean and Graham, 1980; Henis and Tripodi, 1980). Glassy polymeric membranes are nowadays separating hydrogen from nitrogen, hydrogen from hydrocarbons, hydrogen from carbon dioxide, hydrogen from carbon monoxide, carbon dioxide from methane, nitrogen from air, and water from compressed air. Rubbery polymeric membranes found their commericial use in vapor membrane separation at the end of the 80's (Behling *et al.*, 1989; Wijmans and Helm, 1989; Katoh *et al.*, 1989). Since then rubbery membranes has been successfully utilized for hydrocarbon vapor separation and recovery from various gas streams (Ohlrogge *et al.*, 1990; Baker *et al.*, 1996) and for monomer separation and recovery from polyolefin resin degassing (Baker and Jacobs, 1996). The latter application not only introduced a decade increase in the feed capacity of the vapor membrane separation process but also a substantial value of the recovered monomer.

The number of vapor separation applications is expected to increase rapidly, partly due to continuous tightening of local authority regulations on the emission control of volatile organic compounds (VOCs) and hazardous air pollutants (HAPs). In addition, new potential applications for hydrocarbon selective membranes are expected to be found in the refinery and petrochemical processes. Therefore, this dissertation centers on vapor separation with hydrocarbon selective rubbery membranes with deep insight into the transport phenomena involved therein.

1.1 SCOPE OF THE WORK

Membrane separation processes have conventionally been used as end-of-pipe installations. Recent developments (Baker and Jacobs, 1996) have introduced vapor membrane separation also as an integral part of a production process with recycle streams. In such cases, the evaluation of the process configuration is preferably performed with flowsheet simulation, which is nowadays an essential tool in the process development, design, and optimization. However, commercial process simulators do not contain models for gas and vapor membrane separation.

The final goal in this work is to develop a theoretically rigorous unit operation model for vapor membrane separation with rubbery spiral-wound membrane modules. The new model is then implemented into a flowsheet process simulator, FLOWBAT (2001), that allows the studying of the vapor membrane separation with the existing unit operation models, such as distillation and various reactor models. Non-commercial user models of different theoretical levels have already been incorporated into commercial and non-commercial process simulators (Rautenbach *et al.* 1996; Hoting *et al.*, 1997; Tessendorf, 1998).

Mathematical models for spiral-wound modules exist for binary (Pan and Habgood, 1974) and multicomponent gas mixtures (Pan and Habgood, 1978; Shindo *et al.*, 1985; Hickey and Gooding, 1994; Qi and Henson, 1997; Tessendorf *et al.*, 1999). However, these models utilize such assumptions that may lead to an overestimation of the performance of vapor membrane separation process. These assumptions include constant permeability, species permeation as a single species in a mixture, isothermal operation, a negligible pressure drop on the retentate side, and, except for the models of Hickey and Gooding (1994) and Qi and Henson (1997), a negligible pressure drop on the permeate side.

The assumption of constant permeability holds for noncondensable components, such as hydrogen and nitrogen, but not for the condensable components in a mixture. The assumption of species permeation as a single species neglects the diffusive coupling and the bulk flux contribution. The latter effect has been recognized for the organic liquid permeation in homogenous solvent swollen membranes (Paul and Ebra-Lima, 1970; Paul, 1973) and for the gas permeation in glassy membranes (McCandless, 1972; Koros *et al.* 1981). Kamaruddin and Koros (1997) revealed that the bulk flux contribution cannot be neglected either at a low sorption level when penetrants have relative large differences in the individual fluxes.

The assumption of an isothermal operation is erroneous in the thermodynamic sense. Gorissen (1987) has pointed out that enthalpy changes do occur in gas and vapor membrane separation due to changes in the pressure and in the composition of the local product flows. The permeated fraction may be internally cooled or heated within the membrane, since the pressure change may result in a positive or negative temperature change for a real gas. Internal cooling may be expected in vapor membrane separation, since most gases, except for hydrogen, cool on expansion at ordinary temperatures. According to Baker and Lokhandwala (1998), retentate and permeate products exit at about the same temperature or the retentate is the colder stream. As a consequence, local temperature differences may be formed over the membrane and heat is transferred over the thin composite membrane. These non-isothermal effects have been taken into account in recent dissertations (Tessendorf, 1998; Thundyil, 1998).

The assumption of the negligible pressure drop on the retentate side is acceptable for a properly designed process. The flow velocity and the required pressure drop for the flow on the retentate side decreases along the flow due to the permeation of the fluid into the permeate side. However, on the permeate side the flow velocity increases along the flow and so the pressure drop must be carefully verified.

A rigorous modeling approach in this work utilizes thermodynamic models for polymeric systems, multicomponent mass transport theories, transport theories in polymeric systems, and techniques from computational fluid dynamics, CFD. The outline of this work is as follows.

Chapter 2 provides the reader with the background information of vapor membrane separation. In chapter 3, the basic model equations of mass, momentum, and energy are derived for the fluid flow in spiral-wound membrane modules. The flow fields of the bulk retentate and permeate are treated as separate but interlinked flow fields due to local mass and energy flow through the membrane. The basic model equations are discretized in chapter 4. The method of discretization follows the control volume approach by Patankar (1980) that results in discrete model equations, which are able to fulfill the integral conservation of mass, momentum, and energy within a spiral-wound module.

Chapter 5 is devoted to the gas and vapor transport in rubbery membranes. The sorption equilibrium in the membrane is treated by using the classical chemical engineering thermodynamics. The transport equations within the membrane will be derived from the generalized Maxwell–Stefan equations (Taylor and Krishna, 1993). The effect of the membrane swelling on sorption is also considered. Diffusion coefficients are treated as experimental quantities that are obtained from the pure component permeability measurements at different temperatures and pressures. These diffusion coefficients will be used to create a diffusivity correlation and to form a predictive description of permeation in a multicomponent system. When the items above are combined, the model is able to describe the temperature, pressure, and composition dependent permeation through the infinitesimal membrane element.

Chapter 6 introduces equation of state models for polymeric systems. These models are the Sanchez–Lacombe equation of state (Sanchez and Lacombe, 1976; Lacombe and Sanchez, 1976), the perturbed hard-sphere-chain equation of state (Song *et al.*, 1996), and the combined Soave-Redlich–Kwong equation of state–predictive excess Gibbs energy model with the MHV2 mixing rule (Dahl and Michelsen, 1990). UNIFAC-FV (Oishi and Prausnitz, 1978) and a new modification of the UNIFAC model, the exponential UNIFAC, provide the excess Gibbs energy expression for the mixing rule. The latter is developed in this work and may be applied for the estimation of the activity coefficients of gases in polymeric liquid mixtures. In this work, the equation of state models are used to describe the sorption equilibrium at the fluid–membrane interface and the non-ideality of the polymer phase in the transport equations. Therefore, the main part of chapter 7 is devoted to the comparison of the models' ability to predict and correlate binary solvent–polymer vapor–liquid equilibrium in order to find the suitable thermodynamic model for vapor membrane separation. Other subjects of chapter 7 deal with the correlation of pure component diffusion coefficients in a PDMS membrane and the modeling of multicomponent permeation in a laboratory test cell. The detailed solution algorithm for the model equations of mass, momentum, and energy are provided in chapter 8 with industrially relevant example simulations. The final conclusions are then drawn in chapter 9.

2 VAPOR MEMBRANE SEPARATION

Vapor membrane separation may be distinguished as a subsection of gas membrane separation. It has become common practice in the membrane separation literature to deal with vapor and gas membrane separation as separate subjects. Basically, feed, retentate, and permeate are vapors in vapor membrane separation and gases in gas membrane separation. In a thermodynamic sense, the difference between vapor and gas is that vapor may be liquefied by increasing the pressure or decreasing the volume at constant temperature while gas may not. However, vapor membrane separation in this work is associated with a membrane process that treats a vapor laden gas stream and preferentially separates at least a part of the vapor to the permeate product stream. The correct term should then be vapor and gas separation but, in brief, vapor separation is used instead.

An organic vapor contaminated gas stream is formed when a gaseous stream, e.g. air, passes through or over a free surface of evaporating liquid. Vapor compounds may be partially recovered from the gas by compression, condensation, absorption, adsorption, or membrane separation. Alternatively, vapor compounds may be destroyed by thermal or catalytic oxidation, i.e. incineration. The choice of the method depends on economical considerations, the vapor concentration level, and the total flow rate. According to Baker (2000, p. 329), vapor membrane separation is economically favorable at the region of 1-10 vol-% of organic vapor.

Vapor membrane separation alone is not able to fulfil simultaneous high-efficiency separation and the enrichment of the desired component in a single separation stage. Better process performance and economics are obtained when membrane separation is combined with another separation process to form a hybrid process. Thus far vapor membrane separation has been combined with compression–condensation (Kaschemekat *et al.*, 1993), absorption (Katoh *et al.*, 1989), adsorption, and catalytic oxidation (Ohlrogge *et al.*, 1990 and 1993).

This introductory chapter provides with the basic information relevant to the topic of this dissertation. Vapor separation membranes and membrane materials are introduced in section 2.1 and the construction of membrane modules in section 2.2. The transport characteristics of rubbery and glassy polymers are set forth in short in terms of sorption and diffusion in section

2.3. The prevailing macroscopic model for gas and vapor permeation, the solution–diffusion model, is presented in section 2.4.

2.1 MEMBRANES AND MEMBRANE MATERIALS

Modern membranes for separation are either asymmetric integrally skinned or flat sheet composite membranes. Vapor membrane separation utilizes hydrocarbon selective rubbery membranes in the form of composite flat sheets. This allows for the production of mechanically strong membranes from materials that have relatively weak mechanical properties.

Generally, the vapor separation membrane consists of three composite layers as sketched in Figure 2.1. The topmost layer is a dense selective layer, 0.4-10 μm in thickness, made of a material that performs the desired separation. Beneath the selective layer, there is a porous support layer, 40-150 μm in thickness, made of a material that provides the membrane with the required mechanical strength, and which is also physically compatible with the selective layer. The undermost layer is a substrate layer, 100-150 μm in thickness, made of a non-woven fabric, like polyester or polypropylene, that acts as a backing for the membrane.

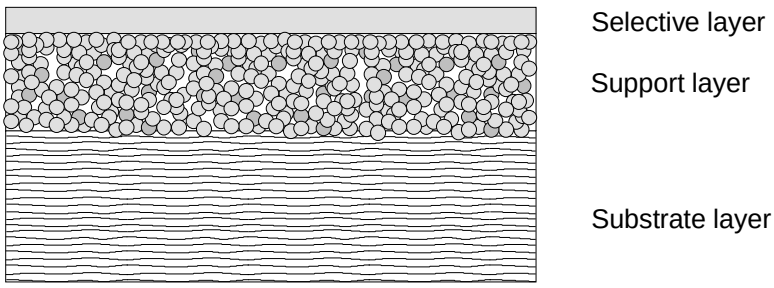

Figure 2.1 Schematic cross-section of a three-layer composite membrane.

Hydrocarbon selective separation layers may be formed from various rubbery polymers as listed in the patents by Baker (1985) and Gottschlich and Jacobs (1998). These materials include nitrile rubber, neoprene, poly(dimethylsiloxane), chlorosulfonated polyethylene, fluoroelastomer, polyurethane, poly(*cis*-butadiene), poly(*cis*-isoprene), and polystyrene-butadiene copolymers.

Hydrocarbon selective layers may also be formed from substituted polyacetylenes that are high permeability glassy polymers (Masuda *et al.*, 1983; Takada *et al.*, 1985; Ichiraku and Stern, 1987; Masuda *et al.*, 1988; Platé *et al.*, 1991). The most permeable member of this family is poly[1-(trimethylsilyl)-1-propyne] (PTMSP), which has the highest permeability for oxygen of the known polymeric materials (Masuda *et al.*, 1983). The high permeability of PTMSP results from the high free volume (Ichiraku and Stern, 1987) that is between 20 and 27% (Platé *et al.*, 1991). The free volume of the polymer is so large that the free volume elements of PTMSP membranes may be connected to form a microporous structure (Auvil *et al.*, 1991; Srinivasan *et al.*, 1994; Pinnau and Toy, 1996). The dominating transport mechanism is surface diffusion (Auvil *et al.*, 1991), which differs from the conventional solution–diffusion mechanism. Condensable components preferably adsorb on the surface of the pores and diffuse through the membrane along the pore wall. At the same time the adsorbed molecules block the pore from the diffusion of less condensable components that migrate through the membrane by bulk or by Knudsen diffusion. This mechanism makes the PTMSP membrane hydrocarbon selective for a mixture of hydrocarbons and non-condensables. Unfortunately, the permeability of PTMSP deteriorates with time due to aging (Langsam and Robeson, 1989; Yampol'skii *et al.*, 1993; Nakagawa *et al.*, 1994); however, PTMSP remains in the group of the most permeable polymeric materials even in the aged form (Yampol'skii *et al.*, 1993). Contrary to above observations, Pinnau *et al.* (1997) discovered in their 47-day-long experiment that the permeability of the PTMSP membrane was quite stable when the membrane was continuously exposed to *n*-butane vapor.

Although the number of suitable polymeric materials is large for vapor membrane separation, a common choice for the selective layer is poly(dimethylsiloxane), PDMS. It is a high permeability polymer and in fact had the highest permeability for oxygen among the known polymeric materials until PTMSP was synthesized. PDMS has low oxygen to nitrogen selectivity, about 2, but it allows hydrocarbons to permeate 10 to 100 times faster than nitrogen (Behling *et al.*, 1989; Wijmans and Helm, 1989). PDMS is hydrophobic and it has a low glass transition temperature, about –123°C.

2.2 MEMBRANE MODULES

Flat sheet hydrocarbon selective membranes for vapor separation are packed in spiral-wound modules (Wijmans and Helm, 1989; Katoh *et al.*, 1989) and in plate-and-frame modules (Behling *et al.*, 1989; Ohlrogge *et al.*, 1993). Membrane Technology and Research, Inc.

manufactures spiral-wound modules under the trade name VaporSep®. Plate-and-frame modules for vapor separation were originally developed by GKSS GmbH but nowadays the manufacturer of these modules is GMT Membrantechnik GmbH. Original equipment manufacturers, such as Aluminium Rheinfelden GmbH and Sterling SAT (SIHI Anlagentechnik), apply the GKSS plate-and-frame modules in the membrane-based vapor recovery units.

2.2.1 Spiral-wound membrane module

Spiral-wound membrane modules consist of multiple flat membrane sheets, feed spacers, and permeate spacers around the central permeate collection pipe. Spiral-wound modules are about 1 meter (40 inch) long and typically 10, 20, or 30 cm (4, 8, or 12 inch) in diameter. According to Baker (1997), a large commercial membrane module may have as many as 30 membrane leaves, each with a membrane area of about 2 m^2. The advance of a multileaf spiral-wound module is the reduced length of the permeate flow path, which effectively minimizes the pressure drop on the permeate side (Baker, 1997).

A spiral-wound membrane module is formed as follows. The membrane sheet is folded over the feed spacer to form a membrane envelope. Then the edges of the membrane and spacer are glued and the leaf end is sealed. The end of a longer permeate spacer sheet is wrapped around a perforated central tube to form a cover to which other membrane leaves and permeate spacers are attached (Figure 2.2). The entirety is then wrapped clockwise to form a spiral-wound assembly. A protective porous cover is wrapped over the surface of the module and antitelescoping devices are attached to the module ends to prevent module telescoping under operation.

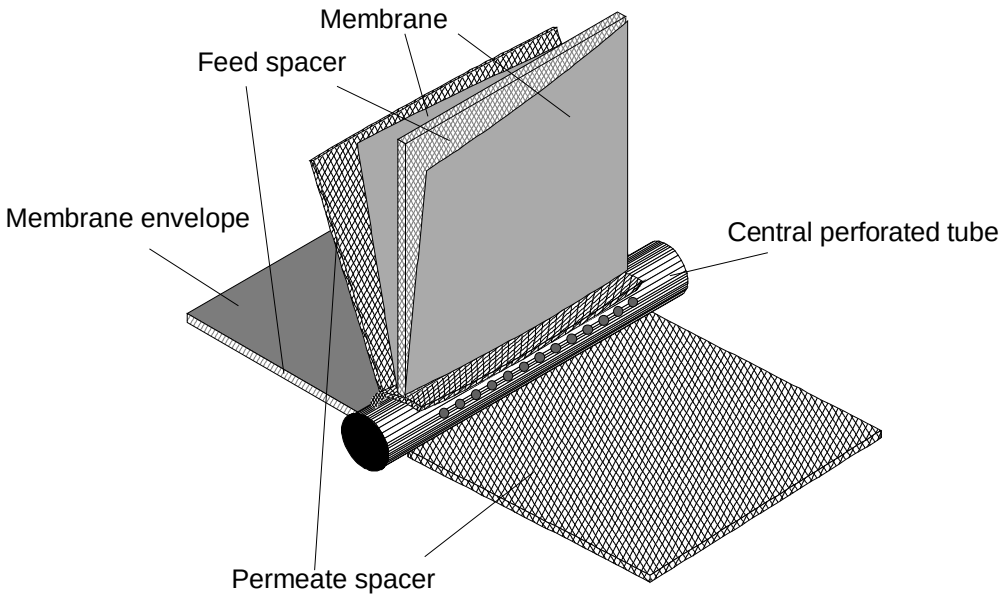

Figure 2.2 Extended spiral-wound membrane module.

A spiral-wound module is shown in Figure 2.3. The feed is introduced axially into the membrane module and further into the membrane leaves. Feed spacers provide the flow paths within the membrane leaves. Part of the feed permeates through the membrane to the low-pressure side so that the residual is depleted from the fastest permeating species. The depleted stream exits almost at feed pressure from the module end as the retentate product. The permeated fraction enters into the low-pressure space between two membrane leaves. In the low-pressure space, the permeated fraction mixes with the bulk permeate and then flows perpendicular to the retentate flow. The permeate spacer provides the spiral flow path within the membrane leaf. At the leaf end, the permeate enters into the central collection tube and exits from the tube end as the low-pressure permeate product.

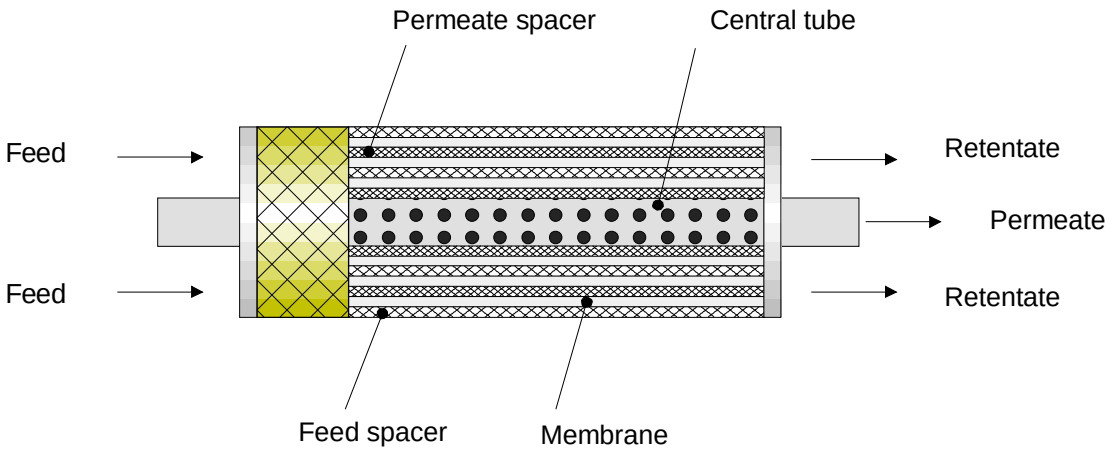

Figure 2.3 Spiral-wound membrane module.

Spiral-wound modules may be installed in parallel and in series to form a membrane separation unit with the desired capacity. The serial modules are connected from the central tubes and may be installed into the same pressure vessel as sketched in Figure 2.4. Then the retentate flow from the previous module forms the mixed feed flow of the next module. This eliminates the flow channeling that may occur in a longer membrane module. Due to the module construction, a membrane replacement in spiral-wound module requires the replacement of the module as a whole.

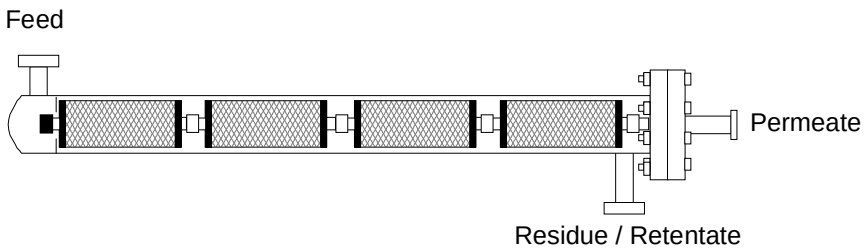

Figure 2.4 Multiple spiral-wound modules connected in series in a pressure vessel.

2.2.2 Plate-and-frame module

Plate-and-frame modules consist of stacked feed spacers and membrane envelopes. The membrane envelopes are formed from the permeate spacer and two round flat sheet membranes sealed at the cutting edges. A desired membrane area per module is constructed from a number of membrane envelopes and feed spacers, which are positioned between the two end plates and along the central permeate tube (Figure 2.5). O-ring gaskets are placed between the membrane envelopes that seal the feed side from the permeate side. A membrane stack is tighten with adapter sleeves and tension nuts while the central tube acts as a tension rod.

The feed is introduced into the module via the upper plate. The baffles inside the module guide the flow path over the stacked membrane envelopes. Part of the feed permeates through the membrane into the membrane envelope and flows radially towards the perforated central tube. The permeate spacer within the membrane envelope provides the flow path for the permeated fraction. The residue becomes depleted from the fastest permeating species and finally exits from the module via the lower plate as the retentate product stream. The permeate is withdrawn from the central tube end or from the both ends of the central tube (Behling *et al.*, 1989).

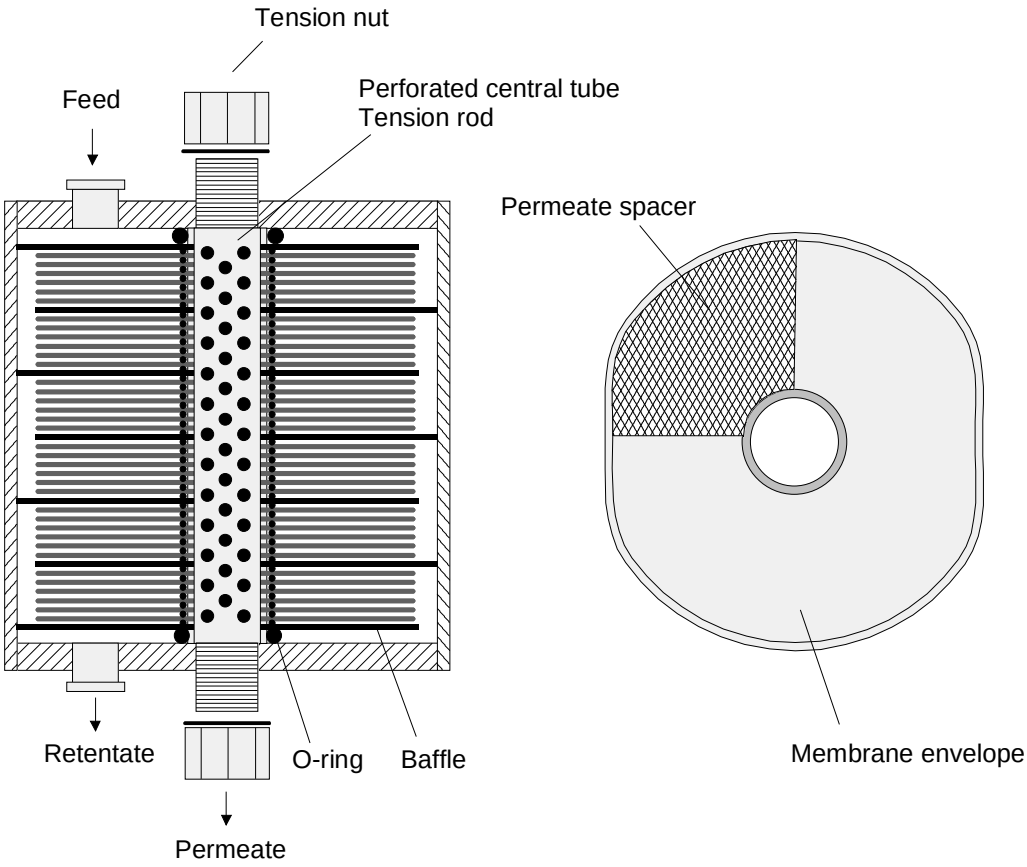

Figure 2.5 Plate-and-frame module and membrane envelope. Feed spacers between the membrane envelopes are omitted for clarity. Adapted from Behling *et al.* (1989) and Ohlrogge *et al.* (1993).

Plate-and-frame modules provide excellent flow patterns for the flows and low permeate side pressure drop (Behling *et al.*, 1989). The membrane stacks may be constructed so that the flow velocity on the high-pressure side remains constant over the membrane module, which may be beneficial to reduce the effect of the concentration polarization. Due to the module construction, the replacement of individual membrane envelopes is possible in a plate-and-frame module.

2.3 PENETRANT TRANSPORT IN AMORPHOUS POLYMERS

Modern polymeric membranes are made from amorphous polymers, which are free from polymer crystallites. Amorphous polymers are classified in two groups based on the glass transition temperature, namely rubbers and glasses (Figure 2.6). Gas or vapor separation with a rubbery membrane is based on the solubility differences in the membrane material. Rubbery membranes sorb more hydrocarbons than permanent gases, like nitrogen, and therefore they are generally utilized in hydrocarbon vapor separation (Baker *et al.*, 1998). Gas separation

with a glassy membrane is based on the diffusion rate differences so that a small molecule generally has a higher diffusion rate through the membrane than a large molecule.

The transport properties of rubbery and glassy polymers are reviewed in short in the following paragraphs. Although rubbers are the preferred choice in vapor membrane separation, glasses are included in the following discussion to enlighten the different transport characteristics of glassy polymers and to give the insight of physical limits of the modeling approach adopted in this work.

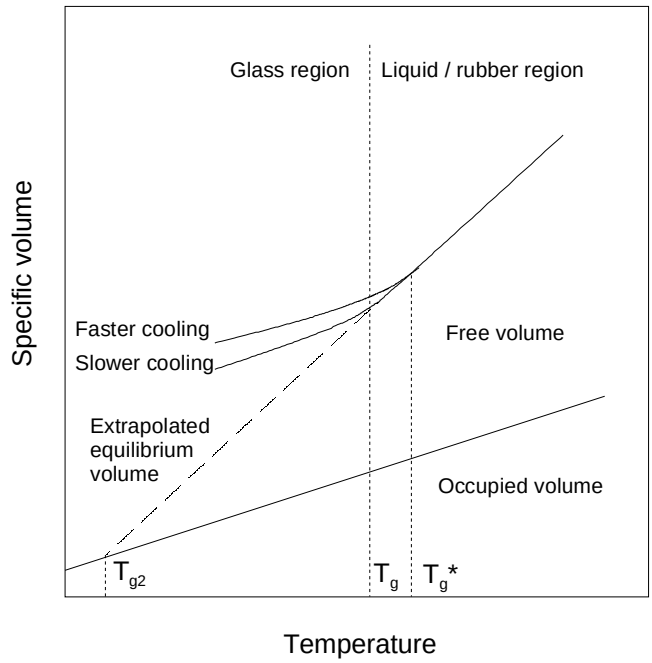

Figure 2.6 Sketch of the volume–temperature behavior of an amorphous polymer. T_g and T_g^* represent the observed glass transition temperatures on slower and faster cooling respectively. Adapted from Matsuoka (1981).

2.3.1 Rubbery polymers

At a low pressure the gas or vapor sorption isotherm in a rubbery or melt polymer is linear with respect to pressure. Then the isotherm follows Henry's law

$$C_1 = k_{D,1} p_1, \tag{2.1}$$

where C_1 is the concentration of the gas or solvent in the polymer, usually in units cm^3 gas (STP)/cm^3 polymer, and p_1 is the partial pressure of the gas. The Henry solubility coefficient k_D is defined as

$$k_{D,1} = \lim_{p_1 \to 0} \frac{C_1}{p_1}. \tag{2.2}$$

The sorption isotherm may deviate from a linear form at moderate or high pressures with components of high solubility (Figure 2.7). Then the isotherm may be described with the Flory-Huggins theory

$$\ln\left(\frac{p_1}{p_1^s}\right) = \ln\phi_1 + (1-\phi_1) + \chi_{12}(1-\phi_1)^2 , \tag{2.3}$$

where p_1^s is the saturation pressure of the solvent, ϕ_1 is the volume fraction of the solvent in the polymer phase, and χ_{12} is the Flory–Huggins interaction parameter between solvent and polymer. Alternatively, fugacities may be used instead of pressure.

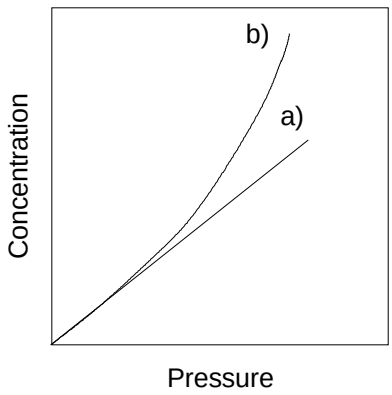

Figure 2.7 Sketches of the gas solubility isotherms for rubbery polymers: a) linear isotherm at low pressure, b) convex isotherm at moderate to high pressure.

Mathematical expressions for molecular diffusion in rubbery or melt polymers base on empirical and phenomenological free volume theories. Although the concept of free volume is an artificial quantity, it is usually invoked for the characterization of the physical behavior of polymers. The free volume is defined as the volume between the observable volume and the occupied volume (Figure 2.6). The occupied volume is not a measurable quantity; it has generally been associated with the van der Waals volume, volume of the liquid at zero temperature, or randomly close packed volume (Bondi, 1968, p. 256).

The concept of free volume was originally introduced in the theory of liquid viscosity by Doolittle (1951) and in the theory of liquid diffusivity by Cohen and Turnbull (1959). Cohen and Turnbull (1959) presumed that the total volume in liquid could be divided into the occupied volume and the free volume. The former is assumed to be inaccessible for diffusing molecules, whereas the latter is available for molecular transport. Cohen and Turnbull's (1959) idealized liquid consists of hard sphere molecules that exist in cavities formed by the nearest neighbors. The molecule is able to vibrate within its cage but migration is possible

only when a hole of sufficient size is formed due to natural thermal fluctuations. The migration results in a successful diffusive step if another molecule occupies the former position. An individual hole may not be large enough to accommodate a diffusing molecule, but the co-operative motion of several neighboring molecules may form a hole of sufficient size.

In polymeric material, the co-operative motion involves of several chain segments (Fujita *et al.*, 1960). This is described by the theory of Pace and Datyner (1979), where polymer chains are bending like flexible rods, with a number of backbone bonds undergoing small rotations. The molecule may move through the polymeric matrix in two ways: along the axis of a channel formed by the adjacent parallel chains or perpendicular to this axis when two polymer chains are separating sufficiently to permit the passage of the molecule. The movement along the axis of a channel is halted whenever the molecule encounters a crosslinking, a crystalline, or a sufficiently large chain entanglement at either end of its confining channel. After this the molecule may continue the permeation process through the membrane only by jumping into an adjoining channel. Pace and Datyner (1979) claimed that the first process occurs at least three orders of magnitude faster than macroscopically observed diffusion rates. This means that a molecule will move backward and forward in its confining channel many times before jumping into an adjacent channel. Molecular dynamic simulations have confirmed diffusion process of this kind for small molecules in amorphous polymers (Sok *et al.*, 1992; Müller-Plathe, 1992).

Two widely cited free volume models for polymers are those of Fujita *et al.* (1960) and Vrentas and Duda (1977a and b). Fujita *et al.* (1960) applied the Doolittle (1951) viscosity relation to describe the temperature and concentration dependence of the penetrant diffusion in a polymer. Their equation was given in the form

$$\frac{D_{T,1}}{RT} = A_d \exp\left(-\frac{B_d}{\phi_{FV}}\right), \tag{2.4}$$

where $D_{T,1}$ is the thermodynamically corrected diffusion coefficient of the penetrant, R is the universal gas constant, A_d and B_d are constants depending on the geometry of the penetrant, and ϕ_{FV} is the fraction of total free volume at the system temperature, pressure, and composition. The parameters A_d and B_d have to be determined from the experimental diffusivity data.

Vrentas and Duda (1977a) outlined that the total free volume cannot be available for the molecular diffusion. In their model, the free volume is comprised of the interstitial free volume, which has large energy for redistribution, and of the hole free volume, which can redistribute with no energy increase. They stated that the latter is the only free volume available for molecular transport. This is in accordance with Matsuoka's (1981) statement that the occupied volume is considerably greater than the crystalline volume and is comprised of a molecular volume with a significant amount of vacancies associated with them.

Vrentas and Duda (1977a) stated that the solvent diffusion in the polymer matrix resembles the Brownian motion in a homogenous medium. Thus, the solvent diffusion may be classified as self-diffusion, which may be described with the following equation

$$D_1 = D_{01} \exp\left(-\frac{E}{RT}\right) \exp\left(\frac{-\gamma\left(w_1 \hat{V}_1^* + w_2 \xi \hat{V}_2^*\right)}{\hat{V}_{FH}}\right), \tag{2.5}$$

where D_1 is the self-diffusion coefficient of the solvent, D_{01} is the pre-exponential factor, w is the weight fraction, E is the activation energy required for a jumping unit to overcome the attractive forces of the neighbor molecules, $\hat{V}_1^*$ and $\hat{V}_2^*$ are the specific hole free volumes for a solvent and polymer molecule required to jump into a new position, factor γ accounts for the overlap between the free volume elements, $\hat{V}_{FH}$ is the average specific hole free volume of the polymeric liquid mixture, and ξ is

$$\xi = \frac{\hat{V}_1^* M_{1j}}{\hat{V}_2^* M_{2j}}, \tag{2.6}$$

where M_{1j} and M_{2j} are the molecular weights of the jumping units of the solvent and polymer respectively. Vrentas and Duda (1977a) deduced that the jumping unit for the pure simple liquid is the entire molecule but for a long chain molecule, a small part of each chain. The parameters of equation (2.5) are determined from the experimental binary diffusivity data and from the Williams–Landel–Ferry (WLF) constants for a polymer as described by Vrentas and Duda (1977b) and Zielinski and Duda (1992). The WLF parameters are already available from Ferry (1980) or may be determined from the experimental temperature–viscosity data. The theory of Vrentas and Duda (1977a and b) is completely reviewed by Duda and Zielinski (1996).

2.3.2 Glassy polymers

Rubbery chain segments are able to move rapidly in a coordinated fashion, which may be seen on the rate change of a specific volume isobar with respect to temperature in Figure 2.6. The motion of individual polymer chains becomes constrained as amorphous rubbers or melts are cooled through the glass transition. The glass transition of an amorphous polymer is not a fixed temperature but a temperature region. McKenna (1989) classifies the glass transition as a kinetic phenomenon with underlying second order thermodynamic transition because of the Gibbs energy and its first partial derivatives are continuous at the glass transition, whereas the second partial derivatives with respect to temperature and pressure — heat capacity, compressibility, and thermal expansion coefficient — are discontinuous at the glass transition.

At the glassy state, polymer chain segments are rigid and movements are merely vibrations and short-range rotations (Sperling, 1992, p.310). Glassy polymers pose non-equilibrium features that may be explained with the concept of free volume. The non-equilibrium features of glassy polymers arise from the excess free volume, which is sketched in Figure 2.6 as the volume between the observed specific volume and the extrapolated equilibrium volume. The excess free volume is captured within the polymeric matrix on cooling through the glass transition (Kovacs, 1958). The faster the cooling rate, the greater the amount of the excess free volume and the observed specific volume. However, no change of specific volume is observed in the rubber or melt region when the amorphous sample is reheated through the glass transition region. Like all non-equilibrium systems, glasses tend to relax towards the equilibrium. However, the relaxation process is slow so that infinite time is required for a glass to relax to the (hypothetical) equilibrium volume.

The sorption isotherm in glassy polymers is generally non-linear and concave to the pressure axis (Figure 2.8a). The sorption isotherm may also behave as in Figure 2.8b, when the penetrant concentration exceeds the level of the solvent induced glass transition (Chiou *et al.*, 1985; Chiou and Paul, 1986). After this inflection point, the sorption isotherm responses to the increase of pressure like rubber.

There are many mathematical expressions for the gas sorption in glassy polymers as can be noted from the review of Barbari and Conforti (1994). However, the dual-mode sorption model is widely used and accepted as a viable model to represent the measured sorption isotherms of non-plasticizing gases in glassy polymers. The sorption isotherms of plasticizing

gases in glassy polymers may be described by the concentration–temperature superposition model of Mi *et al.* (1991).

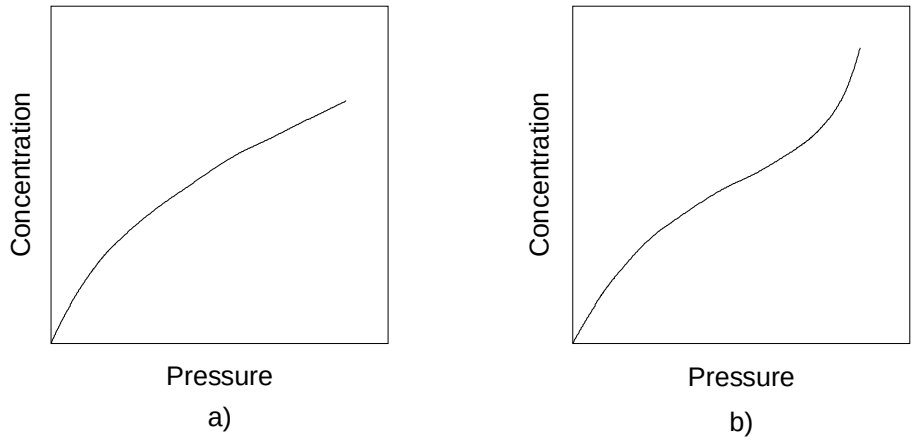

Figure 2.8 Sketches of sorption isotherms for glassy polymers: a) normal isotherm, b) isotherm for plasticizing gas.

The dual-mode sorption model is a phenomenological model, which combines two different sorption phenomena: Henry's law sorption of the amorphous polymer regions and the Langmuir sorption of the microvoids or defects frozen in the polymer matrix at glass transition. The two distinct sorption populations are assumed to be in local equilibrium. The concentration of the gas in the polymer is given by equation

$$C_1 = C_{D,1} + C_{H,1} = k_{D,1} p_1 + \frac{C'_{H,1} b_1 p_1}{1 + b_1 p_1}, \tag{2.7}$$

where C_D is the Henry's type solubility concentration, C_H is the Langmuir type solubility concentration, C'_H is the hole saturation constant, and b is the hole affinity constant. The three model parameters are determined from the measured sorption isotherm. According to Koros *et al*. (1981), the hole saturation constant characterizes the total sorption capacity of the Langmuir sites for a given penetrant and the hole affinity constant characterizes the tendency of a given penetrant to sorb in the Langmuir sites. Equation (2.7) may also be written in terms of fugacities instead of pressure.

Diffusion in glassy polymers does not generally obey Fickian diffusion (Park, 1968; Neogi, 1996) i.e. the fractional mass intake in a sorption experiment is not proportional to the square root of time. Phenomenological gas diffusion models have been developed based on the dual-mode sorption model (Vieth and Sladek, 1965; Paul and Koros, 1976). Vieth and Sladek

(1965) assumed the total immobilization of the Langmuir population and related the diffusion flux to the population sorbed by amorphous polymer regions. Paul and Koros (1976) assumed the partial immobilization of the Langmuir population and described the diffusion flux as a sum of two parallel but separate processes. As a consequence, the model resulted in two diffusion coefficients for a penetrant diffusion in a glassy polymer.

2.4 THE SOLUTION–DIFFUSION MODEL

The solution–diffusion model (Wijmans and Baker, 1995) is widely used to describe permeant transport in dense rubbery and glassy membranes. According to this model, the permeation process occurs in three steps. Penetrants first sorb — or in the terms of usual interpretation dissolve — in the membrane at the interface of the upstream side, then diffuse through the membrane, and finally desorb at the interface of the downstream side. The pressure in the membrane is constant and equal to the pressure on the upstream side. Thus, a step change in the pressure occurs at the interface of the downstream side.

In mass transport theories, component flux N_i is composed of the diffusion flux J_i relative to the mixture and the bulk flux with the mixture (Bird *et al.*, 1960, p. 502)

$$N_i = J_i + x_i N_t \,, \tag{2.8}$$

where x_i is the mole fraction of species *i*. The bulk flux contribution is generally neglected in the modeling of membrane separation processes. In the solution–diffusion model this means that the sorption level has to be so low that x_i approaches zero. Further, when the chemical potential gradient in the membrane is expressed only in terms of the concentration gradient, the transport equations may be written in the form

$$J_i = \frac{p}{RT}\frac{D_i}{\delta_m}\left(x_{im,I} - x_{im,II}\right), \tag{2.9}$$

where J_i is the molar diffusion flux of species *i*, *p* is pressure, *R* is the universal gas constant, *T* is temperature, D_i is the Fick's diffusion coefficient of species *i*, δ_m is the thickness of the selective layer of the membrane, $x_{im,I}$ and $x_{im,II}$ are the mole fractions of species *i* in the membrane at interfaces *I* and *II* (Figure 2.9).

The mole fraction of the gas in the membrane may be described in terms of the partial pressure of the gas

$$x_{im} = S_i p_i , \tag{2.10}$$

where S_i is the solubility coefficient. The same solubility coefficient may be applied both at the high-pressure and low-pressure membrane interface when the Henry's law equation (2.2) applies. Then equation (2.9) may be written in terms of the partial pressures

$$J_i = \frac{1}{RT}\frac{D_i S_i}{\delta_m}\left(p_{iL} - p_{iV}\right) \tag{2.11}$$

and further

$$J_i = \frac{1}{RT}\frac{P_i}{\delta_m}\left(p_{iL} - p_{iV}\right), \tag{2.12}$$

where P_i is the permeability coefficient for component i

$$P_i = D_i S_i . \tag{2.13}$$

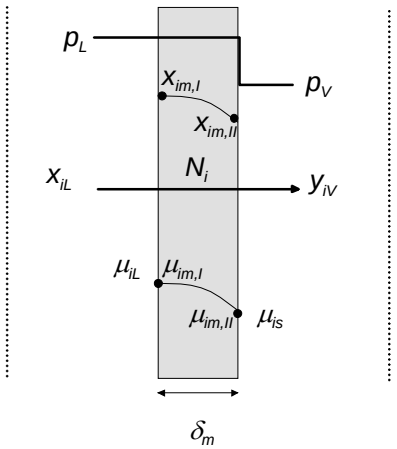

Figure 2.9 Schematic picture of permeation through the dense membrane.

Equation (2.12) is more familiar in terms of the volume flux, J_i^V :

$$J_i^V = \frac{P_i}{\delta_m}\left(p_{iL} - p_{iV}\right). \tag{2.14}$$

As equation (2.13) indicates, the permeability coefficient is composed of the diffusivity (kinetic) term and the solubility (thermodynamic) term. The diffusion and solubility coefficients in a polymer solution are generally concentration dependent. Then, in principle, equation (2.14) should be written as

$$J_i^V = \frac{\overline{P_i}}{\delta_m}\left(p_{iL} - p_{iV}\right), \tag{2.15}$$

where $\overline{P_i}$ is the mean permeability coefficient of component i. The temperature dependence of the permeability coefficient may be described by the Arrhenius type relation

$$\overline{P}_i = P_i^0 \exp\left(-\frac{E_{P,i}}{RT}\right), \tag{2.16}$$

where P_i^0 is the pre-exponential factor and $E_{P,i}$ is the activation energy for permeation. The pressure dependence of the pure component permeability at a constant temperature may be described by relation (Stern *et al.*, 1972)

$$\overline{P}_i = P_i(0)\exp(m\Delta p_i), \tag{2.17}$$

where $P_i(0)$ is the hypothetical permeability coefficient at zero pressure difference over the membrane and m is the slope of the change of $\ln(\overline{P}_i)$ with respect to the pressure difference over the membrane, Δp_i.

Equation (2.15) may be used to obtain the pure component permeability coefficients from the permeability experiments when the membrane sample area and thickness are known. Equations (2.16) and (2.17) may be used to correlate the temperature and pressure dependence of the experimental permeability coefficients when the experiments are performed at various temperatures and pressures. The pure component permeability coefficients may also be used in multicomponent systems when the diffusion within the membrane is assumed to take place at the infinite dilution region and the effect of other components on the sorption equilibrium and on the diffusion process within the membrane is neglected.

3 BASIC MODEL EQUATIONS

Membrane separation process usually consist of multiple membrane modules connected in series and in parallel. Parallel modules may be assumed to operate similarly when the feed is divided equally among the parallel membrane modules and membrane modules are of the same size and type. Then the permeation and the fluid flow have to be modeled only in the serial membrane modules. The division may be taken even further: when all leaves in a membrane module operate similarly, a membrane leaf and a central tube describe an entire spiral-wound module.

The description of a multicomponent non-isothermal fluid flow in a membrane leaf requires the equations of continuity, motion, and energy. In this chapter, these basic equations are derived from the general transport equations (Bird *et al.*, 1960; Deen, 1998) and are then discretized in chapter 4 by the control-volume approach of Patankar (1980). The derivation of the basic model equations for a flow scheme in Figure 3.1 are made by using the following definitions and assumptions:

- The module operates at a steady state and no chemical reactions take place.
- The feed is uniformly distributed along the feed side of a membrane leaf.
- Within the membrane leaf and between the membrane leaves, fluids flow in channels formed by parallel plates with wall spacing of 2B, filled with a permeable medium (spacer).
- Retentate flow within the membrane leaf occurs in z direction, permeate flow between the membrane leaves in x direction, local permeation through the membrane in y direction, and permeate flow in a central tube in z direction.
- The flow is in a laminar region and fluids are described as incompressible Newtonian fluids.
- The gravitational force is the only external force acting on the species in a mixture and is considered negligible.
- Edge effects and entrance effects are ignored.
- Axial and transverse mixing are ignored.

The description of the gas flow as an incompressible Newtonian fluid is erroneous in a thermodynamic sense but the effect of the pressure on density is negligible over the control volume elements applied in this work. Also the assumption of laminar flow in the retentate

channel and in the central tube may not be valid in the real operation. However, the model equations may first be developed for the laminar flow and then be extended to the turbulent flow by changing the velocity, pressure, density, and temperature with the corresponding time-averaged values and fluctuations around the time-averaged values (Bird *et al.*, 1960, pp. 158-159, 377-378).

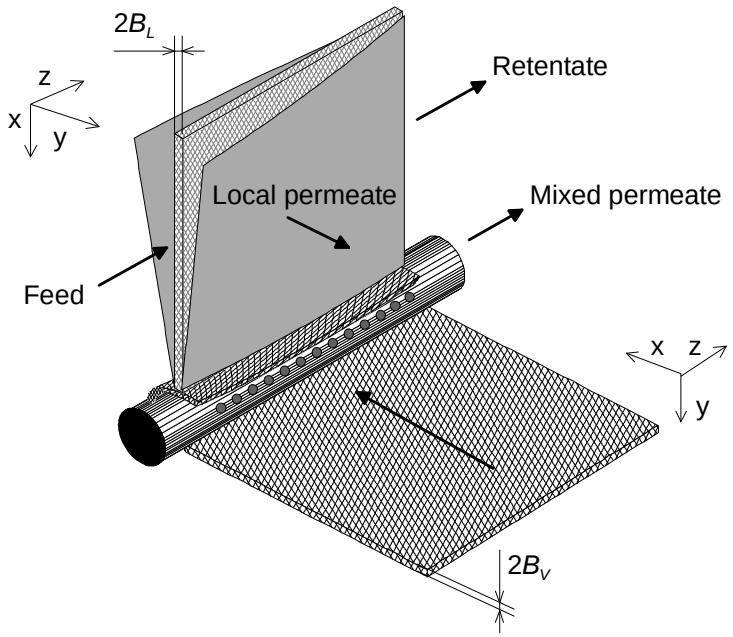

Figure 3.1 Flow scheme in an extended membrane leaf and in a permeate spacer.

3.1 EQUATIONS OF CONTINUITY

The equation of continuity represents the conservation of mass. In multicomponent systems the equation of continuity may be written for each species in the fluid as

$$\frac{\partial \rho_i}{\partial t} + \nabla \cdot \left(\rho_i \mathbf{v}_i \right) = r_i, \quad i = 1, 2, \ldots, nc, \tag{3.1}$$

where ρ_i is the mass density of species *i*, $\mathbf{v}_i$ is the velocity vector of component *i*, *nc* is the number of components, and r_i is the net rate of production of species *i* per unit volume by the chemical reaction. The equation of continuity for the mixture is obtained when all *nc* equations (3.1) are summed up. As a result, the equations of the continuity for the retentate, permeate, and local permeate within the membrane are written as

$$\frac{\partial \rho_L}{\partial t} + \nabla \cdot (\rho_L \mathbf{v}) = 0, \tag{3.2}$$

$$\frac{\partial \rho_V}{\partial t} + \nabla \cdot (\rho_V \mathbf{u}) = 0, \text{ and} \tag{3.3}$$

$$\frac{\partial \rho_M}{\partial t} + \nabla \cdot (\rho_M \mathbf{w}) = 0. \tag{3.4}$$

In equations (3.2), (3.3), and (3.4) ρ is the fluid density, **v** is the retentate velocity vector, **u** is the permeate velocity vector, and **w** is the local permeate velocity vector within the membrane. Subscripts *L*, *V*, and *M* denote the retentate, permeate, and membrane fluid property respectively.

The fluid flow in the spiral-wound module is two-dimensional since we have decided to ignore the transverse mixing so that $v_x = u_z = 0$. Then equations (3.2) and (3.3) are written for the steady fluid flow as

$$\frac{\partial}{\partial y}(\rho_L v_y) + \frac{\partial}{\partial z}(\rho_L v_z) = 0 \text{ and} \tag{3.5}$$

$$\frac{\partial}{\partial x}(\rho_V u_x) + \frac{\partial}{\partial y}(\rho_V u_y) = 0. \tag{3.6}$$

The fluid flow within the membrane is one-dimensional, so that equation (3.4) becomes

$$\frac{\partial}{\partial y}(\rho_M w_y) = 0. \tag{3.7}$$

The bulk permeate from the membrane leaves is assumed to be evenly distributed to the periphery of the central tube so that $u_\theta = 0$ and there is no angular dependence. Then the permeate flow in a central tube is two-dimensional in cylindrical co-ordinates and equation (3.3) becomes

$$\frac{1}{r}\frac{\partial}{\partial r}(\rho_V r u_r) + \frac{\partial}{\partial z}(\rho_V u_z) = 0. \tag{3.8}$$

3.2 EQUATIONS OF MOTION

The equation of motion represents the conservation of momentum in terms of density, viscosity and flow velocity. The equation of motion is presented in the form of the Navier–Stokes equation for a system of constant density and viscosity

$$\rho \frac{D\mathbf{v}}{Dt} = -\nabla p + \mu \nabla^2 \mathbf{v} + \rho \mathbf{g}, \tag{3.9}$$

where μ is the viscosity of the fluid, and **g** is the gravitational acceleration vector. The operator D/Dt is the substantial time derivative,

$$\frac{D}{Dt} = \frac{\partial}{\partial t} + \mathbf{v} \cdot \nabla , \tag{3.10}$$

the derivative following the fluid motion. Based on equation (3.5), the conservation of the momentum in the retentate flow requires the *z* and *y* components of (3.9):

$$\rho_L \left(v_y \frac{\partial v_z}{\partial y} + v_z \frac{\partial v_z}{\partial z} \right) = -\frac{\partial p_L}{\partial z} + \mu_L \left(\frac{\partial^2 v_z}{\partial y^2} + \frac{\partial^2 v_z}{\partial z^2} \right) \text{ and} \tag{3.11}$$

$$\rho_L \left(v_y \frac{\partial v_y}{\partial y} + v_z \frac{\partial v_y}{\partial z} \right) = -\frac{\partial p_L}{\partial y} + \mu_L \left(\frac{\partial^2 v_y}{\partial y^2} + \frac{\partial^2 v_y}{\partial z^2} \right). \tag{3.12}$$

Similarly, based on equation (3.6), the conservation of the momentum in the permeate flow between the membrane leaves requires the *x* and *y* components of (3.9):

$$\rho_V \left(u_x \frac{\partial u_x}{\partial x} + u_y \frac{\partial u_x}{\partial y} \right) = -\frac{\partial p_V}{\partial x} + \mu_V \left(\frac{\partial^2 u_x}{\partial x^2} + \frac{\partial^2 u_x}{\partial y^2} \right) \text{ and} \tag{3.13}$$

$$\rho_V \left(u_x \frac{\partial u_y}{\partial x} + u_y \frac{\partial u_y}{\partial y} \right) = -\frac{\partial p_V}{\partial y} + \mu_V \left(\frac{\partial^2 u_y}{\partial x^2} + \frac{\partial^2 u_y}{\partial y^2} \right). \tag{3.14}$$

Due to the fluid flow in a narrow channel, the pressure in the *y* direction may safely be assumed constant so that $\partial p_L / \partial y = 0$ and $\partial p_V / \partial y = 0$. Also the velocity change in the main flow direction may be assumed to be much smaller than the velocity change in the *y* direction, because of the no-slip condition at the plate wall, so that $\partial^2 v_z / \partial z^2 << \partial^2 v_z / \partial y^2$ and $\partial^2 u_x / \partial x^2 << \partial^2 u_x / \partial y^2$.

The classical lubrication approximation (Deen, 1998, pp. 270-275) may be introduced when the inertial terms of the main flow direction are negligible. According to Deen (1998, p. 274), the requirement is fulfilled in membrane separation when the Reynolds number based on the *y* component velocity at the channel wall is much smaller than one. Then $\rho_L v_z \partial v_z / \partial z << \mu_L \partial^2 v_z / \partial y^2$ and $\rho_V u_x \partial u_x / \partial x << \mu_V \partial^2 u_x / \partial y^2$, and the Navier-Stokes equations (3.11) and (3.13) are reduced to

$$\frac{\partial^2 v_z}{\partial z^2} = \frac{1}{\mu_L} \frac{dp_L}{dz} \text{ and} \tag{3.15}$$

$$\frac{\partial^2 u_x}{\partial x^2} = \frac{1}{\mu_V} \frac{dp_V}{dx} . \tag{3.16}$$

As a result, the main flow direction is the only significant velocity component for the conservation of momentum in a parallel plate channel.

Equations (3.15) and (3.16) are valid for a fluid flow in an empty channel. However, the channels in spiral-wound modules are filled with spacers and each spacer type has its own characteristic resistance for the fluid flow. The above derivation is presented in order to show that the flow in a membrane leaf is adequately described as one-dimensional, for which empirical equations may be applied. One such equation is the Darcy law with empirical spacer permeability, β. Then the velocities of the retentate flow and the permeate flow are given by the following equations:

$$v_z = -\frac{\beta_L}{\mu_L}\frac{dp_L}{dz} \text{ and} \tag{3.17}$$

$$u_x = -\frac{\beta_V}{\mu_V}\frac{dp_V}{dx}. \tag{3.18}$$

Alternatively, we may apply the empirical Fanning friction factors. Then the velocities of the laminar retentate and the laminar permeate flow in parallel plate channels are given by

$$v_z = -\sqrt{\frac{2}{\rho_L}\frac{B_L}{f_L}\frac{dp_L}{dz}} \text{ and} \tag{3.19}$$

$$u_x = -\sqrt{\frac{2}{\rho_V}\frac{B_V}{f_V}\frac{dp_V}{dx}}, \tag{3.20}$$

where f is the Fanning friction factor, B_L is the half distance of the parallel plates in the retentate channel and B_V is the half distance of the parallel plates in the permeate channel. Equations (3.19) and (3.20) are obtained from the analytical solution for the parallel plates. The hydraulic diameter approach (Bird *et al.*, 1960, pp. 188, 401) is used for the turbulent flow in the retentate channel with $2B_L$ as the hydraulic diameter. Then the velocity of the retentate flow is given by

$$v_z = -\sqrt{\frac{1}{\rho_L}\frac{B_L}{f_L}\frac{dp_L}{dz}}. \tag{3.21}$$

One-dimensional empirical equations are not applicable for the central tube due to the fluid flow through the tube wall. The permeate flow in the central tube is essentially two-dimensional and thus the conservation of momentum requires both the r and the z components of (3.9):

$$\rho_V\left(u_r\frac{\partial u_r}{\partial r}+u_z\frac{\partial u_r}{\partial z}\right)=-\frac{\partial p_V}{\partial r}+\mu_V\left(\frac{\partial}{\partial r}\left(\frac{1}{r}\frac{\partial}{\partial r}(ru_r)\right)+\frac{\partial^2 u_r}{\partial z^2}\right) \text{ and} \tag{3.22}$$

$$\rho_V\left(u_r\frac{\partial u_z}{\partial r}+u_z\frac{\partial u_z}{\partial z}\right)=-\frac{\partial p_V}{\partial z}+\mu_V\left(\frac{1}{r}\frac{\partial}{\partial r}\left(r\frac{\partial u_z}{\partial r}\right)+\frac{\partial^2 u_z}{\partial z^2}\right). \tag{3.23}$$

The pressure gradient may be assumed negligible in the radial direction. In the central tube the fluid flow velocity u_z is zero at $z = 0$ but increases with z due to the permeate flow through the perforated tube wall. The radial velocity component at the wall is largest at $z = 0$ and then slightly decreases with z due to the decrease in the local permeation rate. As a consequence, the flow situation is quite complex, extending from the developing laminar to the developing turbulent flow. A fully developed velocity profile will never be attained due to a continuous increase in the mass and the fluid velocity along the axial (main flow) direction. The flow problem resembles the entry region in a tube flow where the viscous effects are less important than in the fully developed region. Then we are allowed to raise the inviscid flow assumption (Deen, 1998, p. 246) to get

$$\rho_V\left(u_r\frac{\partial u_r}{\partial r}+u_z\frac{\partial u_r}{\partial z}\right)=0 \text{ and} \tag{3.24}$$

$$\rho_V\left(u_r\frac{\partial u_z}{\partial r}+u_z\frac{\partial u_z}{\partial z}\right)=-\frac{\partial p_V}{\partial z}. \tag{3.25}$$

3.3 EQUATIONS OF ENERGY

The equation of energy describes the conservation of energy within a volume element. It may be written in terms of the internal and kinetic energy

$$\rho\frac{D}{Dt}\left(\hat{U}+\frac{1}{2}v^2\right)=-\nabla\cdot\mathbf{q}-p(\nabla\cdot\mathbf{v})+\boldsymbol{\tau}:\nabla\mathbf{v}+\sum_{i=1}^{nc}\mathbf{j}_i\cdot\mathbf{g}_i\,, \tag{3.26}$$

where $\hat{U}$ is the specific internal energy, $\mathbf{q}$ is the heat flux vector, $\boldsymbol{\tau}$ is the stress tensor, $\mathbf{j}_i$ is the diffusive flux vector of species i, and $\mathbf{g}_i$ is the external body force per unit mass of species i. The term $\frac{1}{2}v^2$ represents the kinetic energy associated with the observable fluid motion (Bird *et al.*, 1960, p. 311). The term $p(\nabla\cdot\mathbf{v})$ represents the rate of the reversible conversion of mechanical energy to thermal energy and may be positive or negative for a real fluid. The term $\boldsymbol{\tau}:\nabla\mathbf{v}$ is known as the viscous dissipation and it represents the rate of irreversible conversion of mechanical energy to thermal energy, which is always positive for Newtonian fluids (Bird *et al.*, 1960, p. 82). The sign convention of the stress tensor components adopted above describes the force per unit area on the surface exerted by the fluid to the outward

normal direction. This convention follows that of Deen (1998, p. 6) and that used in CFD literature, e.g. Tannehill *et al.* (1997, p. 252) and Ferziger and Perić (1997, p. 5).

The viscous dissipation is clearly unimportant in membrane separation and thus the term $\boldsymbol{\tau} : \nabla \mathbf{v}$ may be dropped. The term $\sum_i \mathbf{j}_i \cdot \mathbf{g}_i$ becomes zero since the gravitational force is the only external force. Then equation (3.26) becomes

$$\rho \frac{D}{Dt}\left(\hat{U} + \frac{1}{2} v^2 \right) = -\nabla \cdot \mathbf{q} - p(\nabla \cdot \mathbf{v}). \tag{3.27}$$

Equation (3.27) is more convenient in terms of the specific enthalpy $\hat{H}$

$$\rho \frac{D}{Dt}\left(\hat{H} + \frac{1}{2} v^2 \right) = -\nabla \cdot \mathbf{q} + \frac{Dp}{Dt}, \tag{3.28}$$

which reduces to the form

$$\rho \mathbf{v} \cdot \nabla \left(\hat{H} + \frac{1}{2} v^2 \right) = -\nabla \cdot \mathbf{q} + \mathbf{v} \cdot \nabla p \tag{3.29}$$

at a steady state. The kinetic energy term and the term $\mathbf{v} \cdot \nabla p$ are negligible for the fluid flow within the membrane leaf and between the membrane leaves when compared to the energy flux. Then equation (3.29) is written as

$$\rho_L \left(v_y \frac{\partial \hat{H}_L}{\partial y} + v_z \frac{\partial \hat{H}_L}{\partial z} \right) = -\left(\frac{\partial q_{L,x}}{\partial x} + \frac{\partial q_{L,y}}{\partial y} + \frac{\partial q_{L,z}}{\partial z} \right) \tag{3.30}$$

for the retentate flow within the membrane leaf and

$$\rho_V \left(u_x \frac{\partial \hat{H}_V}{\partial x} + u_y \frac{\partial \hat{H}_V}{\partial y} \right) = -\left(\frac{\partial q_{V,x}}{\partial x} + \frac{\partial q_{V,y}}{\partial y} + \frac{\partial q_{V,z}}{\partial z} \right) \tag{3.31}$$

for the permeate flow between the membrane leaves. The permeated fraction within the membrane will be exposed to a large pressure gradient due to a pressure difference over the membrane. Then the term $\mathbf{v} \cdot \nabla p$ serves as a heat source in the equation of energy and the heat flux through the membrane is no longer independent of *y*. Thus, the equation of energy for the local permeate within the membrane is

$$\frac{\partial}{\partial y}\left(\rho_M w_y \hat{H}_M \right) = -\frac{\partial q_{M,y}}{\partial y} + w_y \frac{\partial p_M}{\partial y}. \tag{3.32}$$

In a central tube, the kinetic energy term plays an important role since the velocity at the tube end at $z = 0$ is zero, but increases along the flow towards the open tube end due to the permeate flow through the tube wall. The term $\mathbf{v} \cdot \nabla p$ is again negligible and so equation (3.29) for the permeate flow in the central tube becomes

$$\rho_V\left[u_r\frac{\partial}{\partial r}\left(\hat{H}_V+\frac{1}{2}u_r^2\right)+u_z\frac{\partial}{\partial z}\left(\hat{H}_V+\frac{1}{2}u_z^2\right)\right]=-\left(\frac{1}{r}\frac{\partial}{\partial r}\left(rq_{V,r}\right)+\frac{\partial q_{V,z}}{\partial z}\right). \tag{3.33}$$

Equations (3.30), (3.31), (3.32), and (3.33) may also be written in terms of molar densities, *c*, and partial molar enthalpies, $\overline{H}_i$. Then the equations of energy for the retentate flow within the membrane leaf, the permeate flow between the membrane leaves, the local permeate flow within the membrane, and the permeate flow in the central tube yield the following expressions

$$\begin{aligned}&v_y\frac{\partial}{\partial y}\left(\sum_{i=1}^{nc}c_{iL}\overline{H}_{iL}\right)+v_z\frac{\partial}{\partial z}\left(\sum_{i=1}^{nc}c_{iL}\overline{H}_{iL}\right)\\&=-\left(\frac{\partial q_{L,x}}{\partial x}+\frac{\partial q_{L,y}}{\partial y}+\frac{\partial q_{L,z}}{\partial z}\right)+\sum_{i=1}^{nc}\overline{H}_{iL}\frac{\partial J_i}{\partial y},\end{aligned} \tag{3.34}$$

$$\begin{aligned}&u_x\frac{\partial}{\partial x}\left(\sum_{i=1}^{nc}c_{iV}\overline{H}_{iV}\right)+u_y\frac{\partial}{\partial y}\left(\sum_{i=1}^{nc}c_{iV}\overline{H}_{iV}\right)\\&=-\left(\frac{\partial q_{V,x}}{\partial x}+\frac{\partial q_{V,y}}{\partial y}+\frac{\partial q_{V,z}}{\partial z}\right)+\sum_{i=1}^{nc}\overline{H}_{iV}\frac{\partial J_i}{\partial y},\end{aligned} \tag{3.35}$$

$$\frac{\partial}{\partial y}\left(w_y\sum_{i=1}^{nc}c_{iM}\overline{H}_{iM}\right)=-\frac{\partial q_{M,y}}{\partial y}+w_y\frac{\partial p_M}{\partial y}+\sum_{i=1}^{nc}\overline{H}_{iM}\frac{\partial J_i}{\partial y}, \text{ and} \tag{3.36}$$

$$\begin{aligned}&u_r\frac{\partial}{\partial r}\left(\sum_{i=1}^{nc}c_{iV}\overline{H}_{iV}+\frac{1}{2}\frac{c_V}{M_V}u_r^2\right)\\&+u_z\frac{\partial}{\partial z}\left(\sum_{i=1}^{nc}c_{iV}\overline{H}_{iV}+\frac{1}{2}\frac{c_V}{M_V}u_z^2\right)=-\left(\frac{1}{r}\frac{\partial}{\partial r}\left(rq_{V,r}\right)+\frac{\partial q_{V,z}}{\partial z}\right).\end{aligned} \tag{3.37}$$

The equations (3.34), (3.35), (3.36), and (3.37) provide the equations of energy in the preferred form.

4 DISCRETIZATION OF BASIC MODEL EQUATIONS

The differential equations derived in chapter 3 are integrated over the extended membrane leaf (Figure 4.1) at discrete grid points. The solution for the entire leaf is computed in conjunction with the following known boundary conditions:

$$x_i F_L\big|_{z=0} = z_i F_F, \quad i = 1, 2, \ldots, nc, \tag{4.1}$$

$$T_L\big|_{z=0} = T_F, \tag{4.2}$$

$$p_L\big|_{z=0} = p_F, \text{ and} \tag{4.3}$$

$$y_i F_V\big|_{x=0} = 0, \quad i = 1, 2, \ldots, nc. \tag{4.4}$$

In the above boundary condition equations, F_F is the feed molar flow rate, F_L is the retentate molar flow rate, F_V is the permeate molar flow rate, T_F is the feed temperature, T_L is the local retentate temperature, p_F is the feed pressure, p_L is the local retentate pressure, z_i is the mole fraction of component i in the feed, x_i is the mole fraction of component i in the retentate, and y_i is the mole fraction of component i in the permeate. The boundary conditions are fully determined only at the feed side boundary: the permeate temperature, pressure, and composition at the closed leaf end ($x = 0$) are unknown. Thus the balance equations on the permeate side represent a boundary value problem. The boundary value problem of the equation of motion may be converted into the initial value problem by defining the permeate pressure at the permeate outlet as a predetermined (fixed) variable

$$p_V\big|_{x=1, z=1} = p_V, \tag{4.5}$$

where p_V is the permeate pressure.

In the control volume approach (Patankar, 1980), a membrane leaf is divided into non-overlapping control volumes. The main grid points are located at the geometric center of each control volume and staggered grid points at the control volume boundaries. The main grid points contain the discrete flow properties, such as density, pressure, temperature, composition, and in the case of membrane separation, the local permeate fluxes of each species in a mixture. The staggered grid points contain the velocity components, which are supposed to govern the whole boundary. The grid density does not have to be the same in the retentate and permeate flow directions and so a grid mesh of m times n may be formed.

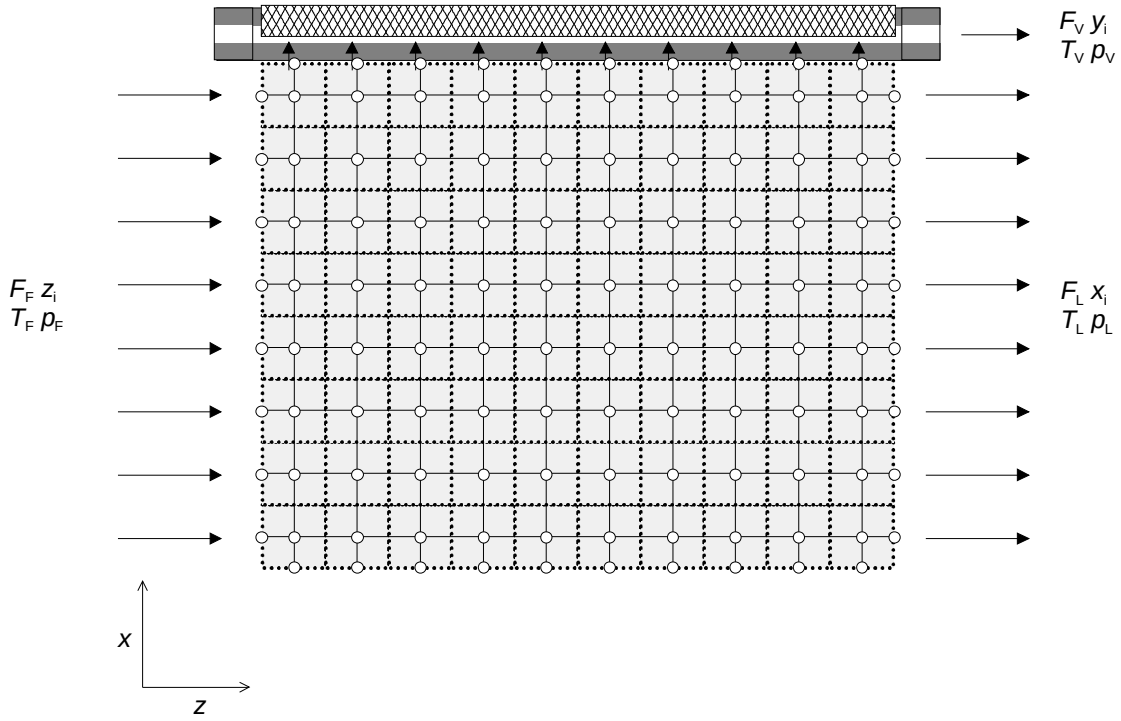

Figure 4.1 Extended membrane leaf with control volumes and main grid points. Grid lines in the permeate flow direction are extended over the central tube to form cylindrical control volumes for the central tube flow.

The grid point formulation for the half of the retentate channel is shown in Figure 4.2. A point *P* is bounded by a west side face *w*, east side face *e*, the flow channel centerline and the membrane. A west neighbor point *W* is located at a distance $(\delta z)_w$ upstream and an east neighbor point *E* at a distance $(\delta z)_e$ downstream. A top neighbor point *T* is located at a distance B_L upwards and a bottom neighbor point *B* at a distance B_L / 2 downwards. The top neighbor point *T* is a symmetry point for *P* and thus the top control volume boundary is a symmetry plane where the temperature gradient is zero. The bottom neighbor point *B* is a boundary point at the membrane–fluid interface within a zero-size control volume.

The grid point formulation for one half of the permeate channel is shown in Figure 4.3. The description for the grid formulation in the permeate channel is similar to the retentate channel with the exception of the bulk flow from south (*S*) to north (*N*) and reversed symmetry and membrane boundary points.

The grid point formulation for the permeate flow in a central tube is shown in Figure 4.4. The system is represented in cylindrical co-ordinates with the bulk flow from west (*W*) to east (*E*) and the permeate flow from the periphery into the tube.

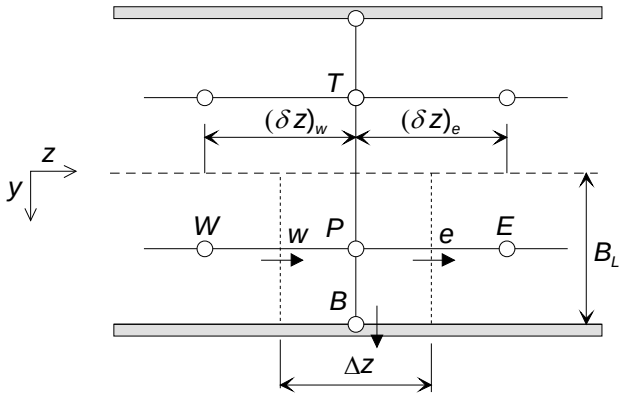

Figure 4.2 Grid point formulation in the retentate flow channel for the bulk flow in the *z* direction and for the local permeate flow through the membrane out of the control volume. The length of the third dimension is *Δx*. A south point *S* is located towards and a north point *N* away from the viewer.

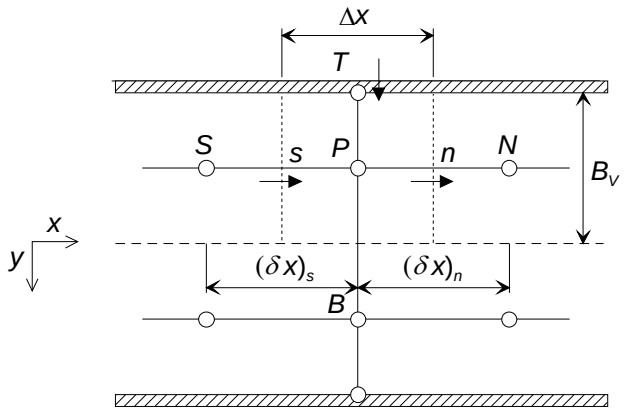

Figure 4.3 Grid point formulation in the permeate flow channel for the bulk flow in the *x* direction and for the local permeate flow through the membrane into the control volume. The length of the third dimension is *Δz*. An east point *E* is located towards and a west point *W* away from the viewer.

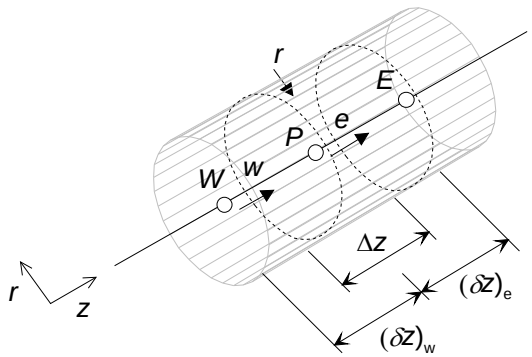

Figure 4.4 Grid point formulation in the central tube for the bulk flow in the *z* direction and for the local permeate flow through the tube wall into the control volume. All dimensions in the *z* direction are equal to the grid point formulation in the retentate flow channel.

The discrete balance equations are formed for each central point *P* to obtain approximations to the integral conservation equations. The flow properties between the main grid points are evaluated by using an interpolation formula or a profile assumption. The staggered grid arrangement guarantees that the velocities at adjacent staggered grid points describe the continuity equation and the pressures at adjacent main grid points determine the pressure gradient for the fluid flow. The resulting solution to the discretized equations then satisfies the integral conservation of mass, momentum, and energy over any group of control volumes and for any number of grid points (Patankar, 1980, pp. 30-31). A specialized discretization form is required when both bulk flow and diffusion terms are included in the balance equations; otherwise, macroscopic balance equations are obtained for a control volume. It should be noted that the current control volume formulation is not able to fulfill the condition of zero velocity at the solid surfaces and hence velocities have to be seen as average velocities.

4.1 EXTENDED MEMBRANE LEAF

In the modeling of the membrane leaf, the conservation of mass is taken care of through the species balances. It is assumed that convection dominates along the direction of the bulk flow — the *z* direction in the retentate channel and the *x* direction in the permeate channel — so that the mass diffusion fluxes of the mixture components may be ignored and all species have equal velocity. Another non-vanishing velocity component of the equation of continuity is the velocity of the finite wall flux. This velocity is different and unique for each species due to the selective permeation through the membrane. As a consequence, less readily permeating species are rejected at the membrane interface so that concentration gradients are formed. The rejected species then diffuse back to the bulk fluid as described by the mass balance equations given in paragraph 4.1.1. The conservation of momentum is taken care of through the momentum balances in paragraph 4.1.2. These balance equations provide the required pressure drop for the given velocity field, which is computed from the molar flow rates, molar volumes, and specified cross-sectional area for the flow. The conservation of energy is then taken care of through the enthalpy balances in paragraph 4.1.3.

4.1.1 Mass balance

The integration of equation (3.5) for each species *i* over the retentate side control volume in Figure 4.2 results in the following species balance equations

$$\left(\rho_{iL} v_z\right)_e B_{L,e} - \left(\rho_{iL} v_z\right)_w B_{L,w} + \left(\rho_{iL} v_y + j_{iL,y}\right)_b \Delta z = 0, \quad i = 1, 2, \ldots, nc, \tag{4.6}$$

where B_L is half of the retentate channel height, j_i is the mass diffusion flux, and subscript *e* denotes properties at control volume interface *e*, subscript *w* properties at the control volume interface *w*, and *b* the properties at control volume interface *b*. Similarly, the species balances over the permeate side control volume in Figure 4.3 are given by

$$\left(\rho_{iV} u_x\right)_n B_{V,n} - \left(\rho_{iV} u_x\right)_s B_{V,s} - \left(\rho_{iV} u_y + j_{iV,y}\right)_t \Delta x = 0, \quad i = 1, 2, \ldots, nc, \tag{4.7}$$

where B_V is half of the permeate channel height and subscript *t* denotes properties at the control volume interface *t*. At the closed leaf end, $u_x = 0$ and so equations (4.7) is reduced to

$$\left(\rho_{iV} u_x\right)_n B_{V,n} - \left(\rho_{iV} u_y + j_{iV,y}\right)_t \Delta x = 0, \quad i = 1, 2, \ldots, nc. \tag{4.8}$$

The local permeate flux of species *i*, n_i, is constant within the membrane although the bulk flux and the species diffusion fluxes vary along the flow. Then the species balances within the membrane are described by equation

$$\left(\rho_{iM} w_y + j_{iM,y}\right)_b - \left(\rho_{iM} w_y + j_{iM,y}\right)_t = 0, \quad i = 1, 2, \ldots, nc. \tag{4.9}$$

The species balances must also hold at the fluid membrane interfaces. Then the species balances of the retentate and permeate sides are interlinked with equations

$$n_i = \left(\rho_{iL} v_y + j_{iL,y}\right)_b = \left(\rho_{iV} u_y + j_{iV,y}\right)_t, \quad i = 1, 2, \ldots, nc. \tag{4.10}$$

The species balance equations in terms of molar fluxes are written similarly, but the mass density is replaced by the molar density, *c*, so that (4.6), (4.7), (4.8), and (4.9) become

$$\left(c_{iL} v_z\right)_e B_{L,e} - \left(c_{iL} v_z\right)_w B_{L,w} + \left(c_{iL} v_y + J_{iL,y}\right)_b \Delta z = 0, \quad i = 1, 2, \ldots, nc, \tag{4.11}$$

for the retentate flow,

$$\left(c_{iV} u_x\right)_n B_{V,n} - \left(c_{iV} u_x\right)_s B_{V,s} - \left(c_{iV} u_y + J_{iV,y}\right)_t \Delta x = 0, \quad i = 1, 2, \ldots, nc, \tag{4.12}$$

for the permeate flow,

$$\left(c_{iV} u_x\right)_n B_{V,n} - \left(c_{iV} u_y + J_{iV,y}\right)_t \Delta x = 0, \quad i = 1, 2, \ldots, nc, \tag{4.13}$$

for the permeate flow at the closed leaf end, and

$$\left(c_{iM} w_y + J_{iM,y}\right)_b - \left(c_{iM} w_y + J_{iM,y}\right)_t = 0, \quad i = 1, 2, \ldots, nc, \tag{4.14}$$

for the local permeate flow within the membrane.

Molar flow rates, *F*, through the control volume faces are obtained when the fluxes are multiplied by Δz or Δx to obtain the corresponding cross-section areas

$$F_{iL,e} = \left(c_{iL} v_z\right)_e B_{L,e} \Delta x, \quad i = 1, 2, \ldots, nc, \tag{4.15}$$

$$F_{iL,w} = \left(c_{iL} v_z\right)_w B_{L,w} \Delta x, \quad i = 1, 2, \ldots, nc, \tag{4.16}$$

$$F_{iV,n} = \left(c_{iV} u_x\right)_n B_{V,n} \Delta z, \quad i = 1, 2, \ldots, nc, \text{ and} \tag{4.17}$$

$$F_{iV,s} = \left(c_{iV} u_x\right)_s B_{V,s} \Delta z, \quad i = 1, 2, \ldots, nc . \tag{4.18}$$

Then the species balance equations may respectively be written as

$$F_{iL,e} - F_{iL,w} + N_{i,b} A_{L,b} = 0, \quad i = 1, 2, \ldots, nc , \tag{4.19}$$

$$F_{iV,n} - F_{iV,s} - N_{i,t} A_{V,t} = 0, \quad i = 1, 2, \ldots, nc , \tag{4.20}$$

$$F_{iV,n} - N_{i,t} A_{V,t} = 0, \quad i = 1, 2, \ldots, nc , \text{ and} \tag{4.21}$$

$$N_{i,b} - N_{i,t} = 0, \quad i = 1, 2, \ldots, nc , \tag{4.22}$$

where

$$A_{L,b} = A_{L,t} = \Delta z \Delta x . \tag{4.23}$$

Total balance equations are obtained when the corresponding species balance equations are summed up. As a result:

$$F_{L,e} - F_{L,w} + \left(\sum_{i=1}^{nc} N_i \right)_b A_{L,b} = 0 , \tag{4.24}$$

$$F_{V,n} - F_{V,s} - \left(\sum_{i=1}^{nc} N_i \right)_t A_{V,t} = 0 , \tag{4.25}$$

$$F_{V,n} - \left(\sum_{i=1}^{nc} N_i \right)_t A_{V,t} = 0 , \text{ and} \tag{4.26}$$

$$\left(\sum_{i=1}^{nc} N_i \right)_b - \left(\sum_{i=1}^{nc} N_i \right)_t = 0 . \tag{4.27}$$

In the above forms, the mass and molar densities, as well the local permeate fluxes N_i through the membrane, are the properties of the central point *P*, whereas the velocities are the properties of the corresponding staggered grid points. Any suitable model may be applied to represent the values of the local permeate fluxes N_i in terms of the membrane transport properties and local fluid properties.

4.1.2 Momentum balance

The integration of the equation of motion is performed over each control volumes around the staggered grid points that are located at the main control volume interfaces, e.g. at *w* and *e* in Figure 4.2, and at *s* and *n* in Figure 4.3.

We have two choices to represent the equation of motion for the fluid flow in a spacer filled channel: the Darcy law, equations (3.17) and (3.18), and the friction factor approach, equations (3.19), (3.20), and (3.21). Both approaches are one-dimensional and they cannot

fulfill the condition of zero velocity on solid surfaces. However, they provide the pressure gradient required for the fluid flow in a porous media in terms of the fluid properties, the geometry of the medium, and the fluid velocity.

The pressure difference between adjacent grid points is obtained by integrating the equation of motion (3.17), (3.19), or (3.21) for the retentate flow and equations (3.18) or (3.20) for the permeate flow over the corresponding staggered grid point. The Darcy law equations result in the following equations for the retentate and permeate flows:

$$p_{L,W} - p_{L,P} = \frac{(\mu_L v_z)_w (\delta z)_w}{\beta_L}, \text{ and} \tag{4.28}$$

$$p_{V,S} - p_{V,P} = \frac{(\mu_V u_x)_s (\delta x)_s}{\beta_V}. \tag{4.29}$$

The friction factor approach results in the following form for the laminar retentate flow

$$p_{L,W} - p_{L,P} = \frac{1}{2}\left(\rho_L v_z^2\right)_w \frac{f_L (\delta z)_w}{B_L} \tag{4.30}$$

and for the turbulent retentate flow

$$p_{L,W} - p_{L,P} = \left(\rho_L v_z^2\right)_w \frac{f_L (\delta z)_w}{B_L}. \tag{4.31}$$

The friction factor f_L has to be determined from an appropriate equation based on the flow conditions. Correspondingly, the friction factor approach for the laminar permeate flow results in

$$p_{V,S} - p_{V,P} = \frac{1}{2}\left(\rho_V u_x^2\right)_s \frac{f_V (\delta x)_s}{B_V}. \tag{4.32}$$

The friction factor is proportional to the inverse of the Reynolds number for the laminar flow

$$f \,\mathrm{Re} = C_f, \tag{4.33}$$

where C_f is a constant characterizing the pressure drop for the steady fluid flow and Re is the Reynolds number

$$\mathrm{Re} = \frac{2B\rho v}{\mu} \tag{4.34}$$

for a flow in a parallel plate channel. The analytical solution of the Navier-Stokes equation yields $C_f = 12$ for parallel plates. In the case of a spacer-filled channel, the constant C_f has to be determined experimentally.

Although not specially indicated, velocity, pressure, and density in equation (4.31) are the corresponding time-averaged values. In the turbulent region for relatively smooth tubes, the proportionality of the Fanning friction factor is no longer linear to the inverse of the Reynolds number but

$$f\,\mathrm{Re}^{n} = C_f\,. \tag{4.35}$$

In the other extreme for relatively coarse tubes, the friction factor becomes independent of the Reynolds number. With n = 0.25 and C_f = 0.0791, equation (4.35) becomes the famous Blasius equation that is valid in the range of 2100< Re <10^5. In the case of a spacer-filled channel, constants n and C_f should be determined experimentally. However, the pressure drop plays a less important role in the high-pressure retentate channel since the amount of flowing fluid decreases along the flow due to permeation. Thereby, the bulk fluid velocity and the required pressure gradient decrease along the flow.

4.1.3 Energy balance

The integration of the equation of energy is performed over the control volumes surrounding the main grid points. The equation of energy for the retentate may be reduced to a two-dimensional equation when the transverse heat conduction is ignored. This is allowed since negligible temperature gradients are expected in the transverse direction. Then equation (3.34) for the retentate flow may be written as

$$\frac{\partial e_{L,y}}{\partial y} + \frac{\partial e_{L,z}}{\partial z} = 0\,, \tag{4.36}$$

where $e_{L,y}$ and $e_{L,z}$ are the multicomponent energy fluxes over the control volume faces:

$$e_{L,y} = \left(\sum_{i=1}^{nc} N_{iL,y}\overline{H}_{iL}\right) - h_L\left(T_{L,B} - T_{L,P}\right) \text{ and} \tag{4.37}$$

$$e_{L,z} = \left(\sum_{i=1}^{nc} N_{iL,z}\overline{H}_{iL}\right) - k_L\,\frac{\partial T_L}{\partial z}\,, \tag{4.38}$$

and where N_i is the molar flux of component i

$$N_i = c_i v + J_i\,. \tag{4.39}$$

The heat transfer coefficient h_L is introduced in equation (4.37) for the interfacial heat transfer on the retentate side.

The energy equation for the permeate is three-dimensional. Equation (3.35) may be written in terms of multicomponent energy fluxes as

$$\frac{\partial e_{V,x}}{\partial x} + \frac{\partial e_{V,y}}{\partial y} + \frac{\partial e_{V,z}}{\partial z} = 0\,, \tag{4.40}$$

where

$$e_{V,x} = \left(\sum_{i=1}^{nc} N_{iV,x} \overline{H}_{iV} \right) - k_V \frac{\partial T_V}{\partial x}\,, \tag{4.41}$$

$$e_{V,y} = \left(\sum_{i=1}^{nc} N_{iV,y} \overline{H}_{iV} \right) - h_V \left(T_{V,P} - T_{V,T} \right), \text{ and} \tag{4.42}$$

$$e_{V,z} = -k_V \frac{\partial T_V}{\partial z}\,. \tag{4.43}$$

The heat transfer coefficient h_V is introduced in equation (4.42) for the interfacial heat transfer on the permeate side. The integration of equations (4.36) and (4.40) over the corresponding control volumes and the multiplying of the resulting equations by Δz or Δx to obtain the corresponding cross-section areas give

$$e_{L,e} A_{L,e} - e_{L,w} A_{L,w} + e_{L,b} A_{L,b} = 0 \text{ and} \tag{4.44}$$

$$e_{V,n} A_{V,n} - e_{V,s} A_{V,s} + e_{V,e} A_{V,e} - e_{V,w} A_{V,w} - e_{V,t} A_{V,t} = 0\,. \tag{4.45}$$

The heat transfer coefficients h_L and h_V are given by the Nusselt number, which is defined for the parallel plates as

$$\mathrm{Nu} = \frac{h 2B}{k}\,. \tag{4.46}$$

The Nusselt number is constant for a laminar flow and depends only on the boundary conditions. The two limiting cases for the heat transfer through the solid wall are the constant wall temperature and the constant wall heat flux. For a laminar flow in parallel plates, the corresponding limiting values are 7.541 and 8.235 respectively (Shah and London, 1978).

The Nusselt number for a turbulent flow is obtained from a tube flow correlation with the hydraulic diameter approach (Bird *et al.*, 1960, pp. 188, 401). Gnielinski (1976) has proposed the following equation for the developing turbulent and developed turbulent flow in the region of $2300 < \mathrm{Re} < 10^6$

$$\mathrm{Nu}_{L,P} = \frac{f_{L,P}/2 \left(\mathrm{Re}_{L,P} - 1000 \right) \mathrm{Pr}_{L,P}}{1 + 12.7 \sqrt{f_{L,P}/2} \left(\mathrm{Pr}_{L,P}^{2/3} - 1 \right)} \left(1 + \frac{2B_L}{\Delta z} \right)^{2/3} \left(\frac{\mu_{L,P}}{\mu_{L,B}} \right)^{0.4}\,, \tag{4.47}$$

where Pr is the Prandtl number and $f_{L,P}$ is the friction factor for a hydraulically smooth channel, which in this work is obtained from the Blasius equation, from (4.35) with $n = 0.25$ and $C_f = 0.0791$. The Prandtl number is defined as

$$\mathrm{Pr}_{L,P} = \frac{\hat{C}_{pL,P}\mu_{L,P}}{k_{L,P}}, \tag{4.48}$$

where $\hat{C}_p$ is the specific heat capacity at constant pressure.

The energy equations of the retentate and permeate flows are coupled by the energy flux through the membrane. The equation of energy within the membrane, equation (3.36), may be written as

$$\frac{\partial e_{M,y}}{\partial y} = \overline{V}_M \left(\sum_{i=1}^{nc} N_{iM,y} \right) \frac{\partial p_M}{\partial y}, \tag{4.49}$$

where $\overline{V}_M$ is the total molar volume of the flowing fluid within the membrane and $e_{M,y}$ is the multicomponent energy flux within the membrane

$$e_{M,y} = \left(\sum_{i=1}^{nc} N_{iM,y} \overline{H}_{iM} \right) - k_M \frac{\partial T_M}{\partial y}. \tag{4.50}$$

The heat convection and the conduction are not constant through the membrane due to the source term on the right hand side of equation (4.49). The source term becomes non-zero under a pressure gradient and for a finite fluid flow. Pressure within the dense selective layer is essentially constant. The permeating fluid is exposed to a pressure gradient at the selective and support layer interfaces and in the porous support and substrate layers. The pressure gradient in the support and substrate layer is, however, essentially small as is the amount of the permeating fluid. Then the source term becomes insignificant at the permeate side interface and the integration of equation (4.49) results in

$$e_{L,b} - e_{V,t} = 0, \tag{4.51}$$

which is the necessary link between equations (4.44) and (4.45). Although the above equation is simple, the evaluation of the boundary fluxes is not since there is a phase change involved. We will deal with this subject later on in this work in conjunction with the mass transfer through the membrane.

The special discretization form has to be derived for the equation of energy since both convection and diffusion terms are included and the evaluation of diffusive energy fluxes requires temperature, or enthalpy, gradients at the control volume interfaces. By following Patankar (1980, p. 98), the total balance equations (4.24) and (4.25) are multiplied by the enthalpy at the corresponding control volume point *P*. The resulting equation is subtracted

from the corresponding energy balance equations (4.44) and (4.45) to yield the following equations:

$$\left(e_{L,e}A_{L,e} - F_{L,e}\overline{H}_{L,P}\right) - \left(e_{L,w}A_{L,w} - F_{L,w}\overline{H}_{L,P}\right) + \left[e_{L,b}A_{L,b} - \left(\sum_{i=1}^{nc} N_i\right)_b A_{L,b}\overline{H}_{L,P}\right] = 0 \text{ and} \tag{4.52}$$

$$\left(e_{V,n}A_{V,n} - F_{V,n}\overline{H}_{V,P}\right) - \left(e_{V,s}A_{V,s} - F_{V,s}\overline{H}_{V,P}\right) + e_{V,e}A_{V,e} - e_{V,w}A_{V,w} - \left[e_{V,t}A_{V,t} - \left(\sum_{i=1}^{nc} N_i\right)_t A_{V,t}\overline{H}_{V,P}\right] = 0. \tag{4.53}$$

The terms in the above equations may be expressed by the discrete total molar enthalpies as

$$a_{L,E}\left(\overline{H}_{L,P} - \overline{H}_{L,E}\right) = e_{L,e}A_{L,e} - F_{L,e}\overline{H}_{L,P}, \tag{4.54}$$

$$a_{L,W}\left(\overline{H}_{L,W} - \overline{H}_{L,P}\right) = e_{L,w}A_{L,w} - F_{L,w}\overline{H}_{L,P}, \tag{4.55}$$

$$a_{L,B}\left(\overline{H}_{L,P} - \overline{H}_{L,B}\right) = e_{L,b}A_{L,b} - \left(\sum_{i=1}^{nc} N_i\right)_b A_{L,b}\overline{H}_{L,P}, \tag{4.56}$$

$$a_{V,N}\left(\overline{H}_{V,P} - \overline{H}_{V,N}\right) = e_{V,n}A_{V,n} - F_{V,n}\overline{H}_{V,P}, \tag{4.57}$$

$$a_{V,S}\left(\overline{H}_{V,S} - \overline{H}_{V,P}\right) = e_{V,s}A_{V,s} - F_{V,s}\overline{H}_{V,P}, \tag{4.58}$$

$$a_{V,E}\left(\overline{H}_{V,P} - \overline{H}_{V,E}\right) = e_{V,e}A_{V,e}, \tag{4.59}$$

$$a_{V,W}\left(\overline{H}_{V,W} - \overline{H}_{V,P}\right) = e_{V,w}A_{V,w}, \text{ and} \tag{4.60}$$

$$a_{V,T}\left(\overline{H}_{V,T} - \overline{H}_{V,P}\right) = e_{V,t}A_{V,t} - \left(\sum_{i=1}^{nc} N_i\right)_t A_{V,t}\overline{H}_{V,P}. \tag{4.61}$$

The substitution of equations (4.54)-(4.61) into equations (4.52) and (4.53) results in the following discrete equations:

$$\left(a_{L,E} + a_{L,W} + a_{L,B}\right)\overline{H}_{L,P} = a_{L,E}\overline{H}_{L,E} + a_{L,W}\overline{H}_{L,W} + a_{L,B}\overline{H}_{L,B}, \text{ and} \tag{4.62}$$

$$\left(a_{V,N} + a_{V,S} + a_{V,E} + a_{V,W} + a_{V,T}\right)\overline{H}_{V,P} = a_{V,N}\overline{H}_{V,N} + a_{V,S}\overline{H}_{V,S} + a_{V,E}\overline{H}_{V,E} + a_{V,W}\overline{H}_{V,W} + a_{V,T}\overline{H}_{V,T}, \tag{4.63}$$

where multipliers a are given by

$$a_{L,E} = \left(\frac{k_L}{C_{pL}}\right)_e \frac{A_{L,e}}{(\delta z)_e} A\left(\left|\mathrm{Pe}_{L,e}\right|\right), \tag{4.64}$$

$$a_{L,W} = \left(\frac{k_L}{C_{pL}}\right)_w \frac{A_{L,w}}{(\delta z)_w} A\left(\left|\mathrm{Pe}_{L,w}\right|\right) + F_{L,w}, \tag{4.65}$$

$$a_{L,B} = \left(\frac{h_L}{C_{pL}}\right)_b A_{L,b} A\left(\left|\mathrm{Pe}_{L,b}\right|\right), \tag{4.66}$$

$$a_{V,N} = \left(\frac{k_V}{C_{pV}}\right)_n \frac{A_{V,n}}{(\delta x)_n} A\left(\left|\mathrm{Pe}_{V,n}\right|\right), \tag{4.67}$$

$$a_{V,S} = \left(\frac{k_V}{C_{pV}}\right)_s \frac{A_{V,s}}{(\delta x)_s} A\left(\left|\mathrm{Pe}_{V,s}\right|\right) + F_{V,s}, \tag{4.68}$$

$$a_{V,E} = \left(\frac{k_V}{C_{pV}}\right)_e \frac{A_{V,e}}{(\delta z)_e}, \tag{4.69}$$

$$a_{V,W} = \left(\frac{k_V}{C_{pV}}\right)_w \frac{A_{V,w}}{(\delta z)_w}, \text{ and} \tag{4.70}$$

$$a_{V,T} = \left(\frac{h_V}{C_{pV}}\right)_t A_{V,t} A\left(\left|\mathrm{Pe}_{V,t}\right|\right) + \left(\sum_{i=1}^{nc} N_i\right) A_{V,t}. \tag{4.71}$$

The function $A\left(\left|\mathrm{Pe}\right|\right)$ depends on the selected interpolation scheme for the enthalpy and the enthalpy gradients at the control volume faces. Various interpolation schemes are available (Patankar, 1980, pp. 81-92; Ferziger and Perić, 1997, pp. 72-76); the power-law scheme (Patankar, 1980, pp. 90-92) is applied in this work. Then the function $A\left(\left|\mathrm{Pe}\right|\right)$ is given by equation

$$A\left(\left|\mathrm{Pe}\right|\right) = \max\left[0, \left(1 - 0.1\left|\mathrm{Pe}\right|\right)^5\right], \tag{4.72}$$

where Pe is the Peclét number, which describes the relative strengths of convection and diffusion. The Peclét number is defined as

$$\mathrm{Pe} = \mathrm{RePr} = \frac{\rho v L \hat{C}_p}{k}, \tag{4.73}$$

where L is the characteristic length. Due to the form of equation (4.72), the diffusive terms become zero at $\mathrm{Pe} \geq 10$. Then the conditions at point P are determined only by the conditions at the upstream grid points and the flow is convection dominated.

The assumption of a convection dominated flow may safely be adopted for the retentate flow, so that the coefficient $a_{L,E}$ in equation (4.62) becomes zero and the molar enthalpy at point P is directly computed from

$$\overline{H}_{L,P} = \frac{a_{L,W}\overline{H}_{L,W} - \sum_{i=1}^{nc} N_{i,b}\overline{H}_{iL,b}A_b + h_L A_b\left(T_{L,B} - T_{L,P}\right)}{a_{L,W} + \left(F_{L,e} - F_{L,w}\right)}. \tag{4.74}$$

where h_L is the heat transfer coefficient on the retentate side and coefficient $a_{L,W}$ is given by equation (4.65).

The discretized energy equations (4.63) along the *x* directed grid line may be represented in a matrix form

$$[a](\overline{H}) = (b), \tag{4.75}$$

where $[a]$ is the coefficient matrix, $(\overline{H})$ is the vector of the molar enthalpies at the main grid points, and (b) is the vector. The coefficient matrix $[a]$ is a tridiagonal matrix with fringes. Equations (4.63) are written for the internal main grid points and thus the vector (b) contains the conditions at the leaf boundaries and the contribution of the top grid points. The tridiagonal matrix with fringes is transformed to a tridiagonal matrix when the contribution of the west and the east grid points is introduced into the vector (b). Then equation (4.75) may be written as

$$\begin{bmatrix} a^1_{V,P} & -a^1_{V,N} & & & & & \\ & \ddots & \ddots & \ddots & & & \\ & & -a^k_{V,S} & a^k_{V,P} & -a^k_{V,N} & & \\ & & & \ddots & \ddots & \ddots & \\ & & & & & -a^n_{V,S} & a^n_{V,P} \end{bmatrix} \begin{pmatrix} \overline{H}^1_V \\ \vdots \\ \overline{H}^{k-1}_V \\ \overline{H}^k_V \\ \overline{H}^{k+1}_V \\ \vdots \\ \overline{H}^n_V \end{pmatrix} \tag{4.76}$$

$$= \begin{pmatrix} a^1_{V,W}\overline{H}_{V,W} + a^1_{V,E}\overline{H}_{V,E} + a^1_{V,T}\overline{H}_{V,T} + a^1_{V,S}\overline{H}^1_{V,S} \\ \vdots \\ a^k_{V,W}\overline{H}^k_{V,W} + a^k_{V,E}\overline{H}^k_{V,E} + a^k_{V,T}\overline{H}^k_{V,T} \\ \vdots \\ a^n_{V,W}\overline{H}_{V,W} + a^n_{V,E}\overline{H}_{V,E} + a^n_{V,T}\overline{H}_{V,T} + a^n_{V,N}\overline{H}^n_{V,N} \end{pmatrix},$$

where superscript *k* and *n* denote the *k*th and the last internal grid point index respectively, and $a_{V,P}$ is the sum of the neighbor coefficients

$$a_{V,P} = a_{V,N} + a_{V,S} + a_{V,E} + a_{V,W} + a_{V,T}. \tag{4.77}$$

The system of equations (4.76) is conveniently solved with the non-symmetric tridiagonal matrix algorithm (Engeln-Mullges and Uhling, 1996).

4.2 CENTRAL TUBE

The balance equations for the central tube are formed similarly as in the previous section. It is again assumed that convection dominates along the direction of the bulk flow so that the mass diffusion fluxes of the mixture components may be ignored both for the radial and the axial directions.

The equation of continuity has two non-vanishing velocity components; they are the velocity of the bulk flow to the *z* direction and the velocity of the permeated fluid through the perforated wall. The resulting mass balance equations are given in paragraph 4.2.1, the momentum balance equation in paragraph 4.2.2, and the energy balance equation in paragraph 4.2.3.

4.2.1 Mass balance

The integration of equation (3.8) for each species *i* over the control volume in Figure 4.4 results in the following species balance equations for the central tube control volume

$$\left(\rho_{iV} u_z\right)_e \frac{1}{2} R_{ct}^2 - \left(\rho_{iV} u_z\right)_w \frac{1}{2} R_{ct}^2 - \left(\rho_{iV} u_r\right)_r R_{ct} \Delta z = 0, \quad i = 1, 2, \ldots, nc, \tag{4.78}$$

where R_{ct} is the radius of the central tube. At the closed tube end, at $z = 0$, $u_z = 0$ and the species balance equations become

$$\left(\rho_{iV} u_z\right)_e \frac{1}{2} R_{ct}^2 - \left(\rho_{iV} u_r\right)_r R_{ct} \Delta z = 0, \quad i = 1, 2, \ldots, nc. \tag{4.79}$$

The above equations may be written in terms of molar density as

$$\left(c_{iV} u_z\right)_e \frac{1}{2} R_{ct}^2 - \left(c_{iV} u_z\right)_w \frac{1}{2} R_{ct}^2 - \left(c_{iV} u_r\right)_r R_{ct} \Delta z = 0, \quad i = 1, 2, \ldots, nc \text{ and} \tag{4.80}$$

$$\left(c_{iV} u_z\right)_e \frac{1}{2} R_{ct}^2 - \left(c_{iV} u_r\right)_r R_{ct} \Delta z = 0, \quad i = 1, 2, \ldots, nc. \tag{4.81}$$

Equations (4.80) and (4.81) may be written in terms of molar fluxes when the equations are multiplied with 2π to yield the corresponding cross-section areas

$$F_{iV,e} - F_{iV,w} - F_{iV,r} = 0, \quad i = 1, 2, \ldots, nc \text{ and} \tag{4.82}$$

$$F_{iV,e} - F_{iV,r} = 0, \quad i = 1, 2, \ldots, nc. \tag{4.83}$$

The summing up of the species balance equations results in the total balance equations

$$F_{V,e} - F_{V,w} - F_{V,r} = 0 \text{ and} \tag{4.84}$$

$$F_{V,e} - F_{V,r} = 0, \text{ at the closed tube end.} \tag{4.85}$$

4.2.2 Momentum balance

The radial component (3.24) and the axial component (3.25) of the momentum are required for the fluid flow in a central tube. The radial component will rapidly become less important with increasing *z* so that the radial component may reasonably be assumed negligible. The axial component of the momentum is further simplified since $\partial u_z / \partial r = 0$ for the inviscid fluid. Then the integration of (3.25) over the staggered grid point in Figure 4.4 yields for the central tube

$$\left(\rho_V \frac{u_z^2}{2}\right)_e - \left(\rho_V \frac{u_z^2}{2}\right)_w = -\left(p_{V,e} - p_{V,w}\right), \tag{4.86}$$

which may be written in terms of molar flow rates and after reorganization as

$$p_{V,w} - p_{V,e} = \frac{1}{2\pi R_{ct}^2}\left[\left(\frac{F_V u_z}{M_V}\right)_w - \left(\frac{F_V u_z}{M_V}\right)_e\right], \tag{4.87}$$

where M_V is the molecular weight of the permeate mixture. The pressure at the open end of the central tube is fixed by the predetermined permeate product pressure, $p_V\big|_{x=1,z=1}$.

4.2.3 Energy balance

The equation of energy (3.37) contains both the radial and axial components. As in the retentate channel, convection dominated flow may safely be assumed in the central tube so that the conductive terms drop out. The radial component of the kinetic energy is small compared to the enthalpy flow through the perforated wall and may thus be neglected.

The integration of (3.37) over the corresponding control volume results in the following energy balance in the central tube:

$$\begin{aligned} &-\left(u_r \sum_{i=1}^{nc} c_{iV}\overline{H}_{iV}\right)_R 2\pi R_{ct}\Delta z \\ &+\left[u_z\left(\sum_{i=1}^{nc} c_{iV}\overline{H}_{iV} + \frac{1}{2}\frac{c_V u_z^2}{M_V}\right)\right]_e \pi R_{ct}^2 - \left[u_z\left(\sum_{i=1}^{nc} c_{iV}\overline{H}_{iV} + \frac{1}{2}\frac{c_V u_z^2}{M_V}\right)\right]_w \pi R_{ct}^2 = 0\,, \end{aligned} \tag{4.88}$$

which may further be written in terms of molar flow rates as

$$\left(F_V \overline{H}_V\right)_e - \left(F_V \overline{H}_V\right)_w - \left(F_V \overline{H}_V\right)_R + \frac{1}{2}\left(\frac{F_V u_z^2}{M_V}\right)_e - \frac{1}{2}\left(\frac{F_V u_z^2}{M_V}\right)_w = 0\,. \tag{4.89}$$

5 TRANSPORT PROCESSES IN RUBBERY MEMBRANES

The local permeate flux through the membrane has made its appearance as a net flow component throughout the equations in the previous chapter. Until now we have not discussed the evaluation of its magnitude; this will be formulated in this chapter.

Gas and vapor transport through the composite membrane is accompanied with various transport resistances such as the concentration polarization on the feed side boundary layer, the selective layer resistance, the porous support layer resistance, and the porous substrate layer resistance. The concentration polarization results form the selective permeation of components through the membrane as discussed in section 4.1. The usual effect of the concentration polarization is to increase the permeability of the less permeable component and to decrease the permeability of the more permeable component. Thus, the effect of the concentration polarization is to decrease the separation selectivity. This has also been confirmed experimentally in gas permeation by Mendes *et al.* (1996) and Lüdtke *et al.* (1998).

The concentration polarization depends strongly on the component fluxes through the membrane. Hence, the effect of the concentration polarization may be diminished as the thickness of the selective layer is increased. Moreover, as the selective layer thickness is increased, the transport resistances of the support and substrate layers are also diminished due to lower fluid flow rate through the porous layers. According to Baker *et al.* (1998), the effect of the concentration polarization and the resistances of the support and substrate layers are negligible when the pressure-normalized nitrogen flux is on the order of $1 \cdot 10^{-4}$ $cm^3(STP)\ cm^{-2}\ s^{-1}\ cmHg^{-1}$ or lower.

In this work, the selective layer resistance remains the only viable resistance for the vapor and gas transport through the composite membrane. The transport process may be described within the selective layer when the sorption equilibrium at the membrane interface is treated by the classical chemical engineering thermodynamics. The general equilibrium condition in section 5.2 may be utilized to obtain the concentration levels of permeating components in the membrane with a suitable thermodynamic model. Some equation of state models for polymers are presented later in chapter 6. Alternatively, Henry's law coefficients may be applied to express the equilibrium condition especially at low pressures. The derivation of the Henry's law coefficient from the general equilibrium condition is presented in section 5.3.

A well-founded theory is required when the diffusive coupling and the convective contribution are accounted for in vapor membrane separation. The generalized Maxwell–Stefan equations (Taylor and Krishna, 1993; Krishna and Wesselingh, 1997) have been used to describe transport in non-ideal gas and liquid mixtures as well as in electrolyte solutions and solid media. Mason and Viehland (1978) derived equations for the transport through open membranes from the statistical-mechanics. These equations include the generalized diffusion, viscous, and inertial term, and result in the form of the generalized Maxwell–Stefan diffusion equations when the last two terms are neglected. Bitter (1991) applied the generalized Maxwell–Stefan equations for liquid and gas permeation in dense membranes, however, without the bulk flux contribution. Heintz and Stephan (1994a and 1994b) used the generalized Maxwell–Stefan equations for the pervaporation of water–organic mixtures. In their work the diffusion coupling was accounted with an adjustable cross-coefficient.

The generalized Maxwell–Stefan equations are also used in this work to describe the penetrant transport within the membrane with equations derived in section 5.4. The transport equations are conveniently solved with the film theory (Taylor and Krishna, 1993, pp. 152-219). The natural choice for the film thickness is the thickness of the selective layer. In principle, the selective layer thickness is a measurable quantity. However, the thickness is different from the dry membrane thickness due to swelling and has to be estimated as discussed in section 5.5.

The transport equations require the diffusion coefficients that have to be treated as experimental quantities. They are obtained from the measured pure component permeability coefficients at different pressures and temperatures as described in section 5.6. Temperature changes are also involved in vapor membrane separation, which results in a combined heat and mass transfer through the membrane. The boundary balances provide the additional equations that are required to solve the combined heat and mass transfer problem. These balances are presented in section 5.7.

Before entering the above subjects, the molecular weight and molecular weight distribution are discussed in short in section 5.1, since these are relevant and characteristic properties of polymeric materials and have an effect on transport processes to a certain extent.

5.1 MOLECULAR WEIGHT AND MOLECULAR WEIGHT DISTRIBUTION

Polymers are high molecular weight mixtures of chemically similar chains of different lengths. Simple molecules are characterized by a single and definite molecular weight value but different molecular weight averages are needed in the case of polymers. The most common molecular weight averages are the number average molecular weight, $\overline{M}_n$

$$\overline{M}_n = \frac{\sum_i \nu_i M_i}{\sum_i \nu_i} \tag{5.1}$$

and the weight average molecular weight, $\overline{M}_w$

$$\overline{M}_w = \frac{\sum_i \nu_i M_i^2}{\sum_i \nu_i M_i} = \sum_i w_i M_i \ , \tag{5.2}$$

where ν_i is the number of molecules i, M_i is the molecular weight of molecules i, and w_i is the weight fraction of molecules i. The number average molecular weight yields the lowest molecular weight value, whereas the weight average molecular weight gives more weight on heavier units. The ratio of $\overline{M}_w$ to $\overline{M}_n$ is the polydispersity index, which describes the width of the molecular weight distribution. Generally, a high molecular weight and a narrow molecular weight distribution are desirable properties for a polymer due to resulting better physical and mechanical properties.

The molecular weight or chain length distribution of the polymeric membrane may be included in the phase equilibrium calculation either by using pseudocomponents or continuous thermodynamics (Cotterman and Prausnitz, 1985). The former uses discrete components and the latter continuous function to describe the polymer chains of different lengths. The pseudocomponent approach may require a large number of pseudocomponents for a polymer and the continuous thermodynamics requires a distribution function for a pure polymer and for each phase considered. In rubbery membranes the polymer chains are crosslinked to form a polymer network. Therefore, the molecular weight of the membrane material becomes very large and the membrane may be described by a single molecular weight value.

The molecular weight and the molecular weight distribution affect also the transport of penetrants in polymers in low molecular weight region. Tanner (1971) studied solvent diffusion in polymer matrices of different molecular weights and observed that solvent

diffusion coefficient is proportional to that of a polymer, when the polymer has a low molecular weight. At higher molecular weights the diffusion coefficient of the solvent becomes less sensitive and, finally, independent of the molecular weight of the polymer. According to Tanner's (1971) study, the effect of molecular weight and hence the effect of molecular weight distribution on the solvent diffusion in polymers become insignificant when the molecular weight of the polymer is higher than 10 000 g/mole. Since rubbery membranes are post-treated to form high molecular weight polymeric networks, the effect of molecular weight is insignificant also in this context.

5.2 GENERAL EQUILIBRIUM CONDITION

The equilibrium between two phases α and β in contact may be expressed in terms of equality of the component chemical potentials μ_i

$$\mu_i^{\alpha} = \mu_i^{\beta}, \quad i = 1, 2, \ldots, nc, \tag{5.3}$$

or alternatively, in terms of equality of the partial fugacities

$$\bar{f}_i^{\alpha} = \bar{f}_i^{\beta}, \quad i = 1, 2, \ldots, nc \tag{5.4}$$

with the constraints

$$T^{\alpha} = T^{\beta} \text{ and} \tag{5.5}$$

$$p^{\alpha} = p^{\beta}. \tag{5.6}$$

When the fugacity of the vapor phase is obtained from an equation of state, e.g. the virial equation, and the non-ideality of the liquid phase is described by the component activities, equation (5.4) may be written as

$$y_i \varphi_i p = x_i \gamma_i \varphi_i^s p_i^s \exp\left[\frac{\overline{V}_i}{RT}\left(p - p_i^0\right)\right], \quad i = 1, 2, \ldots, nc, \tag{5.7}$$

where y_i is the molar fraction of component *i* in the gas phase, φ_i is the fugacity coefficient of component *i* in the mixture at the system pressure *p*, x_i is the mole fraction of component *i* in the liquid phase, γ_i is the activity coefficient of component *i* in the liquid phase, φ_i^s is the pure component fugacity coefficient at the vapor pressure p_i^s, and $\overline{V}_i$ is the partial molar volume of component *i* in the liquid phase. At low pressures the exponential term in equation (5.7) is near unity and may then be neglected to obtain

$$y_i \varphi_i p = x_i \gamma_i \varphi_i^s p_i^s, \quad i = 1, 2, \ldots, nc. \tag{5.8}$$

When the equation of state is applicable for the both phases, we simply get

$$y_i \varphi_{iV} = x_i \varphi_{iL}, \quad i = 1, 2, \ldots, nc, \tag{5.9}$$

where subscripts *V* and *L* denote the vapor and liquid phases respectively.

5.3 HENRY'S CONSTANT

The equilibrium condition between a solvent and a non-volatile polymer phase from equation (5.3) is

$$\mu_1 = \mu_{12}, \tag{5.10}$$

where μ_1 is the chemical potential of the solvent vapor and μ_{12} is the chemical potential of the solvent in the polymer. The equilibrium condition in terms of the solvent fugacities is obtained from equation (5.4) as

$$f_1 = \bar{f}_{12}, \tag{5.11}$$

where f_1 is the fugacity of the solvent vapor and $\bar{f}_{12}$ is the partial fugacity of the solvent in the polymer. When the sorption of the solvent in the polymer is small, the equilibrium condition can be approximated in terms of Henry's constants, H_{12}

$$f_1 = H_{12} x_{12}, \tag{5.12}$$

where x_{12} is the mole fraction of the solvent in the polymer. Equation (5.11) may be written in terms of the fugacity coefficients

$$\varphi_1 p_1 = x_{12} \gamma_{12} \varphi_1^s p_1^s, \tag{5.13}$$

where p_1 is the pressure of the solvent in the vapor phase. At low and moderate pressures the fugacity coefficients on both sides of the equation (5.13) are equal, and hence

$$p_1 = x_{12} \gamma_{12} p_1^s. \tag{5.14}$$

Thus, the solvent vapor pressure is proportional to the mole fraction of the dissolved solvent in the polymer. At low pressures this proportionality is linear and known as Henry's law. Then Henry's constant may be defined in terms of the solvent activity coefficient at infinite dilution γ_{12}^{∞} as

$$H_{12} = \gamma_{12}^{\infty} p_1^s. \tag{5.15}$$

The weight fraction based Henry's constant H_{12}^w is more convenient for polymer solutions. It is defined as

$$H_{12}^{w} = \lim_{w_{12}\to 0} \frac{f_1}{w_{12}} = \Omega_{12}^{\infty} p_1^{s}, \tag{5.16}$$

where w_{12} is the weight fraction of the solvent in the polymer phase and Ω_{12}^{∞} is the weight fraction based activity coefficient of the solvent in the polymer at infinite dilution. The weight fraction based activity coefficient may be calculated from the mole fraction based activity coefficient by equation (Danner and High, 1993, p. 47)

$$\ln \Omega_{12}^{\infty} = \ln \gamma_{12}^{\infty} - \ln\left(w_{12} + (1 - w_{12}) \frac{M_1}{M_2} \right), \tag{5.17}$$

where M_1 is the molecular weight of the solvent and M_2 is the molecular weight of the polymer. When the vapor phase is assumed to be ideal, that is $\varphi_1 = 1$, the equation (5.16) can be written in the form

$$H_{12}^{w} = \lim_{w_{12}\to 0} \frac{p_1}{w_{12}}. \tag{5.18}$$

5.4 MAXWELL–STEFAN EQUATIONS FOR PERMEATION

According to the famous dusty gas model (Mason and Malinauskas, 1983), a porous membrane may be considered to consist of giant molecules uniformly distributed in the space. The transport through the porous membrane occurs by the bulk flow, ordinary diffusion, Knudsen diffusion, and viscous flow. The latter two modes of transport are suppressed in a dense membrane where the molecules form a pore-free structure. Then, the membrane is no longer an inert component in a multicomponent permeation of *nc* components, but the (*nc*+1)th component of the system. The membrane has a zero flux due to the external force provided by the support layer, which holds the membrane fixed in the space. This external force does not affect the diffusion of the other *nc* species. The pressure in the selective layer is assumed to be equal to the pressure on the high-pressure side in accordance with the solution–diffusion model.

The Maxwell–Stefan equations may be written for the system of *nc*+1 components within the membrane as

$$-\frac{x_{im}}{RT} \nabla_{T,p} \mu_{im} = \sum_{\substack{j=1 \\ j\neq i}}^{nc} \frac{x_{jm} N_i - x_{im} N_j}{c_{tm} Đ_{ij}'} + \frac{x_{(nc+1)m} N_i}{c_{tm} Đ_{i(nc+1)}'}, \quad i = 1, 2, \ldots, nc, \tag{5.19}$$

where x_i is the mole fraction of species i, N_i is the molar flux of species i, c_t is the total molar density, $Đ'_{ij}$ is the Maxwell–Stefan diffusion coefficient that relates the friction between species i and j, and subscript m denotes the property in the membrane. Equation (5.19) is inconvenient, since the molar density and the mole fractions are awkward quantities with polymeric systems. By using the mass density and the weight fractions, steep concentration profiles can be avoided. Also the assumption of constant density in the selective layer is more acceptable in terms of the mass density than in terms of the molar density. In terms of the mass density and the weight fractions equation (5.19) transforms into a form

$$-\frac{w_{im}}{RT}\nabla_{T,p}\mu_{im} = \sum_{\substack{j=1 \\ j\neq i}}^{nc}\frac{w_{jm}n_i - w_{im}n_j}{\rho_{tm}Đ_{ij}} + \frac{w_{(nc+1)m}n_i}{\rho_{tm}Đ_{i(nc+1)}}, \quad i = 1, 2, \ldots, nc, \tag{5.20}$$

where n is the mass flux, w is the weight fraction, ρ_t is the total mass density of the mixture, and $Đ$ is defined as the mass fraction based Maxwell–Stefan diffusion coefficient

$$Đ_{ij} = Đ'_{ij}M_j\sum_{k=1}^{nc+1}\frac{w_{km}}{M_k}, \tag{5.21}$$

and where M is the molecular weight. Equations (5.20) may be written in an equivalent and generalized Maxwell–Stefan form as

$$-\frac{w_{im}}{RT}\nabla_{T,p}\mu_{im} = \sum_{\substack{j=1 \\ j\neq i}}^{nc+1}\frac{w_{jm}n_i - w_{im}n_j}{\rho_{tm}Đ_{ij}}, \quad i = 1, 2, \ldots, nc. \tag{5.22}$$

The generalized Maxwell–Stefan equations are valid for dense gas and liquid mixtures. Curtiss and Bird (1996, 1997) derived an equation for polymeric liquids from molecular theory; the equation resembles the generalized Maxwell–Stefan form but stress tensor appears in the driving force expression instead of pressure (Curtiss and Bird, 1999).

The transport equations for permeation are conveniently solved by using the film model. A single component permeation is first considered in paragraph 5.4.1 and multicomponent systems are then treated in paragraphs 5.4.2 and 5.4.3.

5.4.1 Single component permeation

In a single component permeation, or alternatively, when interaction terms are negligible, the cross-terms $Đ_{ij}$ in equation (5.20) are dropped out. Then the component fluxes may be written as

$$n_i = -\rho_{tm} \frac{Đ_{i(nc+1)}}{w_{(nc+1)m}} \frac{w_{im}}{RT} \nabla_{T,p} \mu_{im} . \tag{5.23}$$

Equation (5.23) may be expressed in terms of the weight fraction gradient,

$$n_i = -\rho_{tm} \frac{Đ_{i(nc+1)}}{w_{(nc+1)m}} \Gamma_{im} \nabla w_{im} , \tag{5.24}$$

where Γ is the thermodynamic factor

$$\Gamma_{im} = \frac{w_{im}}{RT} \left. \frac{\partial \mu_{im}}{\partial w_{jm}} \right|_{T,p,\Sigma} . \tag{5.25}$$

In equation (5.25) Σ denotes that the sum of all weight fractions must be unity. For ideal systems, the thermodynamic factor is unity and then

$$n_i = -\rho_{tm} \frac{Đ_{i(nc+1)}}{w_{(nc+1)m}} \nabla w_{im} . \tag{5.26}$$

In gas and vapor permeation, diffusion is assumed to be one-directional and perpendicular to the membrane interface. Equation (5.26) may be approximated with the one-dimensional finite-difference approximation that results in equation

$$n_i = \rho_{tm} \frac{Đ_{i(nc+1)}}{w_{(nc+1)m}} \frac{\left(w_{im,I} - w_{im,II}\right)}{\delta_m} . \tag{5.27}$$

The relation between the Maxwell–Stefan equation and the solution–diffusion model equation can be observed easier if the equation is written — despite the discussion above — in the molar flux form,

$$N_i = c_{tm} \frac{Đ'_{i(nc+1)}}{x_{(nc+1)m}} \frac{\left(x_{im,I} - x_{im,II}\right)}{\delta_m} . \tag{5.28}$$

As the solubility coefficient S_i relates the partial pressure of the gas or the vapor on the feed and the permeate side to the concentration in the membrane, equation (5.28) becomes

$$N_i = \frac{1}{RT} \frac{Đ'_{i(nc+1)} S_i}{x_{(nc+1)m}} \frac{\left(p_{iL} - p_{iV}\right)}{\delta_m} . \tag{5.29}$$

The term $1/x_{(nc+1)m}$ arises from the bulk flux contribution, which is not accounted for in the solution–diffusion model. For a single component permeation we may define an effective Maxwell–Stefan diffusion coefficient for species *i* in the membrane in the form

$$Đ_{iM} = \frac{Đ_{i(nc+1)}}{w_{(nc+1)m}} = \frac{Đ'_{i(nc+1)}}{x_{(nc+1)m}} , \tag{5.30}$$

and write equations (5.27) and (5.29) as

$$n_i = \rho_{tm} Đ_{iM} \frac{\left(w_{im,I} - w_{im,II}\right)}{\delta_m} \text{ and} \tag{5.31}$$

$$N_i = \frac{1}{RT} Đ_{iM} S_i \frac{\left(p_{iL} - p_{iV}\right)}{\delta_m}. \tag{5.32}$$

Now it may be seen that $D_i = Đ_{iM}$ but only in ideal systems. The diffusion coefficient D_i in equation (2.11) must also be defined as an effective diffusion coefficient. However, all diffusion coefficients become equal at the limit of zero penetrant concentration, so that $Đ_{iM} = Đ'_{i(nc+1)} = Đ_{i(nc+1)} = D_i$.

5.4.2 Multicomponent permeation: Matrix method

Equations (5.22) are written in the *nc* dimensional matrix form as (Taylor and Krishna, 1993, pp. 163, 209)

$$[\Gamma]\frac{d(w)}{d\lambda} = [\Phi](w) + (\phi), \tag{5.33}$$

where $[\Phi]$ is the matrix of rate factors, (ϕ) is the vector of rate factors, λ is the dimensionless distance in the film, (w) is the vector of mass fractions, and $[\Gamma]$ is the matrix of thermodynamic factors accounting for the system non-ideality. Equation (5.33) represents a set of *nc* coupled non-linear differential equations, since the diffusion coefficients and the thermodynamic factors are composition dependent. Instead of the exact solution, Taylor and Krishna (1993, p. 209) recommended the Krishna (1977) approximation, where the thermodynamic factors and the diffusion coefficients are considered constant along the diffusion path. This approximation expresses equation (5.33) as a linear matrix differential equation, which may be solved for the *nc* fluxes as

$$\begin{aligned}(n) &= \rho_{tm}[\beta][B_0]^{-1}[\Gamma_{av}][\Xi_0]\frac{\left(w_{m,I} - w_{m,II}\right)}{\delta_m} \\ &= \rho_{tm}[\beta][B_\delta]^{-1}[\Gamma_{av}][\Xi_\delta]\frac{\left(w_{m,I} - w_{m,II}\right)}{\delta_m},\end{aligned} \tag{5.34}$$

where $[\beta]$ is the bootstrap matrix, $[B]$ is the matrix of inverted diffusion coefficients, $[\Gamma_{av}]$ is the matrix of thermodynamic correction factors defined at the average composition, and $[\Xi]$ is the matrix of high flux correction factors. Both $[B]$ and $[\Xi]$ are evaluated at the film interface, either at $y = 0$ or $y = \delta_m$. The matrix $[B]$ has elements given by equations

$$B_{ii} = \frac{w_{im}}{\mathcal{D}_{i(nc+1)}} + \sum_{\substack{k=1 \\ k\neq i}}^{nc+1} \frac{w_{km}}{\mathcal{D}_{ik}} \text{ and} \tag{5.35}$$

$$B_{ij} = -w_{im}\left(\frac{1}{\mathcal{D}_{ij}} - \frac{1}{\mathcal{D}_{i(nc+1)}}\right). \tag{5.36}$$

Note that the mass fraction based Maxwell–Stefan diffusion coefficients are used in the equations (5.35) and (5.36). The matrix of thermodynamic factors $[\Gamma_{av}]$ has elements given by equation

$$\Gamma_{ij,av} = \frac{\overline{w}_{im}}{RT}\left.\frac{\partial \mu_{im}}{\partial w_{jm}}\right|_{T,p,\Sigma}, \tag{5.37}$$

where Σ denotes that for an infinitesimal change of weight fraction j, the sum of all weight fractions must be unity. The matrix of high flux correction factors $[\Xi]$ at $y = 0$ is obtained by equation

$$[\Xi_0] = [\Theta]\left[\exp[\Theta] - [I]\right]^{-1} \tag{5.38}$$

and at $y = \delta_m$ by equation

$$[\Xi_\delta] = [\Theta]\exp[\Theta]\left[\exp[\Theta] - [I]\right]^{-1}, \tag{5.39}$$

where $[\Theta]$ is

$$[\Theta] = [\Gamma_{av}]^{-1}[\Phi]. \tag{5.40}$$

Thus, the thermodynamic factors affect directly the matrix of the correction factors $[\Xi]$. The elements of the matrix of the rate factors $[\Phi]$ are given by the equations

$$\Phi_{ii} = \frac{n_i}{\rho_{tm}\mathcal{D}_{i(nc+1)}/\delta_m} + \sum_{\substack{k=1 \\ k\neq i}}^{nc+1} \frac{n_k}{\rho_{tm}\mathcal{D}_{ik}/\delta_m} \text{ and} \tag{5.41}$$

$$\Phi_{ij} = -n_i\left(\frac{1}{\rho_{tm}\mathcal{D}_{ij}/\delta_m} - \frac{1}{\rho_{tm}\mathcal{D}_{i(nc+1)}/\delta_m}\right). \tag{5.42}$$

Generally, the bootstrap matrix is required to define the fluxes in the system, because there are only nc independent driving forces in the nc+1 component system. Since the membrane flux is zero, the elements of the bootstrap matrix $[\beta]$ are (Taylor and Krishna, 1993, p. 148)

$$\beta_{ik} = \delta_{ik} + \frac{w_{im}}{w_{(nc+1)m}}, \tag{5.43}$$

where δ_{ik} is the Kronecker delta. Computationally, it is more convenient to calculate first the nc independent diffusion fluxes as

$$(j) = \rho_{tm}[B_0]^{-1}[\Gamma_{av}][\Xi_0]\frac{(w_{m,I} - w_{m,II})}{\delta_m} \qquad (5.44)$$
$$= \rho_{tm}[B_\delta]^{-1}[\Gamma_{av}][\Xi_\delta]\frac{(w_{m,I} - w_{m,II})}{\delta_m}.$$

Since

$$\sum_{i=1}^{nc+1} j_i = 0, \qquad (5.45)$$

the total flux is given by the equation

$$n_t = -\frac{j_{nc+1}}{w_{(nc+1)m}} = \frac{\sum_{i=1}^{nc} j_i}{w_{(nc+1)m}} \qquad (5.46)$$

and the component fluxes are obtained from

$$(n) = (j) + (w)n_t. \qquad (5.47)$$

The solution procedure is iterative, since the fluxes are required in the computation of the matrix of high flux correction factors.

5.4.3 Multicomponent permeation: Simplified explicit method

An alternative solution method for a multicomponent permeation is the simplified explicit method for the Stefan diffusion by Burghardt and Krupiczka (1975), which yields explicit expressions for the rate factor Φ and for the high flux correction factor Ξ. As a consequence, the component fluxes can be calculated without iteration. The simplified method for the Stefan diffusion can be generalized for non-ideal fluids by including the matrix of thermodynamic rate factors $[\Gamma]$ (Kubaczka and Bandrowski, 1990; Taylor, 1991). Then the *nc* mass fluxes can be written as

$$(n) = \rho_{tm}[A_{av}]^{-1}[\Gamma_{av}]\,\Xi\frac{(w_{im,I} - w_{im,II})}{\delta_m}, \qquad (5.48)$$

where Ξ is the scalar correction factor and $[A_{av}]$ is the matrix of inverted diffusion coefficients evaluated at the arithmetic average composition with elements

$$A_{ii,\mathrm{av}} = \sum_{\substack{k=1 \\ k\neq i}}^{nc+1} \frac{\overline{w}_{km}}{\overline{\overline{D}}_{ik}} \quad \text{and} \tag{5.49}$$

$$A_{ij,\mathrm{av}} = -\frac{\overline{w}_{im}}{\overline{\overline{D}}_{ij}}. \tag{5.50}$$

The bootstrap condition is already taken into account in the elements of matrix [*A*], thus the matrix $[A]^{-1}$ corresponds to the matrix multiplication $[\beta][B]^{-1}$. The scalar correction factor is defined as

$$\Xi = \frac{1}{2}\Phi\frac{(\exp\Phi+1)}{(\exp\Phi-1)}, \tag{5.51}$$

where the explicit mass transfer rate factor Φ is defined in terms of the weight fractions at the film interfaces 0 and δ_m with

$$\Phi = \ln\left(\frac{w_{(nc+1)m,\delta}}{w_{(nc+1)m,0}}\right). \tag{5.52}$$

According to Taylor and Krishna (1993, pp. 199-200), the scalar correction factor Ξ accounts for the non-linearity of the composition profiles, and gives a clear improvement in the predicted fluxes.

5.5 FILM THICKNESS

Thus far the membrane thickness δ_m has been treated as a constant and known parameter. However, the actual membrane thickness δ_m is not equal to the dry membrane thickness δ_m^0 since sorption causes volume dilation. Paul and Ebra-Lima (1970) and Bitter (1984) have already discussed the effect of swelling on permeation in reverse osmosis and gas separation.

The rate of swelling in the direction of the permeation depends on the mode of swelling, the rate of sorption, and the volume fraction profile of the polymer. Isotropic and anisotropic swelling may be identified as two limiting modes of volume dilation. On isotropic swelling, the volume change in the membrane occurs freely in all dimensions and may be expressed as (Sperling, 1992, p. 415)

$$\alpha_x\alpha_y\alpha_z = \frac{1}{\phi_{(nc+1)m}}, \tag{5.53}$$

where α_x, α_y, and α_z are the swelling ratios in the *x*, *y*, and *z* dimensions, and $\phi_{(nc+1)m}$ is the volume fraction of the polymer in the membrane phase,

$$\phi_{(nc+1)m} = \frac{\overline{V}_{(nc+1)m}}{\overline{V}_{tm}} . \tag{5.54}$$

The partial molar volume of the membrane, $\overline{V}_{(nc+1)m}$, is defined as

$$\overline{V}_{(nc+1)m} = \left. \frac{\partial \overline{V}_{tm}}{\partial x_{(nc+1)m}} \right|_{T,p,\Sigma} , \tag{5.55}$$

where Σ denotes that for an infinitesimal change of the mole fraction of the membrane, the sum of the mole fractions must be unity.

On isotropic swelling, the swelling ratio α_y in the direction of the permeation is

$$\alpha_y = \frac{\delta_m}{\delta_m^0} = \frac{1}{\phi_{(nc+1)m}^{1/3}} . \tag{5.56}$$

On anisotropic swelling, the volume change of the membrane occurs only in the *y* direction since the cross-section area of the membrane is fixed to the direction of the permeation. Then both α_x and α_z in equation (5.53) are equal to unity and thus

$$\alpha_y = \frac{1}{\phi_{(nc+1)m}} . \tag{5.57}$$

However, the volume dilation is not purely isotropic or anisotropic in a real process (Crank and Park, 1968). A geometric mean of the above limiting modes may be applied and then

$$\alpha_y = \frac{1}{\phi_{(nc+1)m}^{2/3}} . \tag{5.58}$$

The volume fraction of the polymer is not constant in the direction of the permeation (Paul and Ebra-Lima, 1970; Bitter, 1984). Therefore, it is convenient to define the average volume fraction $\overline{\phi}_{(nc+1)m}$, which is obtained by integrating the volume fraction profile within the membrane over the membrane thickness

$$\overline{\phi}_{(nc+1)m} = \frac{\int_0^{\delta_m} \phi_{(nc+1)m} dy}{\int_0^{\delta_m} dy} = \int_0^1 \phi_{(nc+1)m} d\lambda , \tag{5.59}$$

where λ is the dimensionless distance in the selective layer, y/δ_m. For simplicity, with an assumption of constant diffusivity and total mass density, the volume fraction of the polymer is obtained from equation

$$\frac{\phi_{(nc+1)m}}{\phi_{(nc+1)m,0}} = \left(\frac{\phi_{(nc+1)m,\delta}}{\phi_{(nc+1)m,0}} \right)^{\lambda}, \tag{5.60}$$

where $\phi_{(nc+1)m,0}$ is the volume fraction of the polymer at $y = 0$ and $\phi_{(nc+1)m,\delta}$ is the volume fraction of the polymer at $y = \delta_m$. The substitution of equation (5.60) into equation (5.59) yields after integration

$$\bar{\phi}_{(nc+1)m} = \frac{\phi_{(nc+1)m,\delta} - \phi_{(nc+1)m,0}}{\ln\left(\frac{\phi_{(nc+1)m,\delta}}{\phi_{(nc+1)m,0}} \right)}. \tag{5.61}$$

Then the ratio of the actual membrane thickness to the dry membrane thickness δ_m / δ_m^0 is obtained for isotropic swelling from equation (5.62), for anisotropic swelling from equation (5.63), and as a geometric mean of the two limiting modes of swelling from equation (5.64).

$$\frac{\delta_m}{\delta_m^0} = \left[\frac{\ln\left(\phi_{(nc+1)m,\delta} / \phi_{(nc+1)m,0}\right)}{\phi_{(nc+1)m,\delta} - \phi_{(nc+1)m,0}} \right]^{1/3} \tag{5.62}$$

$$\frac{\delta_m}{\delta_m^0} = \frac{\ln\left(\phi_{(nc+1)m,\delta} / \phi_{(nc+1)m,0}\right)}{\phi_{(nc+1)m,\delta} - \phi_{(nc+1)m,0}} \tag{5.63}$$

$$\frac{\delta_m}{\delta_m^0} = \left[\frac{\ln\left(\phi_{(nc+1)m,\delta} / \phi_{(nc+1)m,0}\right)}{\phi_{(nc+1)m,\delta} - \phi_{(nc+1)m,0}} \right]^{2/3} \tag{5.64}$$

5.6 DIFFUSION IN RUBBERY MEMBRANES

Binary diffusion coefficients are required between all possible binary pairs to describe the effect of species concentration gradients to the species fluxes in the defined mixture. The binary penetrant–membrane diffusion coefficients are experimental quantities that are obtained from measured pure component permeability coefficients. In order to correlate the temperature, pressure, and concentration dependence of binary penetrant–membrane diffusion coefficients, several permeability measurements are required at different pressures and temperatures for each penetrant.

The permeability coefficients may be determined from a steady state or a transient permeation experiment (Crank and Park, 1968). In the steady state method, the permeate flux through a flat sheet of known thickness is measured at known steady interfacial conditions. A permeability coefficient may then be calculated from equation (2.14). Since the permeability

coefficient is generally concentration dependent, an average permeability coefficient is obtained.

In the transient experiment, the membrane is initially free of a penetrant. Then the upstream side of the membrane is exposed to the constant pressure of the permeating gas or vapor, while the downstream side is maintained on the low pressure. At the beginning of the experiment, both the rate of flow and the concentration in the membrane vary with time and finally become stabilized at the steady state. The permeated gas or vapor is continuously removed from the low-pressure side of the membrane into a permeate chamber. The rate of the pressure increase in the permeate chamber with respect to time is recorded until the steady state increase in the pressure is reached. A permeability coefficient is related to the accumulation rate of the permeated gas or vapor at the steady state

$$P = \frac{\delta_m^0}{p_F}\frac{dQ_t}{dt}, \tag{5.65}$$

where Q_t is the total amount of the permeated fluid per membrane area, t is time, and p_F is the pressure on the upstream side. If the diffusion coefficient of the permeant is constant, i.e. independent of the concentration, the diffusion coefficient is related to the time lag t_g, which is required to attain the steady state (Crank and Park, 1968)

$$t_g = \frac{\delta_m^{0\,2}}{6D}. \tag{5.66}$$

Thus, the permeability and the diffusion coefficient may be determined from a single transient experiment. The solubility coefficient may then be calculated from the definition of the permeability, equation (2.13). For a concentration dependent permeation, an average permeability coefficient is obtained, but equation (5.66) is not applicable for obtaining an average diffusion coefficient.

In fact, the term P_i / δ_m in equation (2.12) and (2.14) is the measured quantity. It is the mass transfer coefficient for permeation that describes the flux with respect to the corresponding conditions over the membrane. The permeability coefficient may be calculated when the thickness of the membrane sample is known. However, the membrane swelling is implicitly included in the experimental permeability coefficient if the dry membrane thickness is applied in the calculation of the permeability coefficient. The actual permeability coefficient may be obtained by observing the volume dilation at a steady state or approximately by including the theoretical swelling correction, equation (5.62), (5.63), or (5.64). An average effective

diffusion coefficient $\overline{Đ}_{iM}$ may then be evaluated from the experimental permeability coefficient with equation

$$\overline{Đ}_{iM} = \frac{\overline{P}_i}{\overline{S}_i \Gamma_{av}} \frac{\delta_m}{\delta_m^0}, \tag{5.67}$$

where the average solubility coefficient, $\overline{S}_i$, has to be calculated from the experimental sorption curve or alternatively, from an appropriate theoretical model.

5.6.1 Diffusion at infinite dilution

The temperature dependence of a penetrant diffusion in polymers above the glass transition is conveniently described by following the free volume theories (Fujita *et al.*, 1960; Vrentas and Duda, 1977). By using the approach of Fujita *et al.* (1960), the temperature dependence of the binary penetrant–membrane Maxwell–Stefan diffusion coefficients at the limit of zero penetrant concentration, $Đ_{12}^0$, may be written in terms of the total free volume of a penetrant free polymer:

$$Đ_{12}^0 = A_d \exp\left(-\frac{B_d}{\phi_{FV}^0}\right), \tag{5.68}$$

where ϕ_{FV}^0 is the fractional free volume of the penetrant-free polymer at the system temperature

$$\phi_{FV}^0 = \frac{V^0(T) - V^*}{V^0(T)}, \tag{5.69}$$

and where $V^0(T)$ is the volume of the pure polymer at the temperature T and at the zero pressure, and V^* is the occupied volume. The definition of the occupied volume will be given later on in this work.

5.6.2 Diffusion in concentrated solutions

Penetrant diffusion in a rubbery membrane resembles the diffusion in a liquid mixture. The diffusion of permanent gases like hydrogen and nitrogen is generally concentration independent. Then the diffusion coefficient corresponds to the diffusivity $Đ_{12}^0$ from (5.68), which includes only the free volume contribution of the pure polymer. The diffusion rate of hydrocarbon vapors increases with concentration since the penetrant molecules increase the total free volume of the system.

The generalized Maxwell–Stefan equations utilize the diffusion coefficients for which the variation with the concentration in binary liquid mixtures is significantly lower than the variation of the Fick diffusion coefficients (Taylor and Krishna, 1993, pp.69-71). Typically, the binary Maxwell-Stefan diffusivities $Đ_{12}$ in binary liquid mixtures follow a linear relation between the limiting diffusivities $Đ_{12}^{0}$ and $Đ_{21}^{0}$, the diffusivity of species 1 at infinite dilution in 2 and the diffusivity of species 2 at infinite dilution in 1. However, in vapor membrane separation the latter limiting diffusivity is not valid since the concentration of penetrant in the membrane is limited by the sorption equilibrium. Then the corresponding limiting diffusivity may be denoted as $Đ_{12}^{\infty}$, the diffusivity at the equilibrium concentration as a result of pure component sorption at the saturation pressure. The diffusion coefficients $Đ_{12}$ at a constant temperature may then be assumed to follow a linear relation between the limiting diffusivities $Đ_{12}^{0}$ and $Đ_{12}^{\infty}$ with respect to the weight fraction

$$Đ_{12} = \left(1 - \frac{w_{1m}}{w_{1m}^{\infty}}\right) Đ_{12}^{0} + \frac{w_{1m}}{w_{1m}^{\infty}} Đ_{12}^{\infty}, \tag{5.70}$$

where w_{1m}^{∞} is the maximum weight fraction of the penetrant in the membrane as a result of the pure component sorption at a constant temperature and the saturation pressure.

5.6.3 Diffusion in multicomponent systems

In multicomponent systems, the cross-coefficients $Đ_{ij}$ between the permeating molecule pairs of *i* and *j* are required in the evaluation of the matrices of the inverted diffusion coefficients $[A]$ or $[B]$. At the moment there is no solid theory to predict the cross-coefficients in a polymeric system. At low pressures and with low solubility components, the permeating molecules in the polymer matrix will be far removed from one another. Then the interactions between the permeating species are negligible compared to the interactions between the permeating species and the membrane. In this case, the matrix $[B]^{-1}$ or $[A]^{-1}$ becomes a diagonal matrix and the multicomponent permeation is described in terms of a single component permeation. The binary penetrant–membrane diffusion coefficient $Đ_{i(nc+1)}$ may then be obtained from equation (5.70) but w_{1m}^{∞}, $Đ_{12}^{0}$, and $Đ_{12}^{\infty}$ replaced by $w_{im}^{\infty}, Đ_{i(nc+1)}^{0}$, and $Đ_{i(nc+1)}^{\infty}$ respectively.

The possibility of interactions between the permeating species increases with pressure — i.e. with the total penetrant concentration in the membrane — and especially in systems containing highly soluble components. According to the free volume theory in paragraph 2.3.1, a hole of a sufficient size is required for a successive diffusive jump. Apparently, a hole of size *x* will also accept all molecules smaller than *x*. Interactions that affect the species diffusion may occur within the period of formation and destruction of the transient hole, if there are more than one molecule in the same channel or if adjacent channels have already accommodated permeating molecules. These interactions either promote or hinder the diffusion of smaller molecules. The former is possible due to increased local free volume for the diffusion and the latter in the form of blocking up the diffusive pathway from the fast moving smaller molecules.

The estimation of multicomponent liquid diffusivities is based on different ways of averaging the infinite dilution diffusion coefficients of the binary pairs in a mixture (e.g. Kooijman and Taylor, 1991). A similar averaging process should be possible for multicomponent diffusivities in a membrane when the mixture of the penetrants and the membrane is considered to be a liquid mixture. Still, the dominating penetrant–membrane interactions are involved also in the penetrant–penetrant interactions. Then, for simplicity, the cross-coefficients $Đ_{ij}$ may be assumed to be proportional to the binary penetrant–membrane diffusion coefficients. The simplest form of the cross-coefficients may be obtained from the geometric average of the limiting diffusion coefficients. The diffusion coefficients at infinite dilution $Đ^{0}_{i(nc+1)}$ give more weight on the cross-coefficients than the diffusion coefficients at a maximum concentration $Đ^{\infty}_{i(nc+1)}$. The binary interactions become important at higher concentration levels, so that following Krishna (1990) for surface diffusion, the cross-coefficients may be chosen to depend on the binary penetrant–membrane diffusion coefficients at a maximum concentration

$$Đ_{ij} = \left(Đ^{\infty}_{i(nc+1)}\right)^{w_i/(w_i+w_j)} \left(Đ^{\infty}_{j(nc+1)}\right)^{w_j/(w_i+w_j)}. \tag{5.71}$$

Equation (5.71) fulfills the criteria $Đ_{ij} = Đ_{ji}$, but it is an empirical equation, which should be confirmed by experiments.

5.7 HEAT TRANSFER THROUGH THE MEMBRANE

The temperature gradient over the selective layer should be known in the evaluation of the component fluxes through the membrane. However, the resulting temperature gradient is so small that the thermal diffusion — the Soret effect — is negligible.

The following interfacial energy balance holds at the interface of the retentate fluid and the membrane (Figure 5.1):

$$\sum_{i=1}^{nc} N_{i,y}\left(\overline{H}_{iL,B} - \overline{H}_{iM,T}\right) + h_L\left(T_{L,B} - T_{L,P}\right) = k_m\left(T_{M,T} - T_{M,P}\right). \tag{5.72}$$

The term $\left(\overline{H}_{iL} - \overline{H}_{iM}\right)$ describes the enthalpy change involved in gas or vapor sorption. Similarly, we may write an interfacial energy balance at the interface of the selective layer and the support layer,

$$k_m\left(T_{M,P} - T_{M,B}\right) = k_s\left(T_{S,T} - T_{S,P}\right) + \sum_{i=1}^{nc} N_{i,y}\left(\overline{H}_{iS,T} - \overline{H}_{iM,B}\right), \tag{5.73}$$

where subscript *S* denotes the support grid point, *s* denotes the support property, and the term $\left(\overline{H}_{iS} - \overline{H}_{iM}\right)$ describes the enthalpy change involved in the gas or vapor desorption and the pressure reduction.

The enthalpy change of sorption and desorption is basically obtained from a thermodynamic model that is suitable both for conventional fluids and polymer solutions. The same model has to be used throughout the energy balance computations in order to maintain energy conservation over the spiral-wound module.

The energy balance equations (5.72) and (5.73) may be combined to yield the macroscopic balance over the selective layer only when the enthalpy change of sorption and desorption is assumed negligible so that

$$\sum_{i=1}^{nc} N_{i,y}\left(\overline{H}_{iL,B} - \overline{H}_{iS,T}\right) + h_L\left(T_{L,B} - T_{L,P}\right) = k_s\left(T_{S,T} - T_{S,P}\right). \tag{5.74}$$

Then heat conduction over the retentate side interface is continuous and the term $\left(\overline{H}_{iL} - \overline{H}_{iS}\right)$ describes the enthalpy change involved in the pressure reduction. Equation (5.74) allows the use of the enthalpy equation derived from the equation of state models for conventional fluids, such as the Soave-Redlich-Kwong equation of state.

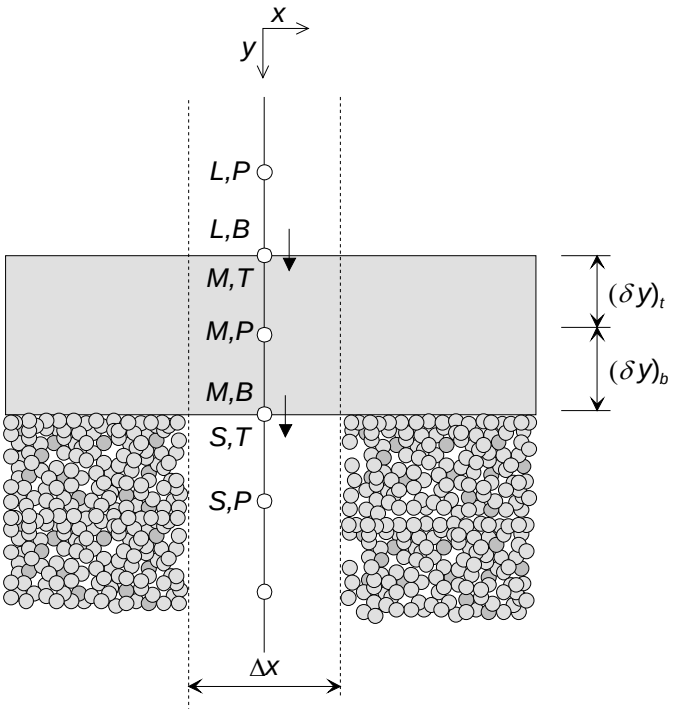

Figure 5.1 Grid point formulation within the membrane for the local permeate flow in the *y* direction. The length of the third dimension is Δz.

The boundary temperatures $T_{L,B}$ and $T_{S,T}$ in (5.74) are not known in advance, but are defined in terms of local mass and energy flux and local external fluid properties on the retentate side. The selective layer thickness is about an order of magnitude smaller than the support layer and at least two orders of magnitudes smaller than the retentate channel height. Then the temperature gradient over the selective layer must indeed be small and the heat transfer is very fast through the thin selective layer and, as a consequence, temperatures $T_{L,B}$ and $T_{S,T}$ become almost equal. In such a case, it would be abnormal to assume a temperature gradient within the support layer, so equation (5.74) becomes

$$\sum_{i=1}^{nc} N_{i,y}\left(\overline{H}_{iL,B} - \overline{H}_{iS,T}\right) + h_L\left(T_{L,B} - T_{L,P}\right) = 0\,. \tag{5.75}$$

Thus, the energy transport through the support and substrate layers to the permeate side occurs only by convection. Then the diffusive term in equation (4.71) becomes zero.

6 EQUATION OF STATE MODELS FOR POLYMER SOLUTIONS

The equation of state models are able to relate *pVT* properties of pure substances and mixtures, and thereby to evaluate important thermodynamic properties, including the equilibrium condition between the two phases in contact. In the case of polymeric systems, the equation of state model should be able to relate *pVT* properties of small solvent molecules and large chain-like macromolecules. The two-parameter cubic equation of state models for normal fluids are usually not able to represent phase behavior in polymeric systems. Therefore, a large number of equation of state models have been specifically developed for polymers. Such models include the Flory EOS (Flory, 1970), the Sanchez–Lacombe EOS (Sanchez and Lacombe, 1976; Lacombe and Sanchez, 1976), the Panayiotou–Vera EOS (Panayiotou and Vera, 1982), the statistical associating fluid theory (SAFT) (Chapman *et al.*, 1989 and 1990), and the perturbed hard-sphere-chain EOS (PHSC) (Song *et al.*, 1994a).

Several combined equation of state–excess Gibbs energy models are proposed in the literature for predicting vapor–liquid equilibria and gas solubility for non-polymer solutions (Heidemann and Khokal, 1990; Michelsen, 1990a,b; Dahl and Michelsen, 1990; Holderbraum and Gmehling, 1991; Wong and Sandler, 1992; Boukouvalas *et al.*, 1994; Twu *et al.*, 1999). These mixing rules combine the excess Gibbs energy expression of an accurate or a predictive activity coefficient model to an equation of state. In the case of polymers, the idea behind the predictive group-contribution model is attractive, because vapor sorption data for polymers may be sparse or not available at all. This is why these new mixing rules have also attained interest in the modeling of polymer–solvent systems (Orbey and Sandler, 1994; Kalospiros and Tassios, 1995; Bertucco and Mio, 1996; Zhong and Masuoka, 1996; Orbey *et al.*, 1997) and thus have extended two-parameter cubic equation of state models also for polymeric systems.

In this chapter, three equation of state models for polymers are presented. The models are the Sanchez–Lacombe equation of state (Sanchez and Lacombe, 1976; Lacombe and Sanchez, 1976) in section 6.1, the perturbed hard-sphere-chain equation of state (Song *et al.*, 1994a, Song *et al.*, 1996) in section 6.2, and the combined Soave-Redlich-Kwong equation of state–group contribution activity coefficient model with the MHV2 mixing rule (Dahl and Michelsen, 1990) in section 6.3.

The original MHV2 model by Dahl and Michelsen (1990) combines the Soave–Redlich–Kwong equation of state with the Lyngby modified UNIFAC by Larsen *et al.* (1987). However, the Lyngby modified UNIFAC, reviewed in section 6.5, is not applicable to polymeric systems, since it greatly overestimates solvent activities in polymer solutions (Kontogeorgis *et al.*, 1994a). In principle, any activity coefficient model may be utilized to express the excess Gibbs energy of the mixture. Thus in polymer solutions, the Lyngby modified UNIFAC should be replaced with the UNIFAC-FV model (Oishi and Prausnitz, 1978), reviewed in section 6.4, or with the exponential UNIFAC modification introduced in section 6.6. The latter model is a new one and is developed during this work.

6.1 SANCHEZ–LACOMBE EQUATION OF STATE

The Sanchez-Lacombe equation of state has two model versions: the original lattice fluid model (Sanchez and Lacombe, 1976; Lacombe and Sanchez, 1976), and the non-lattice model development (Sanchez, 1987). Although the equation of state is the same for the models, the multicomponent chemical potentials yield different expressions. This is why both model versions are considered in this work.

The Sanchez-Lacombe equation of state for pure fluids and mixtures is (Sanchez and Lacombe, 1976; Lacombe and Sanchez, 1976):

$$\tilde{\rho}^2 + \tilde{P} + \tilde{T}\left[\ln(1-\tilde{\rho}) + \left(1-\frac{1}{r}\right)\tilde{\rho}\right] = 0, \tag{6.1}$$

where r is the number of effective segments of the molecule, or the molecular size parameter, $\tilde{T}$, $\tilde{P}$, and $\tilde{\rho}$ are the reduced temperature, pressure, and density respectively. The reduced properties are defined by equations

$$\tilde{T} = \frac{T}{T^*}, \tag{6.2}$$

$$\tilde{P} = \frac{p}{P^*}, \tag{6.3}$$

$$\tilde{\rho} = \frac{\rho}{\rho^*}, \text{ and} \tag{6.4}$$

$$\tilde{v} = \frac{1}{\tilde{\rho}} = \frac{V}{V^*}, \tag{6.5}$$

where T is the temperature, p is the pressure, V is the total volume, V^* is the close packed volume, $\tilde{v}$ is the reduced volume, and T^*, P^*, and ρ^* are the characteristic equation of state parameters.

For a high molecular weight polymer, the number of effective segments is large and hence the term $1/r$ becomes negligible. Then the equation of state becomes

$$\tilde{\rho}^2 + \tilde{P} + \tilde{T}\left[\ln(1-\tilde{\rho}) + \tilde{\rho}\right] = 0\,. \tag{6.6}$$

The roots of the equation of state have to be solved numerically. In general, there are three solutions to the equation of state: the greatest and the smallest real root corresponds to the minimum in the Gibbs energy and the intermediate real solution corresponds to the maximum in the Gibbs energy. The high-density minimum corresponds to a liquid root solution and the lower density minimum to a gas root solution.

6.1.1 Lattice fluid model

A real lattice fluid is completely characterized by the equation of state parameters T^*, P^*, and ρ^* or by the molecular parameters ε^*, v^*, and r, the total interaction energy per mer, the close packed volume per mer, and the number of effective segments respectively. The equation of state parameters and molecular parameters are related with each other by the following equations (Sanchez and Lacombe, 1978)

$$\varepsilon^* = k_B T^*, \tag{6.7}$$

$$v^* = \frac{k_B T^*}{P^*}, \text{ and} \tag{6.8}$$

$$r = \frac{MP^*}{k_B T^* \rho^*} = \frac{M}{\rho^* v^*}, \tag{6.9}$$

where k_B is the Boltzmann constant and M is the molecular weight. For polymers, the number average molecular weight is used.

Lacombe and Sanchez (1976) assumed that the close packed molecular volume of each component is conserved, that is, the number of occupied sites in the pure state r_i^0 is different from the number of occupied sites in the mixture r_i. Later, Sanchez and Lacombe (1978) introduced a more general assumption that the molecule occupies the same number of lattice sites r_i in the mixture as in the pure state. The close packed volume of the mixture, V^* is then given by equation

$$V^* = v^* \sum_i r_i \nu_i = r \nu v^*, \tag{6.10}$$

where v^* is the average close packed mer volume in the mixture and ν_i is the number of molecules of component *i*. The average close packed mer volume in the mixture is obtained from a linear mixing rule

$$v^* = \sum_i \phi_i v_i^* , \tag{6.11}$$

where ϕ_i is the close packed volume fraction

$$\phi_i = \frac{r_i \nu_i}{\sum_j r_j \nu_j} = \frac{w_i / \rho_i^*}{\sum_j w_j / \rho_j^*}, \tag{6.12}$$

and v_i^* is the pure component close packed mer volume. In equation (6.12), w_i is the mass fraction of component *i*, and ρ_i^* is the scaling density of the pure component *i*.

The total volume of the mixture is the sum of occupied and empty lattice sites. Since the filled sites and holes have the same size, the total volume of the mixture may be written as

$$V = (\nu_0 + r \nu) v^* = V^* \tilde{v}, \tag{6.13}$$

where *r* is the number of segments in the mixture

$$r = \sum_i x_i r_i \tag{6.14}$$

and ν_0 is the number of empty lattice sites. The number fraction x_i is defined as

$$x_i = \frac{\nu_i}{\sum_j \nu_j}. \tag{6.15}$$

The total fraction of occupied sites is equal to the reduced density $\tilde{\rho}$

$$\tilde{\rho} = \frac{r \nu}{r \nu + \nu_0}. \tag{6.16}$$

In close packed mixtures, the interaction energies are obtained from the combining rule (Lacombe and Sanchez, 1976)

$$\varepsilon^* = \sum_i \sum_j \phi_i \phi_j \varepsilon_{ij}^* , \tag{6.17}$$

where ε_{ij}^* is the cross-term between *i* and *j*

$$\varepsilon_{ij}^* = \left(\varepsilon_i^* \ \varepsilon_j^*\right)^{1/2} \left(1 - k_{ij}\right) \tag{6.18}$$

and where k_{ij} is the binary energy interaction parameter. The characteristic temperature of the mixture can then be calculated from equation (6.7). The close packed mass density of the mixture is obtained from equation

$$\rho^* = \frac{\sum_i \nu_i M_i}{\sum_i r_i \nu_i v_i^*} = \frac{1}{\sum_i \frac{w_i}{\rho_i^*}}. \tag{6.19}$$

The chemical potential of species i in a mixture is obtained from the partial differential of the Gibbs energy with respect to the number of lattice sites occupied by species i

$$\mu_i = \left(\frac{\partial G}{\partial \nu_i} \right)_{T,p,\nu_{j,i\neq j}}. \tag{6.20}$$

Lacombe and Sanchez (1976) derived the following expression for the intensive Gibbs energy

$$\frac{G}{r\nu} = -\tilde{\rho}\varepsilon^* + p\tilde{v}v^* + k_B T\left[(\tilde{v}-1)\ln(1-\tilde{\rho}) + \frac{1}{r}\ln\tilde{\rho} + \sum_i \frac{\phi_i}{r_i}\ln\frac{\phi_i}{\omega_i} \right], \tag{6.21}$$

where ω_i is the number of configurations available to a molecule in the close packed pure state and depends on the molecule size r_i and flexibility. The chemical potentials may be written in the form of the partial differential equations

$$\mu_i = r\nu \frac{\partial(G/r\nu)}{\partial \nu_i} + \frac{G}{r\nu}\frac{\partial(r\nu)}{\partial \nu_i}, \tag{6.22}$$

where

$$\frac{\partial(r\nu)}{\partial \nu_i} = r_i. \tag{6.23}$$

Since the intensive Gibbs energy is a function of temperature, pressure, and composition,

$$\frac{G}{r\nu} = g(T, p, \phi_1, \phi_2, \ldots, \phi_{nc}), \tag{6.24}$$

the following chain rule may be used in deriving the intensive Gibbs energy with respect to the number of lattice sites occupied by species i:

$$\frac{\partial(g)}{\partial \nu_i} = \sum_j \frac{\partial g}{\partial \phi_j}\frac{\partial \phi_j}{\partial \nu_i}, \tag{6.25}$$

where

$$\frac{\partial \phi_i}{\partial \nu_i} = \frac{\phi_i(1-\phi_i)}{\nu_i} \text{ and} \tag{6.26}$$

$$\frac{\partial \phi_j}{\partial \nu_i} = -\frac{\phi_i \phi_j}{\nu_i}. \tag{6.27}$$

As (6.26) and (6.27) are inserted into equation (6.25), and the resulting equation is substituted into equation (6.22) with (6.23), the partial differential equations become

$$\mu_i = \left.\frac{\partial G}{\partial \nu_i}\right|_{T,p,\nu_j} = r_i\left[g + \frac{\partial g}{\partial \phi_i} - \sum_j \phi_j \frac{\partial g}{\partial \phi_j}\right]. \tag{6.28}$$

The final form of the chemical potentials are obtained when equation (6.28) is derived with the lattice fluid mixing and combining rules

$$\begin{aligned}\frac{\mu_i}{k_B T} = \ln\frac{\phi_i}{\omega_i} + \left(1 - \frac{r_i}{r}\right) + \frac{2 r_i \tilde{\rho}}{k_B T}\left(\varepsilon^* - \sum_j \phi_j \varepsilon_{ij}^*\right) \\ + r_i\left[-\frac{\tilde{\rho}}{\tilde{T}} + \frac{\tilde{P}_i \tilde{v}}{\tilde{T}_i} + (\tilde{v} - 1)\ln(1 - \tilde{\rho}) + \frac{1}{r_i}\ln\tilde{\rho}\right],\end{aligned} \tag{6.29}$$

where

$$\tilde{T}_i = \frac{T}{T_i^*} \text{ and} \tag{6.30}$$

$$\tilde{P}_i = \frac{p}{P_i^*}. \tag{6.31}$$

6.1.2 Non-lattice fluid model

In the lattice fluid version, the filled sites and holes of the lattice mixture have the same size. In the non-lattice version, Sanchez (1987) allowed holes to have an adjustable size. This modification explicitly demonstrates that holes have an entropy-like character.

The model parameters in the non-lattice fluid have different definitions from the lattice fluid. Characteristic temperature T^* is now related to the hole volume v_0^* by the equation

$$k_B T^* = P^* v_0^*. \tag{6.32}$$

The molecular size parameter, *r*, is defined as volume ratio

$$r = \frac{v^*}{v_0^*} = \frac{P^* v^*}{k_B T^*}, \tag{6.33}$$

where v^* is the hard-core molecular volume. The reduced density $\tilde{\rho}$ of the mixture is

$$\tilde{\rho} = \frac{V^*}{\left(V_0 + V^*\right)}, \tag{6.34}$$

where

$$V^* = \sum_i \nu_i v_i^* \quad \text{and} \tag{6.35}$$

$$V_0 = \nu_0 v_0^*, \tag{6.36}$$

are the total hard-core volume and the free volume respectively. Although the choice of the hole volume is arbitrary, the molecular hole volume for the mixture may be calculated by using the reciprocal addition rule

$$\frac{1}{v_0^*} = \sum_i \frac{\phi_i}{v_{0,i}^*} = \sum_i \frac{\phi_i P_i^*}{k_B T_i^*}. \tag{6.37}$$

The characteristic pressure P^* corresponds to the cohesive energy density of the mixture. It is calculated from the pure component characteristic pressures

$$P^* = \sum_i \sum_j \phi_i \, \phi_j \, P_{ij}^*, \tag{6.38}$$

where

$$P_{ij}^* = \left(P_i^* \, P_j^* \right)^{1/2} \left(1 - k_{ij} \right), \tag{6.39}$$

and where k_{ij} is the binary interaction parameter between species *i* and *j*.

Since the physical picture in the non-lattice fluid version is different from the lattice fluid version, the chemical potentials also have different expressions. The Gibbs energy density for the non-lattice fluid is (Sanchez and Panayiotou, 1994)

$$g = \frac{G}{V^*} = -\tilde{\rho} P^* + p\tilde{v} + k_B T \left[\frac{(\tilde{v} - 1)\ln(1 - \tilde{\rho})}{v_0^*} + \frac{\ln \tilde{\rho}}{v^*} + \sum_i \frac{\phi_i \ln \phi_i}{v_i^*} \right]. \tag{6.40}$$

After a similar manipulation as in paragraph 6.1.1, the partial differential expression of the non-lattice fluid chemical potentials may be written as

$$\mu_i = \left. \frac{\partial G}{\partial \nu_i} \right|_{T,p,\nu_j} = v_i^* \left[g + \frac{\partial g}{\partial \phi_i} - \sum_j \phi_j \frac{\partial g}{\partial \phi_j} \right], \tag{6.41}$$

and the analytical expression of the non-lattice fluid chemical potentials as

$$\begin{aligned} \frac{\mu_i}{k_B T} = \ln \phi_i + \left(1 - \frac{v_i^*}{v^*} \right) + \frac{2 v_i^* \tilde{\rho}}{k_B T} \left(P^* - \sum_j \phi_j P_{ij}^* \right) \\ + r_i \left[-\frac{\tilde{\rho} \tilde{P}_i}{\tilde{T}_i \tilde{P}} + \frac{\tilde{P}_i \tilde{v}}{\tilde{T}_i} + (\tilde{v} - 1)\ln(1 - \tilde{\rho}) + \frac{1}{r_i} \ln \tilde{\rho} \right]. \end{aligned} \tag{6.42}$$

6.2 PERTURBED HARD-SPHERE-CHAIN EQUATION OF STATE

A hard-sphere-chain model is based on athermal — zero excess enthalpy — hard-sphere chains, where a chain molecule is modeled by a series of freely jointed tangent hard spheres. According to Song *et al.* (1994a), these models take into account some significant features of real chain-like fluids, like excluded volume effects and chain connectivity.

Total pressure, p, of hard-sphere chains system consists of three parts: a nonbonding contribution of hard-sphere mixtures prior to bonding, a bonding contribution due to chain formation, and van der Waals attractive forces between non-bonded hard-spheres. Song *et al.* (1994b) derived the following perturbed hard-sphere-chain equation of state for the mixtures

$$\frac{p}{\rho k_B T} = 1 + \rho \sum_i \sum_j x_i x_j r_i r_j b_{ij} g_{ij}\left(d_{ij}^{+}\right) - \sum_i x_i \left(r_i - 1\right)\left[g_{ii}\left(d_{ii}^{+}\right) - 1\right] - \frac{\rho}{k_B T} \sum_i \sum_j x_i x_j r_i r_j a_{ij}, \tag{6.43}$$

where p is the pressure, T is the absolute temperature, ρ is the number density, k_B is the Boltzmann constant, r is the number of segments or effective hard spheres per molecule, x_i is the number fraction of component i, b is the second virial coefficient of non-bonded hard-spheres or van der Waals co-volume per segment, $g_{ij}\left(d_{ij}^{+}\right)$ is the radial distribution function of hard-sphere mixtures at contact, and a_{ij} reflects the attractive forces between two non-bonded segments. The number density is defined as

$$\rho = \frac{\sum_i \nu_i}{V}, \tag{6.44}$$

where ν_i is the number of molecules of species i in volume V. The roots of the equation of state have to be solved numerically, since mixing rules are density dependent as will be seen later on. Topliss *et al.* (1988) present a solution procedure for such equation of states.

The analytical expression for the radial distribution function $g_{ij}\left(d_{ij}^{+}\right)$ is unknown. Song *et al.* (1994c) recommend the Carnahan–Starling equation for pure fluids

$$g\left(d^{+}\right) = \frac{1 - \eta/2}{\left(1 - \eta\right)^3} \tag{6.45}$$

and the Boublik–Mansoori–Carnahan–Starling (BMCS) equation for mixtures in the form

$$g_{ij}\left(d_{ij}^{+}\right)=\frac{1}{1-\eta}+\frac{3}{2}\frac{\xi_{ij}}{\left(1-\eta\right)^{2}}+\frac{1}{2}\frac{\xi_{ij}^{2}}{\left(1-\eta\right)^{3}}, \tag{6.46}$$

where η is the packing factor of hard-sphere mixtures,

$$\eta=\frac{\rho}{4}\sum_{i}x_{i}r_{i}b_{i}\,, \tag{6.47}$$

and ξ_{ij} is given by

$$\xi_{ij}=\frac{\rho}{4}\left(\frac{b_{i}b_{j}}{b_{ij}}\right)^{1/3}\sum_{k}x_{k}r_{k}b_{k}^{2/3}\,. \tag{6.48}$$

Alternatively, the equation of state can be expressed in terms of segment fractions ϕ_i:

$$\begin{aligned}\frac{p}{\rho_{r}k_{B}T}=1+\rho_{r}\sum_{i}\sum_{j}\phi_{i}\phi_{j}b_{ij}g_{ij}\left(d_{ij}^{+}\right)-\sum_{i}\phi_{i}\left(1-\frac{1}{r_{i}}\right)g_{ii}\left(d_{ii}^{+}\right)\\ -\frac{\rho_{r}}{k_{B}T}\sum_{i}\sum_{j}\phi_{i}\phi_{j}a_{ij},\end{aligned} \tag{6.49}$$

where ρ_r is the segment density defined as

$$\rho_{r}=\frac{\sum_{i}r_{i}\nu_{i}}{V}=\frac{\nu_{r}}{V} \tag{6.50}$$

and where ν_r the total number of segments in the mixture. The segment fraction is related to the number fraction by

$$\phi_{i}=\frac{r_{i}x_{i}}{\sum_{j}r_{j}x_{j}}\,. \tag{6.51}$$

The cross terms a_{ij} and b_{ij} are obtained from equations

$$a_{ij}(T)=\frac{2\pi}{3}\sigma_{ij}^{3}\varepsilon_{ij}F_{a} \text{ and} \tag{6.52}$$

$$b_{ij}(T)=\frac{2\pi}{3}\sigma_{ij}^{3}F_{b}\,, \tag{6.53}$$

where ε_{ij} is the non-bonded pair interaction energy between segments i and j, σ_{ij} is the segment size, F_a and F_b are the temperature dependent universal functions. The cross terms ε_{ij} and σ_{ij} are obtained from

$$\varepsilon_{ij}=\left(\varepsilon_{i}\varepsilon_{j}\right)^{1/2}\left(1-k_{ij}\right) \text{ and} \tag{6.54}$$

$$\sigma_{ij}=\frac{1}{2}\left(\sigma_{i}+\sigma_{j}\right)\left(1-l_{ij}\right), \tag{6.55}$$

where k_{ij} and l_{ij} are adjustable binary energy interaction and size correction parameters. In the simplified PHSC equation of state (Song *et al.*, 1996) the universal functions F_a and F_b are given by equations

$$F_a = 1.8681\exp\left[-0.0619\left(\frac{k_B T}{\varepsilon_{ij}}\right)\right] + 0.6715\exp\left[-1.7317\left(\frac{k_B T}{\varepsilon_{ij}}\right)^{3/2}\right] \text{ and} \tag{6.56}$$

$$F_b = 0.7303\exp\left[-0.1649\left(\frac{k_B T}{\varepsilon_{ij}}\right)^{1/2}\right] + 0.2697\exp\left[-2.3973\left(\frac{k_B T}{\varepsilon_{ij}}\right)^{3/2}\right]. \tag{6.57}$$

For a pressure explicit equation of state, the chemical potential of component k is obtained from the total Helmholtz energy by partial differentiation

$$\mu_k = \left(\frac{\partial A}{\partial \nu_k}\right)_{T,V,\nu_{j,k\neq j}}. \tag{6.58}$$

According to Song *et al.* (1994b), the Helmholtz energy of the mixture is given by the equation

$$\begin{aligned}\frac{A}{\nu_r k_B T} = \sum_i \phi_i \frac{A_i^0}{\nu_i r_i k_B T} + \\ \rho_r \sum_i \sum_j \phi_i \phi_j b_{ij} W_{ij} - \sum_i \phi_i \left(1 - \frac{1}{r_i}\right) Q_{ii} - \\ \frac{\rho_r}{k_B T} \sum_i \sum_j \phi_i \phi_j a_{ij} + \sum_i \frac{\phi_i}{r_i} \ln\left(\frac{\phi_i}{r_i} \rho_r k_B T\right),\end{aligned} \tag{6.59}$$

where A_i^0 is the Helmholtz energy of pure component i as an ideal gas at temperature T. W_{ij} and Q_{ii} are given by:

$$W_{ij} = K_1 + \frac{3}{2}\xi_{ij} K_2 + \frac{1}{2}\xi_{ij}^2 K_3 \text{ and} \tag{6.60}$$

$$Q_{ii} = -\ln(1-\eta) + \frac{3}{2}\frac{\xi_{ii}}{1-\eta} + \frac{1}{4}\frac{\xi_{ii}^2}{(1-\eta)^2}, \tag{6.61}$$

where

$$K_1 = -\frac{\ln(1-\eta)}{\eta} \text{ and} \tag{6.62}$$

$$K_n = \frac{1}{\eta}\left[-K_{n-1} + \frac{1}{n-1}\frac{1}{(1-\eta)^{n-1}}\right]. \tag{6.63}$$

Thus, the chemical potential of component k is (Song *et al.*, 1994b)

$$\frac{\mu_k}{k_B T} = \frac{\mu_k^0}{k_B T} + 2r_k \rho_r \sum_i \phi_i b_{ik} W_{ik} + \rho_r \sum_i \sum_j \phi_i \phi_j b_{ij} \left(\nu_r \frac{\partial W_{ij}}{\partial \nu_k} \right) - \tag{6.64}$$

$$(r_k - 1) Q_{kk} - \sum_i \phi_i \left(1 - \frac{1}{r_i} \right) \left(\nu_r \frac{\partial Q_{ii}}{\partial \nu_k} \right) - \frac{2 r_k \rho_r}{k_B T} \sum_i \phi_i a_{ik} +$$

$$\ln\left(\frac{\phi_k}{r_k} \rho_r k_B T \right) + 1,$$

where μ_k^0 is the chemical potential of pure component k as an ideal gas at temperature T and

$$\left(\nu_r \frac{\partial W_{ij}}{\partial \nu_k} \right) = \left(\frac{\partial W_{ij}}{\partial \eta} \right) \left(\nu_r \frac{\partial \eta}{\partial \nu_k} \right) + \left(\frac{\partial W_{ij}}{\partial \xi_{ij}} \right) \left(\nu_r \frac{\partial \xi_{ij}}{\partial \nu_k} \right), \tag{6.65}$$

$$\left(\nu_r \frac{\partial Q_{ii}}{\partial \nu_k} \right) = \left(\frac{\partial Q_{ii}}{\partial \eta} \right) \left(\nu_r \frac{\partial \eta}{\partial \nu_k} \right) + \left(\frac{\partial Q_{ii}}{\partial \xi_{ii}} \right) \left(\nu_r \frac{\partial \xi_{ii}}{\partial \nu_k} \right), \tag{6.66}$$

$$\left(\nu_r \frac{\partial \eta}{\partial \nu_k} \right) = \frac{\rho_r}{4} r_k b_k, \text{ and} \tag{6.67}$$

$$\left(\nu_r \frac{\partial \xi_{ij}}{\partial \nu_k} \right) = \left(\frac{b_i b_j}{b_{ij}} \right)^{1/3} \frac{\rho_r}{4} r_k b_k^{2/3}. \tag{6.68}$$

6.3 THE MHV2 MODEL

The MHV2 mixing rule by Dahl and Michelsen (1990) is the second-order approximation of the modified Huron-Vidal (MHV1) mixing rule by Michelsen (1990b). It combines the Soave–Redlich–Kwong equation of state with the group-contribution activity coefficient model with the MHV2 mixing rule.

The Soave–Redlich–Kwong (SRK) equation of state is a cubic equation of state

$$p = \frac{RT}{(v - b)} - \frac{a}{v(v + b)}, \tag{6.69}$$

where p is pressure, T is temperature, v is the molar volume, a is the energy and b the co-volume parameter of the mixture. The mixture co-volume is obtained from the corresponding pure component values

$$b = \sum_i x_i b_i, \tag{6.70}$$

where x_i is the mole fraction. The pure component co-volume is obtained from the component critical pressure and temperature, p_c and T_c:

$$b_i = 0.08664 \frac{RT_{c,i}}{p_{c,i}}. \tag{6.71}$$

The pure component energy parameter, a_i, is obtained from

$$a_i = 0.4286 \frac{\left(RT_{c,i}\right)^2}{p_{c,i}} \beta_i^2, \tag{6.72}$$

where

$$\beta_i = 1 + m_i \left(1 - \sqrt{T_{r,i}}\right) \tag{6.73}$$

and where $T_{r,i}$ is the reduced temperature and m_i is a function of the acentric factor of component i

$$m_i = 0.48 + 1.574\omega_i - 0.176\omega_i^2. \tag{6.74}$$

Instead of equation (6.73), Mathias and Copeman (1983) parameters may be used

$$\beta_i = \begin{cases} 1 + C_{1,i}\left(1 - \sqrt{T_{r,i}}\right) + C_{2,i}\left(1 - \sqrt{T_{r,i}}\right)^2 + C_{3,i}\left(1 - \sqrt{T_{r,i}}\right)^3, & T_{r,i} < 1 \\ 1 + C_{1,i}\left(1 - \sqrt{T_{r,i}}\right), & T_{r,i} > 1 \end{cases}, \tag{6.75}$$

where $C_{1,i}$, $C_{2,i}$, and $C_{3,i}$ are pure component parameters. A list of Mathias–Copeman parameters for the SRK are given by Dahl *et al.* (1991).

The excess Gibbs energy model is introduced into the mixing rule through the excess Helmholtz energy of mixing, A^E

$$\frac{A^E}{nRT} = -\sum_i x_i \ln\left(\frac{v - b}{v_i - b_i}\right) + \frac{a}{bRT} \ln\left(\frac{v}{v + b}\right) - \sum_i x_i \frac{a_i}{b_i RT} \ln\left(\frac{v_i}{v_i + b_i}\right), \tag{6.76}$$

where n is the total number of moles. The excess Gibbs energy and the excess Helmholtz energy are equal at zero and infinite pressures. The equation of state is forced to reproduce the behavior of the excess Gibbs energy model by setting the EOS mixture parameter a at a reference pressure with equation

$$\left(\frac{g^E}{RT}\right)_{EOS} = \left(\frac{g^E}{RT}\right)_{AM}, \tag{6.77}$$

where g^E is the molar excess Gibbs energy, and subscripts EOS and AM denote g^E expression of the equation of state and the activity coefficient model respectively. The zero pressure approach is applied in the MHV2 model and then the molar excess Gibbs energy from the equation of state can be written

$$\left(\frac{g^E}{RT}\right)_{EOS} = -\sum_i x_i \ln\left(\frac{b}{b_i}\right) + Q(\alpha) - \sum_i x_i Q(\alpha_i), \tag{6.78}$$

where

$$\alpha = \frac{a}{bRT} \text{ and} \tag{6.79}$$

$$Q(\alpha) = -1 - \ln(u-1) - \alpha \ln\left(\frac{u+1}{u}\right), \tag{6.80}$$

and where u is the solution obtained from the equation of state, v/b, at zero pressure

$$u = \frac{1}{2}\left[\alpha - 1 - \sqrt{(\alpha^2 - 6\alpha + 1)}\right]. \tag{6.81}$$

The mixture parameter α is given implicitly at zero pressure by equation

$$Q(\alpha) = \sum_i x_i Q(\alpha_i) + \sum_i x_i \ln\left(\frac{b}{b_i}\right) + \left(\frac{g^E}{RT}\right)_{AM}, \tag{6.82}$$

which can be approximated according to Dahl and Michelsen (1990) MHV2 as

$$Q(\alpha) = q_0 + q_1\alpha + q_2\alpha^2, \tag{6.83}$$

where the values of q_0, q_1, and q_2 for the SRK are 0, -0.478, and -0.0047 respectively. The substitution of the above approximation to equation (6.82) results in the MHV2 mixing rule (Dahl and Michelsen, 1990)

$$q_1\left(\alpha - \sum_i z_i\alpha_i\right) + q_2\left(\alpha^2 - \sum_i z_i\alpha_i^2\right) = \sum_i x_i \ln\left(\frac{b}{b_i}\right) + \left(\frac{g^E}{RT}\right)_{AM}. \tag{6.84}$$

The fugacity coefficient, φ_i, both for vapor and liquid is given by

$$\ln\varphi_i = \ln\left[\frac{RT}{p(v-b)}\right] + \left(\frac{1}{v-b} - \frac{\alpha}{v+b}\right)b_i - \ln\left(\frac{v+b}{v}\right)\left(\frac{\partial(n\alpha)}{\partial n_i}\right)_{T,n_j}. \tag{6.85}$$

The composition derivative $\left(\partial(n\alpha)\big/\partial n_i\right)_{T,n_j}$ is obtained from the MHV2 mixing rule by

$$\left(\frac{\partial(n\alpha)}{\partial n_i}\right)_{T,n_j} = \left[q_1\alpha_i + q_2\left(\alpha^2 + \alpha_i^2\right) + \ln\gamma_i - \ln\left(\frac{b_i}{b}\right) + \frac{b_i}{b} - 1\right]\frac{1}{(q_1 + 2\alpha q_2)}, \tag{6.86}$$

where γ_i is the activity coefficient of component i in the mixture.

6.4 UNIFAC AND UNIFAC-FV

Fredenslund *et al.* (1975) introduced the UNIFAC group-contribution model to predict liquid phase activity coefficients. The activity coefficient of a solvent in a solution is formed from combinatorial and residual contributions to the activity coefficient γ_i

$$\ln \gamma_i = \ln \gamma_i^C + \ln \gamma_i^R , \tag{6.87}$$

where superscripts C and R stand for the combinatorial and residual contributions respectively.

Polymer chains in a mixture reduce the free volume of the system. This reduction is not explicitly taken into account in the UNIFAC model, and hence predicted solvent activities tend to be lower than experimentally observed values. The predictions were improved when Oishi and Prausnitz (1978) included the free volume contribution to the solvent activity

$$\ln \gamma_i = \ln \gamma_i^C + \ln \gamma_i^R + \ln \gamma_i^{FV} \quad , \tag{6.88}$$

where superscript FV stands for free volume contribution. This model is known as the UNIFAC-FV model.

6.4.1 Combinatorial contribution

The Staverman–Guggenheim combinatorial part accounts for size and shape differences and uses only pure component properties

$$\ln \gamma_i^C = \ln \frac{\phi_i}{x_i} + \frac{z}{2} q_i \ln \frac{\theta_i}{\phi_i} + l_i - \frac{\phi_i}{x_i} \sum_j x_j l_j , \tag{6.89}$$

where x_i is the mole fraction of component i in the solution, q_i is the surface area parameter of component i, l_i is a parameter for component i, θ_i is the molecular area fraction of component i, and z is the coordination number, usually $z = 10$. The molecular volume fraction ϕ_i is given by

$$\phi_i = \frac{r_i x_i}{\sum_j r_j x_j} , \tag{6.90}$$

where r_i is the volume parameter for component i

$$r_i = \sum_k \nu_k^{(i)} R_k , \tag{6.91}$$

and where R_k is the group volume parameter for group k, $\nu_k^{(i)}$ is the number of groups of type k in molecule i, and subscript k is the group index. The molecular area fraction θ_i for component i is given by

$$\theta_i = \frac{q_i x_i}{\sum_j q_j x_j} \tag{6.92}$$

and the parameter l_i

$$l_i = \frac{z}{2}(r_i - q_i) - (r_i - 1)\,. \tag{6.93}$$

The surface area parameter q_i is determined by

$$q_i = \sum_k \nu_k^{(i)} Q_k\,, \tag{6.94}$$

where Q_k is the group area parameter for group k. The group parameters, R_k and Q_k are obtained from the van der Waals group volume and surface areas, V_{wk} and A_{wk}, as given by Bondi (1968, pp. 450-452)

$$R_k = \frac{V_{wk}}{15.17} \text{ and} \tag{6.95}$$

$$Q_k = \frac{A_{wk}}{2.5\cdot 10^9}\,, \tag{6.96}$$

where the normalization factors, 15.17 and $2.5\cdot10^9$, are determined by the volume and the external surface area of the CH_2 unit in polyethylene. The original UNIFAC group volume and surface area parameters are available by Fredenslund *et al.* (1975) and Hansen *et al.* (1991).

6.4.2 Residual contribution

The residual activity coefficient contribution accounts for group interactions and is given by

$$\ln \gamma_i^R = \sum_k \nu_k^{(i)} \left[\ln \Gamma_k - \ln \Gamma_k^{(i)}\right], \tag{6.97}$$

where Γ_k is the residual activity coefficient of group k in the defined solution at the given temperature and $\Gamma_k^{(i)}$ is the residual activity coefficient of group k in the reference solution containing pure component i at the given temperature. The residual activity coefficient of group k both in the defined solution and in the reference solution is given by equation

$$\ln \Gamma_k = Q_k \left[1 - \ln\left(\sum_{m=1}^{ng} \theta_m \psi_{mk} \right) - \sum_{m=1}^{ng} \left(\frac{\theta_m \psi_{km}}{\sum_{k=1}^{ng} \theta_k \psi_{km}} \right) \right], \tag{6.98}$$

where ng is the number of groups in the solution, ψ_{mk} is the group interaction parameter between groups m and k, and θ_m is the group surface area fraction of group m in the given solution

$$\theta_m = \frac{Q_m X_m}{\sum_{k=1}^{ng} Q_k X_k}, \tag{6.99}$$

and where X_m is the mole fraction of group m in the solution

$$X_m = \frac{\sum_{j=1}^{nc} \nu_{mj} x_j}{\sum_{j=1}^{nc} \sum_{k=1}^{ng} \nu_{kj} x_j}. \tag{6.100}$$

The group interaction parameter function ψ_{mn} is determined for each possible binary group pair m and n by the equation

$$\psi_{mn} = \exp\left(-a_{mn} / T\right), \tag{6.101}$$

where a_{mn} is the group interaction parameter resulting from the interaction of main groups m and n, and T is the temperature in Kelvin. The interaction parameter is not usually symmetric, so that $a_{mn} \neq a_{nm}$. The original UNIFAC group interaction parameters are available by Fredenslund *et al.* (1975) and Hansen *et al.* (1991).

6.4.3 Free volume contribution

The free volume contribution to the activity of component i is obtained by using the Flory equation of state with the simplification that the Flory interaction parameter, χ_{ij}, is zero (Oishi and Prausnitz, 1978)

$$\ln \gamma_i^{FV} = 3\vartheta_i \ln\left[\frac{\left(\tilde{v}_i^{1/3} - 1\right)}{\left(\tilde{v}^{1/3} - 1\right)} \right] - \vartheta_i \left[\left(\frac{\tilde{v}_i}{\tilde{v}} - 1 \right) \left(1 - \frac{1}{\tilde{v}_i^{1/3}} \right)^{-1} \right], \tag{6.102}$$

where ϑ_i is the external degree of freedom parameter for solvents (=1.1). The reduced volume, $\tilde{v}_i$, is given by

$$\tilde{v}_i = \frac{v_i}{15.17 c r_i}, \tag{6.103}$$

where v_i is the molar volume of component i in units of cm^3/mol and c is the proportionality factor. Oishi and Prausnitz (1978) found the best agreement on calculated activities with experimental activities for solvents in polymer solutions with c = 1.28. The reduced volume of the mixture is obtained from equation

$$\tilde{v} = \frac{\sum_j v_j x_j}{15.17 c \sum_j r_j x_j}. \tag{6.104}$$

6.5 LYNGBY MODIFIED UNIFAC

Kikic *et al.* (1980) modified the Staverman–Guggenheim combinatorial term, equation (6.89), and proposed a new form

$$\ln \gamma_i^c = \ln \phi_i' + 1 - \frac{\phi_i'}{x_i} - \frac{z}{2} q_i \left[\ln\left(\frac{\phi_i}{\theta_i}\right) + 1 - \frac{\phi_i}{\theta_i} \right], \tag{6.105}$$

where ϕ and θ are the volume and surface area fractions, as in the original UNIFAC, and ϕ_i' is given by

$$\phi_i' = \frac{x_i r_i^{2/3}}{\sum_j x_j r_j^{2/3}}. \tag{6.106}$$

Kikic *et al.* (1980) chose the volume exponent of 2/3 on the basis of comparison with experimental results for a large number of mixtures of aliphatic hydrocarbons. The combinatorial term, equation (6.105), can be seen as a combination of the modified Flory–Huggins combinatorial of Donohue and Prausnitz (1975) and the Staverman–Guggenheim correction. According to Kikic *et al.* (1980), the modification resulted in improved predictions of activity coefficients in mixtures containing saturated hydrocarbons. Physically reasonable UNIFAC group interaction parameters for olefins and benzene were also obtained and the fit to experimental data was somewhat improved. Furthermore, the modification introduced no adverse effects for mixtures containing strongly interacting functional groups.

Larsen *et al.* (1987) adapted the combinatorial part of Kikic *et al.* (1980) into the Lyngby modified UNIFAC in the form

$$\ln \gamma_i^C = \ln \phi_i^{'} + 1 - \frac{\phi_i^{'}}{x_i}. \tag{6.107}$$

Thus, the combinatorial activity coefficient is then given without the Staverman–Guggenheim correction. The residual part is calculated as in the original UNIFAC by Fredenslund *et al.* (1975), except that the interaction parameters are temperature dependent (Larsen *et al.*, 1987)

$$a_{mn} = a_{mn,1} + a_{mn,2}\left(T - T_0\right) + a_{mn,3}\left[T \ln\left(\frac{T_0}{T}\right) + T - T_0\right], \tag{6.108}$$

where $a_{mn,1}$, $a_{mn,2}$, and $a_{mn,3}$ are the interaction parameter coefficients and T_0 is the reference temperature. The Lyngby modified UNIFAC is used in the MHV2 model with the gas groups extension by Dahl *et al.* (1991). As in the UNIFAC model, the interaction parameters are generally not symmetric, so that $a_{mn,1} \neq a_{nm,1}$, $a_{mn,2} \neq a_{nm,2}$, and $a_{mn,3} \neq a_{nm,3}$.

6.6 EXPONENTIAL UNIFAC FOR POLYMERS

Donohue and Prausnitz (1975) proposed the idea of the exponential volume fraction in the form

$$\phi_i^{'} = \frac{x_i r_i^{\zeta}}{\sum_j x_j r_j^{\zeta}} \tag{6.109}$$

and included it into the combinatorial Flory–Huggins entropy expression in order to combine the ideal solution and Flory–Huggins expressions into one form. Donohue and Prausnitz (1975) stated that the exponent ζ is a function of the ratio of the external surface area q to volume r and it is a measure of the molecules' shape. For a monomer, the exponent is one and when the volume becomes very large, it approaches the value of 2/3 for a linear chain and zero for a sphere. If the exponent in the volume fraction is allowed to lie between zero and one, the combinatorial excess Gibbs energy $g^{E,C}$ from equation (6.107)

$$\frac{g^{E,C}}{RT} = \sum_i x_i \ln \frac{\phi_i^{'}}{x_i} \tag{6.110}$$

has theoretical limits of the ideal solution and the Flory–Huggins combinatorial expression.

Polymer solutions are strongly non-ideal, but the Flory–Huggins expression tends to underestimate the solvent activity coefficient in a solution, since the free volume effects are not included due to incompressibility of the lattice vacancies. Thus, the actual combinatorial excess Gibbs energy lies between the ideal solution and the Flory–Huggins expressions.

In polymer–solvent systems, the polymer molecules gain freedom to exercise their rotational and vibrational motions, whereas the solvent molecules partially loose such freedom (Reid *et al.*, 1987). The Lyngby modified UNIFAC is successful for solutions of small molecules, but the model overestimates the solvent activity coefficients in polymer solutions. In order to include the free volume effects in the modified Flory–Huggins combinatorial term properly, a system dependent exponent is required. Previously, Kontogeorgis *et al.* (1994a) and Voutsas *et al.* (1995) proposed such models. Kontogeorgis *et al.* (1994a) used the Flory–Huggins combinatorial and proposed a system dependent exponent in the form

$$\zeta = 1 - \frac{r_{small}}{r_{large}}. \tag{6.111}$$

Voutsas *et al.* (1995) used the Staverman–Guggenheim combinatorial with

$$\zeta = 0.9\left(1 - \frac{r_{small}}{r_{large}}\right), \tag{6.112}$$

where r_{small} and r_{large} are the pure component volume parameters of the short-chain and long-chain components of the binary mixture respectively. Equations (6.111) and (6.112) may be applied for binary mixtures.

A new exponential form may be proposed by following the original idea of Donohue and Prausnitz (1975) with

$$\zeta = \frac{1}{nc}\sum_i \frac{r_i}{q_i}\left(\frac{q}{r}\right)_{\min}, \tag{6.113}$$

where subscript min denotes the minimum q/r ratio that is used to scale r_i/q_i ratios of the system components. We may assume that a molecule with the lowest q/r ratio is the largest molecule of the system, which defines the packing of the molecules in the lattice. The largest molecule will then have a scaled r_i/q_i ratio equal to one and other molecules will have scaled r_i/q_i ratio smaller than one. As the exponent ζ is formed from the arithmetic average of the scaled pure component r_i/q_i ratios, the free volume effect is introduced into the combinatorial excess Gibbs energy expression and further on the component activities. Different weighting is obtained with the geometric average form

$$\zeta = \left[\prod_i \frac{r_i}{q_i} \left(\frac{q}{r} \right)_{\min} \right]^{1/nc} . \tag{6.114}$$

Equations (6.113) and (6.114) may be used both for binary and multicomponent mixtures. Composition dependent exponent ζ for multicomponent mixtures is excluded, since such exponential form of the combinatorial term does not obey the Gibbs–Duhem relation (Voutsas and Tassios, 1997).

7 MODEL PARAMETERIZATION AND VERIFICATION

The previous chapters provide the theoretical building blocks that form the basis for a unit operation model for vapor membrane separation with rubbery membranes. In this chapter, the individual model parts are verified against the experimental data. The equation of state models from chapter 6 are compared in the prediction and the correlation of binary solvent–liquid polymer equilibrium data and in the prediction of pure component sorption in a PDMS membrane in section 7.1. The diffusion coefficient equations from section 5.6 are used for the correlation of pure component diffusivities in a PDMS membrane in section 7.2. The transport equations for permeation from section 5.4 are then used with thermodynamic models to predict isothermal multicomponent permeation in a laboratory test cell in section 7.3.

7.1 MODELING OF BINARY SOLVENT–POLYMER EQUILIBRIUM

The binary equilibrium data by Covitz and King (1972), Schreiber *et al.* (1973), Lichtenthaler *et al.* (1974), Liu and Prausnitz (1977), Roth and Novak (1986), and Wohlfarth (1994) at infinite dilution is used as reference data for the prediction of Henry's law coefficients. The vapor sorption data by Noda *et al.* (1984) and Iwai and Arai (1989) is used for the evaluation of the equation of state models' capability to predict and correlate binary vapor–liquid equilibrium data. The gas and vapor sorption data in a PDMS membrane by De Angelis *et al.* (1999) is used for the evaluation of the models' capability to predict the experimental sorption curves without the binary interaction parameters. Table 7.1 characterizes the polymers in the reference systems; De Angelis *et al.* (1999) did not provide molecular weight data and hence the molecular weight of PDMS is not reported in Table 7.1.

The lattice and nonlattice fluid versions of the Sanchez–Lacombe equation of state, the perturbed hard-sphere-chain equation of state, and the routines to compute vapor sorption equilibrium at infinite dilution and finite concentrations were coded in Fortran. The models were incorporated into the in-house process simulator (FLOWBAT, 2001). The combined SRK–group-contribution activity coefficient models were obtained by modifying the source codes of the MHV2 and the original UNIFAC in the FLOWBAT simulator.

Table A.1 presents the equation of state parameters for the Sanchez–Lacombe EOS and Table A.2 for the perturbed hard-sphere-chain EOS. Both tables are found in appendix I. Most of the parameters were collected from the literature. The missing EOS parameters for normal

components were determined by minimizing the sum of squares of the relative deviation between the calculated and the experimental saturation vapor pressure and liquid density data from the DIPPR databank (Danner and Gess, 1990). The parameters of the perturbed hard-sphere-chain equation of state for the PDMS were determined from the *pVT* data (Danner and High, 1993) by minimizing the sum of squares of the relative deviation between the calculated and experimental specific density for the different molecular weight samples.

Table 7.1 Molecular weights of polymers in the reference systems.

	$\overline{M}_n$, g/mol	$\overline{M}_w$, g/mol	Ref.
HDPE	-	105 000	Schreiber *et al.* (1973)
LDPE	-	82 000	Schreiber *et al.* (1973)
PP	94 100	461 000	Wohlfarth (1994)
PVAC	83 400	-	Liu and Prausnitz (1977)
PDMS	20 700	95 300	Roth and Novak (1986)
PIB	-	53 000[a)]	Lichtenthaler *et al.* (1974)
PS	63 000	-	Noda *et al.* (1984)
	53 700	247 000	Iwai and Arai (1989)
	96 200	97 600	Covitz and King (1972)
PcB	-	200 000-300 000	Iwai and Arai (1989)

[a)] Viscosity average molecular weight.

The Sanchez–Lacombe and the PHSC are three-parameter equation of state models but only two residual functions may be formed with the saturation vapor pressure and the liquid density data. In order to find the global optimum for the three equation of state parameters, a set of equation of state parameters in local optimum were searched for a number of constant *r*-values in a bounded range. The optimization was then continued from the point of the lowest residual for a number of new *r*-values. The densification of the bounded range was repeated until the chance in the *r*-value became insignificant. For the Sanchez–Lacombe equation of state, the constant *r*-value fixes the relation between the equation of state parameters via equation (6.9). Then the two equation of state parameters to be optimized were T_i^* and P_i^* for the Sanchez–Lacombe equation of state and ε_i / k_B and σ_i for the perturbed hard-sphere-chain equation of state. In the parameterization of the Sanchez–Lacombe equation of state, two sets of EOS parameters were determined for ethane, propane, and propylene. One set was determined from the low-pressure experimental data and the another from the high-pressure experimental data, because all predictions of the Sanchez–Lacombe equation of state are sensitive to the equation of state parameters of the solvent (Hariharan *et al.*, 1993).

The parameterization of the perturbed hard-sphere-chain equation of state for hydrogen was extremely difficult. The parameterization resulted in an average relative deviation of 7.9% for the saturated liquid density and 20.5% for the saturation pressure. Far better results were obtained in the parameterization of other components. For example, the parameterization of the PHSC for nitrogen resulted in an average relative deviation of 0.9% for the saturated liquid density and 0.6% for the saturation pressure. The large residuals indicate that PHSC did not completely fit in the experimental data for hydrogen.

FLOWBAT includes routines to calculate the physical properties of process flows from the flowsheet. These routines may be invoked via a namelist, "FYSPRO". A new property option, "GSISOT", was created for the calculation of gas and vapor sorption isotherms in polymers. For the new property option, the user has to define the polymer name, the molecular weight, the molecular weight distribution, and the thermodynamic model to be used in the property calculation. The UNIFAC groups and equation of state parameters for a number of common polymers were hard-coded into the model, and hence the polymer parameters are retrieved based on the user given polymer specification. Only the solvent functional groups for the UNIFAC models have to be given in the FYSPRO namelist.

The SRK equation of state parameters for normal components were determined from the critical properties obtained from the FLOWBAT (2001) databank. Polymers do not have critical properties, and hence the EOS parameters for polymers were determined from the volumetric data following Kontogeorgis *et al.* (1994b). The SRK equation of state parameters for each polymer were determined from polymer molar volumes v_1 and v_2 at temperatures T_1 and T_2 with equations

$$R\left\{b^2+\left[\frac{v_1v_2(T_2-T_1)+T_1v_1^2-T_2v_2^2}{T_1v_1-T_2v_2}\right]b-v_1v_2\right\}=0 \text{ and} \tag{7.1}$$

$$a=\frac{RT_1\left(v_1^2+bv_1\right)}{\left(v_1-b\right)}, \tag{7.2}$$

where T has units in Kelvin and b and v have units in cubic meters per mole. The required specific volumes of polymers at two different temperatures in the vicinity of each experimental temperature point were obtained from the Tait equation with parameters given by Rodgers (1993). The exponential form of the Tait equation (Rodgers, 1993) can be used to extrapolate beyond the temperature limits of the experimental data, when the thermal expansion coefficient for the polymer is assumed to be constant in a wide temperature range.

Such extrapolation using the polynomial form may be dangerous. Therefore, the perturbed hard-sphere-chain equation of state (Song *et al.*, 1994a) was used with the parameters given in Table A.2 in appendix I when the temperature limits of the polynomial Tait equation were exceeded. The number average molecular weight was used to convert the specific volumes to molar volumes. Table 7.2 presents examples of polymer parameters for the SRK equation of state.

Table 7.2 SRK equation of state parameters for polymers and examples of α values.

Polymer	T K	a J m^3/mol^2	b m^3/mol	α -
HDPE	418.55	2203.9	0.05414	11.698
LDPE	393.15	877.8	0.03485	7.706
PP	448.25	4895.9	0.10221	12.853
PVAC	393.15	2032.4	0.05891	10.554
PDMS	313.15	512.1	0.01731	11.363
PIB	348.15	1051.9	0.02519	14.426
PS	396.45	3736.6	0.08040	14.099
PcB	296.65	2201.7	0.06167	14.475

The SRK energy parameter a for the polymer–solvent mixture was obtained from the MHV2 mixing rule as described in section 6.3. The required excess Gibbs energy expression was calculated from the UNIFAC-FV model (section 6.4) and from the proposed exponential UNIFAC model (section 6.6). These combinations are denoted by SRK1 and SRK2 respectively. The solvent liquid molar volumes for the UNIFAC-FV model were calculated from the Racket equation (Reid *et al.*, 1987, p. 67) with parameters from the FLOWBAT databank. The solvent liquid molar volumes are not needed in the exponential UNIFAC model. The exponent ζ of the volume fraction expression in the exponential UNIFAC model was calculated by using the arithmetic average of the scaled pure component r_i / q_i ratios, equation (6.113).

The polymer–solvent systems were considered to be athermal mixtures so that the residual excess Gibbs energy becomes zero and no interaction parameters are required. This assumption was used for all polymer–solvent systems considered, since the combinatorial contribution and the free volume contribution mainly describe the solvent activity at infinite dilution. The UNIFAC-FV provides activity coefficients that increase with temperature due to the free volume contribution, whereas the proposed exponential UNIFAC modification provides temperature independent activity coefficients.

The Newton-Raphson method was used to compute the polymer phase composition at known p and T. Equation (5.10) was used to determine the equilibrium condition between the polymer and the solvent phases with the Sanchez–Lacombe and the PHSC equation of states. The species-specific constants ω_i cancel, when the lattice fluid chemical potentials from (6.29) are equilibrated with (5.10). Therefore, it is not needed to specify the value of ω_i for the equilibrium calculation. The equilibrium condition (5.11) was applied for the SRK equation of state.

Most of the infinite dilution equilibrium data in paragraph 7.1.1 were reported in terms of experimental specific retention volumes V_g^0. In these cases, the weight fraction based Henry's constants were calculated from the specific retention volumes by equation

$$H_{exp.}^{w} = \frac{RT^0}{V_g^0 M_1}, \tag{7.3}$$

where T^0 is the normal temperature 273.15 K, and M_1 is the molecular weight of the solvent. The predicted weight fraction based Henry's constants were calculated from equation (5.18). The deviation between the calculated and experimental Henry's coefficients was then evaluated from the average absolute deviation for each polymer–solvent system

$$AAD = \frac{1}{DP}\sum_{i=1}^{DP}\frac{\left|H_{i,pred.}^{w} - H_{i,\exp.}^{w}\right|}{H_{i,\exp.}^{w}}, \tag{7.4}$$

where DP is the number of data points. An example of a simulation input file is given in appendix III.

The simulation results for the vapor sorption in paragraph 7.1.2 were obtained by fitting a binary interaction parameter for each polymer–solvent pair at one temperature by minimizing the absolute average deviation between the experimental and the calculated solvent weight fraction in the polymer phase. The fitted binary parameters were then used at other temperatures to study the models' capability to describe the temperature dependence of the phase behavior. The PHSC model has two adjustable binary parameters: the energy interaction parameter k_{ij} and the size correction parameter l_{ij}, equations (6.54) and (6.55). However, either the energy interaction or the size correction parameter was used; the one with the best fit was chosen in each case. The SRK models were further utilized as predictive models with the assumption of athermal polymer–solvent solutions. Therefore, the SRK1 and the SRK2 models are expected to provide reasonable predictions only for systems containing

similar segment structures. An example of a simulation input file for the vapor sorption computation is provided in appendix IV.

The concentration of gases and hydrocarbon vapors in the PDMS membrane in paragraph 7.1.3 was calculated with the Sanchez–Lacombe equation of state and the perturbed hard-sphere-chain equation of state, as described in section 5.2, with the parameters given in Table A.1 and Table A.2. No binary interaction parameters were used in these calculations. The high-pressure range parameters were used for the Sanchez–Lacombe equation of state. The equilibrium concentration in the units of volume of ideal gas sorbed per unit volume of polymer was computed from the solvent weight fraction by equation

$$C_1 = \frac{RT^0}{p^0}\frac{\rho_2 w_1}{M_1 w_2}, \tag{7.5}$$

where T^0 and p^0 are the normal temperature and pressure respectively. An example of a simulation input file for the calculation of gas and vapor sorption in the PDMS membrane is given in appendix V.

7.1.1 Sorption at infinite dilution

Tables 7.3-7.9 provide the absolute average percentage deviations between the calculated and the experimental weight fraction based Henry's constants for solvents in polymers. In these tables, SLLF denotes the lattice fluid version and SLNLF the non-lattice fluid version of the Sanchez–Lacombe equation of state. PHSC is used as an abbreviation for the perturbed hard-sphere-chain equation of state, SRK1 for the combined SRK–UNIFAC-FV model, and SRK2 for the combined SRK–exponential UNIFAC modification with equation (6.113). Some of the experimental Henry's constants are corrected for the carrier gas sorption, while some are not. According to Liu and Prausnitz (1977), the correction is necessary only for low sorption gases, such as ethane and ethylene. The effect of the correction lies within the experimental error for hydrocarbons of a higher sorption level.

As a summary, the mean values of the average AAD values from tables 7.3-7.9 are calculated into Table 7.10. The mean values are calculated separately for the solvent vapors and the gases in order to observe the differences between the models' predictions. There is no calculated mean value for the gases with SRK1 since the original UNIFAC model does not have groups for the gases.

Table 7.3 Results of vapor sorption predictions at infinite dilution in HDPE at temperature range 418.55-426.45 K. Henry's constants calculated from the specific retention volumes reported by Schreiber *et al.* (1973) are not corrected for the carrier gas sorption.

Solvent	DP	AAD, % SLLF	AAD, % SLNLF	AAD, % PHSC	AAD, % SRK1	AAD, % SRK2
Decane	2[a]	5.2	25.4	322.3	28.7	23.9
Dodecane	2[a]	11.1	35.3	391.8	29.3	26.2
Ethylbenzene	2[b]	10.0	18.6	38.2	23.4	21.7
Nonane	2[b]	3.7	17.2	305.3	24.4	23.5
Octane	2[b]	2.4	16.0	277.5	17.6	22.0
Toluene	2[b]	14.3	20.4	21.6	20.4	20.3
m-xylene	2[b]	18.3	21.1	40.7	22.6	18.0
p-xylene	2[b]	16.2	18.4	43.4	20.0	15.8
Total average		10.1	21.6	180.1	23.3	21.4

[a] Temperatures 418.45 and 426.45 K.
[b] Temperatures 418.45 and 425.45 K.

Table 7.4 Results of vapor sorption predictions at infinite dilution in LDPE at temperature range 393.15-418.35 K. Henry's constants calculated from the specific retention volumes reported by Schreiber *et al.* (1973) are not corrected for the carrier gas sorption.

Solvent	DP	AAD, % SLLF	AAD, % SLNLF	AAD, % PHSC	AAD, % SRK1	AAD, % SRK2
Decane	2	10.0	2.1	548.2	31.3	27.2
Dodecane	2	2.4	1.3	690.9	33.0	29.7
Ethylbenzene	2	1.0	12.9	51.5	27.6	26.4
Nonane	2	12.8	4.5	498.4	27.2	26.8
Octane	2	19.0	3.6	431.4	21.4	25.9
Toluene	2	4.3	13.3	32.3	23.8	24.1
m-xylene	2	9.4	17.3	58.0	26.0	21.9
p-xylene	2	8.9	16.9	53.6	24.9	21.2
Total average		8.5	9.0	295.5	26.9	25.4

Table 7.5 Results of vapor and gas sorption predictions at infinite dilution in PP at temperature range 448.2-523.2 K. Henry's constants from the Wohlfarth (1994) data collection are corrected for the carrier gas sorption.

Solvent	DP	AAD, % SLLF	AAD, % SLNLF	AAD, % PHSC	AAD, % SRK1	AAD, % SRK2
Pentane	4	166.4	38.2	49.3	31.4 (1)[b]	21.9
Hexane	4	99.0	16.9	48.3	23.5 (3)[b]	11.3
Heptane	4	117.9	26.5	44.2	19.9	9.0
Octane	4	112.1	26.1	35.1	11.6	4.8
Cyclohexane	4	119.0	60.9	25.0	29.1	3.9
Benzene	4	36.9	32.9	19.8	5.9	4.7
Ethylbenzene	4	60.5	43.0	10.0	5.1	3.4
Nitrogen	4	1792.1	94.2	41.6	-	71.1[c]
Propane	3[a]	233.9	40.4	40.9	-	39.8[c]
Propylene	3[a]	239.9	42.3	24.1	-	33.1[c]
Butane	3[a]	251.9	55.5	49.1	-	28.4[c]
Vapors average		101.7	34.9	33.1	18.1	8.4
Gases average		629.4	58.1	38.9	-	43.1
Total average		293.6	43.4	35.2	18.1	21.1

[a] Maximum temperature 498.2 K.
[b] Calculated data points in parenthesis.
[c] MHV2 group volume and area parameters were divided by two.

Table 7.6 Results of vapor sorption predictions at infinite dilution in PDMS at temperature range 313.15-353.15 K. Henry's constants calculated from the specific retention volumes reported by Roth and Novak (1986) are not corrected for the carrier gas sorption.

Solvent	DP	AAD, % SLLF	AAD, % SLNLF	AAD, % PHSC	AAD, % SRK1	AAD, % SRK2
Pentane	5	27.5	28.3	4.5	11.5	6.7
Hexane	5	30.6	30.6	3.8	19.0	12.8
Heptane	5	36.5	36.5	10.6	25.7	19.2
Octane	5	37.7	38.2	19.5	32.1	26.0
Cyclohexane	5	36.1	27.0	31.6	33.4	23.6
Average		33.7	32.1	14.0	24.3	17.7

Table 7.7 Results of vapor sorption predictions at infinite dilution in PS at temperature range 396.45-447.45 K. Henry's constants calculated from the weight fraction activity coefficients reported by Covitz and King (1972) are not corrected for the carrier gas sorption.

Solvent	DP	AAD, % SLLF	AAD, % SLNLF	AAD, % PHSC	AAD, % SRK1	AAD, % SRK2
Carbon tetrachloride	3	9.1	23.7	114.3	33.7	22.5
Chlorobenzene	3	3.5	4.3	90.3	7.5	-[a]
o-xylene	3	6.7	10.5	167.6	6.7	5.4
m-xylene	3	8.9	12.5	198.7	4.9	5.7
p-xylene	3	10.4	11.3	217.0	5.0	3.4
Styrene	3	-	-	133.0	1.9	3.2
Benzene	3	30.0	5.1	102.0	17.1	5.0
Toluene	3	25.6	2.4	156.8	10.8	3.3
Ethylbenzene	3	36.4	4.5	215.5	6.8	3.2
MEK	3	11.2	30.8	42.2	15.3	8.0
1,4-dioxane	3	24.2	21.2	-	8.1	14.1
Propylbenzene	3	-	-	282.6	3.9	8.0
Total average		16.6	12.6	156.4	10.1	7.4

[a] Groups not available.

Table 7.8 Results of vapor and gas sorption predictions at infinite dilution in PVAC at temperature range 393.15-473.15 K. Henry's constants from Liu and Prausnitz (1977) are corrected for the carrier gas sorption.

Solvent	DP	AAD, % SLLF	AAD, % SLNLF	AAD, % PHSC	AAD, % SRK1	AAD, % SRK2
Acetone	4	8.4	15.4	39.0	11.4	2.7
MEK	4	18.5	19.0	64.4	4.3	4.2
Methyl chloride	4	5.6	13.3	42.9	-[a]	-[a]
Vinyl acetate	4	-	-	-	5.0	30.4
Ethylene	4	73.3	3.7	77.4	-[a]	22.9[b]
Ethane	4	22.9	40.7	31.1	-[a]	44.3[b]
Carbon dioxide	4	69.3	5.7	6.5	-[a]	33.2[b]
Vapors average		10.8	15.9	48.7	6.9	12.4
Gases average		55.2	16.7	38.3	-	33.5
Total average		33.0	16.3	43.5	6.9	22.9

[a] Groups not available.

[b] MHV2 group volume and area parameters were divided by two.

Table 7.9 Results of vapor sorption predictions at infinite dilution in PIB at temperature range 348.15-398.15 K. Henry's constants calculated from the specific retention volumes reported by Lichtenthaler *et al.* (1974) are not corrected for the carrier gas sorption.

Solvent	DP	AAD, % SLLF	AAD, % SLNLF	AAD, % PHSC	AAD, % SRK1	AAD, % SRK2
Hexane	3	12.6	26.7	503.0	1.0	50.0
Cyclohexane	3	6.3	21.6	160.1	1.1	36.6
Benzene	3	39.0	39.1	22.4	19.4	46.0
Total average		19.3	29.2	228.5	7.2	44.2

For solvent vapors in polymers, SRK1 has the best prediction ability as may be seen from Table 7.10. The performance of SRK1 is generally better than SRK2 because the former is able to account for the temperature effect through the free volume contribution. However, a comparison of the AAD values in tables 7.3-7.9 reveals the variation in the models' performance from system to system. For example, SRK2 yields better predictions than SRK1 in the solvent–PP systems but the situation is reversed in the solvent–PIB and solvent–PVAC systems. SLNLF yields comparable results with SRK1 and SRK2 in HDPE but in LDPE the predictions of SLNLF are far better than the predictions of SRK1 and SRK2.

The poor performance of the lattice Sanchez–Lacombe EOS in the solvent–PP systems is somewhat peculiar when it is compared to the performance of the non-lattice Sanchez–Lacombe equation of state. The only explanation to this is the difference in the development picture, since a calculation of both models converged normally and both models use the same equation of state parameters. PHSC yields generally the poorest results, however, the predictions in the solvent–PDMS systems show better agreement than the other models.

Table 7.10 Mean values of the average AAD values for the thermodynamic models in the polymer–solvent systems.

	DP	Mean AAD, % SLLF	Mean AAD, % SLNLF	Mean AAD, % PHSC	Mean AAD, % SRK1	Mean AAD, % SRK2
Vapors	146	28.7	22.2	136.6	16.7	19.6
Gases	25	342.3	37.4	38.6	-	38.3
All	171	59.3	23.5	136.2	16.7	22.9

Earlier studies with non-polymer solutions have revealed that the performance of the MHV2 model becomes poorer as the asymmetry of the system increases (Boukouvalas *et al.*, 1994; Voutsas *et al.*, 1996). Since the MHV2 coefficients are selected to provide particularly accurate approximations in the α value range of 10-13, Michelsen (1996) associates the failure of the MHV2 model to α values that considerably exceed the above mentioned limits of α. Some α values for polymers in Table 7.2 fall outside the limits for accurate

approximations. Table 7.11 presents percentage AAD values between the experimental and the computed weight fraction based activity coefficients for solvents in polystyrene. The Lyngby modified UNIFAC gives unrealistically high weight fraction based activity coefficients, as already observed by Kontogeorgis *et al.* (1994a). The MHV2 model is not applicable for polymeric systems as such. The UNIFAC-FV model and the proposed exponential UNIFAC provide more realistic solvent activities in polymer solutions.

Table 7.11 Average absolute percentage deviation between the experimental and predicted weight fraction activity coefficients for solvents in PS at 396.45 K. The experimental weight fraction activity coefficients were used as reported by Covitz and King (1972).

Solvent	AAD, % Lyngby mod. UNIFAC	AAD, % UNIFAC-FV	AAD, % Exponential UNIFAC eq. (6.113)
Carbon tetrachloride	397.8	0.7	6.8
o-xylene	485.4	16.6	17.0
m-xylene	474.5	14.3	18.5
p-xylene	492.9	10.9	15.9
Styrene	564.5	6.7	9.2
Benzene	563.0	2.7	18.3
Toluene	531.6	6.4	15.8
Ethylbenzene	497.0	9.1	14.3
MEK	323.3	10.4	14.4
1,4-dioxane	470.8	11.1	5.0
Propylbenzene	434.1	15.2	18.7
Average	475.9	9.5	14.0

In gas sorption predictions, the models can be compared only in the PP and PVAC systems. Based on Table 7.10, SLNLF, PHSC, and SRK2 seem to produce gas sorption predictions with equal accuracy but again a comparison of the AAD values in the individual binary systems reveals the variation in the models' performance. Liu and Prausnitz (1977) reported an experimental error of 37% for the ethane sorption in PVAC at 200°C without the carrier gas correction and 15% with the carrier gas correction. Thus, the gas sorption predictions in Table 7.5 and Table 7.8 are mainly beyond the experimental error.

The gas sorption predictions with SRK2 were not successful with the original MHV2-UNIFAC group volume and area parameters by Dahl *et al.* (1991). For example, the AAD value for the nitrogen sorption in PP was 229% with the original MHV2-UNIFAC parameters. The predictions were improved when the original MHV2-UNIFAC group volume and area parameters for the gases were divided by two. This manipulation was performed due to the contrarious numerical manipulation with the preliminary values of the gas group volume and area parameters for the MHV2-UNIFAC model (Fredenslund and Soresen, 1994). The new group volume and area parameters for ethane, ethylene, carbon dioxide, and nitrogen

were observed to be equal to the group volume and area parameters used in the LCVM model (Spiliotis *et al*, 1994). The results for the gas sorption with SRK2 in Table 7.5 and Table 7.8 are computed with the new group volume and area parameters, and hence, e.g. the AAD value for nitrogen in PP reduced to 71%. As a comparison, the AAD values for the gas sorption in PP and PVAC were over 1000% with the MHV2 model of Dahl and Michelsen (1990).

7.1.2 Sorption in concentrated solutions

The correlated and predicted weight fractions of benzene and nonane in polystyrene are presented in Figures 7.1-7.7, and the weight fractions of ethylbenzene and nonane in poly(1,4-*cis*-butadiene) in Figures 7.8-7.13. The fitted parameters for the binary systems, the binary energy interaction parameter k_{ij} for the Sanchez–Lacombe equation of state, and the energy interaction parameter k_{ij} or the size correction parameter l_{ij} for the perturbed hard-sphere-chain equation of state, are presented in Table 7.12.

Table 7.12 The binary interaction parameters for the polymer–solvent systems.

Data from	System	Model	Fitted parameter	AAD, %	DP
Noda *et al.* (1984)	benzene–PS	SLLF	-0.0106	4.7	7
		SLNLF	0.0051	1.2	“
		PHSC[a)]	-0.0245[c)]	5.1	“
Iwai and Arai (1989)	nonane–PS	SLLF	0.0095	6.9	5
		SLNLF	0.0252	6.3	“
		PHSC[b)]	-0.0494	11.3	“
Iwai and Arai (1989)	ethylbenzene–PcB	SLLF	0.0102	1.7	12
		SLNLF	0.0096	1.7	“
		PHSC[a)]	-0.0275	1.6	“
Iwai and Arai (1989)	nonane–PcB	SLLF	0.0253	4.3	12
		SLNLF	0.0084	4.1	“
		PHSC[b)]	-0.0439	6.0	“

[a)] Size correction parameter
[b)] Energy interaction parameter
[c)] Gupta and Prausnitz (1996) reported a value of –0.024.

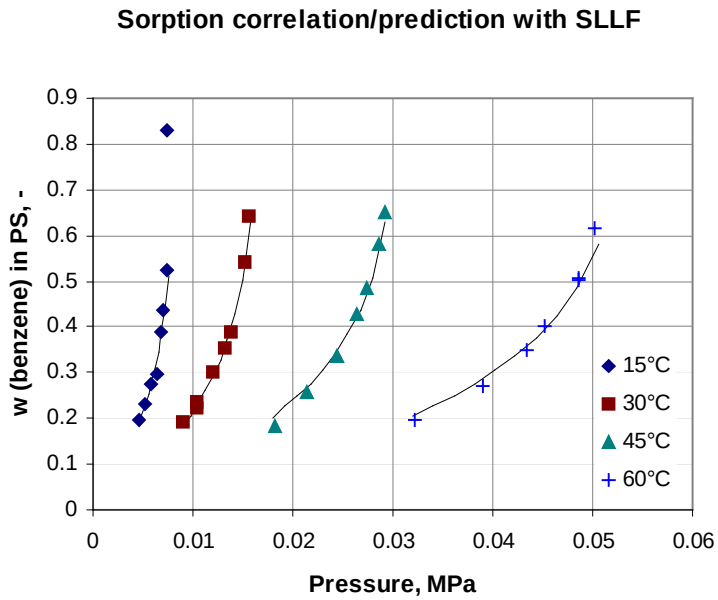

Figure 7.1 Correlation and prediction of benzene sorption in PS with the lattice Sanchez–Lacombe equation of state. The energy interaction parameter (k_{ij} = -0.0106) was fitted at 60°C, the same value was used at the other temperatures. The polymer number average molecular weight is 63 000 g/mole. Data from Noda *et al.* (1984).

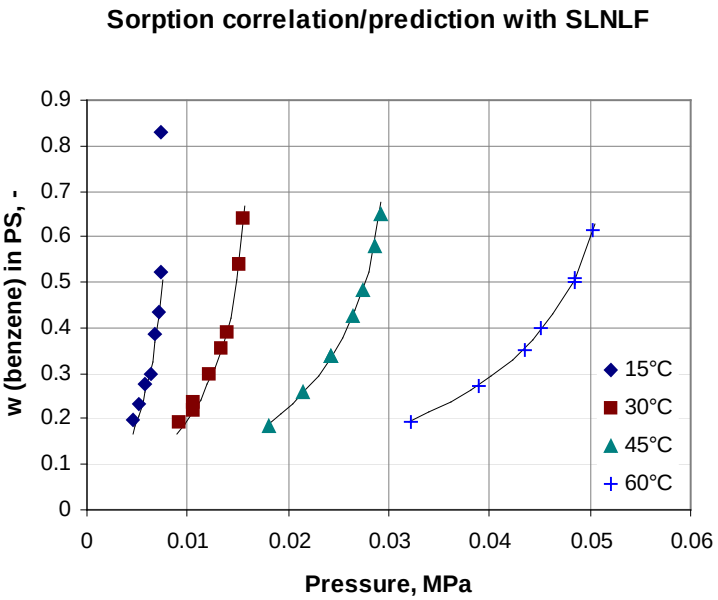

Figure 7.2 Correlation and prediction of benzene sorption in PS with the non-lattice Sanchez–Lacombe equation of state. The energy interaction parameter (k_{ij} = 0.0051) was fitted at 60°C, the same value was used at the other temperatures. The polymer number average molecular weight is 63 000 g/mole. Data from Noda *et al.* (1984).

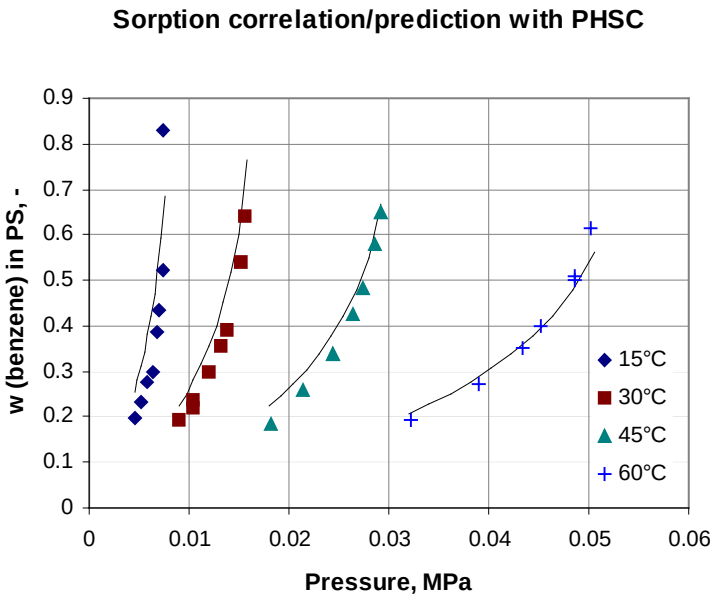

Figure 7.3 Correlation and prediction of benzene sorption in PS with the perturbed hard-sphere-chain equation of state. The size correction parameter (l_{ij} = -0.0245) was fitted at 60°C, the same value was used at the other temperatures. The polymer number average molecular weight is 63 000 g/mole. Data from Noda *et al.* (1984).

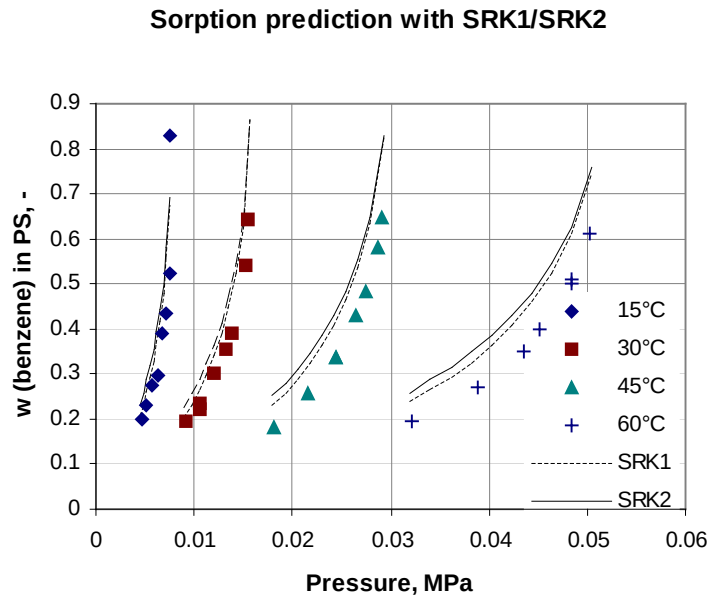

Figure 7.4 Prediction of benzene sorption in PS with SRK1 and SRK2. The polymer number average molecular weight is 63 000 g/mole. Data from Noda *et al.* (1984).

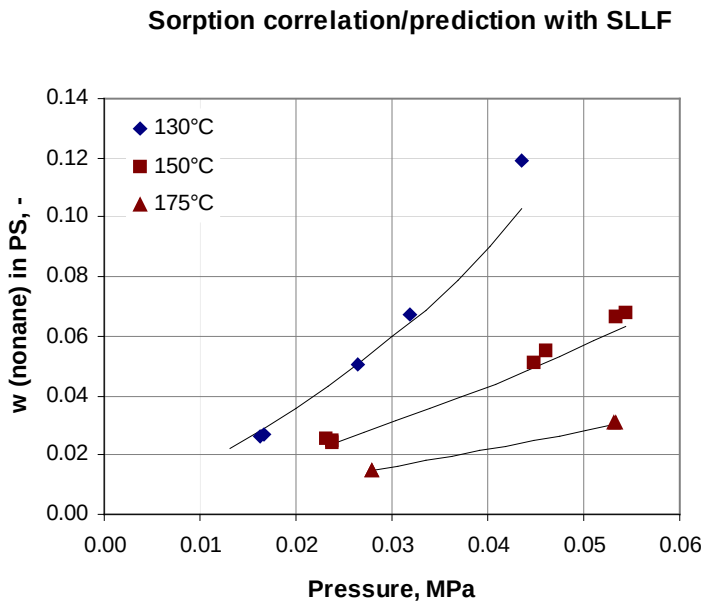

Figure 7.5 Correlation and prediction of nonane sorption in PS with the lattice Sanchez–Lacombe equation of state. The energy interaction parameter (k_{ij} = 0.0095) was fitted at 130°C, the same value was used at the other temperatures. The polymer number average and the weight average molecular weights are 53 700 g/mole and 247 000 g/mole respectively. Data from Iwai and Arai (1989).

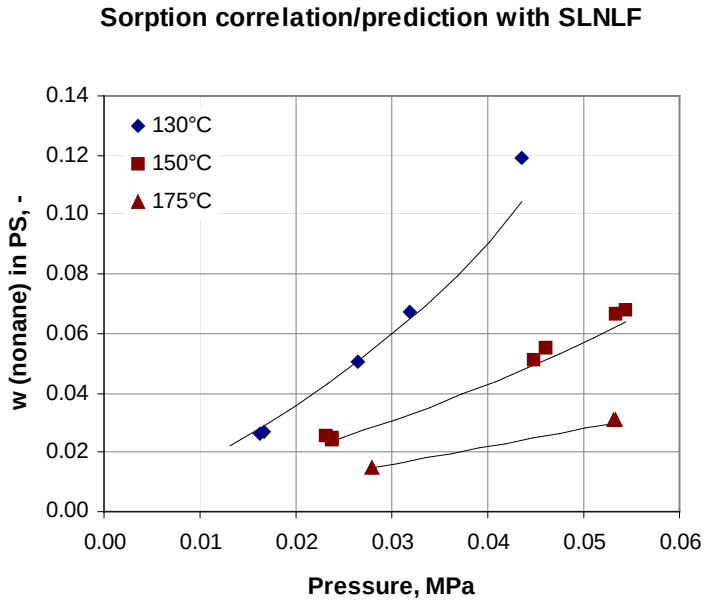

Figure 7.6 Correlation and prediction of nonane sorption in PS with the non-lattice Sanchez–Lacombe equation of state. The energy interaction parameter (k_{ij} = 0.0252) was fitted at 130°C, the same value was used at the other temperatures. The polymer number average and the weight average molecular weights are 53 700 g/mole and 247 000 g/mole respectively. Data from Iwai and Arai (1989).

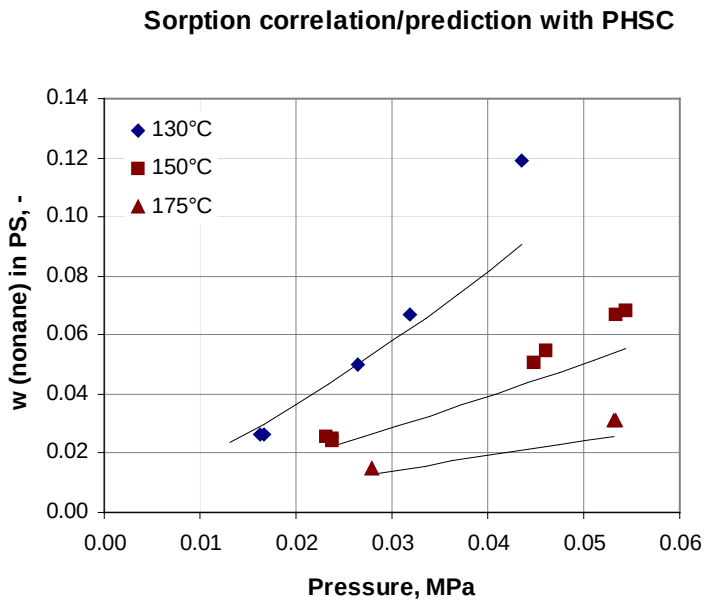

Figure 7.7 Correlation and prediction of nonane sorption in PS with the perturbed hard-sphere-chain equation of state. The energy interaction parameter (k_{ij} = -0.0494) was fitted at 130°C, the same value was used at the other temperatures. The polymer number average and the weight average molecular weights are 53 700 g/mole and 247 000 g/mole respectively. Data from Iwai and Arai (1989).

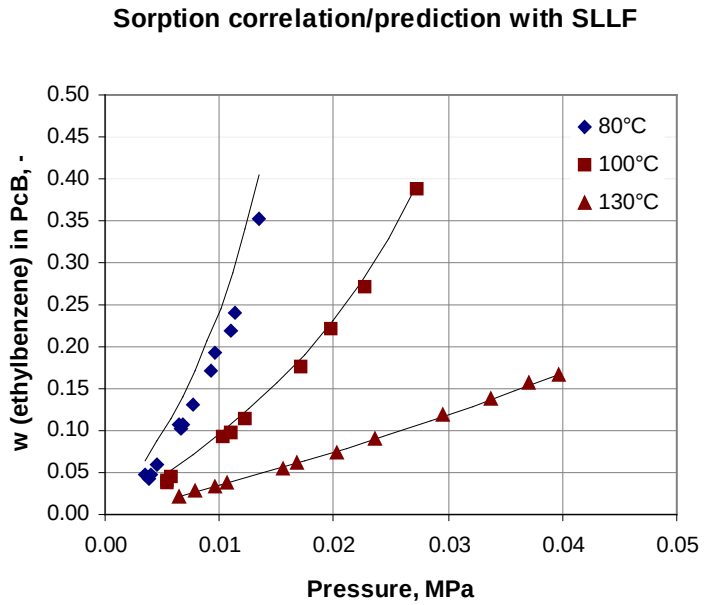

Figure 7.8 Correlation and prediction of ethylbenzene sorption in PcB with the lattice Sanchez–Lacombe equation of state. The energy interaction parameter (k_{ij} = 0.0102) was fitted at 130°C, the same value was used at the other temperatures. The polymer weight average molecular weight is 200 000-300 000 g/mole. Data from Iwai and Arai (1989).

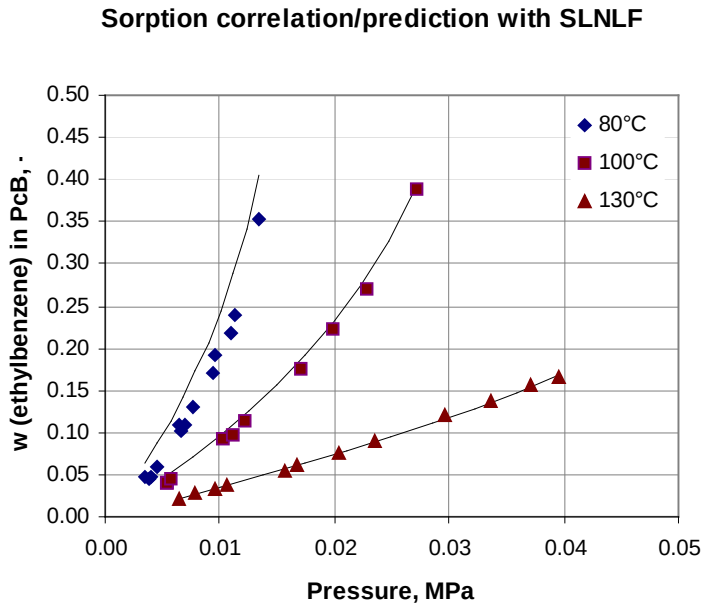

Figure 7.9 Correlation and prediction of ethylbenzene sorption in PcB with the non-lattice Sanchez–Lacombe equation of state. The energy interaction parameter (k_{ij} = 0.0096) was fitted at 130°C, the same value was used at the other temperatures. The polymer weight average molecular weight is 200 000-300 000 g/mole. Data from Iwai and Arai (1989).

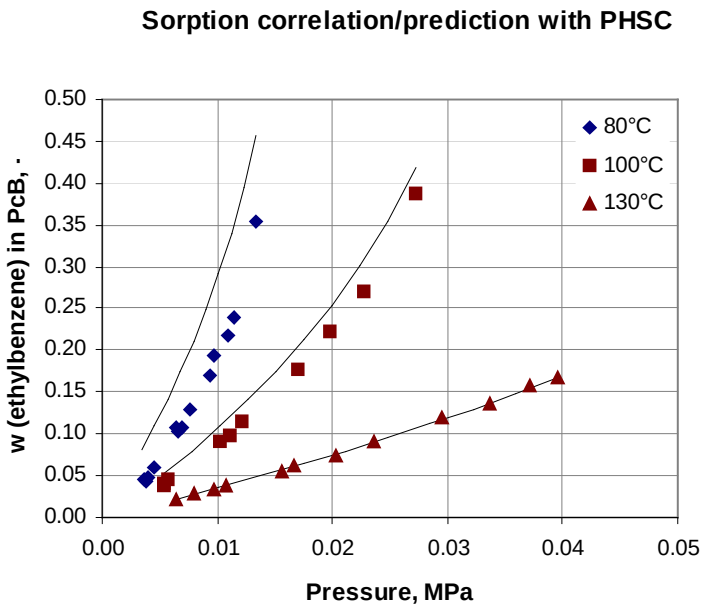

Figure 7.10 Correlation and prediction of ethylbenzene sorption in PcB with the perturbed hard-sphere-chain equation of state. The size correction parameter (l_{ij} = -0.0275) was fitted at 130°C, the same value was used at the other temperatures. The polymer weight average molecular weight is 200 000-300 000 g/mole. Data from Iwai and Arai (1989).

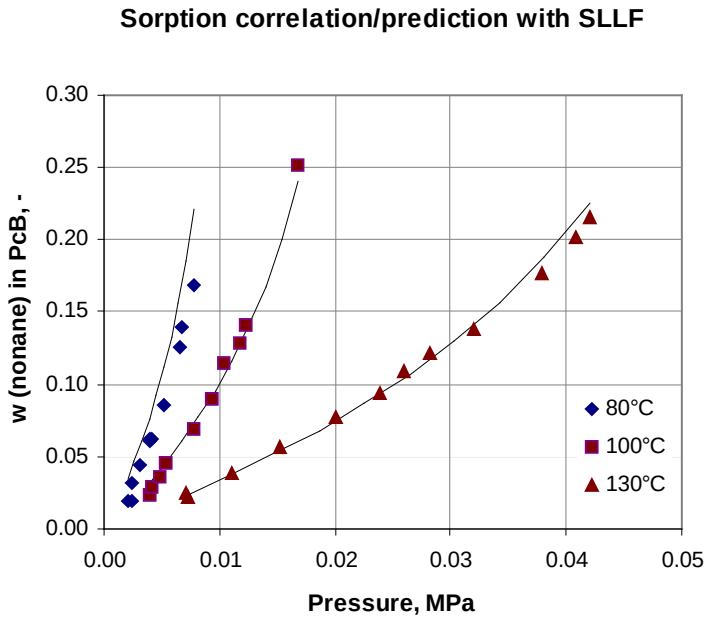

Figure 7.11 Correlation and prediction of nonane sorption in PcB with the lattice Sanchez–Lacombe equation of state. The energy interaction parameter (k_{ij} = 0.0253) was fitted at 130°C, the same value was used at the other temperatures. The polymer weight average molecular weight is 200 000-300 000 g/mole. Data from Iwai and Arai (1989).

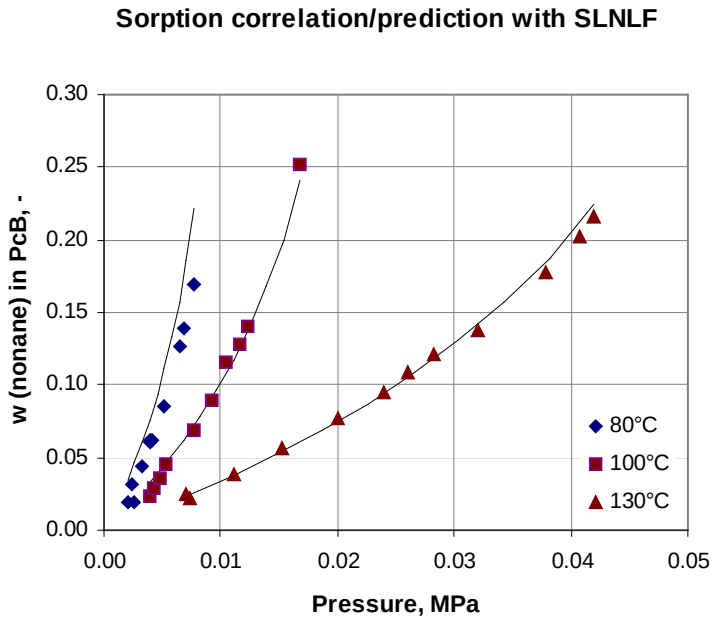

Figure 7.12 Correlation and prediction of nonane sorption in PcB with the non-lattice Sanchez–Lacombe equation of state. The energy interaction parameter (k_{ij} = 0.0084) was fitted at 130°C, the same value was used at the other temperatures. The polymer weight average molecular weight is 200 000-300 000 g/mole. Data from Iwai and Arai (1989).

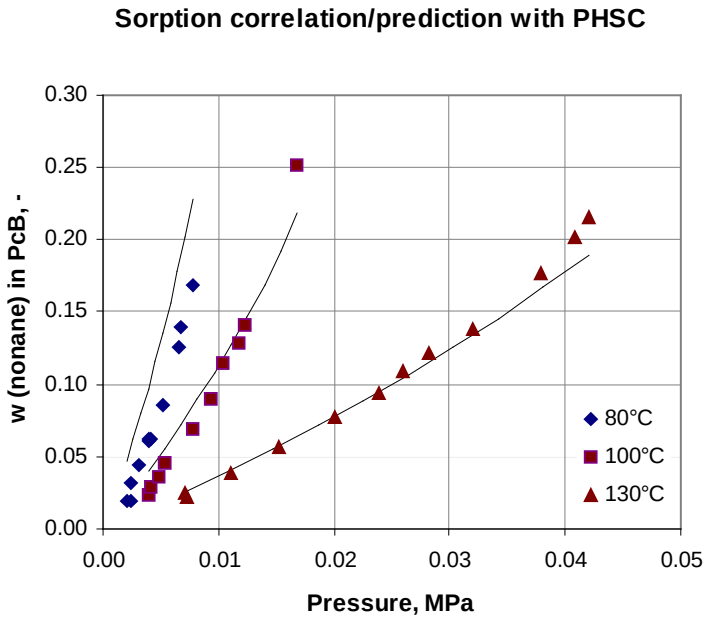

Figure 7.13 Correlation and prediction of nonane sorption in PcB with the perturbed hard-sphere-chain equation of state. The energy interaction parameter (k_{ij} = -0.0439) was fitted at 130°C, the same value was used at the other temperatures. The polymer weight average molecular weight is 200 000-300 000 g/mole. Data from Iwai and Arai (1989).

The best results in parameter fitting were obtained with the non-lattice Sanchez–Lacombe equation of state. The SLNLF model seems to have enough flexibility for an accurate description of the binary equilibrium data with an adjustable parameter. The performance of PHSC in the ethylbenzene–PcB system at 130°C is comparable with the performance of the Sanchez–Lacombe models, but the predictions at the other temperatures become poorer (Figure 7.10). The perturbed hard-sphere-chain equation of state is a more complicated model than the Sanchez–Lacombe models and perhaps both the energy interaction and the size correction parameter are required for accurate phase behavior correlations.

The ability of the Sanchez–Lacombe equation of state to predict and correlate gas and vapor sorption in polymers has already been observed in earlier studies (Kiszka *et al.*, 1988; Sanchez and Rodgers, 1990; Pope *et al.* 1991; Bicerano, 1992; De Angelis *et al.*, 1999). Earlier studies have applied either the lattice fluid or the non-lattice fluid version. Based on the above simulation results, the non-lattice version yields slightly better results than the lattice fluid development.

The combined SRK–group contribution models SRK1 and SRK2 provided reasonable predictions only in the benzene–polystyrene system (Figure 7.4), where both the solvent and

the polymer contain similar segmental structures. SRK1 obtains better predictions than SRK2 as the temperature increases, because the UNIFAC-FV accounts for the temperature dependence through the free volume contribution. Clearly, the temperature effect should be included at concentrated solutions. Group interaction parameters for the proposed exponential UNIFAC modification should be determined in order to use the proposed model at concentrated solutions. The original UNIFAC interaction parameters (Fredenslund *et al.*, 1975) may be used for the UNIFAC-FV model.

7.1.3 Sorption in PDMS membrane

Thermodynamic model for vapor membrane separation should be able to describe qualitatively gas and vapor sorption in the membrane material. SRK1 can not be used to predict gas sorption since the UNIFAC-FV model does not contain the groups for gases. The application of SRK2 would require a considerable amount of work to determine a new group interaction parameter table. Since SRK2 is not able to predict gas sorption in a polymer any better than SLNLF or PHSC, the determination of the new group interaction parameter table is considered non-profitable for the purposes of this work. Therefore, only the lattice and nonlattice fluid versions of the Sanchez–Lacombe equation of state and the perturbed hard-sphere-chain equation of state are used from this point onwards.

Poly(dimethylsiloxane) is still the most important commercial membrane material in vapor membrane separation. The computed sorption curves for various gases and vapors in a PDMS membrane are presented in Figures 7.14-7.19. The resulted absolute average deviations between the experimental and the predicted sorption curves are provided in Table 7.13. All computations were performed without the binary interaction parameters.

Table 7.13 Absolute average deviations between the experimental sorption curves (De Angelis *et al.*, 1999) and the equation of state predictions in a PDMS membrane at 35°C.

System	DP	AAD, % SLLF	AAD, % SLNLF	AAD, % PHSC
Nitrogen	9	62.6	60.7	23.0
Oxygen	9	46.5	60.2	40.4
Carbon dioxide	10	21.4	37.1	333.6
Methane	10	36.3	28.2	13.6
Ethane	7	6.7	29.6	7.0
Propane	7	32.6	53.5	10.0

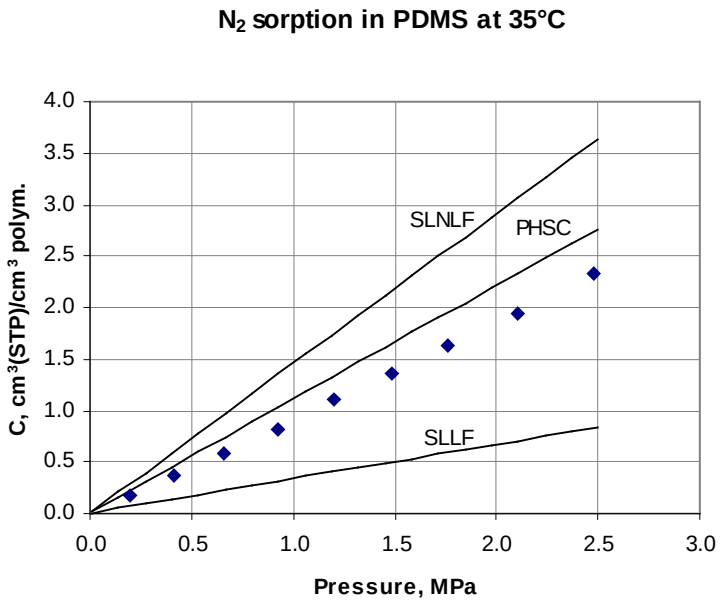

Figure 7.14 Nitrogen sorption in the PDMS membrane with the equation of state models without the binary interaction parameters. Data from De Angelis *et al.* (1999).

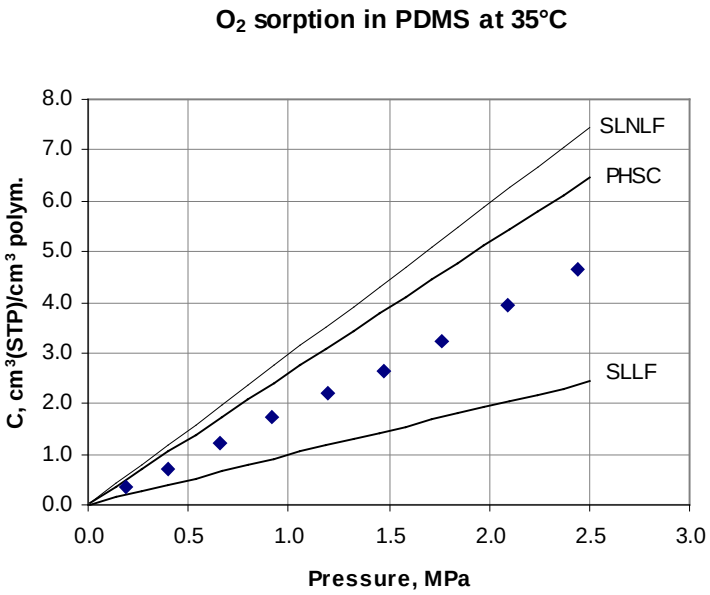

Figure 7.15 Oxygen sorption in the PDMS membrane with the equation of state models without the binary interaction parameters. Data from De Angelis *et al.* (1999).

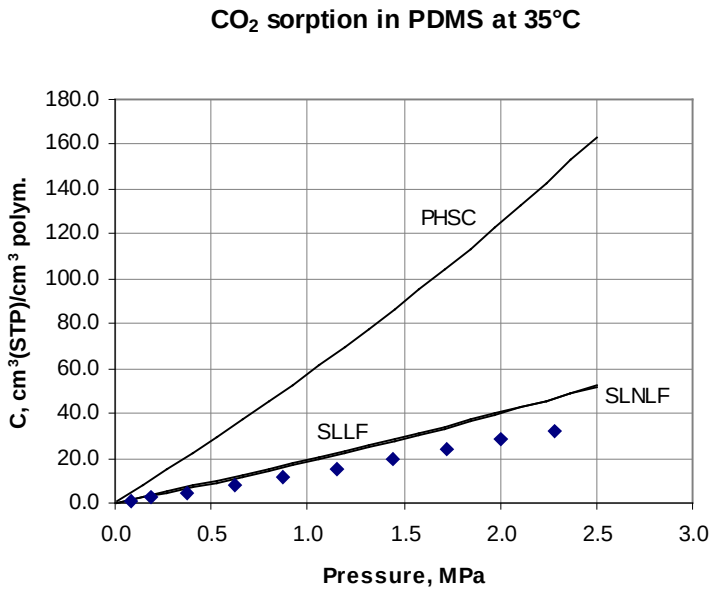

Figure 7.16 Carbon dioxide sorption in the PDMS membrane with the equation of state models without the binary interaction parameters. Data from De Angelis *et al.* (1999).

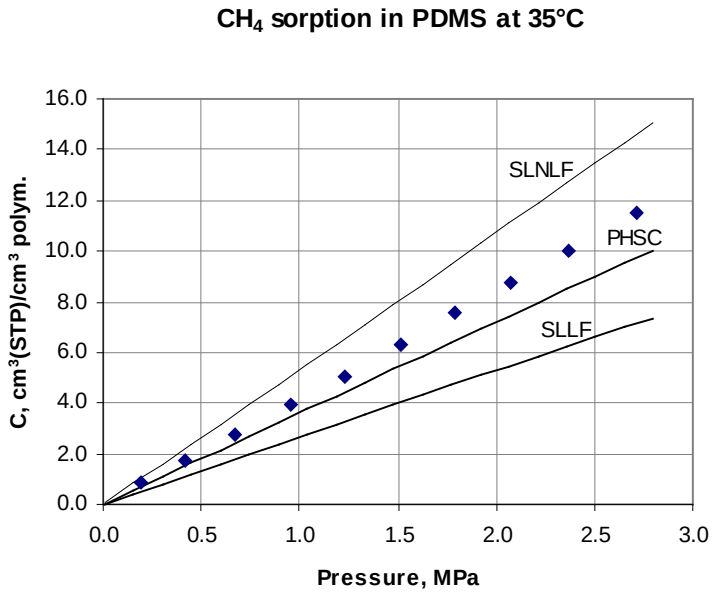

Figure 7.17 Methane sorption in the PDMS membrane with the equation of state models without the binary interaction parameters. Data from De Angelis *et al.* (1999).

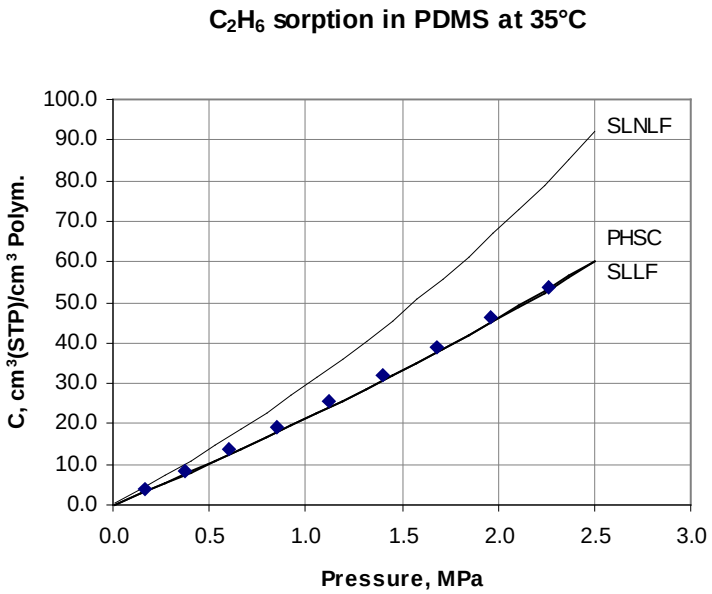

Figure 7.18 Ethane sorption in the PDMS membrane with the equation of state models without the binary interaction parameters. Data from De Angelis *et al.* (1999).

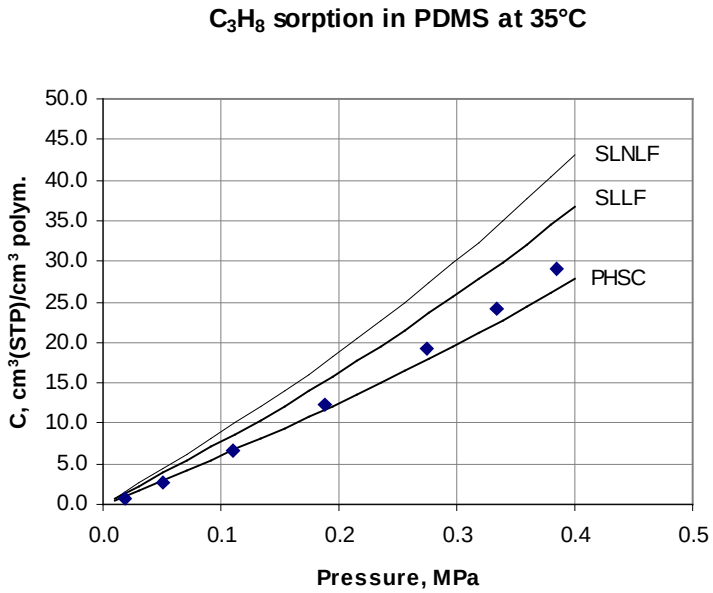

Figure 7.19 Propane sorption in the PDMS membrane with the equation of state models without the binary interaction parameters. Data from De Angelis *et al.* (1999).

The perturbed hard-sphere-chain equation of state is able to predict sorption curves in the PDMS membrane better than the versions of the Sanchez–Lacombe equation of state. At least the AAD value for nitrogen with the PHSC is within the experimental error; this may also be

the case for hydrocarbons with the PHSC and for ethane with the SLLF. The better performance of PHSC in the linear alkane–PDMS systems may also be observed in Henry's constant predictions in Table 7.6. However, the prediction for polar CO_2 sorption is coarsely overestimated. The perturbed hard-sphere-chain equation of state predicts that the sorption level of CO_2 in a PDMS membrane is of the same order than the sorption level of propane, as if CO_2 molecules appears in the form of a chain-like molecule.

Generally, the lattice fluid model seems to underestimate the sorption curves and the non-lattice fluid model seems to overestimate the sorption curves. In paragraph 7.1.2, the binary interaction parameters were determined from the experimental data at one temperature in order to improve the models' ability to predict the equilibrium concentration at the other temperatures. Usually this binary interaction parameter is associated with the energetic interaction between molecules i and j. The Sanchez–Lacombe models have an energy interaction parameter, which appears in equation (6.18) for the lattice fluid and in equation (6.39) for the nonlattice fluid. The perturbed hard-sphere-chain equation of state has two adjustable parameters: the energy interaction parameter, in equation (6.54), and the size correction parameter in equation (6.55).

A model is forced to reproduce binary experimental data accurately with an adjustable binary interaction parameter. Ideally, the same interaction parameter describes the interaction also in a multicomponent system. However, the binary adjustable parameter also smoothes out shortcomings in the model's physical picture. According to Sanchez and Panayiotou (1994), hole volumes v^* in the lattice fluid model and v_0^* in the non-lattice fluid model are erroneous, non-physical quantities incorporated to introduce the free volume into the mixture volume. The hole volume in the lattice fluid model is equal to an occupied lattice size, which is given by equation (6.11). The hole volume in the non-lattice fluid model, equation (6.37), is in principle an adjustable quantity. It may be argued that the lattice fluid model underestimates the total free volume, whereas the non-lattice fluid model overestimates the total free volume. This error is corrected implicitly in the Sanchez–Lacombe models through the binary interaction parameter in equations (6.18) and (6.39).

The figures in the previous paragraph clearly show a good generalization ability of the studied thermodymanic models, which is gained thought the parameter fitting from limited experimental binary data. The generalization with binary pairs is generally retained in

multicomponent gas and liquid mixtures. However, it is not clear whether the generalization will also be retained in multicomponent asymmetric systems, such as encoutered in vapor membrane separation. Moreover, experimental VLE data for penetrant–membrane binary pairs are rather limited. Therefore, in this work the equation of state models are preferably used without an adjustable binary interaction parameter, that is, the models are used in a predictive mode.

7.2 CORRELATION OF BINARY DIFFUSION DATA IN PDMS MEMBRANE

The mass transport model requires the diffusion coefficients, which have to be treated as experimental quantities. The binary penetrant–membrane diffusion coefficients are determined from the experimental permeability data as described in section 5.6.

A large number of experimental permeability coefficient in PDMS membranes can be found in open literature, but the values of the experimental permeability coefficients may deviate considerably between different studies (e.g. Jordan *et al.* 1987; Jordan and Koros, 1990). These deviations may occur due to differences in membrane compositions and different film forming procedures that may result in different crosslinking densities in the final membranes. Therefore, care should be taken when permeability data is combined from the different sources.

A consistent data for the correlation of pure component diffusion in a membrane is the one measured with the same membrane in the same device at different temperatures and pressures. Unfortunately, such consistent data is rare (Barrer and Chio, 1965; Stern *et al.*, 1987; Thundyil, 1997). Both Barrer and Chio (1965) and Stern *et al.* (1987) utilized silica reinforced membrane, which gives rise to the dual-mode sorption (Kamiya *et al.*, 1990), thus restricting the use of equation of state models as such at high sorption levels. Thundyil (1997) utilized a crosslinked filler-free membrane and this data for hydrogen, methane, ethane, ethylene, propane, and propylene is adopted here. Unfortunately, data for other components of interest have to be search from the different sources. The data of Barrer and Chio (1965) is adopted for nitrogen and the data of Stern and Bhide (1989) for hydrogen sulfide.

Barrer and Chio (1965) applied two PDMS membrane samples of a different filler content (5.5 and 18.2 vol-%). This makes it possible to extrapolate the experimental permeabilities of nitrogen at the same temperature to the zero filler content. This treatment may be inadequate

to eliminate the space-filling effect of the silica filler, since the filler particles are not always fully wetted by the polymer (Barrer, 1968) to prevent the penetrant adsorption. However, the resulting data is adequate for the parameterization of equation (5.68) since the nitrogen permeability coefficient is concentration independent.

Stern and Bhide (1989) provide the parameters for equation

$$\log_{10} \overline{P} = \log_{10} \overline{P}(0) + m\Delta p \,, \tag{7.6}$$

to compute the hydrogen sulfide permeability coefficients at temperatures of 10, 35, and 55°C in a silica-filled membrane (4.9 vol-%). This data was used to generate the required permeability data for the parameterization of equation (5.68) for hydrogen sulfide. Corrections for the filler effect were not made for the calculated permeability coefficients.

The Maxwell–Stefan diffusion coefficients at different temperatures and pressures for hydrogen, methane, ethane, ethylene, propane, propylene, nitrogen, and hydrogen sulfide in a PDMS were calculated from the permeability coefficients by using equation (5.67). The solubility coefficients and the thermodynamic factors were obtained from the lattice fluid and the non-lattice fluid models of the Sanchez–Lacombe equation of state with the parameters given in Table A.1, and from the perturbed hard-sphere-chain equation of state with the parameters given in Table A.2. Again, the high-pressure parameters were used for the Sanchez–Lacombe equation of state. The theoretical swelling correction was calculated from the geometric average of the anisotropic and isotropic swelling, equation (5.64). As an example, Table 7.14, Table 7.15, and Table 7.16 present the values of the polymer mass or segment fractions, the Fick diffusion coefficients, the effective Maxwell-Stefan diffusion coefficients, the solubility coefficients, the thermodynamic factors, and the swelling factors for hydrogen and propane in the PDMS membrane. The values of the polymer mass or segment fractions are the averages of the values at the membrane interfaces.

As the thermodynamic models are used without the binary interaction parameters, there is a systematic deviation in the predicted sorption curves with respect to the experimental data. The amount and the direction of the deviation depend on the thermodynamic model and the chemical species involved. Thus, the values of the solubility coefficients S_1, the diffusion coefficients D_{12} and $Đ_{1M}$, the swelling factors δ_m / δ_m^0, and the thermodynamic factors Γ_1 in tables 7.14 to 7.16 differ from table to table. The resulting error in S_1, D_{12}, and δ_m / δ_m^0 equals to the amount of the deviation in the sorption curve at a specified pressure.

Table 7.14 The polymer mass fractions, the Fick diffusion coefficients, the effective Maxwell-Stefan diffusion coefficients, the solubility coefficients, the thermodynamic factors, and the swelling factors for hydrogen and propane in PDMS. The results are computed with SLLF at 303.15 K.

	p, MPa	w_2, -	D_{12}, 10^{-5} cm^2/s	$Đ_{1M}$, 10^{-5} cm^2/s	S_1, cm^3 (STP)/ (cm^3 polym. MPa)	Γ_{12}, -	$\frac{\delta_m}{\delta_m^0}$, -
H_2	0.345	1.000	5.460	5.473	0.985	0.998	1.001
	0.690	1.000	5.448	5.473	0.984	0.997	1.001
	1.379	1.000	5.415	5.463	0.983	0.993	1.002
	2.068	1.000	5.382	5.452	0.983	0.990	1.003
C_3H_8	0.345	0.957	0.458	0.563	103.208	0.870	1.069
	0.517	0.935	0.513	0.703	119.935	0.807	1.107
	0.690	0.906	0.566	0.895	145.812	0.732	1.157
	0.862	0.864	0.571	1.118	194.416	0.631	1.235

Table 7.15 The polymer mass fractions, the Fick diffusion coefficients, the effective Maxwell-Stefan diffusion coefficients, the solubility coefficients, the thermodynamic factors, and the swelling factors for hydrogen and propane in PDMS. The results are computed with SLNLF at 303.15 K.

	p, MPa	w_2, -	D_{12}, 10^{-5} cm^2/s	$Đ_{1M}$, 10^{-5} cm^2/s	S_1, cm^3 (STP)/ (cm^3 polym. MPa)	Γ_{12}, -	$\frac{\delta_m}{\delta_m^0}$, -
H_2	0.345	1.000	6.195	6.208	0.868	0.998	1.001
	0.690	1.000	6.183	6.209	0.867	0.997	1.001
	1.379	1.000	6.150	6.199	0.866	0.994	1.002
	2.068	1.000	6.117	6.189	0.865	0.991	1.003
C_3H_8	0.345	0.951	0.390	0.490	121.285	0.862	1.083
	0.517	0.924	0.428	0.608	143.637	0.796	1.129
	0.690	0.889	0.459	0.766	179.790	0.715	1.193
	0.862	0.836	0.438	0.938	253.221	0.606	1.297

Table 7.16 The polymer segment fractions, the Fick diffusion coefficients, the effective Maxwell-Stefan diffusion coefficients, the solubility coefficients, the thermodynamic factors, and the swelling factors for hydrogen and propane in PDMS. The results are computed with PHSC at 303.15 K.

	p, MPa	ϕ_2, -	D_{12}, 10^{-5} cm^2/s	$Đ_{1M}$, 10^{-5} cm^2/s	S_1, cm^3 (STP)/ (cm^3 polym. MPa)	Γ_{12}, -	$\frac{\delta_m}{\delta_m^0}$, -
H_2	0.345	1.000	16.970	16.980	0.317	1.000	1.000
	0.690	1.000	16.940	16.960	0.317	0.999	1.000
	1.379	1.000	16.870	16.910	0.316	0.998	1.000
	2.068	1.000	16.800	16.850	0.315	0.997	1.000
C_3H_8	0.345	0.958	0.598	0.685	78.981	0.893	1.023
	0.517	0.937	0.705	0.866	87.307	0.843	1.035
	0.690	0.913	0.815	1.093	101.183	0.784	1.050
	0.862	0.880	0.897	1.355	123.760	0.709	1.071

The experimental solubility coefficient for hydrogen in PDMS is 0.832 cm^3 (STP)/(cm^3 polym. MPa) at 25°C (Kamiya *et al.*, 1997). The computed solubility coefficients for hydrogen with SLNLF (Table 7.15) are in good agreement with the experimental value, but the computed solubility coefficients with PHSC are about three times smaller. In consequence of the relation (2.13), the computed diffusion coefficients for hydrogen with PHSC are about three times higher than the computed diffusion coefficients with SLLF or SLNLF. In the case of propane, PHSC is able to predict the sorption curve well and perhaps within the experimental error (Table 7.13). Since SLLF and SLNLF overestimate the sorption level of propane by 30% and 50% respectively, the corresponding deviations are observed also in the computed diffusion coefficients D_{12} and the solubility coefficients S_1 with respect to the values obtained with PHSC. Despite the large deviations in the predicted sorption curves, the thermodynamic factors Γ_1 for propane differ only by a factor of 1.2 at maximum due to the fact that Γ_1 is a relative property, cf. equation (5.25).

The calculated binary penetrant–membrane diffusion coefficients were correlated as follows. The effective binary penetrant–membrane diffusion coefficients $\overline{Đ}_{1M}$ at a constant temperature were extrapolated to the zero penetrant concentration with respect to the average values of the penetrant mass or segment fractions to obtain the diffusion coefficients at the infinite dilution $Đ_{12}^0$. The parameters A_d and B_d were then obtained from the least squares fits for equation (5.68). Equation (5.69) was used to compute the fractional free volume of a pure polymer at the system temperature. The occupied volume was defined to be the volume of the glass at 0 K, for which Seitz (1993) obtained the following correlation:

$$V^* = 1.42 V_w , \tag{7.7}$$

where V_w is the van der Waals molecular volume and may be estimated from groups given by Bondi (1968, pp. 450-452). The van der Waals molecular volume of 0.595 cm^3/g was obtained for a PDMS chain.

The effective binary penetrant–membrane diffusion coefficients $Đ_{1M}$ at a constant temperature were then multiplied by the average values of the polymer mass or segment fractions to obtain the binary Maxwell–Stefan diffusion coefficients $Đ_{12}$. The mass fraction based Maxwell–Stefan diffusivities were observed to be of a linear form with respect to the

retentate pressure at a constant temperature. This temperature dependent behavior was conveniently captured by a relation

$$\frac{Đ_{12}(w_1,T)}{Đ_{12}^0(T)} = 1 + C_d \exp\left(\frac{E_d}{RT}\right)p, \tag{7.8}$$

where C_d and E_d are component specific parameters and the latter may be associated with the energy of the diffusion.

The resulted parameters and the coefficients of determination for equations (5.68) and (7.8) are presented in Table 7.17, Table 7.18, and Table 7.19 for SLLF, SLNLF, and PHSC respectively. As an example, Figure 7.20 presents the Maxwell–Stefan diffusion coefficients for ethylene and Figure 7.21 the Maxwell–Stefan diffusion coefficients for propane in PDMS.

Table 7.17 The parameters of equations (5.68) and (7.8) for the penetrant diffusion in the PDMS membrane to be used with SLLF.

	A_d, 10^{-3} cm^2/s	B_d -	C_d, 10^{-5} MPa^{-1}	E_d / R K	R^2 for (5.68)	R^2 for (7.8)
Nitrogen	1.495	0.5200	-	-	0.999	-
Hydrogen sulfide	0.116	0.5534	-	-	0.890	-
Hydrogen	0.820	0.4986	-	-	0.999	-
Methane	0.531	0.5769	-	-	1.000	-
Ethane	0.573	0.8189	3.776	2899.6	0.999	1.000
Ethylene	0.633	0.7615	15.029	2370.5	1.000	0.988
Propane	0.152	0.7193	43.983	2599.2	0.979	0.993
Propylene	0.792	0.9795	2.036	3533.0	0.996	0.996

Table 7.18 The parameters of equations (5.68) and (7.8) for the penetrant diffusion in the PDMS membrane to be used with SLNLF.

	A_d, 10^{-3} cm^2/s	B_d -	C_d, 10^{-5} MPa^{-1}	E_d / R K	R^2 for (5.68)	R^2 for (7.8)
Nitrogen	1.299	0.7667	-	-	0.998	-
Hydrogen sulfide	0.172	0.4677	-	-	0.863	-
Hydrogen	0.825	0.4766	-	-	0.999	-
Methane	0.510	0.6960	-	-	1.000	-
Ethane	0.483	0.8341	4.685	2780.9	1.000	1.000
Ethylene	0.572	0.8114	14.756	2327.8	1.000	0.982
Propane	9.340	0.6360	201.570	2059.3	0.955	0.965
Propylene	0.371	0.8383	13.509	2853.6	1.000	1.000

Good coefficients of determination were resulted for the components, except for hydrogen sulfide. Hydrogen, methane, nitrogen, and hydrogen sulfide are able to diffuse in the PDMS membrane without the associated energy of activation and thus only equation (5.68) is required. The activation energy for the diffusion should increase with the molecular size. As the values of E_d / R are examined, the parameters in Table 7.19 follow the correct trend. The

physically meaningful behavior of E_d / R is violated in Table 7.17 and in Table 7.18 due to the large deviations in the predicted sorption level with the Sanchez–Lacombe models.

Table 7.19 The parameters of equations (5.68) and (7.8) for the penetrant diffusion in the PDMS membrane to be used with PHSC.

	A_d, 10^{-3} cm^2/s	B_d -	C_d, 10^{-5} MPa^{-1}	E_d / R K	R^2 for (5.68)	R^2 for (7.8)
Nitrogen	8.529	1.0340	-	-	0.999	-
Hydrogen sulfide	0.350	0.7190	-	-	0.926	-
Hydrogen	1.877	0.4410	-	-	0.995	-
Methane	1.033	0.7545	-	-	0.998	-
Ethane	1.489	0.9926	1.261	3197.6	0.996	0.999
Ethylene	1.384	0.9365	4.908	2670.2	1.000	0.989
Propane	1.489	1.1290	2.094	3599.5	1.000	0.998
Propylene	2.024	1.1360	1.558	3555.5	0.992	0.995

The use of the parameters for equations (5.68) and (7.8) and the thermodynamic models must be consistent. Only then the model is able to produce a reasonable prediction for the penetrant transport and the experimental pure component permeability coefficients may be reproduced within the numerical accuracy. Table 7.20 presents the permeability coefficients that are calculated with the rearranged equation (5.67) and with the values from Table 7.14, Table 7.15, and Table 7.16.

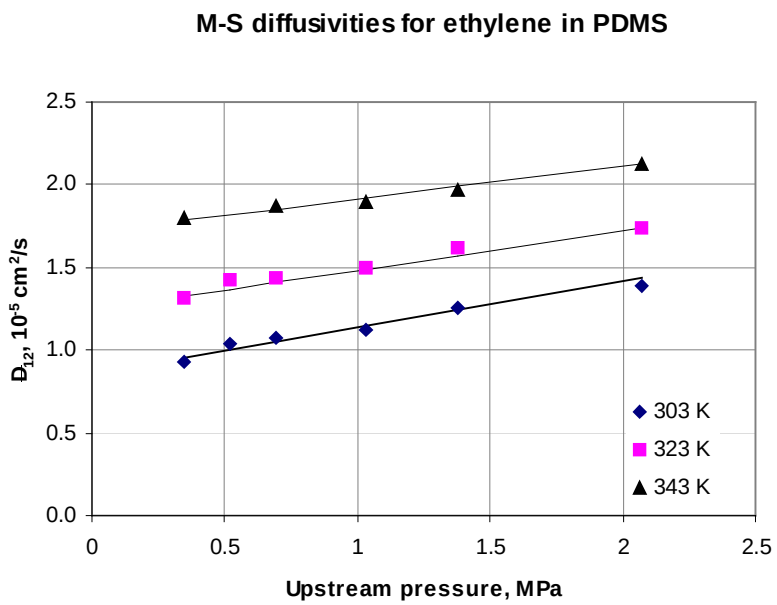

Figure 7.20 Concentration and temperature dependence of the M-S diffusion coefficients for ethylene in PDMS. The diffusivity data is computed from the permeability coefficient data of Thundyil (1997). The solid lines are calculated from equations (5.68) and (7.8) with the parameters given in Table 7.19.

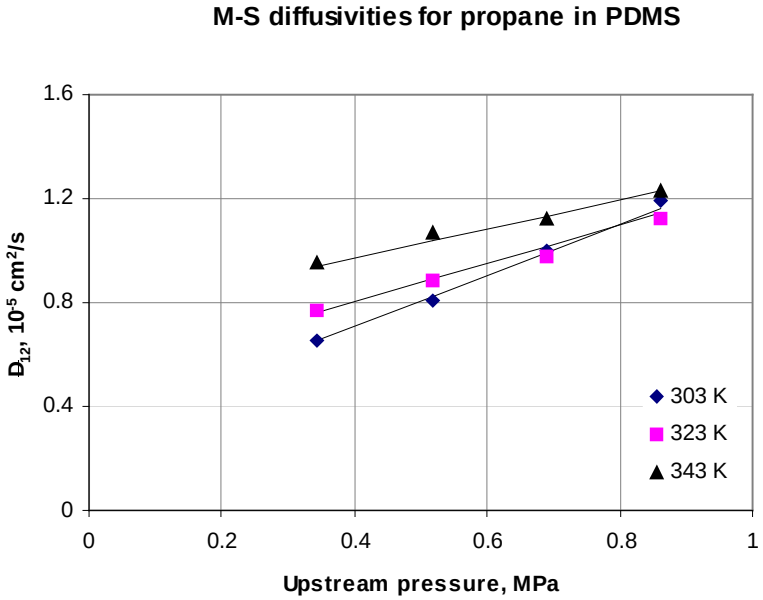

Figure 7.21 Concentration and temperature dependence of the M-S diffusion coefficient for propane in PDMS. The diffusivity data is computed from the permeability coefficient data of Thundyil (1997). The solid lines are computed from equations (5.68) and (7.8) with the parameters given in Table 7.19.

Table 7.20 The recalculated permeability coefficients for hydrogen and propane in the PDMS membrane in the units of 10^{-5} cm^3 (STP) cm /(cm^2 s MPa).

	p, MPa	SLLF	SLNLF	PHSC
H_2	0.345	5.375	5.373	5.378
	0.690	5.362	5.362	5.363
	1.379	5.326	5.323	5.327
	2.068	5.290	5.290	5.288
C_3H_8	0.345	47.246	47.249	47.234
	0.517	61.499	61.524	61.517
	0.690	82.536	82.514	82.524
	0.862	111.055	110.983	111.045

7.3 MODELING OF ISOTHERMAL MULTICOMPONENT PERMEATION

A permeation model is formed when the transport equations are combined with an equation of state model. The unknown variables of the model are the *nc* component fluxes, the *nc* + 1 mass fractions at a high-pressure phase interface, and the *nc* + 1 mass fractions at a low-pressure phase interface. Hence, the permeation through the membrane has to be computed by iteration.

The component fluxes through the rubbery membrane may deviate by orders of magnitude, which may cause numerical problems. Therefore, the component fluxes are scaled with the initial fluxes that are obtained from a simplified computation procedure. The penetrant mass fractions at the high-pressure phase interface are assumed to be equal to the equilibrium sorption at a local retentate composition, temperature, and pressure as described in section 7.1. The penetrant mass fractions at the low-pressure phase interface are set to zero. The initial component fluxes through the membrane are then obtained by computing the component fluxes with the simplified method (paragraph 5.4.3).

During the first iteration the scaled flux value is one for all components. The composition in the membrane support is equal to the local permeate composition

$$w_{im,II} = \frac{n_i}{n_t}, \quad i = 1, 2, \ldots, nc. \tag{7.9}$$

The concentration in the membrane at the permeate side interface is then obtained by computing the equilibrium sorption at the local permeate composition and the applied permeate pressure. This corresponds to the assumption that there is no chemical potential gradient over the support layer and the backmixing is negligible in the membrane support (Rautenbach and Helmus, 1994). The permeation fluxes may then be computed for the known driving force over the selective layer. This system of the $3nc + 2$ unknowns is solved with the Newton–Raphson method. The $3nc + 2$ residual functions are formed from the deviations between the estimated and computed component fluxes and the chemical potentials at phase interfaces, and from the natural logarithms of sum of weight fractions at the selective layer interfaces.

Thundyil (1997) performed a multicomponent permeation experiment in an isothermal Millipore test cell at 30°C. The test gas mixture contained 10.20% hydrogen, 10.00% methane, 9.97% ethane, 20.00% propylene, and 49.83% propane. The gas mixture supplier guaranteed the gas mixture within 2% of the smallest component. The experiment was conducted with the feed pressure of 411.4 kPa, the permeate pressure of under 6.7 kPa, and the stage cut of 0.00415. The sum of the reported permeate composition exceeded 100% but this error was adjusted by re-scaling.

The multicomponent permeation experiment of Thundyil (1997) was simulated with the transport model equations. The simulations were performed with the simplified explicit

method and with the matrix method by using the three thermodynamic models. An example of an input file for a FLOWBAT simulation is given in appendix VI.

The results for the simplified explicit method without the cross-coefficients $Đ_{ij}$ are presented in Table 7.21. The high-pressure parameters were used for the Sanchez–Lacombe equation of state. The simplified explicit method and the matrix method yielded exactly the same results, and therefore these results are presented in the same Table 7.22. The cross-coefficients $Đ_{ij}$ for these simulations were determined from equation (5.71). The permeation with PHSC was calculated with the equations given in chapter 5, except for that the segment fractions (6.51) and the molar segment density (6.50) were used instead of the weight fractions and the mass density where ever they appeared.

Table 7.21 Predicted permeate composition with the simplified explicit method (diagonal matrix [*A*]).

	Exp. mole-%	SLLF mole-%	AAD %	SLNLF mole-%	AAD %	PHSC mole-%	AAD %
Hydrogen	2.350	3.059	30.2	2.353	0.1	2.699	14.8
Methane	2.809	2.537	9.7	2.704	3.7	3.003	6.9
Ethane	7.618	5.617	26.3	6.063	20.4	6.522	14.4
Propylene	23.283	21.050	9.6	24.684	6.0	24.925	7.1
Propane	63.940	67.737	5.9	64.196	0.4	62.851	1.7
Total av.			16.3		6.1		9.0

Table 7.22 Predicted permeate composition with the simplified explicit method (full matrix [*A*]) and the exact method (full matrix [*B*]).

	Exp. mole-%	SLLF mole-%	AAD %	SLNLF mole-%	AAD %	PHSC mole-%	AAD %
Hydrogen	2.350	2.548	8.4	1.777	24.4	1.745	25.8
Methane	2.809	2.370	15.6	2.605	7.3	3.029	7.8
Ethane	7.618	5.591	26.6	6.053	20.5	6.800	10.7
Propylene	23.283	21.184	9.0	24.815	6.6	25.803	10.8
Propane	63.940	68.307	6.8	64.750	1.3	62.623	2.1
Total av.			13.3		12.0		11.4

The composition of the permeate without the cross-coefficients $Đ_{ij}$ was better predicted with the transport model equations combined with SLNLF. The poorer performance of PHSC without the cross-coefficients with respect to SLNLF may be associated with the deviation in the predicted solubility coefficient for hydrogen (section 7.2). When the cross-coefficients $Đ_{ij}$ were included to the transport equations, comparable results were obtained with the model equations combined with PHSC and SLNLF. In all cases, the deviation in ethane mole

fraction is large. Since the deviation seems to be systematic, this may be due to the composition accuracy of the feed gas mixture.

Due to the form of equation (5.71), the obvious consequence of including the cross-coefficients $Đ_{ij}$ to the diffusion coefficient matrix $[A]$ or $[B]$ is to decrease the flux of molecules with lower permeability (high diffusivity, low solubility). As highlighted in the previous section, the binary Maxwell–Stefan diffusion coefficients were calculated from the experimental permeability coefficients. When the estimated solubility coefficients deviate from the experimental solubility coefficients, the deviation is transmitted to the binary diffusion coefficients, and further to the cross-coefficients $Đ_{ij}$ via equation (5.71). Therefore, the predicted permeate composition became worse with SLNLF and PHSC when the cross-coefficients were included.

The simplified explicit solution and the matrix solution yielded the same results. The fluxes in the matrix solution were initialized with the simplified solution and then the matrix solution converged in one additional iteration loop. According to Taylor and Krishna (1993, p. 204), the rate factor defined in equation (5.52) is an exact eigenvalue of the matrix $[\Phi]$ for the Stefan diffusion, and the eigenvalues of $[\Phi]$ characterize the correction factor matrix $[\Xi]$ in the exact solution. Therefore, we may conclude that the simplified explicit solution method is adequate for the modeling of multicomponent vapor permeation in rubbery membranes.

In the transport model for pervaporation of binary mixture, Heintz and Stephan (1994b) applied the cross-coefficient $Đ_{12}$ as an adjustable parameter. However, in multicomponent systems the cross-coefficients have to be estimated. In this work the estimation was carried out with equation (5.71) but the form was not successful. Hence, the cross-coefficients are dropped out from the model of multicomponent permeation. Without the cross-coefficients, the transport equations should be combined with the non-lattice fluid version of the Sanchez–Lacombe equation of state or with the perturbed hard-sphere-chain equation of state.

8 MODELING OF SPIRAL-WOUND MODULES

The model for gas and vapor permeation was qualitatively verified in the previous chapter. In this chapter, the permeation model is combined with the basic model equations derived from chapter 3 to form a model for vapor membrane separation with spiral-wound modules. The model is then implemented into the FLOWBAT process simulator.

FLOWBAT is an in-house process simulator for steady-state processes. It includes various unit operation models varying from simple short-cut models to unique and very specialized models. In an input file, the user defines the process flowsheet with suitable unit modules, connects the modules with material and energy streams, and selects the thermodynamic models and the estimation methods for the missing thermodynamic properties. For input file rules and specification, see *FLOWBAT user's instruction manual* (2001).

FLOWBAT is used at Neste Engineering Oy and at some universities. It has continuously been improved and extended with new calculation and estimation methods and new unit operation models. Recent published improvements have dealt with estimating plate efficiencies in distillation and reactive distillation (Ilme, 1997; Klemola and Ilme, 1996; Klemola, 1998), modeling a trickle-bed (Toppinen *et al.*, 1996), and a multiphase stirred tank reactor (Alopaeus et al., 1999; Alopaeus, 2001). This work is a continuation in this series. The model for vapor membrane separation is developed and implemented into FLOWBAT that provides

- access to the databank of over 4000 components for basic thermodynamic properties,
- tested methods of the simulator to compute physical and thermodynamic properties both for pure components and mixtures, and
- tested solvers of linear and non-linear equations and matrix algorithms.

A new FLOWBAT unit model was created for vapor membrane separation. The unit specifications are given within a namelist SDGMEM, where the user defines the feeds to the unit, the product streams from the unit, the permeate product pressure, the total membrane area, the module specification, the module arrangement, the selection of the thermodynamic model, the selection of the calculation methods, and the parameters for the diffusion coefficient correlation. The module specification includes the selective layer material, the polymer molecular weight and the molecular weight distribution, the selective layer thickness,

the number of membrane leaves in a module, the leaf length, the flow channel heights, and the number of grid points.

A membrane separation stage may consist of parallel and serial membrane modules. There may be l — up to four — serial modules in a separation stage. A membrane leaf is divided into m times n non-overlapping control volumes as in Figure 4.1. A set of non-linear model equations is written for each control volume. The equations are non-linear due to composition, temperature, and pressure dependent transport parameters. The composition of the fluid flow on the retentate side is continuously changing along the flow due to the selective permeation. The mass and energy transfer through the membrane is computed by iteration since local permeate fluxes, local penetrant concentrations at the membrane interfaces, and permeated fraction temperature at the support layer are the unknown variables. This system of the $3\,nc + 3$ unknowns is solved with the Newton-Raphson method. The residual functions are formed as in section 7.3 but equation (5.75) serves as an additional residual function for the permeated fraction temperature.

The mass and energy transfer through the membrane is basically computed at each control volume so that there are $l\,m\,n(3\,nc + 3)$ variables associated with the mass and energy transfer alone. In addition, there are $l\ m\ n$ unknown molar enthalpies and pressures both on the retentate and permeate side and $l\,n$ unknown molar enthalpies and pressures in a central tube. Altogether, $4\,l\,m\,n + 2\,l\,n$ variables are associated with the fluid flow problem. For example, for a system of five components, 50 times 50 grid points per membrane leaf, and two serial modules, the total number of variables is 110200. It may not be necessary to compute the mass and energy transfer through the membrane at each control volume. Instead, they may be computed at the median properties of a grid line along the permeate flow. This reduces the number of the mass and energy transfer related variables to $l\ m\ (3\ nc + 3)$ and the total number of variables to 22000 in the above mentioned case.

Apparently, simultaneous solution of all variables is not feasible. The approximation of one-way space coordinate on the retentate side introduces the natural solution method for the entire membrane leaf. The solution starts from the feed inlet boundary and proceeds towards the retentate exit boundary line-by-line. The model equations are solved by iteration at each x directed grid line j, the grid line along the permeate flow. Only component fluxes through the membrane, retentate temperatures, permeate temperatures, and permeated fraction

temperatures are kept in the memory for all control volumes and membrane leaves. Other variables and transport parameters allocate memory only for a line *j*, for which a solution is searched, and for the neighbor lines $j - 1$ and $j + 1$ that are needed to evaluate the gradients at the control volume interfaces (Figure 8.1). The convergence of the line *j* is determined from the residual vector for the local permeate flow field and the convergence of the membrane leaves from the residual vector for the entire permeate side temperature profile. Iterations to obtain the solution for the line *j* are denoted as inner iterations. Iterations to solve the permeate temperature profile over all membrane leaves are denoted as outer iterations. The solution procedure is described in detail in section 8.1.

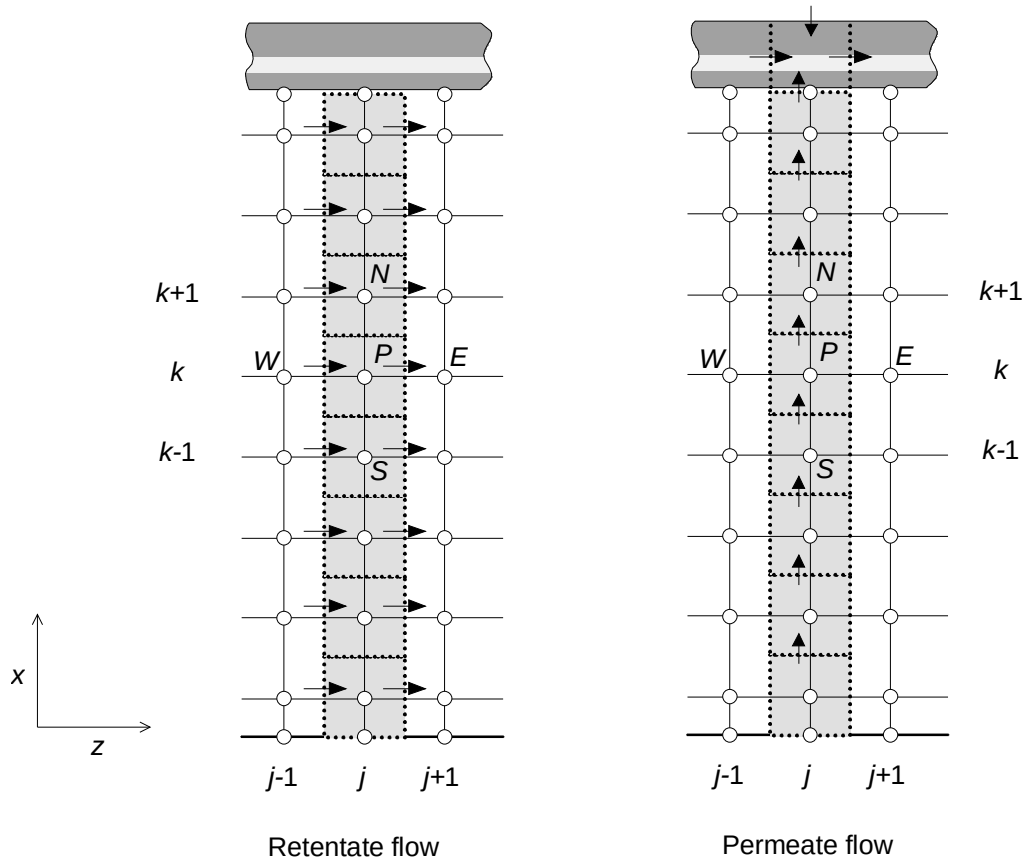

Figure 8.1 Illustration of a line-by-line solution in a membrane leaf.

The converged flux profiles, the retentate and permeate temperature profiles, and the pressure profile in a central tube are written into a binary file. The binary file exists during the flowsheet simulation and is used to initialize the unit model in the following evaluations of the unit model. An ASCII –format file and an EXCEL readable text file are written from the binary file when the whole flowsheet simulation is converged. The ASCII file allows the user to exchange the unit profiles between different simulation runs and the EXCEL file allows the

user to explore the unit results in graphical form, which is currently not possible within the FLOWBAT simulator itself.

It is obvious that the computation time required to solve the model equations depends on the grid density. This is illustrated in section 8.2 with an example simulation of selective removal of hydrocarbons from hydrogen. Another example simulation, propylene recovery from polypropylene resin degassing in section 8.3, illustrates the flowsheet solution of a vapor membrane separation process with recycle streams. Based on these example simulations, the final combination and legitimate simplifications of the model equations are concluded.

8.1 SOLUTION PROCEDURE

A membrane leaf or membrane leaves connected in series are solved by the line-by-line relaxation method with the following solution procedure. The flowchart of the solution procedure is given in Appendix II.

1. Check for an existing binary or ASCII file: if old profiles exist and are appropriate for the simulation, use them to initialize the flow field. Otherwise, create an initial flow field for a coarser grid as follows. Divide the number of user given grid points in z and x directions by two and round upwards to the nearest integer when necessary. Set the temperature and pressure on the retentate side equal to the feed temperature and pressure. Set the temperature on the permeate side equal to the feed temperature, but the pressure equal to the preset permeate product pressure.
2. Step on the first x directed internal grid line and designate it with an index j. On the retentate side, the previous line $j - 1$ corresponds to the feed boundary. On the permeate side, set the gradients at the west side interface of the control volumes to zero by setting the properties at the edge of the membrane equal to the properties at the line j.
3. Compute the component and energy fluxes through the membrane with the current properties at the line j. Compute the combined heat and mass transfer along the x directed grid line at each grid point. Alternatively, compute the heat and mass transfer at the median grid line properties and then assume the fluxes to be valid over the whole grid line j. Use the latter at least in the initialization stage. Describe the penetrant transport through the membrane with the simplified solution method by Burghardt and Krupiczka (1975) and the penetrant sorption with the non-lattice Sanchez–Lacombe equation of state or with the perturbed hard-sphere-chain equation of state. Solve the equations with the non-linear

equation solver as in section 7.3 but now include equation (5.75) for the permeated fraction temperature.

4. Compute the molar flow rates at the control volume interfaces directly from the computed permeate fluxes so that the mass conservation equation is fulfilled.
5. Obtain the discrete transport parameters, heat capacities, viscosities, and thermal conductivities along the line *j* from the physical property package of FLOWBAT (2001).
6. Discretize the energy equations to the forms of equations (4.74) and (4.76). There is no fluid and heat flow at the closed leaf end in the permeate channel (x = 0) so that coefficient $a_{V,S}^{1}$ is zero. The convective contribution may be assumed to dominate at the outflow boundary of the permeate channel so that coefficient $a_{V,N}^{n}$ becomes zero. Then the discrete equations in the permeate channel are written only for internal control volumes. Obtain the heat transfer coefficient h_L according to the flow conditions at the line *j*. Neglect the heat transfer resistance of the selective layer. For the laminar flow, obtain the heat transfer coefficient h_L from the limiting case of the constant wall temperature i.e. Nu = 7.541. For the turbulent or developing turbulent flow, apply equation (4.47) with $\mu_{L,P} / \mu_{L,B} = 1$.
7. Compute the retentate enthalpies from (4.74). Solve (4.76) along the corresponding permeate grid line with the non-symmetric tridiagonal matrix algorithm (Engeln-Mullges and Uhling, 1996).
8. Update the retentate and permeate temperature field from the converged enthalpy field by the one-variable Newton-Raphson method. Use the polynomial extrapolation (Press *et al.*, 1999, pp. 102-104) to obtain the exit boundary temperature on the permeate side.
9. If the iteration counter is below or equal to three, obtain the mass and energy fluxes through the membrane as in step 3. Update the molar flow rates and transport parameters as in step 4 and 5. If the iteration counter is greater than three, update the fluxes and transport parameters only on every third iteration count.
10. Return to 6 and repeat until the change in the temperature field along the grid line is below the preset tolerance, i.e. the absolute average norm of the residual vector is below 0.005 K or the maximum number of inner iterations is exceeded. Limit the maximum number of inner iterations to five in the initialization stage.
11. Set the properties and transport parameters at the line *j* as the properties and transport parameters at the line *j* – 1. Move to the next grid line, designate it with an index *j* and use the converged solution from the previous grid line *j* – 1 as the initial guess for the variables if the old profiles do not exist.

12. Repeat 3-11 until the leaf end of the last serial module is reached. At the retentate exit boundary of each module, mix the retentate and determine the flow temperature from the enthalpy before feeding the retentate into the next module.
13. If the computation was performed for the coarser grid, copy the recent discrete flow field values at each grid point to the four nearest grid points in the original grid spacing (Figure 8.2). Save the temperature profile on the permeate side for the entire flow field.
14. Repeat 3-12 over the serial membrane leaves to obtain a new temperature profile of the permeate side over the membrane leaves. Check the convergence and repeat 3-12 until the average and the maximum changes in the permeate temperature profile are below the preset tolerances, i.e. the absolute average norm of the residual vector is below 0.01 K and the maximum norm of the residual vector is below 0.05 K.
15. Solve the pressure and temperature profiles in the central tube fulfilling the balances of the mass, the momentum, and the energy given in section 4.2. Use the Newton-Raphson iteration: start from the open tube end where the permeate product pressure is predefined and proceed step-by-step to the closed tube end. Note that the total permeate flow in the central tube equals to the permeate flow from a membrane leaf multiplied by the number of the membrane leaves in a spiral-wound module.
16. Set the permeate pressure profile in the permeate channels between the membrane leaves equal to the local pressure in the permeate collection tube along the x directed grid line. Compute the discrete velocity field for the retentate and permeate from the molar flow rates, molar volumes, and specified cross-section area for the flow. Compute the required pressure drop for the fluid flow in a membrane leaf and between the membrane leaves from the equations (4.30), (4.31), and (4.32) with an appropriate friction factor equation. For the permeate channel, use equation (4.33) with $C_f = 48$ (Hickey and Gooding, 1994). Repeat 3-15 for the pressure profile computation, but check the convergence of each grid line j from the pressure profile and the convergence of the entire membrane leaf from the permeate temperature profile. Grid line j is solved when the absolute average norm of the residual vector is below 1 Pa. The membrane leaves are solved when the changes in the permeate temperature profile are below the preset tolerances, as in step 14.

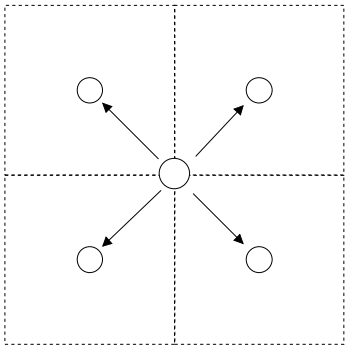

Figure 8.2 Information transfer from a coarser grid to a finer grid.

8.2 EXAMPLE SIMULATION: SELECTIVE REMOVAL OF HYDROCARBONS FROM HYDROGEN

The effect of the grid density on the computation time and the stage cut — the fraction of feed permeating through the membrane — was studied by running several simulations with different numbers of grid lines. A mixture of hydrogen, methane, ethane, propane, and hydrogen sulfide was used as a simulation example. Nitrogen and propylene with zero mole fractions were included in the mixture since a flowsheet model should handle zero components without convergence problems. Preferentially, hydrocarbons and hydrogen sulfide permeate through the PDMS membrane over hydrogen, so this simulation example is called the selective removal of hydrocarbons from hydrogen.

The feed mixture composition and the constant conditions in the simulation runs are given in Table 8.1. An example of a simulation input file is given in appendix VII, the same thermodynamic and physical property selections were applied in all simulations. The component and energy fluxes through the membrane were evaluated at median grid line properties. For comparison, two additional simulations were performed: one with the fluxes evaluated at each main grid point and another with an assumption of isothermal separation. The permeate side pressure drop was included in all the above simulations, but the retentate side pressure drop was neglected. As a comparison, a third additional simulation run was carried out without the permeate side pressure drop.

The computation times on Digital AlphaServer 2100 Model 5/375 with four processors are presented in Table 8.2. The computation of component and energy fluxes through the membrane requires the greatest computational effort. Therefore, the greatest effect of the grid density, or the number of control volumes, concerns the computation time and the increase in the computation time is linear with the increasing number of the grid lines.

Table 8.1 The feed properties and constant conditions used in the simulations of the selective removal of hydrocarbons from hydrogen.

Total feed, kg/h	1000
Composition, mole-%	
H_2	85.0
CH_4	7.0
C_2H_6	4.0
C_3H_6	0.0
C_3H_8	2.5
H_2S	1.5
N_2	0.0
Feed pressure, kPa	2750
Feed temperature, °C	40
Permeate pressure, kPa	800
Membrane area, m^2	80
Number of parallel modules	2
Number of serial modules	2
Number of membrane leaves in a module	10
Selective layer material	PDMS
Selective layer thickness, μm	4
Leaf length, m	0.9
Number of *z* directed grid lines	50

Table 8.2 also reveals the vast difference between the used thermodynamic models. The model equations with SLNLF are solved approximately 35 times faster than the model equations with PHSC, when the fluxes are computed at the median grid line properties, and approximately 100 times faster in the isothermal system. The composition dependent mixing and combining rules of SLNLF requires less computational effort than the mixing and combining rules of PHSC, which depend on the composition, temperature, and density. Moreover, the mixing and combining rules of SLNLF have to be computed only once, after which the roots of the equation (6.1) may be solved, whereas the mixing and combining rules of PHSC have to be computed on each iteration count that is spent to solve the roots of the equation (6.49).

The computed component and energy fluxes are assumed to be valid over the control volume. This assumption resembles the numerical integration with constant step size and midpoint rule. Then, in principle, an increasing of the number of control volumes will provide more accurate approximation to the profiles of the individual component fluxes through the membrane over the membrane module. Also the stage cut is approximated more accurately. However, the effect of the number of control volumes on stage cut is insignificant based on Figure 8.3. This is due to the selected system that mainly consists of hydrogen and methane,

for which diffusion in the membrane is concentration independent and the flux through the membrane is constant over the membrane modules (Figure 8.4 and Figure 8.5). The change in the stage cut remains insignificant when the component and energy fluxes are computed at each main grid point, instead of the median properties of the *x* directed grid lines and, further, when the permeate side pressure drop is neglected. Changes in the sixth decimal of the stage cut were observed in the above mentioned cases.

Table 8.2 The effect of the number of *x* directed grid lines on computing time on Digital AlphaServer 2100 Model 5/375 with four processors.

No. of *x* directed grids	Model equations with SLNLF CPU, sec.	Model equations with PHSC CPU, sec.
6	10	383
8	15	512
10	13	503
20	25	894
40	44	1510
60	63	2270
80	83	2880
100	103	3550
60[a)]	505	40700
60[b)]	17	1760
60[c)]	68	2250

[a)] Fluxes computed at each control volume.
[b)] Isothermal permeation.
[c)] Pressure drop neglected both on the permeate and retentate sides.

Despite the insignificance of the change in the stage cut, there is an observable trend in the calculated stage cut values with respect to the grid density. The behavior of the computed stage cut curves is unstable below 40 *x* directed grid lines, reflecting an insufficient number of control volumes. The minimum number of *x* directed grid lines for this example simulation is 40, since predicted stage cut curves start to decline as the number of grid lines is increased. Obviously, the decline of the curves would level off when the number of *x* directed grid lines is further increased — in theory to infinity.

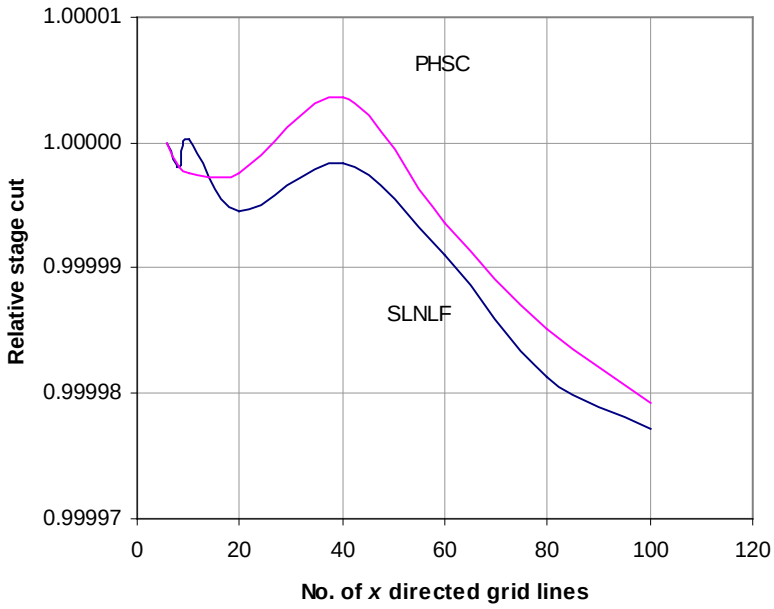

Figure 8.3 Change in relative stage cut with respect to number of *x* directed grid lines.

The simulated permeate and retentate flow properties are given in Table 8.3 and the separation factors

$$\alpha_{ij} = \frac{y_{iV} x_{jL}}{x_{iL} y_{jV}} \tag{8.1}$$

over hydrogen are provided in Table 8.4. This simulation example can be classified as an isothermal separation since the model equations predicted a temperature decrease of 0.1°C. In this case, the cooling of hydrocarbons is just balanced with the heating of hydrogen on expansion.

Hydrocarbon selective membranes could be used to selectively remove enriching hydrocarbon components from hydrogen rich recycle streams in refinery hydroprocessing units as described in a recent patent by Lokhandwala and Baker (2001). The PDMS membrane preferentially permeates hydrocarbons and hydrogen sulfide so that recovered hydrogen is obtained at high pressure, contrary to hydrogen selective membranes. The predicted separation selectivity in Table 8.4 is only 3.4-3.5 for hydrogen sulfide and 2.2-2.4 for propane over hydrogen. Usually, an ideal separation factor α_{ij}^{0} is used to characterize the separation between components *i* and *j*

$$\alpha_{ij}^{0} = \frac{P_i}{P_j}, \tag{8.2}$$

where P_i and P_j are the pure component permeabilities of components *i* and *j* respectively. Based on the pure component permeability coefficients in Table 7.20, the ideal separation factor for propane over hydrogen is 8.8 at 0.345 MPa. For a comparison, a value of 8.5 may be calculated from the permeability data provided by Bhide and Stern (1991). Due to the nature of the vapor membrane separation, the real separation factor will be far from the ideal separation factor and will decrease with the increase of the stage cut.

Despite the low separation factors, the simulated membrane process has clear advantages. The process will remove about half of hydrogen sulfide and 40% of propane from the feed with a simultaneous hydrogen loss of about 70 kg/h. When the same amount of hydrogen sulfide or propane is removed by purging, the hydrogen loss will be about 150 kg/h and about 120 kg/h respectively.

Table 8.3 Simulation results for the selective removal of hydrocarbons from hydrogen. The separation was computed with the non-isothermal model equations with 60 *x* directed grid lines and 50 *z* directed grid lines.

	Model equations with SLNLF		Model equations with PHSC	
	Permeate	Retentate	Permeate	Retentate
Mass flow, kg/h	314	686	317	683
Molar flow, kmole/h	42.3	134.6	43.7	133.2
Temperature, °C	39.9	39.9	39.9	39.9
Pressure, kPa	800	2750	800	2750
Composition, mole frac.				
H_2	0.798	0.866	0.803	0.865
CH_4	0.069	0.070	0.068	0.070
C_2H_6	0.058	0.034	0.057	0.034
C_3H_6	0.000	0.000	0.000	0.000
C_3H_8	0.043	0.019	0.040	0.020
H_2S	0.031	0.010	0.031	0.010
N_2	0.000	0.000	0.000	0.000
Component cut, -				
H_2	0.225	0.775	0.233	0.767
CH_4	0.237	0.763	0.242	0.758
C_2H_6	0.348	0.652	0.352	0.648
C_3H_6	-	-	-	-
C_3H_8	0.408	0.592	0.398	0.602
H_2S	0.501	0.499	0.509	0.491
N_2	-	-	-	-

The individual component flux profiles are provided in Figure 8.4 and Figure 8.5. As already mentioned, hydrogen and methane flux profiles are nearly constant over the serial membrane modules. This is due to concentration independent diffusivity within the selective layer and, to a great extent, due to an almost constant mole fraction of hydrogen and methane in the

retentate flow (Table 8.3). The mole fractions of ethane, propane, and hydrogen sulfide were originally low in the feed (Table 8.1). Then the sorption and diffusion within the selective layer take place at the infinite dilution region and hence the flux profiles are decreasing linearly along the flow.

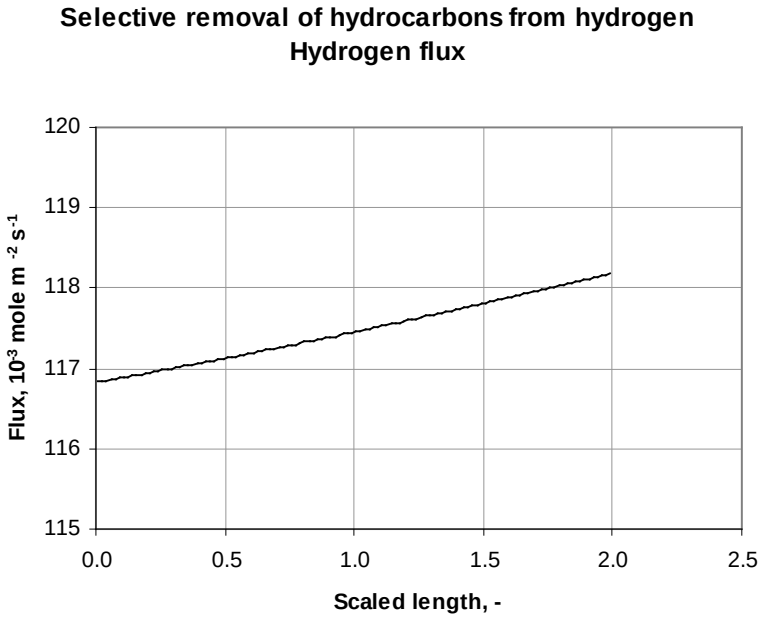

Figure 8.4 Predicted hydrogen flux through the PDMS membrane. The flux profile was computed from the non-isothermal model equations combined with SLNFL.

Table 8.4 Separation factors for the selective removal of hydrocarbons.

	Model equations with SLNLF	Model equations with PHSC
H_2	1.000	1.000
CH_4	1.073	1.046
C_2H_6	1.842	1.784
C_3H_6	-	-
C_3H_8	2.376	2.171
H_2S	3.458	3.404
N_2	-	-

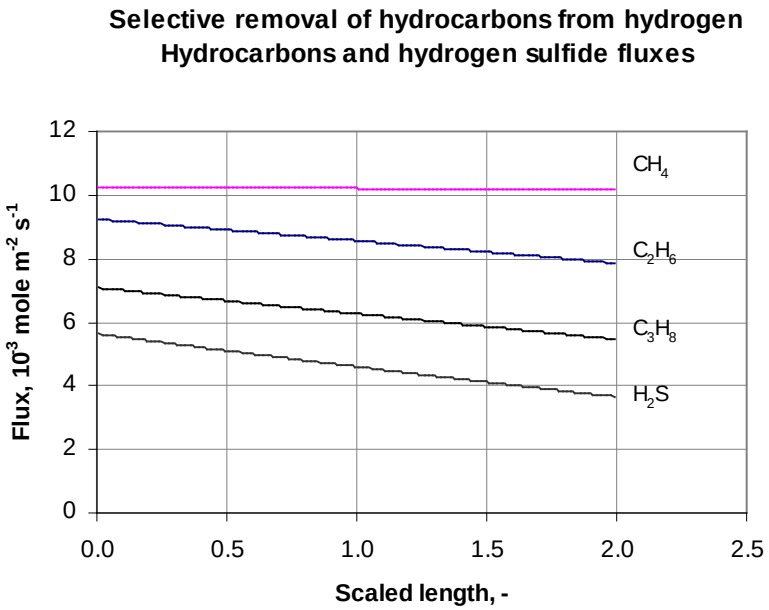

Figure 8.5 Predicted fluxes of hydrocarbons and hydrogen sulfide through the PDMS membrane. The flux profiles were computed from the non-isothermal model equations combined with SLNFL.

8.3 EXAMPLE SIMULATION: PROPYLENE RECOVERY

A membrane separation process of commercial interest is the monomer recovery from the polypropylene resin degassing (Baker and Jacobs, 1996). The two-stage process shown in Figure 8.6 is currently in operation at the DSM polypropylene plant in Geleen, the Netherlands. Baker and Jacobs (1996) provide a design material balance for this process, which has approximately 50 membrane modules providing an approximately 280 m^2 total membrane area (*Filtration and Separation*, 1996). Although the material balance by Baker and Jacobs (1996) is a design material balance, it is used as a quantitative point of comparison for the simulation results of this section. Basic data for this two-stage process is given in Table 8.5.

The first separation stage of the two-stage process, ST-1 in Figure 8.6, performs the bulk separation of hydrocarbons from nitrogen to produce a hydrocarbon lean nitrogen product stream. The second separation stage, ST-2, is required to enrich the separated hydrocarbon fraction, stream no. 3, to a hydrocarbon rich product stream that can be recycled directly into the polypropylene reactor feed. The hydrocarbon depleted retentate stream from the ST-2 (no. 4) is recycled into the feed of the ST-1. The process requires two compressors: one for the compression of the feed into the unit and another for the compression of the permeate from

the stripping stage. The feed temperatures to the separation stages were not specified in the literature; therefore the feed temperatures were set to 20°C in this work.

Table 8.5 Basic data for the two-stage propylene recovery process (Baker and Jacobs, 1996; Baker *et al.* 1998).

Feed flow, kg/h (lb/h)	1597 (3520)
Feed pressure, kPa (psia)	103 (15)
Feed composition, vol-%	
N_2	86.7
$C_2H_4 + C_2H_6$	0.3
C_3H_6	10.0
C_3H_8	3.0
Nitrogen product flow, kg/h (lb/h)	1334 (2940)
Nitrogen product pressure, kPa (psia)	1379 (200)
Nitrogen product composition, vol-%	
N_2	96.4
$C_2H_4 + C_2H_6$	0.1
$C_3H_6 + C_3H_8$	3.5
Hydrocarbon product flow, kg/h (lb/h)	263 (580)
Hydrocarbon product pressure, kPa (psia)	103 (15)
Hydrocarbon product composition, vol-%	
N_2	15.5
$C_2H_4 + C_2H_6$	1.5
$C_3H_6 + C_3H_8$	83.0

An example of an input file for the two-stage process is given in appendix VIII. The stream no. 4 was set as a cut stream and, therefore, the initial guesses for the flow rate and the composition were given in the flow specifications. The membrane modules are specified in Table 8.6; similar membrane modules were used in the separation stages ST-1 and ST-2. The module arrangement in the separation stages was searched by trial and error. The first separation stage was discovered to consist of four serial and 11 parallel modules, providing a total membrane area of 264 m^2. The second separation stage was discovered to consist of two parallel modules, providing a total membrane area of 12 m^2. The ideal gas law was selected for the calculation method of the vapor specific molar volumes due to the low pressure on the permeate side and the medium pressure on the retentate side. The method of Aasberg-Petersen *et al.* (1991) was specified for the calculation of the vapor viscosity. In these simulations, the permeate side pressure drop was included but the retentate side pressure drop was neglected.

The process simulations were carried out by computing the membrane separation stage performances from the model equations combined with SLNLF and PHSC. The resulted material balances from these simulations are given in Table 8.7 and in Table 8.8 respectively. In these simulations, the component and energy fluxes through the membrane were computed at median properties of a grid line. As a comparison, an additional simulation was carried out

without the permeate side pressure drop. The resulted material balance from this simulation is presented in Table 8.9.

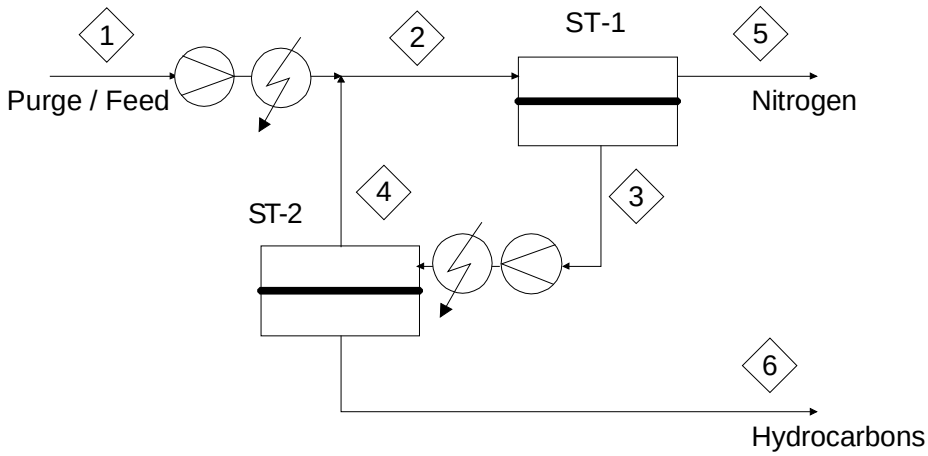

Figure 8.6 Two-stage membrane separation process for the propylene recovery from the polypropylene resin degassing (adapted from Baker and Jacobs, 1996). ST-1 is a stripping stage and ST-2 is an enriching stage.

Table 8.6 Spiral-wound module specification.

Module membrane area, m^2	6.0
Selective layer material	PDMS
Selective layer thickness, μm	4.0
No. of leaves in a module	4
Leaf length, m	0.9
Feed channel height, mm	1.3
Permeate channel height, mm	1.0
No. of *x* directed grid lines	76
No. of *z* directed grid lines	20

The calculated results correspond rather well with the design material balance by Baker and Jacobs (1996). A comparison to the design material balance in Table 8.5 reveals that the smaller amount of nitrogen product, the greater amount of hydrocarbon product, the higher purity of the nitrogen product, and the higher recovery of the C3 fraction were obtained in the current material balances. The absolute deviations in the nitrogen product flow rates are 2% with SLNLF and 2.3% with PHSC. The corresponding absolute deviations in the hydrocarbon product flow rates are 10.7% and 11.9% respectively.

Table 8.7 and Table 8.9 provide the predicted material balances based on the same model equations, but in the latter the permeate side pressure drop was neglected. As a result, the propane recovery increased by 0.1 per cent units and small differences in the flow

compositions are noted mainly for nitrogen and propane. However, these changes are negligible: the permeate side pressure drop seems indeed to have an insignificant effect on the productivity of a multileaf membrane module.

Table 8.7 Predicted material balance for the propylene recovery computed from the model equations with SLNLF. The resulted propylene recovery is 86.4%, nitrogen recovery 97.8%, and propane recovery 84.0%.

Flow no.	1	2	3	4	5	6
Pressure, kPa	101	1380	150	1385	1380	103
Temperature, °C	25.0	20.0	16.7	17.0	13.8	18.1
Mass flow, kg/h	1587	2966	1663	1379	1303	283
Molar flow, kmol/h	53.1	95.2	49.2	42.1	46.0	7.0
Composition, mole %						
Nitrogen	86.70	77.99	59.44	67.00	97.81	14.23
Ethylene	0.15	0.30	0.48	0.49	0.10	0.46
Ethane	0.15	0.13	0.25	0.10	13 ppm	1.12
Propylene	10.00	16.18	29.88	23.99	1.54	65.17
Propane	3.00	5.40	9.95	8.43	0.55	19.01

Table 8.8 Predicted material balance for the propylene recovery computed from the model equations with PHSC. The resulted propylene recovery is 84.8%, nitrogen recovery 97.2%, and propane recovery 73.7%.

Flow no.	1	2	3	4	5	6
Pressure, kPa	150	1380	150	1385	1380	103
Temperature, °C	25.0	20.0	16.6	17.5	13.5	18.4
Mass flow, kg/h	1587	2966	1850	1570	1307	280
Molar flow, kmol/h	53.1	95.2	55.1	48.1	46.0	7.1
Composition, mole %						
Nitrogen	86.70	77.54	61.17	67.42	97.16	18.56
Ethylene	0.15	0.29	0.45	0.44	0.10	0.46
Ethane	0.15	0.29	0.47	0.46	0.09	0.53
Propylene	10.00	16.25	28.35	23.15	1.73	63.82
Propane	3.00	5.63	9.56	8.52	0.91	16.63

Table 8.9 Predicted material balance for the propylene recovery computed from the model equations with SLNLF. The permeate side pressure drop was neglected. The resulted propylene recovery is 86.4%, nitrogen recovery 97.8%, and propane recovery 84.1%.

Flow no.	1	2	3	4	5	6
Pressure, kPa	101	1380	150	1385	1380	103
Temperature, °C	25.0	20.0	16.7	17.0	13.8	18.1
Mass flow, kg/h	1587	2966	1663	1379	1303	283
Molar flow, kmol/h	53.1	95.2	49.2	42.1	46.0	7.0
Composition, mole %						
Nitrogen	86.70	77.99	59.43	66.98	97.81	14.23
Ethylene	0.15	0.30	0.49	0.49	0.10	0.46
Ethane	0.15	0.13	0.25	0.10	13 ppm	1.12
Propylene	10.00	16.18	29.89	23.99	1.53	65.18
Propane	3.00	5.41	9.95	8.44	0.55	19.02

Non-isothermal separation is clearly present in this simulation example. The retentate product flow temperature decreases from the feed temperature of 20°C over 6°C in the first stage

(Figure 8.10) and over 3°C in the second stage (Figure 8.14). The retentate product flow is noted to exit at a lower temperature than the permeate product flow (Table 8.7, Table 8.8, and Table 8.9) because energy is continuously removed from the flow element in the retentate channel to the flow element in the permeate channel. The local permeate flow from the membrane leaves mixes with the permeate flow in the central tube. Hence the permeate product temperature is approximately an average of the local permeate temperatures.

The retentate and permeate temperature profiles in the stripping stage (Figure 8.10) are almost equal. The temperature difference of fluids over the membrane is 0.35°C at the beginning of the stripping stage, after which it decreases steadily along the distance from the feed inlet to almost zero at the retentate exit boundary. The temperature profiles stay further apart in the enriching stage (Figure 8.14) in the range of 0.3-0.4°C due to the lower stage cut and the lower heat transfer area than in the stripping stage.

The nitrogen flux profile through the membrane in the stripping stage is presented in Figure 8.7 and in the enriching stage in Figure 8.11. As expected, these profiles are quite stable because the nitrogen diffusivity is concentration independent within the selective layer. The nitrogen flux through the membrane first increases in the enriching stage due to an increase in the concentration of the retentate flow, and then starts to decrease in the second serial module due to an overcome by the effect of the temperature decrease on permeation. The effect of the temperature decrease is absent in the enriching stage due to a small fraction of feed allowed to permeate through the membrane.

The ethylene and ethane fluxes through the membrane in the stripping stage are presented in Figure 8.8 and in the enriching stage in Figure 8.12. The corresponding profiles for propylene and propane are presented in Figure 8.9 and Figure 8.13. The purpose of the stripping stage is to recover the maximum amount of propylene from the nitrogen so that the enriching stage is able to fulfil the product purity and recovery requirements. The recovery in the stripping stage is achieved by allowing a large fraction of the feed to permeate through the membrane. At the same time a large quantity of propane is recovered. The flux profiles decay exponentially along the distance from the feed inlet due to the concentration and temperature dependent permeation. For example, the propylene flux reduces to a tenth of the initial flux rate. At the same time ethylene and ethane are recovered from the nitrogen, however, at the lower rate due to the low concentration of components in the feed.

The enriching of propylene is achieved by allowing only the richest fraction of the feed to permeate through the membrane in the enriching stage so that the propylene flux is at its highest level. This means that a low fraction of the feed is taken to the permeate product and the amount of the product depends on the purity requirements. Therefore, the flux profiles of hydrocarbons do not change a great deal in the enriching stage and the ethylene and ethane concentrations remain essentially constant (Table 8.8).

All simulations required seven iterations for a flowsheet convergence. The computation times of the various modeling combinations are given in Table 8.10. The computation time interval is provided for the outer iteration; the smallest correspond to the solution time of the serial leaves during the final flowsheet iteration and the greatest to the solution time of the serial leaves just after the initialization stage. The computation time difference between the model equations with SLNLF and PHSC is again vast. The computation time of the former is counted in minutes while the computation time of the latter is counted in hours. The explanation for this is already given in the previous section. Interestingly, the omitting of the permeate side pressure drop did not decrease the computation time.

Table 8.10 Computation times on Digital AlphaServer 2100 Model 5/375 with four processors for the propylene recovery simulations.

		Initialization CPU sec.	Outer iteration CPU sec.	Total simulation CPU sec.
Model equations with SLNLF, fluxes at median grid line properties	ST-1	31	39-125	993
	ST-2	11	19-47	
Model equations with PHSC, fluxes at median grid line properties	ST-1	1174	1439-5280	36745
	ST-2	359	834-1512	
Model equations with SLNLF, no permeate side pressure drop	ST-1	32	52-131	1027
	ST-2	12	14-45	

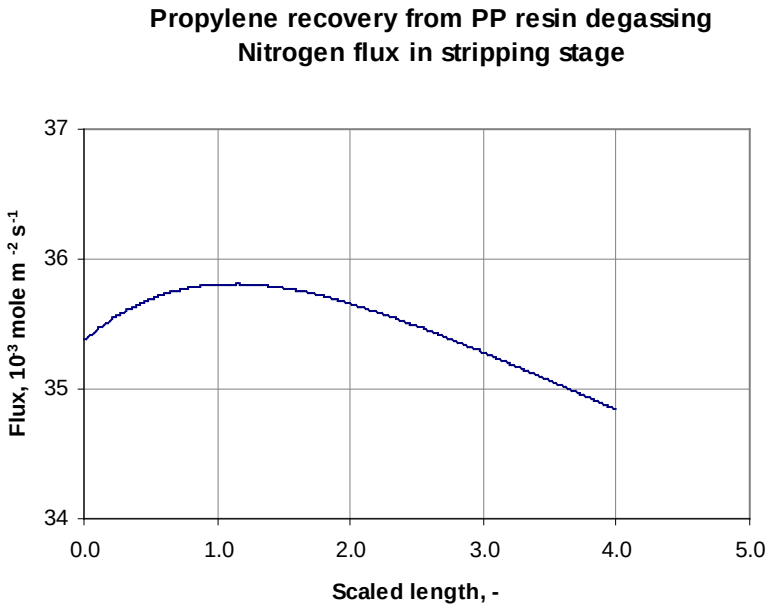

Figure 8.7 Nitrogen flux through the PDMS membrane in the stripping stage. The flux profile is obtained from the model equations combined with PHSC.

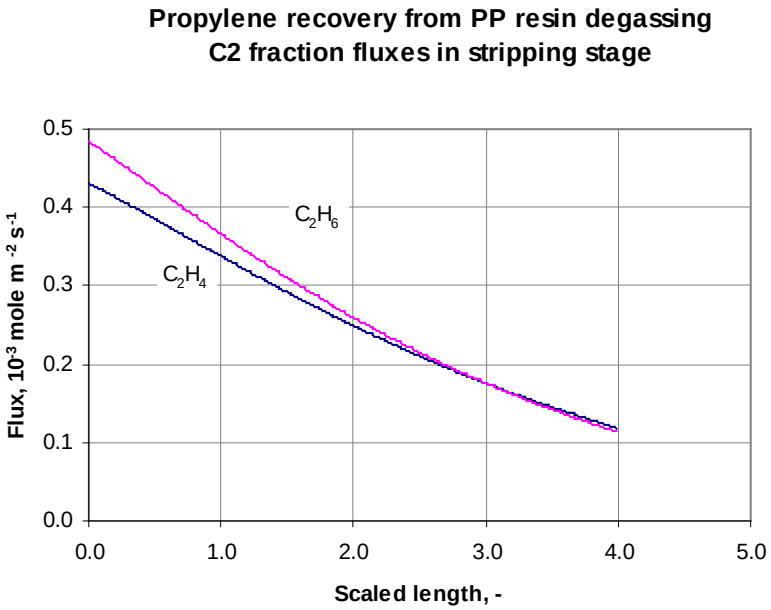

Figure 8.8 Ethylene and ethane fluxes through the PDMS membrane in the stripping stage. The flux profiles are obtained from the model equations combined with PHSC.

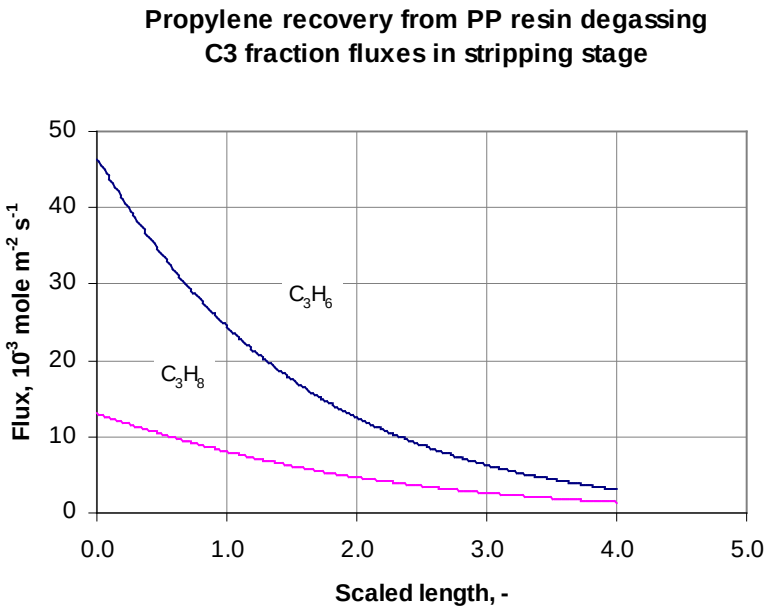

Figure 8.9 Propylene and propane fluxes through the PDMS membrane in the stripping stage. The flux profiles are obtained from the model equations combined with PHSC.

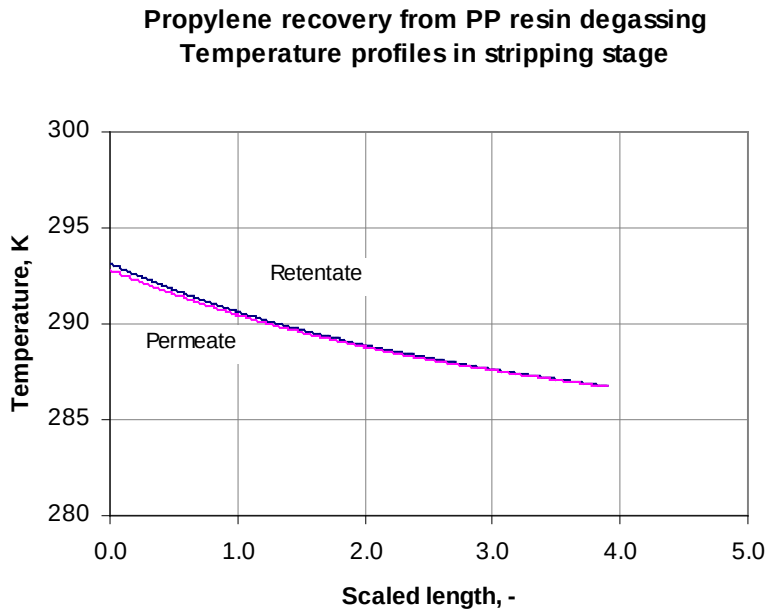

Figure 8.10 Temperature profiles in the stripping stage.

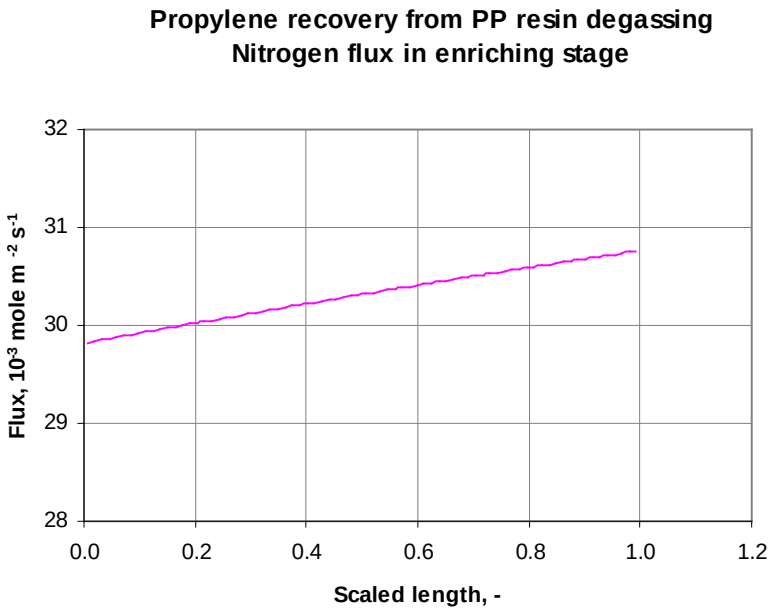

Figure 8.11 Nitrogen flux through the PDMS membrane in the enriching stage. The flux profile is obtained from the model equations combined with PHSC.

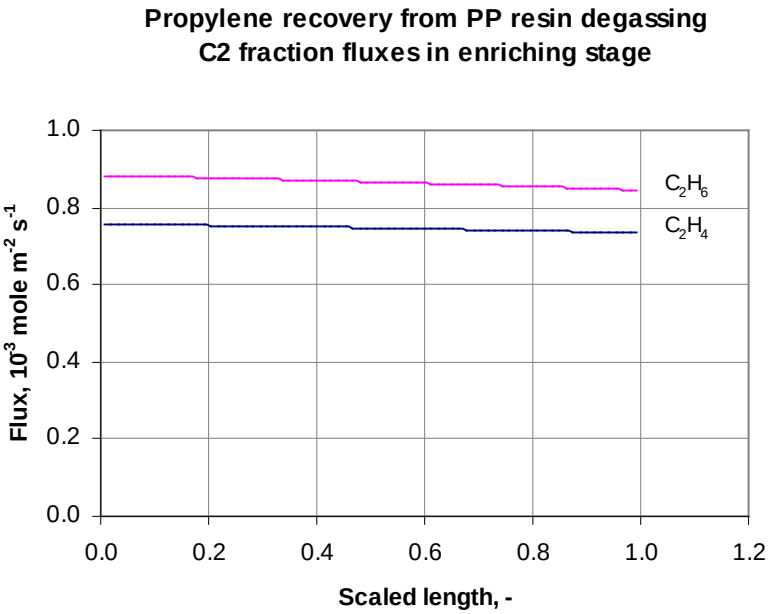

Figure 8.12 Ethylene and ethane fluxes through the PDMS membrane in the enriching stage. The flux profiles are obtained from the model equations combined with PHSC.

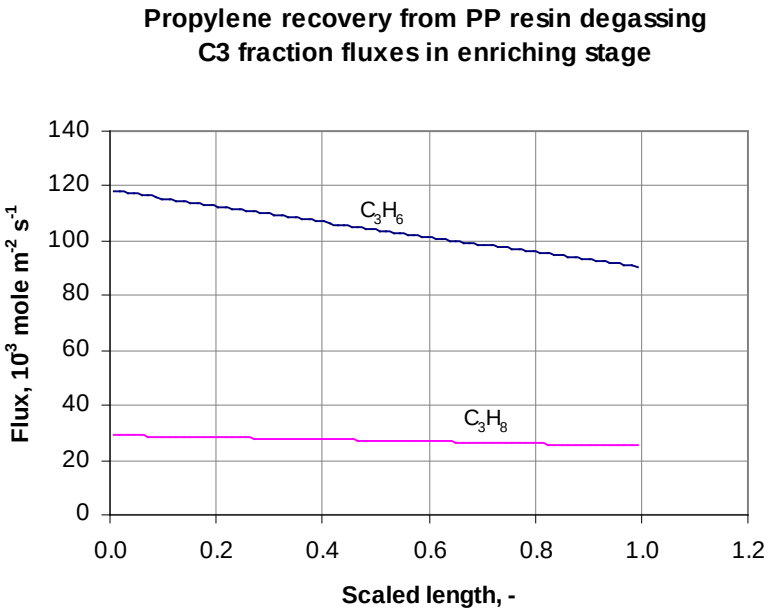

Figure 8.13 Propylene and propane fluxes through the PDMS membrane in the enriching stage. The flux profiles are obtained from the model equations combined with PHSC.

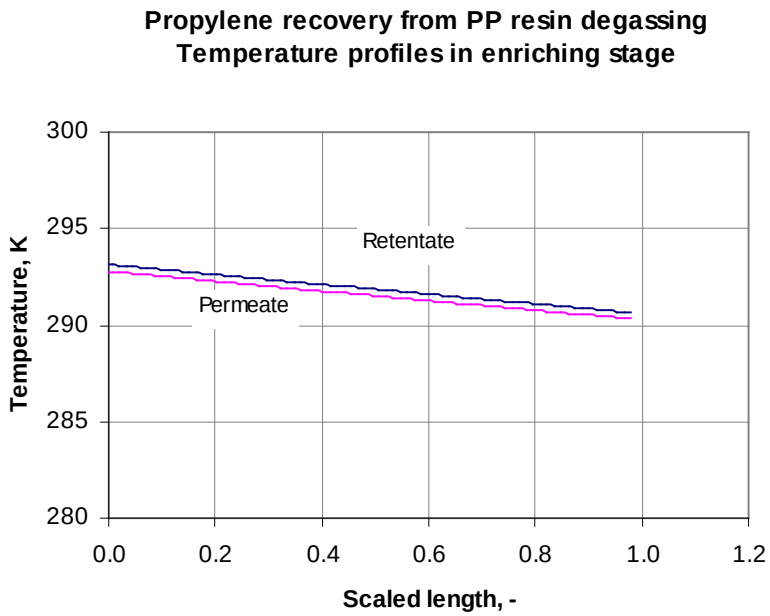

Figure 8.14 Temperature profiles in the enriching stage.

9 CONCLUSIONS

In this work, a new unit operation model was developed for vapor membrane separation with rubbery membranes. The new model utilizes thermodynamic models for polymeric systems, multicomponent mass transport theories, transport theories in polymeric systems, and techniques from computational fluid dynamics.

Various thermodynamic models were compared in the modeling of vapor and gas sorption in melt or rubber polymers. These models included equation of state models for polymeric systems and combined equation of state–excess Gibbs energy models with the MHV2 mixing rule by Dahl and Michelsen (1990). The group of equation of state models for polymers included both the lattice and nonlattice fluid development of the Sanchez–Lacombe equation of state (Sanchez and Lacombe, 1976; Lacombe and Sanchez, 1976; Sanchez, 1987), and the perturbed hard-sphere-chain equation of state (Song *et al.*, 1994a and 1996). The group of combined EOS–G^E models included the combinations of the Soave–Redlich–Kwong equation of state with the UNIFAC-FV model by Oishi and Prausnitz (1978) and the exponential UNIFAC modification proposed in this work. The difference between the two activity coefficient models is that the UNIFAC-FV model uses solvent liquid molar volumes to account for the free volume effect in a polymeric system, whereas the exponential UNIFAC modification accounts for the free volume effect directly in the combinatorial part without any liquid volume data.

In the thermodynamic model verification, the combined EOS-G^E models provided better Henry's law coefficient predictions in various solvent–polymer systems than the other equation of state models. Gas sorption predictions are not possible with the UNIFAC-FV model, since gas group volume and surface area parameters are not available in the original UNIFAC model and the free volume contribution requires liquid volume data. Gas sorption predictions are possible with the exponential UNIFAC model; however, the gas sorption predictions were not any better than those with SLNLF or PHSC and the determination of the new group interaction parameter table was considered non-profitable. Therefore, this model was excluded from any further use in this work. The non-lattice model version of the Sanchez–Lacombe equation of state (Sanchez, 1987) and the perturbed hard-sphere-chain equation of state (Song *et al.*, 1996) were found to provide feasible predictions and hence to be the appropriate models for the purposes of this work. PHSC was found to be very

appropriate in PDMS systems, but this model should be applied with caution in other polymeric systems, especially without binary interaction parameters. The computational effort of PHSC is considerably greater than that of the non-lattice fluid version of the Sanchez–Lacombe equation of state.

The penetrant transport within the membrane was described with the Maxwell–Stefan based equations of multicomponent mass transfer. The binary penetrant–membrane diffusion coefficients for the transport equations are determined from the pure component permeability coefficients. Experimental permeability data at different temperatures and pressures are required to capture the temperature and concentration dependent behavior of the binary penetrant–membrane diffusion coefficients. The binary penetrant–membrane diffusion coefficients at infinite dilution were conveniently correlated with the classical free volume theory of Fujita *et al.* (1960). A new equation was developed for the correlation of the concentration dependence of the binary penetrant–membrane diffusion coefficients in a polymeric membrane. This approach captures the behavior of the binary penetrant–membrane diffusion coefficients very well and provides the basis for the diffusion coefficients in multicomponent systems.

The transport equations within the membrane were solved by using the film model with the Krishna (1977) approximation of the exact matrix solution and the simplified solution of Burghardt and Krupiczka (1975) for the Stefan diffusion. The former is an iterative solution method, while the latter provides the component fluxes through the membrane without iteration. The film models were used in the generalized form, i.e. the matrix of thermodynamic factors was included to account for the system non-ideality. In the transport equations, the membrane, or to be exact, the chain segments of the polymer, were allowed to have a finite diffusion flux against the fluxes of penetrant components. This gives rise to the bulk flux contribution in the permeation.

The Krishna (1977) approximation of the exact matrix solution and the simplified solution of Burghardt and Krupiczka (1975) for the Stefan diffusion yielded exactly the same results. The simplified solution is preferred, since it provides component fluxes without iteration. The cross-coefficients $Đ_{ij}$ in the transport equations were computed from the geometric average of the binary penetrant–membrane diffusion coefficients at maximum penetrant concentration. The effect of including the cross-coefficients was to suppress the flux of the components of

high diffusivity — which is the correct effect of flux coupling — but the results without the cross-coefficients were in better agreement with the low-pressure experimental data. Therefore, the transport equations were later on used without the cross-coefficients. More experimental data is required in order to draw any definite conclusions about the effect of the diffusional coupling in vapor membrane separation.

The permeation model was combined with the model for the fluid flow in multileaf spiral-wound modules. In the flow model, the operation of a spiral-wound module was described by a membrane leaf and a central tube. Equations for the discretized flow field were developed from the basic conservation equations of mass, momentum, and energy. The discretization of the model equation was performed by following the control volume approach of Patankar (1980). The non-isothermal operation of spiral-wound modules was expected since a real fluid is exposed to internal heating or cooling on expansion. This was clearly shown in the example simulation of the propylene recovery from the polypropylene resin degassing. The example simulation of the selective removal of hydrocarbons from hydrogen was almost isothermal, because the effect of internal cooling of hydrocarbons was balanced by the internal heating of hydrogen on expansion.

A line-by-line solution procedure was provided for solving the combined permeation and fluid flow model in a membrane leaf or membrane leaves in series. The membrane leaves have to be solved many times to allow the initial fluid flow field to relax to the final converged flow field. The control volume method describes the flow field in discrete grid points and the description becomes more accurate when the grid density is increased. The optimal grid density is such that the increase in the grid density would not significantly change the profiles of the component fluxes and the flow temperatures. A routine could have been created that starts from a coarse grid solution, then finds the solution for a denser grid spacing, observes the changes in profiles, and repeats the densification until the change in profiles becomes insignificant so that the optimum solution is found for the flow field. However, it was decided to use a constant number of control volumes in order to save computation time. This choice will never be destructive in view of flowsheet simulation, since, as stated by Patankar (1980, pp. 30-31), the control volume approach satisfies the integral conservation of mass, momentum, and energy over any group of control volumes and for any number of grid points.

A multileaf spiral-wound membrane module provides short permeate flow paths. It was observed from the example simulations that the resulting pressure drop is insignificant in terms of the module productivity. As a consequence, the component and energy fluxes through the membrane do not have to be calculated at each grid point. The evaluation of the fluxes at the median properties of a grid line provides an adequate description, since the local permeate fluxes through the membrane remain almost constant along the grid line for the permeate flow. This diminishes the computation time considerably since the evaluation of the component and energy fluxes requires the greatest computational effort.

The developed model was implemented into an in-house process simulator (FLOWBAT, 2001) that makes it possible to combine vapor membrane separation with other existing unit operation models. This implementation is useful in the identification and the evaluation of potential new applications for vapor membrane separation and it also aids in the designing of vapor membrane separation processes for optimal performance.

The developed model has its bases on well-founded theoretical equations. Conventional approaches follow the solution–diffusion model in its simplest form so that the permeation flux through the membrane is related to the exterior conditions over the membrane by a permeability coefficient. In this work, the thermodynamic and kinetic contribution to permeation as well as the real fluid effects were treated with the theoretical models so that the temperature, pressure, and concentration dependent permeation through the rubbery membrane can be more profoundly accounted for. The rigorousness and the complexity of the new model well exceed the level of the previous mathematical models for gas and vapor membrane separation. However, the reward of this effort is the greater confidence on the model’s predictions on multicomponent mixture separations especially in regions where experimental data is not available.

10 NOMENCLATURE

A	Total Helmhotz energy Flow area
$A(\lvert Pe \rvert)$	Interpolation function, eq. (4.72)
A^E	Excess Helmholtz energy
A_d	Penetrant dependent pre-exponential factor in the diffusivity relation
A_{wk}	van der Waals surface area of group k
A^0	Helmholtz energy of pure substance
a	Energy parameter Coefficient in discretized energy equation
a_{mn}	Group interaction parameter of main groups m and n in the original UNIFAC
$a_{mn,1}$, $a_{mn,2}$, $a_{mn,3}$	Group interaction parameters of main groups m and n in the modified UNIFAC
B	Half distance of parallel plates
B_d	Penetrant dependent constant in the diffusivity relation
b	Co-volume parameter Hole affinity constant in (2.7)
C_D	Henry's type solubility concentration
C_d	Penetrant dependent constant in the diffusivity relation
C_f	Constant in the friction factor correlation
C_H	Langmuir type solubility concentration
$C_H^{'}$	Hole saturation constant
C_i	Concentration of penetrant in the membrane at standard temperature and pressure
C_p	Heat capacity at constant pressure
C_1, C_2, C_3	Mathias–Copeman pure component parameters
c	Proportionality constant to solvent activity in UNIFAC-FV
c_i	Molar density
D	Fick's diffusion coefficient
D_{01}	Pre-exponential factor in the solvent self-diffusivity relation
D_1	Solvent self-diffusion coefficient
$Đ$	Maxwell–Stefan diffusion coefficient in the mass fraction form
$Đ_{iM}$	Effective M–S diffusion coefficient for binary penetrant–membrane pair
D_T	Thermodynamically corrected diffusion coefficient
$Đ^{'}$	Maxwell–Stefan diffusion coefficient in the mole fraction form
$Đ^0$	Binary penetrant–membrane M–S diffusion coefficient at infinite dilution
$Đ^\infty$	Binary penetrant–membrane M–S diffusion coefficient at maximum penetrant weight fraction
DP	Number of data points
E	Activation energy
E_d	Penetrant dependent parameter in the diffusivity relation
E_P	Activation energy for permeation
e	Multicomponent energy flux
F_a	Universal function in PHSC for the energy parameter

F_b	Universal function in PHSC for the co-volume parameter
F_F	Total molar flow rate of feed
F_L	Total molar flow rate of retentate
F_V	Total molar flow rate of permeate
f	Fugacity
	Fanning friction factor
G	Total Gibbs energy
g	Intensive Gibbs energy
$g_{x,y,z}$	Gravitational force components
$g_{ij}(d_{ij}^{+})$	Radial distribution function
g^{E}	Molar excess Gibbs energy
$g^{E,C}$	Combinatorial molar excess Gibbs energy
H_i	Molar fraction based Henry's constant of component *i*
H_i^w	Weight fraction based Henry's constant of component *i*
$H_{\text{exp.}}^w$	Experimental weight fraction based Henry's constant
$\hat{H}$	Specific enthalpy
$\overline{H}$	Molar enthalpy
h	Heat transfer coefficient
J	Molar diffusive flux
J^V	Volume diffusive flux
j	Mass diffusive flux
k	Thermal conductivity
k_B	Boltzmann's constant
k_D	Henry law solubility coefficient
k_{ij}	Binary interaction parameter
L	Characteristic length
l	Number of serial modules
l_{ij}	Binary size correction parameter
M	Molecular weight
M_{1j}	Molecular weight of the solvent jumping unit
M_{2j}	Molecular weight of the polymer jumping unit
$\overline{M}_n$	Number average molecular weight
$\overline{M}_w$	Weight average molecular weight
m	Number of grid lines in *x* direction
N_i	Molar flux of component *i*
N_t	Total molar flux
Nu	Nusselt number, $\text{Nu} = h2B/k$
n	Total number of moles
	Number of grid lines in *z* direction
n_i	Mass flux of component *i*
n_t	Total mass flux
nc	Number of components
ng	Number of groups
P_i	Permeability coefficient of component *i*

P_f^0	Pre-exponential factor
Pe	Peclét number, Pe = RePr
Pr	Prandtl number, Pr = $\hat{C}_p \mu / k$
$\tilde{P}$	Reduced pressure
P^*	Characteristic pressure
p	Pressure
$p_{c,i}$	Critical pressure of component *i*
p^s	Saturation pressure
Q_k, Q_m	Group area parameters of groups *k* and *m*
Q_t	Total amount of permeated fluid per membrane area
q_i	Surface area parameter of component *i*
q_0, q_1, q_2	MHV2 parameters
R	Gas constant
R_{ct}	Radius of the central tube
R_k	Group volume parameter of group *k*
Re	Reynolds number, Re = $\rho v 2B / \mu$
r	Molecular size parameter Volume parameter in UNIFAC models Radial co-ordinate
r_i	Net rate of production of species *i* per unit volume
S_i	Solubility coefficient of component *i*
T	Temperature
$T_{c,i}$	Critical temperature of component *i*
T_r	Reduced temperature, $T_r = T / T_c$
T_0	Reference temperature
$\tilde{T}$	Reduced temperature, $\tilde{T} = T / T^*$
T^*	Characteristic temperature
t	Time
t_g	Time lag
$\hat{U}$	Specific internal energy
$u_{x,y,z}$	Permeate velocity components
V	Volume
V_{wk}	van der Waals volume of group *k*
V^*	Total close packed volume (lattice fluid) Total hard-core volume (non-lattice fluid) Occupied volume
V_0	Empty (free) volume
V_g^0	Specific retention volume at standard pressure and temperature
$\hat{V}_{FH}$	Average specific hole free volume
$\hat{V}_1^*$	Required minimum local free volume for a diffusive jump of the solvent
$\hat{V}_2^*$	Required minimum local free volume for a diffusive jump of the polymer
v	Molar volume
$v_{x,y,z}$	Retentate velocity components
v^*	Close packed mer volume (lattice fluid) Hard-core molecular volume (non-lattice fluid)

v_0^*	Hole volume
$\tilde{v}$	Reduced volume of the mixture
$\tilde{v}_i$	Reduced volume of component *i*
w	Mass fraction
w_y	Permeate velocity within the membrane
w^∞	Maximum weight fraction
X_m	Molar fraction of group *m*
x, y, z	Mole and number fractions Cartesian co-ordinates
z	Coordination number

Greek

α	Mixture α value, eq. (6.79)
α_i	Pure component α value
$\alpha_x, \alpha_y, \alpha_z$	Swelling ratios
α_{ij}	Separation factor of component *i* over *j*
α_{ij}^0	Ideal separation factor of component *i* over *j*
β	Darcy's law permeability
χ	Flory–Huggins interaction parameter
δ_{ik}	Kronecker delta: $\delta_{ik} = \begin{cases} 1 & , i = k \\ 0 & , i \neq k \end{cases}$
δ_m	Selective layer thickness
δ_m^0	Selective layer thickness of a penetrant free membrane
ε_{ij}	Non-bonded pair energy interaction between segments *i* and *j*
ε^*	Interaction energy per segment
Φ	Explicit mass transfer rate factor
φ	Fugacity coefficient
ϕ	Volume or segment fraction
ϕ'	Exponential volume fraction
Γ	Thermodynamic correction factor
Γ_k	Residual activity coefficient of group *k*
γ	Molar fraction activity coefficient
γ^C	Combinatorial contribution to the molar fraction activity coefficient
γ^{FV}	Free volume contribution to the molar fraction activity coefficient
γ^R	Residual contribution to the molar fraction activity coefficient
γ^∞	Molar fraction activity coefficient at infinite dilution
η	Packing factor
λ	Dimensionless distance in the film or in the selective layer
μ	Viscosity
μ_i	Chemical potential of species *i*
μ_i^0	Chemical potential of species *i* at the reference state

ν	Number of molecules
ν_r	Number of segments
ν_0	Number of empty lattice sites or holes
$\nu_k^{(i)}$	Number of groups *k* in component *i*
θ	Surface area fraction
ϑ	External degree of freedom for solvents in UNIFAC-FV
ρ	Mass density Number density in PHSC
ρ_r	Segment density
ρ^*	Characteristic density
$\tilde{\rho}$	Reduced density, $\tilde{\rho} = \rho / \rho^*$
σ_{ij}	Segment size
Ω^∞	Weight fraction based activity coefficient at infinite dilution
ω	Acentric factor, $\omega = -\log_{10}\left[p_r\left(T_r = 0.7\right)\right] - 1$
ω_i	Component specific constant in SLLF
Ξ	Explicit high flux correction factor
ξ	Parameter, eq. (2.6)
ξ_{ij}	Function, eq. (6.48)
ψ_{mn}	Group interaction parameter
ζ	Exponent in volume fraction of the exponential UNIFAC

Abbreviations

AAD	Absolute average deviation
AAN	Absolute average norm
CV	Control volume
EOS	Equation of state
HAP	Hazardous air pollutant
HDPE	High density poly(ethylene)
LCVM	Linear combination of the Vidal and Michelsen mixing rules
LDPE	Low density poly(ethylene)
MHV1	Modified Huron–Vidal mixing rule
MHV2	Second-order approximation of the Modified Huron-Vidal mixing rule
PcB	Poly(*cis*-1,4-butadiene)
PDMS	Poly(dimethylsiloxane)
PHSC	Perturbed hard-sphere-chain equation of state
PIB	Poly(isobutylene)
PP	Poly(propylene)
PS	Poly(styrene)
PTMSP	Poly[1-(trimetylsilyl)-1-propyne]
PVAC	Poly(vinyl acetate)
SLLF	Lattice fluid version of the Sanchez–Lacombe equation of state
SLNLF	Non-lattice fluid version of the Sanchez–Lacombe equation of state
SRK1	Soave–Redlich–Kwong equation of state with UNIFAC-FV
SRK2	Soave–Redlich–Kwong equation of state with the exponential UNIFAC

STP	Standard temperature and pressure: 273.15 K and 101325 Pa
UNIFAC	UNIQUAC functional-group activity coefficient
UNIFAC-FV	UNIQUAC fuctional-group activity coefficient with a free volume correction
UNIQUAC	Universal quasi-chemical activity coefficient
VOC	Volatile organic compound

Subscripts and superscripts

av	Average property
F	Feed property
FV	Free volume
i, j, k	Component indexes
j, k	Grid line indexes
k, m, n	Group indexes
L	Retentate property
m	Membrane or selective layer property
N, S, E, W, T, B	Grid point indexes
n, s, e, w	Control volume face indexes
o	Old value
r, θ, z	Radial co-ordinate indexes
s	Support layer property
t	Total property
V	Permeate property
x, y, z	Rectangular co-ordinate indexes
δ	Property at the end of the film
λ	Local property in the film
0	Property at the beginning of the film
1	Solvent
2	Polymer
I	Retentate–membrane interface
II	Membrane–permeate interface

Matrices and vectors

$[A]$	Matrix of inverted diffusion coefficient for Stefan diffusion
$[a]$	Matrix of coefficients of discretized energy equations
$[B]$	Matrix of inverted diffusion coefficients
(b)	Right hand side vector of the discretized energy equations
$(\overline{H})$	Vector of molar enthalpies of the discretized energy equations
$[I]$	Identity matrix
(j)	Vector of mass diffusion fluxes
(n)	Vector of mass fluxes
(w)	Vector of weight fractions
$[\beta]$	Bootstrap matrix

$[\Phi]$	Matrix of mass transfer rate factors
(ϕ)	Vector of rate factors
$[\Gamma]$	Matrix of thermodynamic correction factors
$[\Theta]$	Matrix of augmented rate factors
$[\Xi]$	Matrix of high flux correction factors
$\mathbf{g}$	Gravitational acceleration vector
$\mathbf{q}$	Conductive heat flux vector
$\mathbf{j}$	Mass diffusion vector
$\boldsymbol{\tau}$	Stress tensor
$\mathbf{v}$	General velocity vector
$\mathbf{v}$	Retentate velocity vector
$\mathbf{w}$	Local permeate velocity within the membrane
$\mathbf{u}$	Permeate velocity vector

Overlines

$\bar{}$	Average property, or partial intensive property
$\wedge$	Property per unit mass
$\sim$	Reduced property

11 REFERENCES

Aasberg-Petersen, K., Knudsen, K., Fredenslund, A. (1991). Prediction of viscosities of hydrocarbon mixtures, *Fluid Phase Equilib.* **70**, 293-308.

Alopaeus, V. (2001). Calculation of multicomponent mass transfer between dispersed and continuous phases, Acta Polytechnica Scandinavica, Chemical Technology Series, No. 283, Espoo.

Alopaeus, V., Koskinen, J., Keskinen, K. I. (1999). Simulation of the population balances for liquid-liquid systems in a nonideal stirred tank, Part 1 Description and qualitative validation of the model, *Chem. Eng. Sci.* **54**, 5887-5899.

Auvil, S. R., Srinivasan, R., Burban, P. M. (1991), Mechanism of gas transport in poly(1-trimethylsilyl-1-propyne), *Polym. Prepr.* **32**, 380-381.

Baker, R. W. (1985). Process for recovering organic vapors from air, *U.S. Patent* 4 553 983.

Baker, R. W. (1997). Membrane technology, in *Encyclopedia of separation technology*, vol. 2, Ruthven, D. M. (ed.), John Wiley & Sons, Inc., New York, 1212-1270.

Baker, R. W. (2000). *Membrane technology and applications*, McGraw-Hill, New York.

Baker, R. W., Jacobs, M. (1996). Improve monomer recovery from polyolefin resin degassing, *Hydrocarbon Processing* **75**, no. 3, 49-51.

Baker, R. W., Kaschemekat, J., Wijmans, J. G. (1996). Membrane systems to profitable VOC recovery, *Chemtech*, July, 37-43.

Baker, R. W., Lokhandwala, K. A. (1998). Membrane expansion process for organic component recovery from gases, U. S. Patent 5762685.

Baker, R. W., Wijmans, J. G., Kaschemekat, J. H. (1998). The design of membrane vapor–gas separation systems, *J. Membrane Sci.* **151**, 55-62.

Barbari, T. A., Conforti, R. M. (1994). Recent theories of gas sorption in polymers, *Polym. Adv. Tech.* **5**, 698-707.

Barrer, R. M. (1968). Diffusion and permeation in heterogeneous media, in *Diffusion in polymers*, Crank, J., Park, G. S. (eds.), Academic Press, London, 165-217.

Barrer, R. M., Chio, H.T. (1965). Solution and diffusion of gases and vapors in silicone rubber membranes, *J. Polym. Sci., Part C.* no. 10, 111-138.

Behling, R.-D., Ohlrogge, K., Peinemann, K.-V. (1989). The separation of hydrocarbons from waste vapor streams, *AIChE Symp. Ser.* **85**, no. 272, 68-73.

Bertucco, A., Mio, C. (1996). Prediction of vapor-liquid equilibrium for polymer solutions by a group-contribution Redlich-Kwong-Soave equation of state, *Fluid Phase Equilib.* **117**, 18-25.

Bhide, B. D., Stern, S. A. (1991). Permeability of silicone polymers to hydrogen, *J. Appl. Polym. Sci.* **42**, 2397-2403.

Bicerano, J. (1992). Statistical-thermodynamic modeling of the transport of penetrants through polymers: sorption of carbon dioxide, *Comp. Polym. Sci.* **2**, 177-201.

Bird, R. B., Stewart, W. E., Lightfoot, E. N. (1960). *Transport phenomena*, John Wiley & Sons, Inc., New York.

Bitter, J. G. A. (1984). Effect of crystallinity and swelling on the permeability and selectivity of polymer membranes, *Desalination* **51**, 19-35.

Bitter, J. G. A. (1991). *Transport mechanisms in membrane separation processes*, Plenum Press, New York.

Bondi, A., (1968). *Physical properties of molecular crystals, liquids, and glasses*, John Wiley & Sons, Inc., New York.

Boukouvalas, C., Spiliotis, N., Coutsikos, P., Tzouvaras, N., Tassios, D. (1994). Prediction of vapor-liquid equilibrium with the LCVM model: a linear combination of the Vidal and Michelsen mixing rules coupled with the original UNIFAC ant the t-mPR equation of state,

Fluid Phase Equilib. **92**, 75-106.

Burghardt, A., Krupiczka, R. (1975). Wnikanie masy w ukladach wielaskladnikowych-teortyczna analiza zagadnienia I okreslenie wspolczynnikow wnikania masy, *Inz. Chem.* **5**, 487-510.

Chapman, W. G., Gubbins, G., Jackson, M., Radoz, M. (1989). SAFT: equation-of –state solution model for associating fluids, *Fluid Phase Equilib.* **52**, 31-38.

Chapman, W. G., Gubbins, G., Jackson, M., Radoz, M. (1990). New reference equation of state for associating fluids, *Ind. Eng. Chem. Res.* **29**, 1709-1721.

Chiou, J. S., Maeda, Y., Paul, D. R. (1985). Gas and vapor sorption in polymers just below T_g, *J. Appl. Polym. Sci.* **30**, 4019-4029.

Chiou, J. S., Paul, D. R. (1986). Sorption and transport of CO_2 in PVF_2/PMMA blends, *J. Appl. Polym. Sci.* **32**, 2897-2918.

Cohen, M. H., Turnbull, D. (1959). Molecular transport in liquids and gases, *J. Chem. Phys.*, **31**, 1164-1169.

Cotterman, R. L., Prausnitz, J. M. (1985). Flash calculations for continuous or semicontinuous mixtures using an equation of state, *Ind. Eng. Chem. Process Des. Dev.* **24**, 434-443.

Covitz, F. H., King, J. W. (1972). Solute absorption into molten polystyrene, *J. Polym. Sci., Part A-1* **10**, 689-699.

Crank, J, Park, G. S. (1968). Methods of measurement, in *Diffusion in polymers*, Crank, J., Park, G. S. (eds.), Academic Press, London, 1-39.

Curtiss, C. F., Bird, R. B. (1996). Multicomponent diffusion in polymeric liquid, *Proc. Natl. Acad. Sci. USA* **93**, 7440-7445.

Curtiss, C. F., Bird, R. B. (1997). Fokker–Planck equation for the one-molecule distribution function in polymer mixtures and its solution, *J. Chem. Phys.* **106**, 9899-9921.

Curtiss, C. F., Bird, R. B. (1999). Multicomponent diffusion, *Ind. Eng. Chem. Res.* **38**, 2515-2522.

Dahl, S., Fredenslund, A., Rasmusen, P. (1991). The MHV2 model: A UNIFAC-based equation of state model for prediction of gas solubility and vapor–liquid equilibria at low and high pressures, *Ind. Eng. Chem. Res.* **30**, 1936-1945.

Dahl, S., Michelsen, M. L. (1990). High-pressure vapor-liquid equilibrium with a UNIFAC-based equation of state, *AIChE J.* **36**, 1829-1836.

Danner, R. P., Gess, M. A. (1990). A data base standard for the evaluation of vapor-liquid-equilibrium models, *Fluid Phase Equilib.* **56**, 285-301.

Danner, R. P., High, M. S. (1993). *Handbook of polymer solution thermodynamics*, AIChE, New York, 42-63.

De Angelis, M. G., Merkel, T. C., Bondar, V. I., Freeman, B. D., Doghieri, F., Sarti, G. C. (1999). Hydrocarbon and fluorocarbon solubility and dilation in poly(dimethylsiloxane): Comparison of experimental data with predictions of the Sanchez–Lacombe equation of state, *J. Polym. Sci., Part B: Polym. Phys.* **37**, 3011-3026.

Deen, W. M. (1998). *Analysis of transport phenomena*, Oxford University Press, New York.

Donohue, M.D., Prausnitz, J. M. (1975). Combinatorial entropy of mixing molecules that differ in size and shape. A simple approximation for binary and multicomponent mixtures, *Can. J. Chem. Eng.* **53**, 1586-1592.

Doolittle, A. K. (1951). Studies in Newtonian flow. II. Dependence of viscosity of liquids on free-space, *J. Appl. Phys.* **22**, 1471-1475.

Duda, J. L., Zielinski, J. M. (1996). Free-volume theory, in *Diffusion in polymers*, Neogi, P. (ed.), Marcel Dekker, Inc., New York, pp. 143-171.

Engeln-Mullges, G., Uhling, F. (1996). *Numerical algorithms with fortran*, Springer-Verlag, Berlin.

Ferry, J. D. (1980). *Viscoelastic properties of polymers*, 2nd revised edition, John Wiley & Sons, Inc., New York.

Ferziger, J. H., Perić, M. (1997). *Computational methods for fluid dynamics*, 2nd edition, Springer-Verlag, Berlin.

Filtration and Separation **33**, no. 1, p. 2, 1996.

Flory, P. J. (1970). Thermodynamics of polymer solutions, *Discuss. Faraday Soc.* **49**, 7-29.

FLOWBAT user's instruction manual (2001). Keskinen, K. I., Aittamaa, J. (eds.), Neste Engineering Oy.

Fredenslund, Aa., Jones, R. L., Prausnitz, J. M. (1975). Group-contribution estimation of activity coefficients in nonideal liquid mixtures, *AIChE J.* **21**, 1086-1099.

Fredenslund, A., Soresen, J. M. (1994). Group contribution estimation methods, in *Models for thermodynamic and phase equilibria calculations*, Sandler, S. I. (ed.), Marcel Dekker, Inc., New York.

Fujita, H., Kishimoto, A., Matsumoto, K. (1960). Concentration and temperature dependence of diffusion coefficients for systems polymethylacrylate and n-alkyl acetates, *Trans. Faraday Soc.* **56**, 424-437.

Gnielinski, V. (1976). New equations for heat and mass transfer in turbulent pipe and channel flow, *Int. Chem. Eng.* **16**, 359-368.

Gorissen, H. (1987). Temperature changes involved in membrane gas separations, *Chem. Eng. Process.* **22**, 63-67.

Gottschlich, D., Jacobs, M. (1998). Monomer recovery process, *U. S. Patent* 5 769 927.

Gupta, R. B., Prausnitz, J. M. (1996). Vapor–liquid equilibria for solvent–polymer systems from a perturbed hard-sphere-chain equation of state, *Ind. Eng. Chem. Res.* **35**, 1225-1230.

Hansen, H. K, Rasmussen, P., Fredenslund, Aa., Schiller, M., Gmehling, J. (1991). Vapor-liquid equilibria by UNIFAC group contributions. 5. Revision and extension, *Ind. Eng. Chem. Res.* **30**, 2352-2355.

Hariharan, R., Freeman, B. D., Carbonell, R. G., Sarti, G. C. (1993). Equation of state predictions of sorption isotherms in polymeric materials, *J. Appl. Polym. Sci.* **50**, 1781-1795.

Heidemann, R. A., Khokal, S. L. (1990). Combined excess free energy models and equation of state, *Fluid Phase Equilib.* **56**, 17-37.

Heintz, A, Stephan, W. (1994a). A generalized solution–diffusion model of the pervaporation process through composite membranes. Part I. Prediction of mixture solubilities in the dense active layer using the UNIQUAC model, *J. Membrane Sci.* **89**, 143-151.

Heintz, A, Stephan, W. (1994b). A generalized solution–diffusion model of the pervaporation process through composite membranes. Part II. Concentration polarization, coupled diffusion and the influence of the porous support layer, *J. Membrane Sci.* **89**, 153-169.

Henis, J. M. S., Tripodi, M. K. (1980). Multicomponent membranes for gas separation, *U. S. Patent* 4 230 463.

Hickey, P. J., Gooding, C. H. (1994). Modeling spiral wound membrane modules for the pervaporative removal of organic compounds from water, *J. Membrane Sci.* **88**, 47-68.

Holderbraum, T., Gmehling, J. (1991). PSRK: A group contribution equation of state based on UNIFAC, *Fluid Phase Equilib.* **70**, 251-265.

Hoting, B., Nitsche, V., Alpers, A. (1997). Integration of design methods for membrane-based gas separation into a modern process simulator, Poster presented at Euromembrane '97, Progress in membrane science and technology, University of Twente, The Netherlands.

Ichiraku, Y., Stern, S. A. (1987). An investigation of the high permeability of poly(1-trimethylsilyl-1-propyne), *J. Membrane Sci.* **34**, 5-18.

Ilme, J. (1997). Estimating plate efficiencies in simulation of industrial scale distillation columns, Doctoral thesis, Lappeenranta University of Technology, Lappeenranta.

Iwai, Y., Arai, Y. (1989). Measurement and prediction of solubilities of hydrocarbon vapors in molten polymers, *J. Chem. Eng. Japan* **22**, 155-161.

Jordan, S. M., Koros, W. J. (1990). Permeability of pure and mixed gases in silicone rubber at

elevated pressures, *J. Polym. Sci., Part B: Polym. Phys.* **28**, 795-809.

Jordan, S. M., Koros, W. J., Fleming, G. K. (1987). The effects of CO_2 exposure on pure and mixed gas permeation behavior: comparison of glassy polycarbonate and silicone rubber, *J. Membrane Sci.* **30**, 191-212.

Kalospiros, N. S., Tassios, D. (1995). Prediction of vapor–liquid equilibria in polymer solutions using an equation of state/excess Gibbs free energy model, *Ind. Eng. Chem. Res.* **34**, 2117-2124.

Kamaruddin, H. D., Koros, W. J. (1997). Some observations about the application of Fick's first law for membrane separation of multicomponent mixtures, *J. Membrane Sci.* **135**, 147-159.

Kamiya, Y., Naito, Y., Hirose, T. (1990). Sorption and partial molar volume of gases in poly(dimethylsiloxane), *J. Polym. Sci., Part B: Polym. Phys.* **28**, 1297-1308.

Kamiya, Y., Naito, Y., Mizoguchi, K., Terada, K., Moreau, J. (1997). Thermodynamic interactions in rubbery polymer/gas systems, *J. Polym. Sci., Part B: Polym. Phys.* **35**, 1049-1053.

Kaschemekat, J., Baker, R. W., Wijmans, J. G. (1993). Process for removing condensable components from gas streams, *U.S. Patent* 5202843.

Katoh, M., Inoue, N., Bitoo, T., Hashimoto, K., Tsuneizumi, H., Furuno, N. (1989). Hydrocarbon vapor recovery with membrane technology, *NKK Tech. Rev.*, no. 56, 67-72.

Kikic, I., Alessi, P., Rasmussen, P., Fredenslund, A. (1980). On the combinatorial part of the UNIFAC and UNIQUAC models, *Can. J. Chem. Eng.* **58**, 253-258.

Kiszka, M. B., Meilchen, M. A., McHugh, M. A. (1988). Modeling high-pressure gas–polymer mixtures using the Sanchez–Lacombe equation of state, *J. Appl. Polym. Sci.* **36**, 583-597.

Klemola, K. T. (1998). Efficiencies in distillation and reactive distillation, Acta Polytechnicia Scandinavica, Chemical Technology Series, No. 257, Espoo.

Klemola, K. T., Ilme, J. (1996). Distillation efficiencies of an industrial-scale *i*-butane/*n*-butane fractionator, *Ind. Eng. Chem. Res.* **35**, 4579-4586.

Kontogeorgis, G. M., Coutsikos, P., Tassios, D., Fredenslund, A. (1994a). Improved models for the prediction of activity coefficients in nearly athermal mixtures, *Fluid Phase Equilib.* **92**, 35-66.

Kontogeorgis, G. M., Harismiadis, V. I., Fredenslund, Aa., Tassios, D. P. (1994b). Application of the van der Waals equation of state to polymers I. Correlation, *Fluid Phase Equilib.* **96**, 65-92.

Kooijman, H. A., Taylor, R. (1991). Estimation of diffusion coefficients in multicomponent liquid systems, *Ind. Eng. Chem. Res.* **30**, 1217-1222.

Koros, W. J., Chern, R. T., Stannett, V., Hopfenberg, H. B. (1981). A model for permeation of mixed gases and vapors in glassy polymers, *J. Polym. Sci., Polym. Phys. Ed.* **19**, 1513-1530.

Kovacs, A. J. (1958). La contraction isotherme du volume des polymères amorphes, *J. Polym. Sci.* **30**, 131-147.

Krishna, R. (1977). A generalized film model for mass transfer in non-ideal fluid mixtures, *Chem. Eng. Sci.* **32**, 659-667.

Krishna, R. (1990). Multicomponent surface diffusion of adsorbed species. A description based on the generalized Maxwell–Stefan diffusion equations, *Chem. Eng. Sci.* **45**, 1779-1791.

Krishna, R., Wesselingh, J. A. (1997). The Maxwell–Stefan approach to mass transfer, *Chem. Eng. Sci.* **52**, no. 6, 861-911.

Kubaczka, A., Bandrowski, J. (1990). An explicit approximate solution of the generalized Maxwell–Stefan equations for the multicomponent film model, *Chem. Eng. Comm.* **95**, 89-97.

Lacombe, R. H., Sanchez, I. C. (1976). Statistical thermodynamics of fluid mixtures, *J. Phys. Chem.* **80**, 2568-2580.

Langsam, M., Robeson, L. M. (1989). Substituted propyne polymers — Part II. Effects of aging on the gas permeability properties of poly[1-(trimethylsilyl)propyne] for gas separation membranes, *Polym. Eng. Sci.* **29**, 44-54.

Larsen, B. L., Rasmussen, P., Fredenslund, Aa. (1987). A modified UNIFAC group-contribution model for prediction of phase equilibria and heats of mixing, *Ind. Eng. Chem. Res.* **26**, 2274-2286.

Lichtenthaler, R. N., Liu, D. D., Prausnitz, J. M. (1974). Polymer–solvent interactions from gas–liquid chromatography with capillary columns, *Macromolecules* **7**, 565-570.

Liu, D. D., Prausnitz, J. M. (1977). Solubilities of volatile solutes in poly(vinyl acetate) from 125 to 200°C, *J. Polym. Sci., Polym. Phys. Ed.* **15**, 145-153.

Loeb, S., Sourirajan, S. (1963). Sea water demineralization by means of an osmotic membrane, *Adv. Chem. Ser.* **38**, 117-132.

Lokhandwala, K. A., Baker, R. W. (2001). Selective purging for hydroprocessing reactor loop, U.S. Patent 6190540.

Lüdtke, O., Behling, R.-D., Ohlrogge, K. (1998). Concentration polarization in gas permeation, *J. Membrane Sci.* **146**, 145-157.

Mason, E. A., Malinauskas, A. P. (1983). *Gas transport in porous media: The dusty gas model*, Elsevier, Amsterdam.

Mason, E. A., Viehland, L. A. (1978). Statistical–mechanical theory of membrane transport for multicomponent systems: passive transport through open membranes, *J. Chem. Phys.* **68**, 3562-3573.

Masuda, T., Iguchi, Y., Tang, B.-Z., Higashimura, T. (1988). Diffusion and solution of gases in substituted polyacetylene membranes, Polymer 29, 2041-2049.

Masuda, T., Isobe, E., Higashimura, T., Takada, K. (1983). Poly[1-(trimethylsilyl)-1-propyne]: a new high polymer synthesized with transition-metal catalysts and characterized by extremely high gas permeability, *J. Am. Chem. Soc.* **105**, 7473-7474.

Mathias, P. M., Copeman, T. W. (1983). Extension of the Peng–Robinson equation of state to complex mixtures: Evaluation of the various forms of the local composition concept, *Fluid Phase Equilib.* **13**, 91-108.

Matsuoka, S. (1981). Free volume, excess entropy and mechanical behavior of polymeric glasses, *Polym. Eng. Sci.* **21**, 907-921.

MacLean, D. L, Graham, T. E. (1980). Hollow fibers recover hydrogen, *Chem. Eng.*, Feb., 54-55.

McCandless, F. P. (1972). Separation of binary mixtures of CO and H_2 by permeation through polymeric films, *Ind. Eng. Chem. Process Des. Dev.* **11**, 470-478.

McKenna, G. B. (1989). Glass formation and glassy behavior, in *Comprehensive polymer science*, vol. 2, Polymer properties, Allen, G., Bevington, J. C., Booth, C., Price, C. (eds.), Pergamon Press, plc., Oxford, pp. 311-362.

Mendes, A. M. M., Alpers, A., Peinemann, K. V., Ohlrogge, K. (1996). Concentration polarization in gas permeation, in 5th World Congress of Chemical Engineering, San Diego, California, July 14-18, volume III, 136-142.

Mi, Y., Zhou, S., Stern, S. A. (1991). Representation of gas solubility in glassy polymer by a concentration–temperature superposition principle, *Macromolecules* **24**, 2361-2367.

Michelsen, M. L. (1990a). A method for incorporating excess Gibbs energy models in equation of state, *Fluid Phase Equilib.* **60**, 47-58.

Michelsen, M. L. (1990b). A modified Huron–Vidal mixing rule for cubic equation of state, *Fluid Phase Equilib.* **60**, 213-219.

Michelsen, M. L. (1996). Matching equation of state mixing rules to activity coefficient model expressions, *Fluid Phase Equilib.* **121**, 15-26.

Müller-Plathe, F. (1992). Molecular dynamics simulation of gas transport in amorphous polypropylene, *J. Chem. Phys.* **96**, 3200-3205.

Nakagawa, T., Fujisaki, S., Nakano, H., Higuchi, A. (1994). Physical modification of poly[1-(trimethylsilyl)-1-propyne] membranes for gas separation, *J. Membrane Sci.* **94**, 183-193.

Neogi, P. (1996). Transport phenomena in polymer membranes, in *Diffusion in polymers*, Neogi, P. (ed.), Marcel Dekker, Inc., New York, pp. 173-209.

Noda, I., Higo, Y., Ueno, N., Fujimoto, T. (1984). Semidilute region for linear polymers in good solvents, *Macromolecules* **17**, 1055-1059.

Ohlrogge, K., Peinemann, K.-V., Wind, J., Behling, R.-D. (1990). The separation of hydrocarbon vapors with membranes, *Sep. Sci. Tech.* **25**, 1375-1386.

Ohlrogge, K., Wind, J., Behling, R.-D. (1993). Membranverfahren in der chemischen und petrochemischen industrie, *Erdöl Kohle-Erdgas* **46**, no. 9, 326-332.

Oishi, T., Prausnitz, J. M. (1978). Estimation of solvent activities in polymer solutions using a group-contribution method, *Ind. Eng. Chem. Process Des. Dev.* **17**, 333-339.

Orbey, H., Chen, C.-C., Bokis, C. P. (1997). An extension of cubic equation of state to vapor–liquid equilibria in polymer–solvent mixtures, *Fluid Phase Equilib.* **145**, 169-192.

Orbey, N., Sandler, S. I. (1994). Vapor–liquid equilibrium of polymer solutions using a cubic equation of state, *AIChE J.* **40**, 1203-1209.

Pace, R. J., Datyner, A. (1979). Statistical-mechanical model for diffusion of simple penetrants in polymers. I. Theory, *J. Polym. Sci, Polym. Phys. Ed.* **17**, 437-451.

Pan, C. Y., Habgood, H. W. (1974). An analysis of the single-stage gaseous permeation process, *Ind. Eng. Chem. Fundam.* **13**, 323-331.

Pan, C. Y., Habgood, H. W. (1978). Gas separation by permeation. Part I. Calculation methods and parametric analysis, *Can. J. Chem. Eng.* **56**, 197-209.

Panayiotou, C. G., Vera, J. H. (1982). Statistical thermodynamics of r-mer fluids and their mixtures, *Polymer* **14**, 681-694.

Park, G. S. (1968). The glassy state and slow process anomalies, in *Diffusion in polymers*, Crank, J., Park, G. S. (eds.), Academic Press, London, pp. 141-163.

Patankar, S. V. (1980). *Numerical heat transfer and fluid flow*, Hemisphere Publishing Corporation, New York.

Paul, D. R. (1973). Relation between hydraulic permeability and diffusion in homogeneous swollen membranes, *J. Polym. Sci., Polym. Phys. Ed.* **11**, 289-296.

Paul, D. R., Ebra-Lima, O. M. (1970). Pressure-induced diffusion of organic liquids through highly swollen polymer membranes, *J. Appl. Polym. Sci.* **14**, 2201-2224.

Paul, D. R., Koros, W. J. (1976). Effect of partially immobilizing sorption on permeability and the diffusion time lag, *J. Polym. Sci., Polym. Phys. Ed.* **14**, 675-685.

Pinnau, I., Casillas, C. G., Moristo, A., Feeman, B. D (1997). Long-time permeation properties of poly(1-trimethylsilyl-1-propyne) membranes in hydrocarbon–vapor environment, *J. Polym. Sci., Part B: Polym. Phys.* **35**, 1483-1490.

Pinnau, I., Toy, L. G. (1996), Transport of organic vapors through poly(1-trimethylsilyl-1-propyne), *J. Membrane Sci.* **116**, 199-209.

Platé, N. A., Bokarev, A. K., Kaliuzhnyi, N. E., Litvinova, E. G., Khotimskii, V. S., Volkov, V. V., Yampol'skii, Yu. P. (1991). Gas and vapor permeation and sorption in poly(trimethylsilylpropyne), *J. Membrane Sci.* **60**, 13-24.

Pope, D. S., Sanchez, I. C., Koros, W. J., Fleming, G. K. (1991). Statistical thermodynamic interpretation of sorption/dilation behavior of gases in silicone rubber, *Macromolecules* **24**, 1779-1783.

Press, W. H., Teukolsky, S. A., Vetterling, W. T., Flannery, B. P. (1999). *Numerical Recipes*, second edition, vol. 1, Cambridge University Press, Cambridge.

Qi, R., Henson, M. A. (1997). Modeling of spiral-wound permeators for multicomponent gas separations, *Ind. Eng. Chem. Res.* **36**, 2320-2331.

Rautenbach, R., Helmus, F. P. (1994). Some considerations on mass-transfer resistances in solution–diffusion-type membrane processes, *J. Membrane Sci.* **87**, 171-181.

Rautenbach, R., Knauf, R., Struck, A., Vier, J. (1996). Simulation and design of membrane plants with AspenPlus, *Chem. Eng. Technol.* **19**, 391-397.

Reid, R. C., Prausnitz, J. M., Poling, B. E. (1987). *The properties of gases & liquids*, 4th edition, McGraw-Hill Book Company, New York.

Rodgers, P. A. (1993). Pressure–volume–temperature relationships for polymeric liquids: A review of equations of state and their characteristic parameters for 56 polymers, *J. Appl. Polym. Sci.* **48**, 1061-1080.

Roth, H, Novak, J. (1986). Thermodynamics of poly(dimethylsiloxane)–alkane systems by gas–liquid chromatography, *Macromolecules* **19**, 364-369.

Sanchez, I. C. (1987). Polymer phase separation, in *Encyclopedia of physical science and technology*, vol. 11, Meyers, R. A. (ed.), Academic Press, Inc., Orlando Fa.

Sanchez, I. C., Lacombe, R. H. (1976). An Elementary molecular theory of classical fluids. Pure fluids, *J. Phys. Chem.* **80**, 2352-2362.

Sanchez, I. C., Lacombe, R. H. (1978). Statistical Thermodynamics of polymer solutions, *Macromolecules* **11**, 1145-1156.

Sanchez, I. C., Panayiotou, C. G. (1994). Equation of state thermodynamics of polymer and related solutions, in *Models for thermodynamic and phase equilibria calculations*, Sandler, S. I. (ed.), Marcel Dekker, Inc., New York, 187-285.

Sanchez, I. C., Rodgers, P. A. (1990). Solubility of gases in polymers, *Pure Appl. Chem.* **62**, 2107-2114.

Schreiber, H. P., Tewari, Y. B., Patterson, D. (1973). Thermodynamics interactions in polymer systems by gas–liquid chromatography. III. Polyethylene–hydrocarbons, *J. Polym. Sci., Polym. Phys. Ed.* **11**, 15-24.

Seitz, J. T. (1993). The estimation of mechanical properties of polymers from molecular structure, *J. Appl. Polym. Sci.* **49**, 1331-1351.

Shah, R. K., London, A. L. (1978). *Laminar flow forced convection in ducts*, Academic Press, New York.

Shindo, Y., Hakuta, T., Yoshitome, H., Inoue, H. (1985). Calculation methods for multicomponent gas separation by permeation, *Sep. Sci. Tech.* **20**, 445-459.

Sok, R. M., Berendsen, H. J. C., van Gunsteren, W. F. (1992). Molecular dynamics simulation of the transport of small molecules across a polymer membrane, *J. Chem. Phys.* **96**, 4699-4704.

Song, Y., Hino, T., Lambert, S. M., Prausnitz, J. M. (1996). Liquid-liquid equilibria for polymer solutions and blends, including copolymers, *Fluid Phase Equilib.* **117**, 69-76.

Song, Y., Lambert, S. M., Prausnitz, J. M. (1994a). A perturbed hard-sphere-chain equation of state for normal fluids and polymers, *Ind. Eng. Chem. Res.* **33**, 1047-1057.

Song, Y., Lambert, S. M., Prausnitz, J. M. (1994b). Liquid–liquid phase diagrams for binary polymer solutions from a perturbed hard-sphere-chain equation of state, *Chem. Eng. Sci.* **49**, 2765-2775.

Song, Y., Lambert, S. M., Prausnitz, J. M. (1994c). Equation of state for mixtures of hard-sphere chains including copolymers, *Macromolecules* **27**, 441-448.

Sperling, L. H. (1992). *Introduction to physical polymer science*, John Wiley & Sons, Inc., New York, p. 108-113.

Spiliotis, N., Boukouvalas, C., Tzouvaras, N., Tassios, D. (1994). Application of the LCVM model to multicomponent systems: Extension of the UNIFAC interaction parameter table and prediction of the phase behavior of synthetic gas condensate and oil systems, *Fluid Phase Equilib.* **101**, 187-210.

Srinivasan, R., Auvil, S. R., Burban, P. M. (1994), Elucidating the mechanism(s) of gas transport in poly[1-(trimethylsilyl)-1-propyne] (PTMSP) membranes, *J. Membrane Sci.* **89**,

67-86.

Stern, S. A., Bhide, B. D. (1989). Permeability of silicone polymers to ammonia and hydrogen sulfide, *J. Appl. Polym. Sci.* **38**, 2131-2147.

Stern, S. A., Fang, S.-M., Frisch, H. L. (1972). Effect of pressure on gas permeability coefficients. A new application of "free volume" theory, *J. Polym. Sci., Part A-2* **10**, 201-219.

Stern, S. A., Shah, V. M., Hardy, B. J. (1987). Structure-permeability relationships in silicone polymers, *J. Polym. Sci, Polym. Phys. Ed.* **25**, 1263-1298.

Takada, K., Matsuya, H., Masuda, T., Higashimura, T. (1985). Gas permeability of polyacetylenes carrying substituents, *J. Appl. Polym. Sci.* **30**, 1605-1616.

Tannehill, J.C., Anderson, D. A., Pletcher, R. H. (1997). Computational fluid mechanics and heat transfer, 2nd edition, Taylor & Francis, Washington, DC.

Tanner, J. E. (1971). Diffusion in polymer matrix, *Macromolecules* **4**, 748-750.

Taylor, R. (1991). On an explicit approximate solution of the generalized Maxwell–Stefan equations for the multicomponent film model, *Chem. Eng. Comm.* **103**, 53-56.

Taylor, R., Krishna, R. (1993). *Multicomponent mass transfer*, John Wiley & Sons, Inc., New York.

Tessendorf, S. (1998). *Modeling, analysis, and design of membrane-based gas separation systems*, Ph.D. thesis, Department of Chemical Engineering, Technical University of Denmark.

Tessendorf, S., Gani, R., Michelsen, M. L. (1999). Modeling, simulation and optimization of membrane-based gas separation systems, *Chem. Eng. Sci.* **54**, 943-955.

Thundyil, M. J. (1997). Hydrocarbon permeabilities in silicone rubber, Unpublished report to Neste Oy.

Thundyil, M. J. (1998). Characterization, analysis and modeling of non-ideal effects in polymeric membrane based natural gas processing, Ph.D. dissertation, University of Texas, Austin.

Topliss, R. J., Dimitrelis, D., Prausnitz, J. M. (1988). Computational aspects of a non-cubic equation of state for phase-equilibrium calculations. Effect of density-dependent mixing rules, *Comput. Chem. Engng.* **12**, 483-489.

Toppinen, S., Aittamaa, J., Salmi, T. (1996). Interfacial mass transfer in trickle-bed reactor modelling, *Chem. Eng. Sci.* **51**, 4335-4345.

Twu, C. H., Coon, J. E., Bluck, D., Tilton, B. (1999). CEOS/A^E mixing rules from infinite pressure to zero pressure and then no reference pressure, *Fluid Phase Equilib.* **158-160**, 271-281.

Vieth, W. R., Sladek, K. J. (1965). A model for diffusion in a glassy polymer, *J. Colloid Sci.* **20**, 1014-1033.

Voutsas, E. C., Boukouvalas, C. J., Kalospiros, N. S., Tassios, P. (1996). The performance of EOS/G^E models in the prediction of vapor–liquid equilibria, *Fluid Phase Equilib.* **116**, 480-487.

Voutsas, E. C., Kalospiros, N. S., Tassios, D. P. (1995). A combinatorial activity coefficient model for symmetric and asymmetric mixtures, *Fluid Phase Equilib.* **109**, 1-15.

Voutsas, E. C., Tassios, D. P. (1997). On the extension of the *p*-FV and *R*-UNIFAC models to multicomponent mixtures, *Fluid Phase Equilib.* **128**, 271-272.

Vrentas, J. S., Duda, J. L. (1977a). Diffusion in polymer–solvent systems. I. Reexamination of the free-volume theory, *J. Polym. Sci., Polym. Phys. Ed.* **15**, 403-416.

Vrentas, J. S., Duda, J. L. (1977b). Diffusion in polymer–solvent systems. II. A predictive theory for the dependence of diffusion coefficients on temperature, concentration, and molecular weight, *J. Polym. Sci., Polym. Phys. Ed.* **15**, 417-439.

Wijmans, J. G., Baker, R. W. (1995). The solution–diffusion model: a review, *J. Membrane Sci.* **107**, 1-21.

Wijmans, J. G., Helm, V. D. (1989). A membrane system for the separation and recovery of organic vapors from gas streams, *AIChE Symp. Ser.* **85**, no. 272, 74-79.

Wohlfarth, C. (1994). *Vapor–liquid equilibrium data of binary polymer solutions*, Vapor pressures, Henry–constants and segment molar excess Gibbs free energies, Physical sciences data 44, Elsevier, Amsterdam.

Wong, D. S. H., Sandler, S. I. (1992). A theoretically correct mixing rule for cubic equation of state, *AIChEJ.* **38**, 671-680.

Yampol'skii, Y. P., Shishatskii, S. M., Shantorovich, V. P., Antipov, E. M., Kuzmin, N. N., Rykov, S. V., Khodjaeva, V. L., Platé, N. A. (1993). Transport characteristics and other physicochemical properties of aged poly(1-(trimethylsilyl)-1-propyne), *J. Appl. Polym. Sci.* **48**, 1935-1944.

Zhong, C., Masuoka, H. (1996). Prediction of Henry's constants for polymer-containing systems using the SRK equation of state coupled with a new modified UNIFAC model, *Fluid Phase Equilib.* **126**, 1-12.

Zielinski, J. M., Duda, J. L. (1992). Influence of concentration on the activation energy for diffusion in polymer–solvent systems, *J. Polym. Sci., Part B: Polym. Phys.* **30**, 1081-1088.

APPENDIX I EQUATION OF STATE PARAMETERS

Table A.1 Sanchez–Lacombe EOS parameters for normal components and polymers.

	T^*, K	P^*, MPa	ρ^*, kg/m^3	Ref.
Carbon dioxide	304.6	591.1	1518.0	This work
Nitrogen	137.1	189.5	932.0	“
Oxygen	168.5	278.3	1290.0	“
Hydrogen sulfide	369.4	628.3	1090.0	“
Hydrogen	52.10	32.7	76.13	“
Methane	211.2	245.1	474.4	“
Ethane [a)]	315.0	327.0	640.0	Sanchez and Panayiotou (1994)
Ethane [b)]	311.0	328.5	632.8	This work
Ethylene	278.0	340.0	668.0	Pope *et al.* (1991)
Propane [a)]	371.0	313.0	690.0	Sanchez and Panayiotou (1994)
Propane [b)]	364.1	326.4	698.4	This work
Propylene [a)]	365.0	338.4	728.5	“
Propylene [b)]	350.7	357.0	729.8	“
Butane	403.0	322.0	736.0	Sanchez and Panayiotou (1994)
Pentane	441.0	310.0	755.0	“
Hexane	476.0	298.0	775.0	“
Heptane	487.0	309.0	800.0	“
Octane	502.0	308.0	815.0	“
Nonane	517.0	307.0	828.0	“
Decane	530.0	304.0	837.0	“
Dodecane	552.0	301.0	854.0	“
o-Xylene	571.0	394.0	965.0	“
m-Xylene	560.0	385.0	952.0	“
p-Xylene	561.0	381.0	949.0	“
Cyclohexane	497.0	383.0	902.0	“
Benzene	523.0	444.0	994.0	“
Ethylbenzene	537.0	403.0	965.0	“
Chlorobenzene	585.0	437.0	1206.0	“
Toluene	543.0	402.0	966.0	“
Acetone	484.0	533.0	917.0	“
Methyl ethyl ketone	513.0	447.0	913.0	“
Methyl chloride	448.0	460.0	1125.0	“
Carbon tetrachloride	535.0	381.0	1788.0	“
1,4-dioxane	519.0	536.0	1163.0	“
HDPE	425.0	649.0	904.0	“
LDPE	359.0	673.0	887.0	“
PP	771.0	281.0	852.0	“
PVAc	590.0	509.0	1283.0	“
PDMS	476.0	302.0	1104.0	“
PIB	354.0	643.0	974.0	“
PS	735.0	357.0	1105.0	“
PcB	552.0	424.0	990.0	“

[a)] Parameters used in liquid polymer systems
[b)] Parameters used in PDMS membrane systems

Table A.2 Perturbed hard-sphere-chain equation of state parameters for normal components and polymers.

	r, -[a]	ε/k_B, K	σ, Å	Ref.
Carbon dioxide	3.368	140.3	2.574	This work
Nitrogen	1.313	99.4	3.628	“
Oxygen	1.225	127.5	3.489	“
Hydrogen sulfide	1.789	242.9	3.357	“
Hydrogen	0.382	63.4	4.945	“
Methane	1.000	182.1	4.126	Song *et al.* (1996)
Ethane	1.694	206.3	3.916	“
Ethylene	1.609	196.8	3.839	“
Propane	2.129	219.0	3.998	“
Propylene	2.029	221.9	3.951	“
Butane	2.496	231.3	4.085	“
Pentane	3.149	226.0	3.995	“
Hexane	3.446	235.6	4.084	“
Heptane	4.255	225.9	3.947	“
Octane	5.055	219.6	3.850	“
Nonane	5.748	217.3	3.804	“
Decane	6.616	212.7	3.723	“
Dodecane	7.712	214.8	3.733	“
o-Xylene	3.620	285.4	3.998	“
m-Xylene	3.721	276.4	3.977	“
p-Xylene	3.455	287.9	4.104	“
Cyclohexane	2.723	286.7	4.215	“
Benzene	2.727	291.6	3.958	“
Ethylbenzene	3.607	279.4	4.018	“
Propylbenzene	4.137	270.6	4.007	“
Styrene	3.291	304.3	4.083	“
Chlorobenzene	3.144	305.3	3.975	“
Toluene	3.138	287.0	4.019	“
Acetone	3.164	250.9	3.510	“
Methyl ethyl ketone	3.344	255.8	3.694	“
Methyl chloride	2.018	256.7	3.591	“
Carbon tetrachloride	2.507	301.7	4.187	“
HDPE	0.04938	324.1	3.825	“
LDPE	0.04408	327.2	3.977	“
PP	0.02831	392.1	4.705	“
PVAc	0.05166	292.6	3.364	“
PDMS	0.03680	253.6	3.968	This work
PIB	0.04024	331.9	3.725	Song *et al.* (1996)
PS	0.03834	385.4	3.899	“
PcB	0.07049	276.6	3.301	“

[a] For polymers r/M_w, mol/g

APPENDIX II FLOWCHART FOR THE MEMBRANE LEAF COMPUTATION

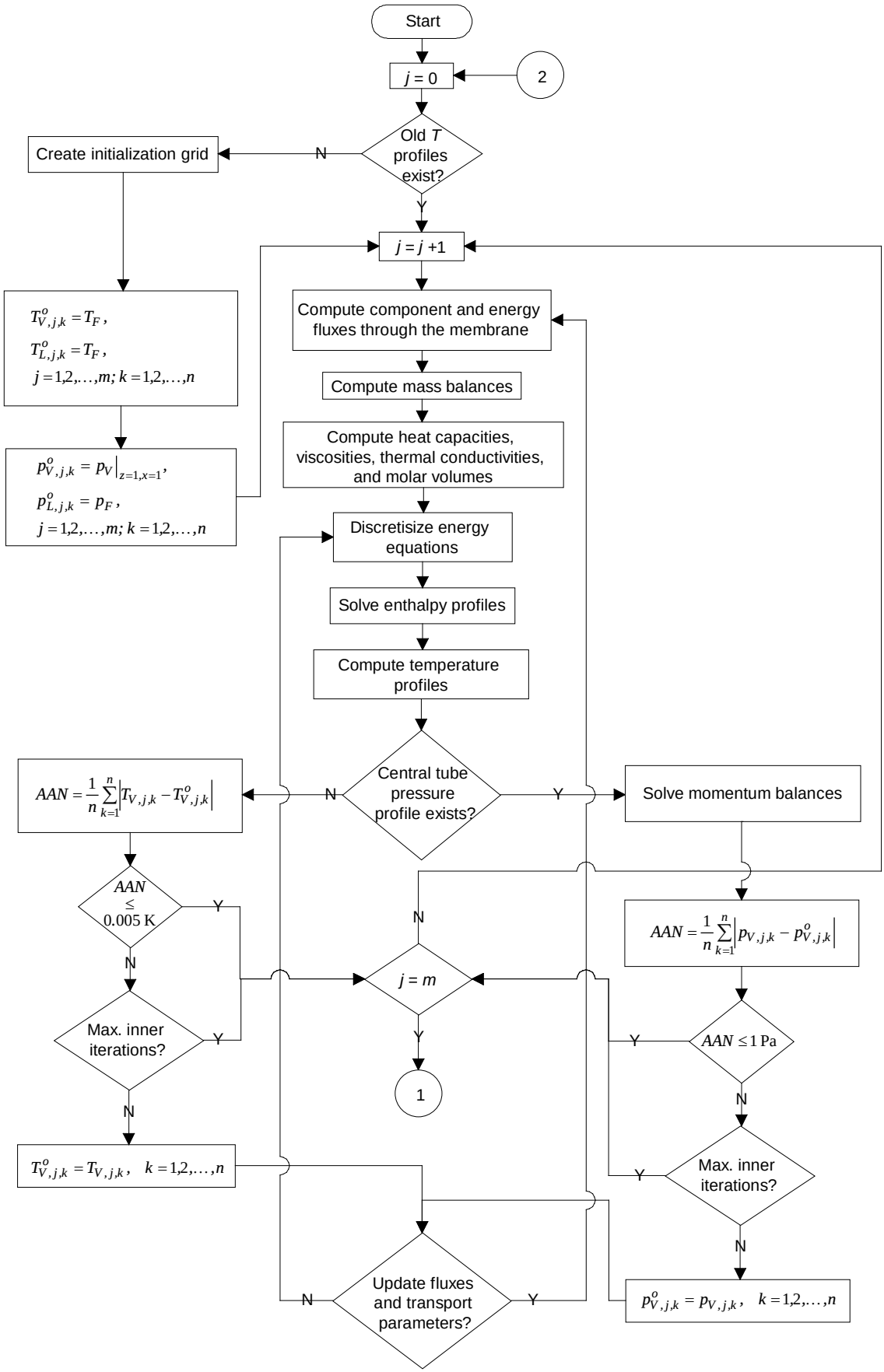

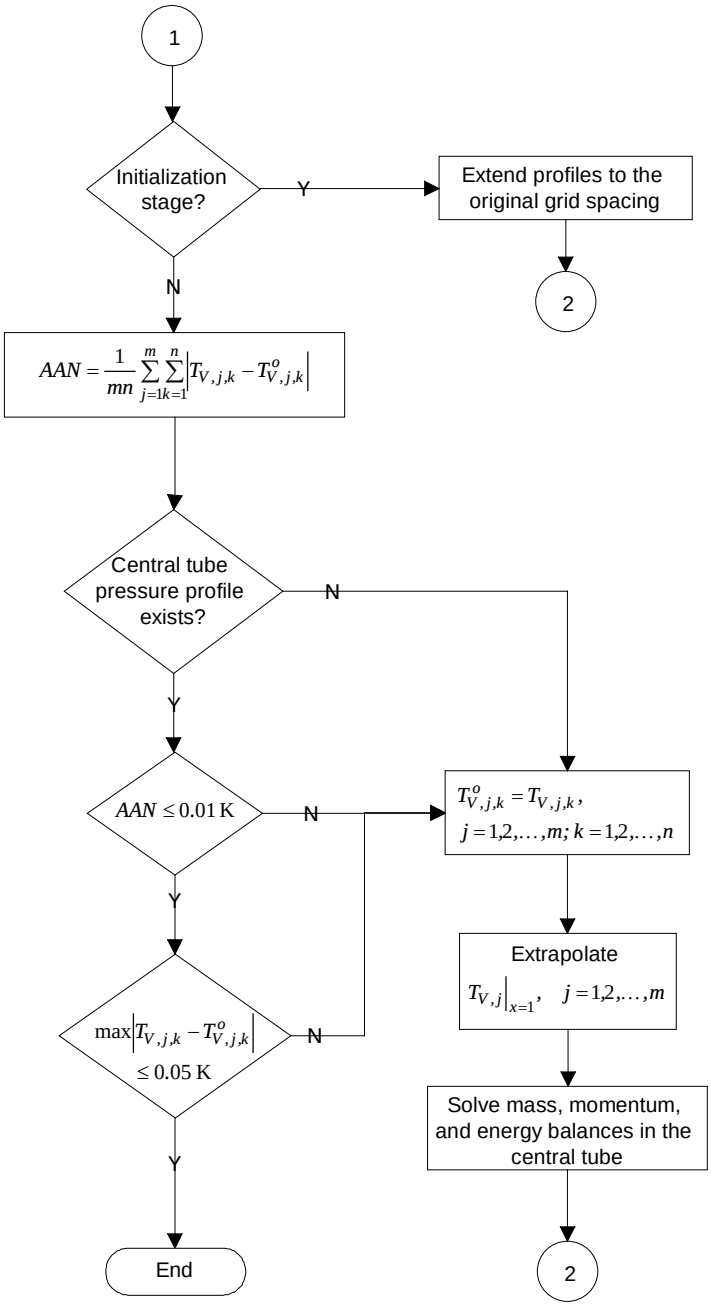
1
Initialization stage?
Y
Extend profiles to the original grid spacing
2
N
$AAN = \frac{1}{mn}\sum_{j=1}^{m}\sum_{k=1}^{n}\left|T_{V,j,k} - T^{o}_{V,j,k}\right|$
Central tube pressure profile exists?
N
Y
$AAN \le 0.01\,\mathrm{K}$
N
$T^{o}_{V,j,k} = T_{V,j,k}$,
$j = 1,2,\ldots,m;\ k = 1,2,\ldots,n$
Y
Extrapolate
$T_{V,j}\big|_{x=1}, \quad j = 1,2,\ldots,m$
$\max\left|T_{V,j,k} - T^{o}_{V,j,k}\right| \le 0.05\,\mathrm{K}$
N
Solve mass, momentum, and energy balances in the central tube
Y
End
2

APPENDIX III INPUT FILE FOR THE HENRY'S COEFFICIENT ESTIMATION

```
 $TITLE
  USER = 'PSAVO', PROJEC = 'GKB81', PROBLE = 'Henry coef.',
 $END

! Units in the simulation

 $UNITS
  MODELS = 'IFLASH',
  MAXITE = 100
 $END

! Components in the simulation:
! Nitrogen

 $THERMO
  COMPNU = 31,
  MDATA = 0
  IMACOP = 1             ! Use Mathias-Copeman parameters
  KTYPE = 'IDEAL'        ! Ideal vapor and liquid phase
                         ! => fugacity coefficients and Poynting correction
                         ! set to one, pressure ratio from pure component
                         ! vapor pressure equation (Antoine or equivalent)
  IPRINT(20) = 1         ! Printing indicator
 $END

 $FLOWS
  FNAMES = 'VAP1',       ! Flow name
  PRES = 0.0101325,
  TEMP = 423.15,
  FLOWTO = 1000.0
  FLOWDI = 'MOL'         ! Flow dimensions: mol/h
  FLOWEN = 'NON-COMPUTE' ! Do not compute flow enthalpy
  FLOW1 = 1.0,           ! Flow composition
 $END

! Isothermal flash unit

 $IFLASH
  UNNAME = 'PROPER1',
  FEEDS = 'VAP1'
  PRODUC = 'GAS1', 'LIQ1'  ! Vapor and liquid product
  TEMP = 423.15            ! Flash temperature
  PRES = 0.0101325         ! Flash pressure
 $END

! Physical properties for the flows of the simulation

 $FYSPRO
  IPR = 0
  FLOWNA = 'GAS1', 'GAS1',              ! Flow for which properties
                                        ! are calculated
  PROPER = 'GSISOT', 'GSISOT',          ! Property: Gas sorption isotherm
  POLY = 'PP', 'PP',                    ! Polymer phase: polypropylene
  POLYMW = 94100.0, 94100.0,            ! Polymer number average Mw
  PDIS = 4.9, 4.9,                      ! Polydispersity index
  PTHERM = 'MHV2P', 'MHV2PO',           ! Polymer thermodynamics: MHV2
                                        ! with the exponential UNIFAC,
                                        ! and the Lyngby modified UNIFAC
                                        ! (original MHV2)
  TINIC = 175.05, 175.05,               ! Initial temperature in Celcius
  TFINC = 250.05, 250.05,               ! Final temperature in Celcius
```

```
  DT = 25.0, 25.0,                        ! Temperature step size
  POINTS = 4, 4,                          ! Number of property points
  PINKPA = 0.00101325, 0.00101325,        ! Initial pressure in kPa
  PFIKPA = 0.00101325, 0.00101325,        ! Final pressure in kPa
  VLEMAT(1,48) = 1                        ! N2 functional group of
                                          ! the MHV2-UNIFAC
$END
```

APPENDIX IV INPUT FILE FOR THE VAPOR SORPTION CALCULATION

```
 $TITLE
  USER = 'PSAVO', PROJEC = 'GKB81', PROBLE = 'Isotermitesti',
 $END

! Units in the simulation

 $UNITS
  MODELS = 'IFLASH',
  MAXITE = 100
 $END

! Components in the simulation
! Benzene

 $THERMO
  COMPNU = 254,
  MDATA = 1              ! Read CRDATA input
  KTYPE = 'MHV2'         ! Thermodynamic selection: MHV2
  VLEMAT(1, 10) = 6      ! Vapor-liquid group parameters
  IPRINT(20) = 0         ! Printing indicator
  IMACOP = 1             ! Use the Mathias-Copeman parameters
 $END

! EOS parameters for PHSC and SL EOS

 &CRDATA
  PHSCR = 2.727,
  PHSCE = 291.6,
  PHSCS = 3.958,
  SLPRES = 444.0,
  SLTEMP = 523.0,
  SLDEN = 994.0,
!
! Energy correction factor matrix for SLLF
!
  SLECOR(1,1) = 0.0, -0.0106
  SLECOR(1,2) = -0.0106, 0.0
!
! Size correction factor matrix for PHSC
!
  PHSCSC(1, 1) = 0.0, -0.0245,
  PHSCSC(1, 2) = -0.0245, 0.0,
 &END

 $FLOWS
  FNAMES = 'TESTGAS1',      ! Flow name
  PRES = 0.101325,          ! Pressure
  TEMP = 298.15,            ! Temperature
  FLOWTO = 1000.0,          ! Total flow rate
  FLOWDI = 'MOL',           ! Flow dimensions: mol/h
  FLOWEN = 'NON-COMPUTE',   ! Do not compute the flow enthalpy
  FLOW1 = 1.0,              ! Flow composition
 $END

! Isothermal flash unit

 $IFLASH
  UNNAME = 'PROPER1',
  FEEDS = 'TESTGAS1'
  PRODUC = 'GAS1', 'LIQ1'   ! Vapor and liquid product
  TEMP = 333.15             ! Flash temperature
```

```
  PRES = 0.00101325         ! Flash pressure
 $END

! Physical properties for the flows of the simulation
!
! ***** SLCOR for SLLF: ignore results for SLNLF *****

 $FYSPRO
! Printing indicator
  IPR = 0
! Flows for which properties are calculated
  FLOWNA = 'GAS1', 'GAS1', 'GAS1', 'GAS1',
           'GAS1', 'GAS1', 'GAS1', 'GAS1',
           'GAS1', 'GAS1', 'GAS1', 'GAS1',
           'GAS1', 'GAS1', 'GAS1', 'GAS1',
           'GAS1', 'GAS1', 'GAS1', 'GAS1'
! Gas sorption isotherms
  PROPER = 'GSISOT', 'GSISOT', 'GSISOT',
           'GSISOT', 'GSISOT', 'GSISOT',
           'GSISOT', 'GSISOT', 'GSISOT',
           'GSISOT', 'GSISOT', 'GSISOT',
           'GSISOT', 'GSISOT', 'GSISOT',
           'GSISOT', 'GSISOT', 'GSISOT',
           'GSISOT', 'GSISOT',
! Polymer phase: polystyrene
  POLY = 'PS', 'PS', 'PS', 'PS', 'PS', 'PS', 'PS', 'PS',
         'PS', 'PS', 'PS', 'PS', 'PS', 'PS', 'PS', 'PS',
         'PS', 'PS', 'PS', 'PS'
! Polymer number average Mw
  POLYMW = 63000.0, 63000.0, 63000.0, 63000.0, 63000.0,
           63000.0, 63000.0, 63000.0, 63000.0, 63000.0,
           63000.0, 63000.0, 63000.0, 63000.0, 63000.0,
           63000.0, 63000.0, 63000.0, 63000.0, 63000.0
! Polydispersity index
  PDIS = 3.97, 3.97, 3.97, 3.97, 3.97, 3.97, 3.97, 3.97,
         3.97, 3.97, 3.97, 3.97, 3.97, 3.97, 3.97, 3.97,
         3.97, 3.97, 3.97, 3.97,
! Polymer thermodynamics
  PTHERM = 'PHSC', 'SLLF', 'SLNLF', 'MHV2P',
           'PHSC', 'SLLF', 'SLNLF', 'MHV2P',
           'PHSC', 'SLLF', 'SLNLF', 'MHV2P',
           'PHSC', 'SLLF', 'SLNLF', 'MHV2P', ! Perturbed Hard-sphere-chain
                                             ! EOS, Sanchez-Lacombe lattice
                                             ! fluid EOS, Sanchez-Lacombe
                                             ! non-lattice fluid EOS
                                             ! and MHV2 with the
                                             ! exponential UNIFAC
           'MHV2PO', 'MHV2PO', 'MHV2PO',
           'MHV2PO'                          ! MHV2 with the Lyngby
                                             ! modified UNIFAC (original
                                             ! MHV2)
! Initial temperatures in Celsius
  TINIC = 15.0, 15.0, 15.0, 15.0,
          30.0, 30.0, 30.0, 30.0,
          45.0, 45.0, 45.0, 45.0,
          60.0, 60.0, 60.0, 60.0,
          15.0, 30.0, 45.0, 60.0
! Final temperatures in Celsius
  TFINC = 15.0, 15.0, 15.0, 15.0,
          30.0, 30.0, 30.0, 30.0,
          45.0, 45.0, 45.0, 45.0,
          60.0, 60.0, 60.0, 60.0,
          15.0, 30.0, 45.0, 60.0
```

```
! Initial pressures in kPa
  PINKPA = 4.5, 4.5, 4.5, 4.5,
           9.0, 9.0, 9.0, 9.0,
           18.0, 18.0, 18.0, 18.0,
           32.0, 32.0, 32.0, 32.0,
           4.5, 9.0, 18.0, 32.0
! Final pressures in kPa
  PFIKPA = 7.5, 7.5, 7.5, 7.5,
           15.7, 15.7, 15.7, 15.7,
           29.2, 29.2, 29.2, 29.2,
           50.5, 50.5, 50.5, 50.5,
           7.5, 15.7, 29.2, 50.5
! Number of property points
  POINTS = 10, 10, 10, 10, 10, 10,
           10, 10, 10, 10, 10, 10,
           10, 10, 10, 10, 10, 10,
           10, 10
! Lyngby modified UNIFAC group parameter for benzene
  VLEMAT(1,10)=6
 $END
```

APPENDIX V INPUT FILE FOR THE GAS AND VAPOR SORPTION IN PDMS

```
 $TITLE
  USER = 'PSAVO', PROJEC = 'HUU01', PROBLE = 'Isotermitesti',
 $END

 $UNITS
  MAXITE = 100
 $END

! Components in the simulation
! CO2, N2, O2, H2, CH4, C2H6, C2H4, C3H8, C3H6

 $THERMO
  COMPNU = 50,
           31,
           35,
           20,
           66,
           105,
           93,
           138,
           126,
  MDATA = 1             ! Read CRDATA input
  KTYPE = 'SRK'
 $END

! SL EOS and PHSC EOS parameters

 $CRDATA
  SLTEMP = 304.6, 133.7, 168.5, 53.55, 211.2, 311.0, 287.0, 364.1, 350.7
  SLPRES = 591.1, 195.4, 278.3, 31.7, 245.1, 328.5, 337.7, 326.4, 357.0
  SLDEN = 1518.0, 935.6, 1290.0, 75.27, 474.4, 632.8, 661.0, 698.4, 729.8
  PHSCR = 3.368, 1.313, 1.225, 1.225, 1.000, 1.694, 1.694, 2.129, 2.129
  PHSCE = 140.3, 99.4, 127.5, 127.5, 182.1, 206.3, 206.3, 219.0, 219.0
  PHSCS = 2.574, 3.628, 3.489, 3.489, 4.126, 3.916, 3.916, 3.998, 3.998
 $END

 $FLOWS
  FNAMES = 'GAS1',
           'GAS2',
           'GAS3',
           'GAS4',
           'GAS5',
           'GAS6',
           'GAS7',
           'GAS8',
           'GAS9'
  PRES = 9*0.101325,
  TEMP = 9*308.15,
  FLOWTO = 9*1000.0,           ! Total flow rate
  FLOWDI = 9*'MOL',            ! Flow dimensions: mol/h
  FLOWEN = 9*'COMPUTE',        ! Compute the flow enthalpy
!
! Flow compositions: pure component flows
!
  FLOW1 = 1.0, 8*0.0
  FLOW2 = 0.0, 1.0, 7*0.0
  FLOW3 = 2*0.0, 1.0, 6*0.0
  FLOW4 = 3*0.0, 1.0, 5*0.0
  FLOW5 = 4*0.0, 1.0, 4*0.0
  FLOW6 = 5*0.0, 1.0, 3*0.0
```

```
  FLOW7 = 6*0.0, 1.0, 2*0.0
  FLOW8 = 7*0.0, 1.0, 0.0
  FLOW9 = 8*0.0, 1.0
 $END

! Physical properties for the flows in the simulation

 $FYSPRO
  IPR = 0
  FLOWNA = 'GAS1', 'GAS2', 'GAS3', 'GAS4', 'GAS5',
           'GAS6', 'GAS7', 'GAS8', 'GAS9',
! Gas sorption isotherms
  PROPER = 'GSISOT', 'GSISOT', 'GSISOT', 'GSISOT',
           'GSISOT', 'GSISOT', 'GSISOT', 'GSISOT', 'GSISOT',
! Polymer phase: polydimethylsiloxane
  POLY = 'PDMS', 'PDMS', 'PDMS', 'PDMS', 'PDMS',
         'PDMS', 'PDMS', 'PDMS', 'PDMS'
! Number average Mw
  POLYMW = 1500000.0, 1500000.0, 1500000.0, 1500000.0,
           1500000.0, 1500000.0, 1500000.0, 1500000.0, 1500000.0,
! Polydispersity index
  PDIS = 1.0, 1.0, 1.0, 1.0, 1.0, 1.0, 1.0, 1.0, 1.0,
! Polymer thermodynamics
  PTHERM = 'SLNLF', 'SLNLF', 'SLNLF', 'SLNLF', 'SLNLF',
           'SLNLF', 'SLNLF', 'SLNLF', 'SLNLF',
! Initial and final temperatures in Celsius
  TINIC = 35.0, 35.0, 35.0, 35.0, 35.0, 35.0, 35.0, 35.0, 35.0,
  TFINC = 35.0, 35.0, 35.0, 35.0, 35.0, 35.0, 35.0, 35.0, 35.0
! Number of points in each isotherm
  POINTS = 20, 20, 20, 20, 20, 20, 20, 20, 20,
! Initial and final pressures in kPa
  PINKPA = 10.0, 10.0, 10.0, 10.0, 10.0, 10.0, 10.0, 10.0, 10.0,
  PFIKPA = 2500.0, 2500.0, 2500.0, 2500.0, 2800.0, 2500.0,
           6760.0, 400.0, 1000.0,
 $END
```

APPENDIX VI INPUT FILE FOR THE ISOTHERMAL PERMEATION

```
$TITLE
 USER = 'PSAVO', PROJEC = 'GKB81', PROBLE = 'Testaus',
$END

! Units in the simulation

$UNITS
 MODELS = 'IFLASH', 'SDGMEM'
 MAXITE = 100
$END

! Components in the simulation
! H2, CH4, C2H6, C3H6, C3H8

$THERMO
 COMPNU = 20,
          66,
          105,
          126,
          138          ! Component numbers in the FLOWBAT databank
 KTYPE = 'SRK-DG'     ! Method to compute the phase equilibrium:
                      ! Daubert and Graboski modification of SRK
 MTHENT = 6,          ! Method to compute the specific enthalpy:
                      ! Pressure correction from SRK-DG
 MTHLSV = 6,          ! Method to compute the liquid specific molar
                      ! volume: Chueh, Prausnitz, Lyckman, Eckert
                      ! saturated liquid
 MVSPVO = 6,          ! Method to compute the vapor specific molar volume:
                      ! SRK-DG
 ISRKSC = 1           ! Use alpha-equations for the supercritical
                      ! components
 MDATA = 1            ! Indicator to read the namelist CRDATA
$END

! EOS parameters for PHSC

$CRDATA
 PHSCR = 0.382, 1.0, 1.694, 2.029, 2.129,
 PHSCE = 63.4, 182.1, 206.3, 221.9, 219.0,
 PHSCS = 4.945, 4.126, 3.916, 3.951, 3.998,
$END

! Feed flow of the simulation

$FLOWS
 FNAMES = 'TESTGAS1',
 PRES = 0.101325,          ! Pressure in MPa
 TEMP = 313.15,            ! Temperature in K
 FLOWTO = 1.7D0            ! Total flow rate
 FLOWDI = 'MOL',           ! Flow dimensions moles/h
 FLOWEN = 'NON-COMPUTE',   ! Selection not to compute the feed enthalpy
 FLOW1 = 10.20, 10.0,
         9.97, 20.00,
         49.83             ! Feed flow composition
$END

! Isothermal flash unit

$IFLASH
 IPR = 0                   ! Output printing suppressed
 UNNAME = 'PROPER1',       ! Block/Unit name
```

```
 FEEDS = 'TESTGAS1',      ! Feed to the unit
 PRODUC = 'GAS1', 'LIQ1'  ! Product flows from the unit
 TEMP = 313.15            ! Block temperature
 PRES = 0.41161           ! Block pressure
$END

! Gas/vapor membrane separation unit

 $SDGMEM
 IPR = 2                 ! Moderate output printing
 UNNAME = 'TESTCELL'     ! Block/Unit name
 FEEDS = 'GAS1'          ! Feed to the unit
 PRODUC = 'RETE', 'PERM' ! Product flows from the unit
 TEMP = 303.15           ! Block temperature
 PRES = 0.4116169929,    ! Feed/Retentate pressure
 PRESV = 0.06666118      ! Permeate product pressure
 PDROP = 'NO'            ! Do not compute pressure drop
 A = 0.0011400918        ! Membrane area
 DMEM = 195.0D0          ! Membrane thickness in microm.
 MODTYP = 'TC'           ! Module type: flat sheet test cell,
                         ! Cross-flow permeate with 1 control volume
 POLY = 'PDMS'           ! Membrane material
 MWP = 50000.0           ! Polymer molecular weight (number average)
 PDIS = 1.5              ! Polydispersity index
 MASSTR = 'simplified'   ! Method to compute the mass transfer:
                         ! The simplified method used
 DCOEF = 'free'          ! Diffusion coefficients from the free volume
                         ! correlations
 CROSS = 'no'            ! Do not compute the cross coefficients
 SOLVER = 'newton'       ! Selection for the Newton-Raphson
                         ! nonlinear equation solver
 PTHERM = 'phsc'         ! Thermodynamics selection for the polymeric
                         ! system
 !
 ! Parameters for the diffusion coefficient correlation
 !
 AD = 1.8774E-3, 1.0327E-3, 1.4892E-3, 2.0242E-3, 1.4891E-3
 BD = 0.441, 0.7545, 0.9926, 1.136, 1.129
 CD = 0.0, 0.0, 1.26118E-5, 1.55793E-5, 2.09383E-5
 ED = 0.0, 0.0, 3197.643, 3555.543, 3599.526
 ENERGY = 'NO'           ! Exclude energy equations: isothermal system
 MAXITE = 100            ! Maximum number of iterations for
                         ! the nonlinear equation solver
 TOL = 1.0D-8            ! Tolerance for nonlinear equation solver
 TUNITS = 3600.0         ! Time units (seconds/units in the simulation)
$END
```

APPENDIX VII INPUT FILE FOR THE SELECTIVE REMOVAL OF HYDROCARBONS FROM HYDROGEN

```
 $TITLE
  USER = 'PSAVO', PROJEC = 'GKB81', PROBLE = 'Testaus',
 $END

 $UNITS
  MODELS = 'IFLASH', 'SDGMEM', 'IFLASH', 'SDGMEM',
  MAXITE = 100
  FLFILE = 'hcpurge.flw'   ! Flow file name of the simulation
  UNFILE(2) = 'memb1.pro'  ! Block/Unit file name for 2nd block
  UNFILE(4) = 'memb2.pro'  ! Block/Unit file name for 4th block
$END

 ! Components in the simulation
 ! H2, CH4, C2H6, C3H6, C3H8, H2S, N2

 $THERMO
  COMPNU = 20, 66,
           105, 126,
           138, 22,
           31           ! Component numbers in the FLOWBAT databank
  KTYPE = 'SRK-DG'
  MTHENT = 6,           ! Method to compute the specific enthalpy:
                        ! Pressure correction from SRK-DG
  MTHLSV = 6,           ! Method to compute the liquid specific molar
                        ! volume: Chueh, Prausnitz, Lyckmann,
                        ! Eckert saturated liquid
  MVSPVO = 6            ! Method to compute the vapor specific molar volume:
                        ! SRK-DG
  ISRKSC = 1            ! Use alpha-equations for the supercritical
                        ! components
  MDATA = 1             ! Indicator to read the namelist CRDATA
 $END

! EOS parameters for the SLNLF and the PHSC

 $CRDATA
  SLTEMP = 53.55, 211.2, 311.0, 350.7, 364.1, 369.4, 133.7
  SLPRES = 31.7, 245.1, 328.5, 357.0, 326.4, 628.3, 195.4
  SLDEN = 75.27, 474.4, 632.8, 729.8, 698.4, 1090.0, 935.6
  PHSCR = 0.382, 1.0, 1.694, 2.029, 2.129, 1.789, 1.131
  PHSCE = 63.4, 182.1, 206.3, 221.9, 219.0, 242.9, 99.4
  PHSCS = 4.945, 4.126, 3.916, 3.951, 3.998, 3.357, 3.628
 $END

! Feed flows

 $FLOWS
  FNAMES = 'PG1', 'PG2'
  PRES = 2*2.75,           ! Flow pressures [MPa]
  TEMP = 2*313.15,         ! Flow temperatures [K]
  FLOWTO = 2*176899.73,    ! Total flow rates
  FLOWDI = 2*'MOL',        ! Flow dimensions [mole/h]
  FLOWEN = 2*'COMPUTE',    ! Compute the flow specific enthalpies
  FLOW1 = 85.0, 7.0, 4.0, 0.0, 2.5, 1.5, 0.0
  FLOW2 = 85.0, 7.0, 4.0, 0.0, 2.5, 1.5, 0.0
 $END

! Components in the simulation
! H2, CH4, C2H6, C3H6, C3H8, H2S, N2
```

```
! Isothermal flash unit, models the feed compression and cooling

 $IFLASH
  IPR = 0
  UNNAME = 'FDCOMP1',
  FEEDS = 'PG1',
  PRODUC = 'HPPG1', 'DUMMY-LIQ1'
  TEMP = 313.15
  PRES = 2.75
 $END

! Gas/vapor membrane separation unit

 $SDGMEM
  IPR = 1
  UNNAME = 'MEMB1'        ! Feed flow to the unit
  FEEDS = 'HPPG1'
  PRODUC = 'PURGE1',
           'PERM1'        ! Product flows from the unit
  PRESV = 0.8,            ! Permeate product pressure [MPa]: design spec
  A = 80.0                ! Total membrane area
  POLY = 'PDMS'           ! Selective layer material
  MWP = 50000.0           ! Polymer molecular weight (number average)
  PDIS = 1.5              ! Polydispersity index
  DMEM = 4.0D0            ! Selective layer thickness [microm]
  MODTYP = 'spiral'       ! Module type: spiral-wound
  DTUBE = 0.02921         ! Central tube diameter: 1.15 in
  NMOD = 2                ! Number of parallel modules
  NMODS = 2               ! Number of serial modules
  NLEAF = 10,             ! Number of membrane leaves in a module
  LLEAF = 0.9144,         ! Leaf length
  HFC = 0.0013,           ! Height of the feed/retentate channel
  HPC = 0.001             ! Height of the permeate channel
  INMAX = 20              ! Maximum number of inner iterations
  OUTMAX = 6              ! Maximum number of outer iterations
  MPDROP = 2              ! Method to compute the pressure drop:
                          ! compute from the friction factors
  FANV = 48.0             ! The fanning friction factor constant
                          ! for the permeate side
  NLSECT = 60,            ! Number of x directed grid lines
  NVSECT = 50             ! Number of z directed grid lines
  MAXITE = 100            ! Maximum number of iterations
                          ! for the nonlinear equation solver
  MTHITE = 1              ! Selection for the Newton-Raphson
                          ! nonlinear equation solver
  TOL = 1.0D-8            ! Tolerance for the nonlinear equation solver
  MASSTR = 'simplified'   ! Method to compute the mass transfer:
                          ! The simplified method used
  DCOEF = 'free'          ! Diffusion coefficients from the free volume
                          ! correlation
  CROSS = 'no'            ! Do not compute the cross coefficients
  PTHERM = 'slnlf'        ! Thermodynamics selection for the polymeric
                          ! system
  !
  ! Parameters for the diffusion coefficient correlation
  !
  AD = 8.2533E-4, 5.1042E-4, 4.8253E-4,
       3.7110E-4, 9.3439E-5, 1.7159E-4, 1.2985E-3
  BD = 0.4766, 0.696, 0.8341, 0.8383, 0.636, 0.4677, 0.7667
  CD = 0.0, 0.0, 4.6846E-5, 1.3509E-4, 2.0157E-3, 0.0, 0.0
  ED = 0.0, 0.0, 2780.859, 2853.632, 2059.340, 0.0, 0.0
  TUNITS = 3600.0         ! Time units (seconds/units in the simulation)
```

```
 CVFLUX = 'all'          ! Selection for the control volume flux
                         ! computation:
                         ! Compute fluxes at all control volumes
 ENERGY = 'yes'          ! Include energy equations: non-isothermal system
$END

! Isothermal flash unit, models the feed compression and cooling

$IFLASH
 IPR = 0
 UNNAME = 'FDCOMP2',
 FEEDS = 'PG2',
 PRODUC = 'HPPG2', 'DUMMY-LIQ2'
 TEMP = 313.15
 PRES = 2.75
$END

! Gas/vapor membrane separation unit

$SDGMEM
 IPR = 1
 UNNAME = 'MEMB2'        ! Feed flow to the unit
 FEEDS = 'HPPG2'
 PRODUC = 'PURGE2',
          'PERM2'        ! Product flows from the unit
 PRESV = 0.8,            ! Permeate product pressure [MPa]: design spec
 A = 80.0                ! Total membrane area
 POLY = 'PDMS'           ! Selective layer material
 MWP = 50000.0           ! Polymer molecular weight (number average)
 PDIS = 1.5              ! Polydispersity index
 DMEM = 4.0D0            ! Selective layer thickness [microm]
 MODTYP = 'spiral'       ! Module type: spiral-wound
 DTUBE = 0.02921         ! Central tube diameter: 1.15 in
 NMOD = 2                ! Number of parallel modules
 NMODS = 2               ! Number of serial modules
 NLEAF = 10,             ! Number of membrane leaves in a module
 LLEAF = 0.9144,           ! Leaf length
 HFC = 0.0013,           ! Height of the feed/retentate channel
 HPC = 0.001             ! Height of the permeate channel
 INMAX = 20              ! Maximum number of inner iterations
 OUTMAX = 6              ! Maximum number of outer iterations
 MPDROP = 2              ! Method to compute the pressure drop:
                         ! compute from the friction factors
 FANV = 48.0             ! The Fanning friction factor constant
                         ! for the permeate side
 NLSECT = 60,            ! Number of x directed grid lines
 NVSECT = 50             ! Number of z directed grid lines
 MAXITE = 100            ! Maximum number of iterations
                         ! for the nonlinear equation solver
 MTHITE = 1              ! Selection for the Newton-Raphson
                         ! nonlinear equation solver
 TOL = 1.0D-8            ! Tolerance for the nonlinear equation solver
 MASSTR = 'simplified'   ! Method to compute the mass transfer:
                         ! The simplified method used
 DCOEF = 'free'          ! Diffusion coefficients from the free volume
                         ! correlation
 CROSS = 'no'            ! Do not compute the cross coefficients
 PTHERM = 'phsc'         ! Thermodynamics selection for the polymeric
                         ! system
 !
 ! Parameters for the diffusion coefficient correlation
 !
 AD = 1.8774E-3, 1.0327E-3, 1.4892E-3,
```

```
     2.0242E-3, 1.4891E-3, 3.4955E-4, 8.5285E-3
 BD = 0.4410, 0.7545 0.9926, 1.1360, 1.1260, 0.7190, 1.0340
 CD = 0.0, 0.0, 1.26118-5, 1.55793E-5, 2.09383E-5, 0.0, 0.0
 ED = 0.0, 0.0, 3197.643211, 3555.543053, 3599.525725, 0.0, 0.0
 TUNITS = 3600.0         ! Time units (seconds/units in the simulation)
 CVFLUX = 'all'          ! Selection for the control volume flux
                         ! computation:
                         ! Compute fluxes at all control volumes
 ENERGY = 'yes'          ! Include energy equations: non-isothermal system
$END
```

APPENDIX VIII INPUT FILE FOR THE PROPYLENE RECOVERY

```
$TITLE
 USER = 'PSAVO', PROJEC = 'GKB81', PROBLE = 'Testaus',
$END

! Units in the simulation

$UNITS
 MODELS = 'IFLASH', 'IFLASH', 'SDGMEM',
         'IFLASH', 'SDGMEM',
 MAXITE = 100
 FLFILE = 'ppmtr.flw'      ! Flow file name of the simulation
 UNFILE(3) = 'memb1.pro',  ! Block/Unit file name for 3rd block
 UNFILE(5) = 'memb2.pro'   ! Block/Unit file name for 5th block
$END

! Components in the simulation
! N2, C2H4, C2H6, C3H6, C3H8,

$THERMO
 COMPNU = 31,
          93,
         105,
         126,
         138          ! Component numbers in the FLOWBAT databank
 KTYPE = 'SRK-DG'
 MTHENT = 6,          ! Method to compute the specific enthalpy:
                      ! Pressure correction from SRK-DG
 MTHLSV = 6,          ! Method to compute the liquid specific molar
                      ! volume:
                      ! Chueh, Prausnitz, Lyckman, Eckert saturated liquid
 MVSPVO = 1,          ! Method to compute the vapor specific molar volume:
                      ! ideal gas
 ISRKSC = 1           ! Use alpha-equations for the supercritical
                      ! components
 MVVISC = 2           ! Method to compute the vapor viscosity:
                      ! Aasber-Petersen et al. (1991)
 MDATA = 1            ! Indicator to read the namelist CRDATA
$END

! EOS parameters for the PHSC

$CRDATA
 PHSCR = 1.131, 1.609, 1.694, 2.029, 2.129
 PHSCE = 99.4, 196.8, 206.3, 221.9, 219.0
 PHSCS = 3.628, 3.839, 3.916, 3.951, 3.998
$END

! Feed flows and initial estimates for the cut flows.

$FLOWS
 FNAMES = 'PG', 'RECY'      ! Feed and cut flow
 PRES = 0.101325, 1.3       ! Flow pressures
 TEMP = 298.15, 283.15      ! Flow temperatures
 FLOWTO = 53061.61419,
          15172.0           ! Total flow rates
 FLOWDI = 'MOL', 'MOL'      ! Flow dimensions
 FLOWEN = 'COMPUTE',
          'COMPUTE'         ! Compute the flow specific enthalpies
 FLOW1 = 86.7,
         0.15,
         0.15,
```

```
         10.0,
          3.0               ! Feed flow composition,
 FLOW2 = 82.0,
          0.3,
          0.2,
         12.0,
          5.5               ! Cut flow composition
$END

! Isothermal flash unit, models the feed compression and cooling

$IFLASH
 IPR = 0
 UNNAME = 'FDCOMP',
 FEEDS = 'PG',
 PRODUC = 'HPPG', 'DUMMY-LIQ'
 TEMP = 298.15
 PRES = 1.38
$END

! Isothermal flash unit, models the mixing of the feed
! and the recycle flow

$IFLASH
 IPR = 0
 UNNAME = 'PROPER1',
 FEEDS = 'PG',
 FEEDS = 'HPPG', 'RECY'
 PRODUC = 'ST1-FD', 'DUMMY-L1'
 TEMP = 293.15
 PRES = 1.38
$END

! Gas/vapor membrane separation unit, stripping stage

$SDGMEM
 IPR = 1
 UNNAME = 'MEMB1'
 FEEDS = 'ST1-FD'        ! Feed flow to the unit
 PRODUC = 'PURGE',
          'PERM'         ! Product flows from the unit
 PRESV = 0.15,           ! Permeate product pressure: design spec
 A = 264.0               ! Total membrane area
 POLY = 'PDMS'           ! Selective layer material
 MWP = 50000.0           ! Polymer molecular weight (number average)
 PDIS = 1.5              ! Polydispersity index
 DMEM = 4.0D0            ! Selective layer thickness [microm]
 MODTYP = 'spiral'       ! Module type: spiral-wound
 DTUBE = 0.02921         ! Central tube diameter: 1.15 in
 NMOD = 11               ! Number of parallel modules
 NMODS = 4               ! Number of serial modules
 NLEAF = 4,              ! Number of membrane leaves in a module
 LLEAF = 0.9144,         ! Leaf length
 HFC = 0.0013,           ! Height of the feed/retentate channel
 HPC = 0.001             ! Height of the permeate channel
 INMAX = 20              ! Maximum number of inner iterations
 OUTMAX = 6              ! Maximum number of outer iterations
 MPDROP = 2              ! Method to compute the pressure drop:
                         ! compute from the friction factors
 FANV = 48.0             ! The Fanning friction factor constant
                         ! for the permeate side
 NLSECT = 75,            ! Number of x directed grid lines
 NVSECT = 20             ! Number of z directed grid lines
```

```
 MAXITE = 100            ! Maximum number of iterations
                         ! for the nonlinear equation solver
 MTHITE = 1              ! Selection for the Newton-Raphson
                         ! nonlinear equation solver
 TOL = 1.0D-6            ! Tolerance for the nonlinear equation solver
 MASSTR = 'simplified'   ! Method to compute the mass transfer:
                         ! The simplified method used
 DCOEF = 'free'          ! Diffusion coefficients from the free volume
                         ! correlation
 CROSS = 'no'            ! Do not compute the cross coefficients
 PTHERM = 'phsc'         ! Thermodynamics selection for the polymeric
                         ! system
 !
 ! Parameters for the diffusion coefficient correlation
 !
 AD = 8.5285E-3, 1.3838E-3, 1.4892E-3, 2.0242E-3, 1.4891E-3
 BD = 1.0340, 0.9365, 0.9926, 1.1360, 1.1290
 CD = 0.0, 4.90811E-5, 1.26118E-5, 1.55793E-5, 2.09383E-5
 ED = 0.0, 2670.212, 3197.643, 3555.543, 3599.526
 TUNITS = 3600.0         ! Time units (seconds/units in the simulation)
 CVFLUX = 'median'       ! Selection for the control volume flux
                         ! computation:
                         ! Compute fluxes at median properties
 ENERGY = 'yes'          ! Include energy equations: non-isothermal system
$END

! Isothermal flash unit, models the compression and cooling of
! permeate stream from the striping stage.

$IFLASH
 IPR = 0
 UNNAME = 'PROPER2',
 FEEDS = 'PERM',
 PRODUC = 'ST2-FD', 'DUMMY-L2'
 TEMP = 293.15
 PRES = 1.385
$END

! Gas/vapor membrane separation unit, enriching stage

$SDGMEM
 IPR = 1
 UNNAME = 'MEMB2'
 FEEDS = 'ST2-FD'        ! Feed flow to the unit
 PRODUC = 'RECY',
          'HC'           ! Product flows from the unit
 PRESV = 0.103,          ! Permeate product pressure: design spec
 A = 12.0                ! Total membrane area
 POLY = 'PDMS'           ! Selective layer material
 MWP = 50000.0           ! Polymer molecular weight (number average)
 PDIS = 1.5              ! Polydispersity index
 DMEM = 4.0D0            ! Selective layer thickness [microm]
 MODTYP = 'spiral'       ! Module type: spiral-wound
 DTUBE = 0.02921         ! Central tube diameter: 1.15 in
 NMOD = 2                ! Number of parallel modules
 NMODS = 1               ! Number of serial modules
 NLEAF = 4,              ! Number of serial modules
 LLEAF = 0.9144,         ! Leaf length
 HFC = 0.0013,           ! Height of the feed/retentate channel
 HPC = 0.001             ! Height of the permeate channel
 INMAX = 10              ! Maximum number of inner iterations
 OUTMAX = 4              ! Maximum number of outer iterations
 MPDROP = 2              ! Method to compute the pressure drop:
```

```
                          ! compute from the friction factors
 FANV = 48.0              ! The Fanning friction factor constant
                          ! for the permeate side
 NLSECT = 75,             ! Number of x directed grid lines
 NVSECT = 20              ! Number of z directed grid lines
 MAXITE = 100             ! Maximum number of iterations
                          ! for the nonlinear equation solver
 MTHITE = 1               ! Selection for the Newton-Raphson
                          ! nonlinear equation solver
 TOL = 1.0D-6             ! Tolerance for the nonlinear equation solver
 MASSTR = 'simplified'    ! Method to compute the mass transfer:
                          ! The simplified method used
 DCOEF = 'free'           ! Diffusion coefficients from the free volume
                          ! correlations
 CROSS = 'no'             ! Do not compute the cross coefficients
 PTHERM = 'phsc'          ! Thermodynamics selection for the polymeric
                          ! system
 !
 ! Parameters for the diffusion coefficient correlation
 !
 AD = 8.5285E-3, 1.3838E-3, 1.4892E-3, 2.0242E-3, 1.4891E-3
 BD = 1.0340, 0.9365, 0.9926, 1.1360, 1.1290
 CD = 0.0, 4.90811E-5, 1.26118E-5, 1.55793E-5, 2.09383E-5
 ED = 0.0, 2670.212, 3197.643, 3555.543, 3599.526
 TUNITS = 3600.0          ! Time units (seconds/units in the simulation)
 CVFLUX = 'median'        ! Selection for the control volume flux
                          ! computation:
                          ! Compute fluxes at median properties
 ENERGY = 'yes'           ! Include energy equations: non-isothermal system
$END

! Convergence and calculation tolerances

$SOLVER
 CUTFLO = 'RECY',         ! Cut flow specification
 MAXITE = 100,            ! Maximum number of iterations
$END
```

ACTA UNIVERSITATIS LAPPEENRANTAENSIS

81. HAUTA-KASARI, MARKKU. Computational techniques for spectral image analysis. 1999. U.s. Diss.

82. FRYDRYCH, MICHAEL. Color vision system based on bacteriorhodopsin. 1999. 87 s. Diss.

83. MAKKONEN, MATTI. Size effect and notch size effect in metal fatigue. 1999. 93 s., liitt. Diss.

84. 7th NOLAMP Conference. 7th Nordic Conference in Laser Processing of Materials. Ed. by Veli Kujanpää and John Ion. Vol. I-II. 1999. 559 s.

85. Welding Conference LUT JOIN´99. International Conference on Efficient Welding in Industrial Applications (ICEWIA). Ed. by Jukka Martikainen and Harri Eskelinen. 1999. 418 s.

86. PARTANEN, TEUVO. On the application of beam on elastic foundation theory to the analysis of stiffened plate strips. 1999. 102 s. Diss.

87. ESKELINEN, HARRI. Tuning the design procedures for laser processed microwave mechanics. 1999. 172 s. Diss.

88. ROUVINEN, ASKO. Use of neural networks in robot positioning of large flexible redundant manipulators. 1999. 71 s. Diss.

89. MAKKONEN, PASI. Artificially intelligent and adaptive methods for prediction and analysis of superheater fireside corrosion in fluidized bed boilers. 1999. 187 s. Diss.

90. KORTELAINEN, JARI. A topological approach to fuzzy sets. 1999. U.s. Diss.

91. SUNDQVIST, SATU. Reaction kinetics and viscosity modelling in the fusion syntheses of Ca- and Ca/Mg-resinates. 1999. U.s. Diss.

92. SALO, JUSSI. Design and analysis of a transversal-flux switched-reluctance-linear-machine pole-pair. 1999. 156 s. Diss.

93. NERG, JANNE. Numerical modelling and design of static induction heating coils. 2000. 86 s. Diss.

94. VARTIAINEN, MIKA. Welding time models for cost calculations in the early stages of the design process. 2000. 89 s., liitt. Diss.

95. JERNSTRÖM, EEVA. Assessing the technical competitiveness of printing papers. 2000. 159 s., liitt. Diss.

96. VESTERINEN, PETRI. On effort estimation in software projects. 2000. U.s. Diss.

97. LUUKKO, JULIUS. Direct torque control of permanent magnet synchronous machines – analysis and implementation. 2000. 172 s. Diss.

98. JOKINEN, ARTO. Lobbying as a part of business management. 2000. 244 s. Diss.

99. JÄÄSKELÄINEN, EDUARD. The role of surfactant properties of extractants in hydrometallurgical liquid-liquid extraction processes. 2000. U.s. Diss.

100. Proceedings of 3rd Finnish-French Colloquium on Nuclear Power Plant Safety. 2000. 118 s.

101. TANSKANEN, PASI. The evolutionary structural optimization (ESO) method: theoretical aspects and the modified evolutionary structural optimization (MESO) method. 2000. 67 s., liitt. Diss.

102. JERNSTRÖM, PETTERI. The effects of real-time control of welding parameters on weld quality in plasma arc keyhole welding. 2000. 69 s., liitt. Diss.

103. KAARNA, ARTO. Multispectral image compression using the wavelet transform. 2000. U.s. Diss.

104. KOTONEN, ULLA. Rahavirta-analyysit, erityisesti kassavirtalaskelma, kunnan talouden ohjauksen apuvälineenä. 2000. 209 s., liitt. Väitösk.

105. VARIS, JUHA. A novel procedure for establishing clinching parameters for high strength steel sheet. 2000. 84 s., liitt. Diss.

106. PÄTÄRI, EERO. Essays on portfolio performance measurement. 2000. 201 s. Diss.

107. SANDSTRÖM, JAANA. Cost information in engineering design – potentials and limitations of activity-based costing. 2001. 143 s., liitt. Diss.

108. TOIVANEN, JOUKO. Balanced Scorecardin implementointi ja käytön nykytila Suomessa. 2001. 216 s. Väitösk.

109. PESONEN, MAUNO. Applying AHP and A´WOT to strategic planning and decision making: case studies in forestry and forest industry. 2001. U.s. Diss.

110. Proceedings of Fifth International Seminar on Horizontal Steam Generators. Ed. by Juhani Vihavainen. 2001. 255 s.

111. LAINE, PERTTI. Kohti vesiensuojelun aikaa: veden laadun muutokset eteläisellä Saimaalla. 2001. 264 s. Väitösk.

112. SILVENTOINEN, PERTTI. Electromagnetic compatibility and EMC-measurements in DC-voltage link converters. 2001. 115 s. Diss.

113. TERVONEN, ANTERO. Laadun kehittäminen suomalaisissa yrityksissä. 2001. 206 s. Väitösk.

114. SALMINEN, ANTTI. The effects of filler wire feed on the efficiency, parameters and tolerances of laser welding. 2001. 82 s., liitt. Diss.

115. HORTTANAINEN, MIKA. Propagation of the ignition front against airflow in packed beds of wood particles. 2001. U.s. Diss.

116. IKONEN, JOUNI. Improving distributed simulation in a workstation environment. 2001. U.s. Diss.

117. WU, HUAPENG. Analysis, design and control of a hydraulically driven parallel robot manipulator. 2001. U.s. Diss.

118. REUNANEN, ARTTU. Experimental and numerical analysis of different volutes in a centrifugal compressor. 2001. 150 s. Diss.

119. TAAVITSAINEN, VELI-MATTI. Strategies for combining soft and hard modelling in some physicochemical problems. 2001. U.s. Diss.

120. SAVOLAINEN, RAIJA. The use of branched ketene dimers in solving the deposit problems related to the internal sizing of uncoated fine paper. 2001. U.s. Diss.

121. SARAVIRTA, ALI. Project success through effective decisions: case studies on project goal setting, success evaluation and managerial decision making. 2001. 286 s. Diss.

122. BLOMQVIST, KIRSIMARJA. Partnering in the dynamic environment: the role of trust in asymmetric technology partnership formation. 2002. 296 s., liitt. Diss.

123. KARVONEN, VESA. Development of fiber recovery process. 2002. U.s. Diss.

ISBN 951-764-647-X
ISSN 1456-4491

Lappeenranta 2002

Errata

Page 28

Equations of energy (3.34), (3.35), and (3.36) in terms of partial molar enthalpies should be written as

$$v_y \frac{\partial}{\partial y}\left(\sum_{i=1}^{nc} c_{iL}\overline{H}_{iL}\right) + v_z \frac{\partial}{\partial z}\left(\sum_{i=1}^{nc} c_{iL}\overline{H}_{iL}\right) = -\left(\frac{\partial q_{L,x}}{\partial x} + \frac{\partial q_{L,y}}{\partial y} + \frac{\partial q_{L,z}}{\partial z}\right), \tag{3.34}$$

$$u_x \frac{\partial}{\partial x}\left(\sum_{i=1}^{nc} c_{iV}\overline{H}_{iV}\right) + u_y \frac{\partial}{\partial y}\left(\sum_{i=1}^{nc} c_{iV}\overline{H}_{iV}\right) = -\left(\frac{\partial q_{V,x}}{\partial x} + \frac{\partial q_{V,y}}{\partial y} + \frac{\partial q_{V,z}}{\partial z}\right), \text{ and} \tag{3.35}$$

$$\frac{\partial}{\partial y}\left(w_y \sum_{i=1}^{nc} c_{iM}\overline{H}_{iM}\right) = -\frac{\partial q_{M,y}}{\partial y} + w_y \frac{\partial p_M}{\partial y}. \tag{3.36}$$

Page 149

Nomenclature for $\mathbf{q}$ should be “Heat flux vector” instead of “Conductive heat flux vector”.

Page 159

Sanchez–Lacombe equation of state parameters for hydrogen in Table A.1 should be T^* = 53.55 K, P^* = 31.7 MPa, and ρ^* = 75.27 kg/m^3 as used in the example simulations (Appendix VII).